UNIVERSIDAD NACIONAL AUTÓNOMA DE MÉXICO

Maestría y Doctorado en Ciencias Bioquímicas

La proteína inhibidora de la ATPasa (IF_1) de *Caenorhabditis elegans* se localiza en la mitocondria y es necesaria para la sobrevivencia en condiciones de estrés.

TESIS

QUE PARA OPTAR POR EL GRADO DE:

Doctor en Ciencias

PRESENTA:
M. en C. LAURA PAULETTE FERNÁNDEZ CÁRDENAS

TUTOR PRINCIPAL
ROSA ESTELA NAVARRO GONZÁLEZ
INSTITUTO DE FISIOLOGÍA CELULAR, UNAM

MIEMBROS DEL COMITÉ TUTOR
DRA. MARIETTA TUENA SANGRI
INSTITUTO DE FISIOLOGÍA CELULAR, UNAM
DR. CHRISTOPHER WOOD
INSTITUTO DE BIOTECNOLOGÍA, UNAM

Ciudad de México. Octubre, 2017

Agradecimientos Académicos

Esta tesis doctoral se realizó bajo la dirección de la Dra. Rosa Estela Navarro González en el laboratorio 206 sur del Instituto de Fisiología Celular de la Universidad Nacional Autónoma de México.

Este trabajo fue posible gracias a los apoyos de los proyectos de Consejo Nacional de Ciencia y Tecnología (CONACYT-SEP) 103856-Q y 220987 y del Programa de Apoyo a la Innovación e Investigación Tecnológica (PAPIIT-UNAM) IN207412 e IN207415

La alumna Laura Paulette Fernández Cárdenas recibió una beca durante la realización de sus estudios de Doctorado por parte del Consejo Nacional de Ciencia y Tecnología (CONACYT, México) con número de registro 378014 y una beca para conclusión de estudios del Programa de Apoyo a la Innovación e Investigación Tecnológica (PAPIIT-UNAM) IN207415.

A el comité tutotal que asesoró el desarrollo de esta tesis estuvo formado por:

Dra. Rosa Estela Navarro González	Instituto de Fisiología Celular, UNAM
Dra. Marietta Tuena Sangri	Instituto de Fisiología Celular, UNAM
Dr. Chritopher Wood	Instituto de Biotecnología, UNAM

Al jurado de examen doctoral compuesto por:

Dra. Soledad Funes Argüello	Instituto de Fisiología Celular, UNAM
Dr. Juan Miranda Ríos	Instituto de Investigaciones Biomédicas, UNAM
Dr. José de Jesús García Trejo	Facultad de Química, UNAM
Dr. Roberto Coria Ortega	Instituto de Fisiología Celular, UNAM
Dr. Jesús Aguirre Linares	Instituto de Fisiología Celular, UNAM

Se reconoce la colaboración de la Dra. Marietta Tuena Sangri, del Departamento de Bioquímica y Biología Estructural del Instituto de Fisiología Celular, UNAM, por su asesoría en el desarrollo del proyecto y en cuyo laboratorio se realizaron los experimentos para determinar la proporción de dímero y monómero de la ATPasa.

A la M. en C. Laura Silvia Salinas Velázquez del Departamento de Biología Celular y del Desarrollo del Instituto de Fisiología Celular, UNAM, por su apoyo técnico y colaboración en la cuantificación de la apoptosis de *C. elegans.*

A la Q.F.B Concepción José Nuñez del Departamento de Bioquímica y Biología Estructural del Instituto de Fisiología Celular, UNAM, por su apoyo técnico y colaboración en la determinación de la proporción de dímero y monómero de la ATPasa.

Al Dr. Salvador Uribe Carvajal, M. en C. Emilio Espinoza Simón, Dr. Alfredo Cabrera Oréfice y M. en C. Cristina Uribe Álvarez del Departamento de Bioquímica y Biología Estructural del Instituto de Fisiología Celular por su apoyo, asesoría, préstamo de reactivos y préstamo de equipo.

A Fermín Domínguez Díaz del Instituto de Fisiología Celular, UNAM por su apoyo en el laboratorio.

A la Maestra Sandra Moncada Hernández, Javier Gallegos Infante y Nadia Brisa Robles Vidal de la Biblioteca Dr. Armando Gómez Puyou por su ayuda, apoyo y organización.

Al Dr. Roberto Coria por todo su apoyo como coordinador del Posgrado en Ciencias Bioquímicas.

A Leticia García Gutierrez, Rosa Lilia de la Rocha, Julio Ignacio Palacios Ordoñez Viñas, M. en C. Norma Trejo Medina, Adelina González Pérez por su ayuda, organización y colaboración en la gestión académica relacionada con el Posgrado en Ciencias Bioquímicas.

A la Dra. Laura Ongay Larios y al personal de la Unidad de Biología Molecular del Instituto de Fisiología Celular, UNAM: Guadalupe Códiz Huerta y Minerva Mora Cabrera.

A los ingenieros Gerardo Coello, Juan Manuel Barbosa, Francisco Pérez e Ivette Rosas por su asesoría y ayuda en el área de computo.

Al personal del taller, el Ing. Aurey Galván Lobato e Ing. Manuel Ortínez Benavides.

Índice

Resumen 11
Abstract 12
Abreviaturas 13

I. Introducción 15

i. La mitocondria. La central energética de la célula. 16

¿Qué es la mitocondria? 16
El origen de la mitocondria**.** 17
Enfermedades mitocondriales. Herencia y heterogeneidad. 18
Metabolismo celular de organismos aerobios. Generalidades. 19
Características generales de las ATPasas que rotan. 22
La F_oF_1-ATP Sintasa. 23
Estructura de la F_oF_1-ATP sintasa. 23
El mecanismo de la F_oF_1-ATP sintasa. 25
Las F-ATPasa forman dímeros. 28
Regulación de la F_oF_1-ATP sintasa por la proteína inhibidora (IF_1). 30
Secuencia mínima de inhibición y estructura de la IF_1. 32
Dimerización de la IF_1 y su efecto en la ultra-estructura mitocondrial. 35
La función de la IF_1 en la regulación de la sobrevivencia y muerte celular. 36
Mantenimiento del $\Delta\psi_m$ por IF_1 y su efecto en la mitocondria. 37
Efecto de la sobre-expresión de IF_1 en el cáncer. 38

ii. Características y fisiología de *Caenorhabditis elegans.* 40

Generalidades de *C. elegans.* 40
Ciclo de vida de *C. elegans.* 41
El sistema reproductor del *C. elegans*. 43
La apoptosis fisiológica de las células germinales del *C. elegans*. 44
Mecanismo por el cual se lleva acabo la apoptosis de las células germinales en *C. elegans.* 45
Participación de la mitocondria en la apoptosis de *C. elegans.* 47
Inducción de la apoptosis de las células germinales por estrés. 48

II. Antecedentes 50

III. Planteamiento del Problema e hipótesis. 52

IV. Objetivos. 54

V. Materiales y Métodos. 56

Mantenimiento de cepas. 57
Generación de los reporteros traduccionales *mai-1::gfp*, *mCherry::mai-1* y *tomm-20::mCherry* por MosSCI. 58

Adquisición de imágenes y procesamiento de los animales transgénicos. 61
Generación de los alelos de *mai-2* por CRISPR-Cas9. 61
Extracción de RNA. 63
Cuantificación de la expresión del mRNA de *mai-2* por RT-PCR semicuantitativo. 64
Tiempo de vida. 64
Conteo de progenie y letalidad embrionaria. 64
Visualización de las mitocondrias 65
Consumo de oxígeno 66
Cuantificación de ATP 66
Purificación de mitocondrias, electroforésis de 1D y SDS-PAGE 67
Ensayos de sobrevivencia 68
Ensayos de apoptosis 68

VI. Resultados 70

MAI-1 no se expresa en la mitocondria. 72
MAI-2 se expresa en la mitocondria de *C. elegans*. 74
Las mutantes en *mai-2* no muestran fenotipo en condiciones fisiológicas. 77
Los animales mutantes en *mai-2* no muestran defectos en las redes mitocondriales ni en la dimerización de ATP sintasa pero si muestra un $\Delta\psi_m$ incrementado. 78
MAI-2 se requiere para que los animales resistan al estrés. 82
MAI-2 se requiere para inducir apoptosis por estrés. 83

VII. Discusión 86

VIII. Conclusiones 91

IX. Perspectivas 93

X. Referencias Bibliográficas 96

XI. Apéndice I 110

XII. Apéndice II 115

Índice de Figuras

Figura 1. La mitocondria. 17
Figura 2. La cadena transportadora de electrones. 21
Figura 3. Criomicroscopía electrónica de 3 diferentes ATPasas. 23
Figura 4. La F_oF_1-ATP sintasa mitocondrial. 24
Figura 5. Estructura y mecanismo de rotación de F_o. 26
Figura 6. Modelo de la síntesis/hidrólisis de ATP de acuerdo con el modelo de sitios alternantes de Paul Boyer. 27
Figura 7. La ATP sintasa dimérica. 29
Figura 8. Interacción de la IF_1 con la F_oF_1-ATP sintasa 31
Figura 9. Alineamiento de los residuos 1-60 de la IF_1 madura de bovino y sus regiones equivalentes en levadura y otras especies. 32
Figura 10. Estructura de la IF_1 de bovino. 33
Figura 11. Estructura y mecanismo de unión de la IF_1 de bovino. 34
Figura 12. Modelo de dimerización de ATP sintasas. 35
Figura 13. Ciclo de vida del *C. elegans*. 42
Figura 14. La gónada de *C. elegans.* 44
Figura 15. La maquinaria de apoptosis se encuentra conservada entre organismos. 48
Figura 16. Representación de MosSCI. 59
Figura 17. Identificación de las mutaciones en mutantes *mai-2(xm18)* y *mai-2(xm19)* por digestión y PCR. 63
Figura 18. Alelos y reporteros traduccionales utilizados para el estudio de la función de la proteína inhibidora de la ATPasa mitocondrial en *C. elegans.* 71
Figura 19. GFP::MAI-1 y MAI-1::mCherry se expresa en el citoplasma y no en la mitocondria. 73
Figura 20. MAI-2::GFP se expresa en el soma y la línea germinal. 75
Figura 21. El reportero MAI-2::GFP se expresa en la mitocondria de *C. elegans.* 76
Figura 22. El mRNA de *mai-2* es poco abundante en las mutantes de *mai-2.* 77
Figura 23. Los animales mutantes en *mai-2* no muestran defectos en el número de progenie ni en el tiempo de vida. 78
Figura 24. Las mutantes en *mai-2* tiene un $\Delta\psi_m$ más elevado. 81
Figura 25 MAI-2 se requiere para la sobrevivencia en condiciones de estrés. 83
Figura 26. MAI-2 es importante para inducir apoptosis en condiciones fisiológicas o en condiciones de estrés. 85

Índice de Tablas.

Tabla 1. Cepas 57
Tabla 2. Oligonucleótidos utilizados en este trabajo. 60
Tabla 3. Los animales mutantes en *mai-2* no muestran diferencias significativas en la apoptosis somática. 84

Resumen

Cuando el gradiente electroquímico se abate en la mitocondria, la proteína inhibidora de la ATPasa (IF_1) inhibe la actividad hidrolítica y reversa de la F_oF_1-ATP sintasa, permitiendo a las células conservar el ATP a expensas de la pérdida del potencial de membrana mitocondrial ($\Delta\psi_m$). La función de la IF_1 se ha estudiado en diferentes líneas celulares, pero estos estudios han generado resultados contradictorios, que no han ayudado a entender el papel de estas proteínas en un organismo completo. En este trabajo estudiamos la función de la proteína IF_1 en *Caenorhabditis elegans* en un intento por entender su papel *in vivo*. *C. elegans* tiene dos proteínas inhibidoras de F_oF_1-ATPasa llamadas MAI-1 y MAI-2. Para determinar su localización en *C. elegans*, se generaron dos reporteros traduccionales y encontramos que la fusión MAI-2::GFP se expresa de forma ubicua en la mitocondria. En cambio, la fusión GFP::MAI-1 se encontró en el citoplasma y en el núcleo de ciertos tejidos. Para estudiar la función de *mai-2* en el nematodo, se generaron dos alelos mutantes por CRISPR-Cas-9. Los animales mutantes en *mai-2* no presentan un fenotipo evidente en cuanto a su fertilidad, desarrollo embrionario o expectativa de vida. En contraste con los resultados previos de otros grupos obtenidos en líneas celulares, no encontramos defectos en la morfología de las redes mitocondriales, la proporción dímero/monómero de ATP sintasa, la concentración de ATP, ni en el consumo de oxígeno. Sin embargo, los animales mutantes en IF_1 tienen un incremento en el potencial de membrana ($\Delta\psi_m$) y presentan menor apoptosis fisiológica. Por otro lado, los animales mutantes en *mai-2* son más sensibles al estrés por choque de calor, el estrés oxidativo y a la inhibición de la cadena transportadora de electrones. Además, encontramos que MAI-2 es importante para inducir la apoptosis de las células germinales bajo ciertos tipos de estrés. Nuestros resultados sugieren que algunos de las funciones previamente atribuidos a IF_1 en líneas celulares no reflejan exactamente la función de esta proteína en un organismo entero y podrían deberse a líneas celulares específicas o a los métodos de silenciamiento o sobre-expresión utilizados. Proponemos que MAI-2 podría jugar un papel en la apoptosis y la regulación del $\Delta\psi_m$. Adicionalmente, sugerimos que la función de IF_1 resulta evidente bajo condiciones de estrés y que en condiciones fisiológicas esta proteína parece no jugar un papel esencial.

Abstract

When the electrochemical proton gradient is disrupted in mitochondria, IF_1 inhibits the reverse hydrolytic activity of the F_oF_1-ATP synthase thereby allowing cells to conserve ATP at the expense of loosing the mitochondrial membrane potential ($\Delta\psi_m$). The function of IF_1 has been studied mainly in different cell lines but these studies have generated contrasting results, which have not been helpful to understand the real role of this protein in a whole organism. In this work, we studied IF_1 function in *Caenorhabditis elegans* in an attempt to understand IF_1´s role *in vivo. C. elegans* has two inhibitor proteins of the F_oF_1-ATPase known as MAI-1 and MAI-2. To determine its protein localization in *C. elegans,* we generated translational reporters and found that MAI-2 is expressed ubiquitously in the mitochondria. Conversely, MAI-1 was found in the cytoplasm and the nuclei of certain tissues. By CRISPR/Cas9 genome editing we generated *mai-2* mutant alleles. Here we showed that *mai-2* mutant animals have normal progeny, embryonic development and lifespan. Contrasting with the results previously obtain in cell lines, we did not find evident defects in the mitochondrial network, dimer/monomer ATP synthase ratio, ATP concentration or respiration. Our results suggest that some of the roles previously attribute to IF_1 in cell lines could not reflect the function of this protein in a whole organism and could be attributed to specific cell lines or methods use to silence, knockout or overexpress this protein. However, we did observe that animals lacking IF_1 had an enhanced $\Delta\psi_m$ and lower physiological germ cell apoptosis. Importantly, we found that *mai-2* mutant animals have to be stress out to observe the role of IF_1. Accordantly we observed that *mai-2* mutant animals were more sensitive to heat shock, oxidative and electron transport chain blockage. Furthermore we observed that IF_1 is important to induce germ cell apoptosis under certain types of stress. Here we propose that MAI-2 might play a role in apoptosis by regulating the $\Delta\psi_m$. Additionally, we suggest that IF_1 function is mainly observed under stress and that in physiological conditions this protein does not play an essential role.

Abreviaturas

1D BN-PAGE	Siglas en inglés para electroforesis en dos dimensiones de geles de poliacrilamida con dodecilsulfato de sodio.
A	Absorbancia
ADP	Adenosin difosfato
ATP	Adenosín-5'-trifosfato
CED	Siglas en inglés para células anormales en la muerte celular
CoA	Coenzima A
cDNA	Siglas en inglés de ácido desoxiribonucléico complementario
CRISPR	Siglas en inglés de repeticiones palindrómicas cortas agrupadas y regularmente inter-espaciadas)
Cyt *c*	Siglas en inglés de Citocoromo *c*
$\Delta\psi_m$	Potencial de membrana mitocondrial
Δp	Fuerza electrón motriz
DI	Dominio de inhibición
DIC	Microscopía de contraste diferencial interferencial
EGL-1	Siglas en inglés para el fenotipo
GFP	Siglas en inglés de proteína verde fluorescente
RRH	Región rica en histidinas
IF_1	Proteína inhibidora 1
kDa	Kilodaltons
MAI	Siglas en inglés de el inhibidor de la ATPasa mitocondrial.
MosSCI	Siglas en inglés de inserción monocopia por recombinación con la transposasa Mos
mRNA	Siglas en inglés de ácido ribonucléico mensajero
mtDNA	Siglas en inglés de ácido desoxiribonucléico mitocondrial
MosSCI	Siglas en inglés de inserción monocopia por recombinación con la transposasa Mos
MTS	Siglas en inglés de secuencia de transporte mitocondrial
NADH	Nicotina adenina dinucleótido (forma reducida)
NES	Siglas en inglés de secuencia de exportación nuclear.
NGM	Siglas en inglés de secuencia de medio de crecimiento normal
OXPHOS	Siglas en inglés de fosforilación oxidativa
PAGE	Siglas en inglés de geles de poliacrilamida con dodecilsulfato de sodio
pb	Pares de bases
PCR	Siglas en inglés de la reacción en cadena de la polimerasa
Pi	Siglas en inglés de fosfato inorgánico
PTP	Siglas en inglés para el poro de transición de permeabilidad
rt	Retro-transcriptasa
rpm	Revoluciones por minuto
RNAi	Siglas en inglés de RNA interferencia
ROS	De las siglas en inglés para nombrar a las especies reactivas de oxígeno
SDS	Siglas en inglés de dodecilsulfato de sodio
SEM	Siglas en inglés de error estándar
sgRNA	Siglas en inglés de RNA guía único
ssDNA	Siglas en inglés del DNA de una sola hebra.
TA	Temperatura ambiente

TMRM	Tetrametilrodamina metil ester
UQ	Ubiquinona
UV	Ultravioleta
UTR	Siglas en inglés de la región no traducida de un RNA mensajero

I. Introducción

i. La mitocondria. La central energética de la célula.

¿Qué es la mitocondria?

En la célula existen muchos procesos que son espontáneos, por ejemplo la formación de la bicapa lipídica al ensamblarse los fosfolípidos en el medio acuoso del citosol o el plegamiento de algunas proteínas, sin embargo, también existen procesos que no son espontáneos y requieren de energía para llevarse acabo, tal es el caso de la síntesis de proteínas, que necesita liberar la energía almacenada en el ATP y GTP. El ATP es una molécula utilizada en muchos procesos celulares y por ende necesita ser sintetizada en grandes cantidades. En la célula, el organelo que se encarga de sintetizar la mayor cantidad de ATP es la mitocondria. La mitocondria es el módulo funcional que ayuda a maximizar la cantidad de ATP que se genera a partir de los alimentos que consumimos.

La mitocondria es un organelo dinámico, que dependiendo del tipo celular y el estadio del desarrollo muestra gran variabilidad en forma, número y estructura (Mootha y colaboradores, 2003). Cada mitocondria está compuesta por dos membranas: la interna y externa (Figura 1). El proteoma de la membrana externa está compuesta de canales que permiten la difusión de iones y moléculas pequeñas al interior de la mitocondria (porinas) y también de enzimas involucradas en la síntesis de lípidos. La membrana interna está compuesta por invaginaciones llamadas crestas, es rica en cardiolipina y es impermeable a iones y moléculas pequeñas. El 76% de las proteínas que componen a la mitocondria se localizan en la membrana interna, dichas proteínas abarcan las enzimas que componen a la cadena transportadora de electrones, transportadores y a la enzima F_oF_1-ATP sintasa encargada de la síntesis de ATP (Nelson y Cox, 2017).

Las dos membranas que comprenden a la mitocondria establecen dos regiones discretas en el organelo: el espacio intermembranal y la matriz. En la matriz mitocondrial se encuentran las enzimas del ciclo de Krebs y el DNA mitocondrial, el cual codifica en mamíferos para 13 proteínas de los complejos de la cadena transportadora de electrones. Mientras que en el espacio intermembranal puede encontrarse un proteoma muy diferente al de la matriz, algunas proteínas incluso son específicas de este compartimento, como es el caso del citocromo *c* (cyt *c*).

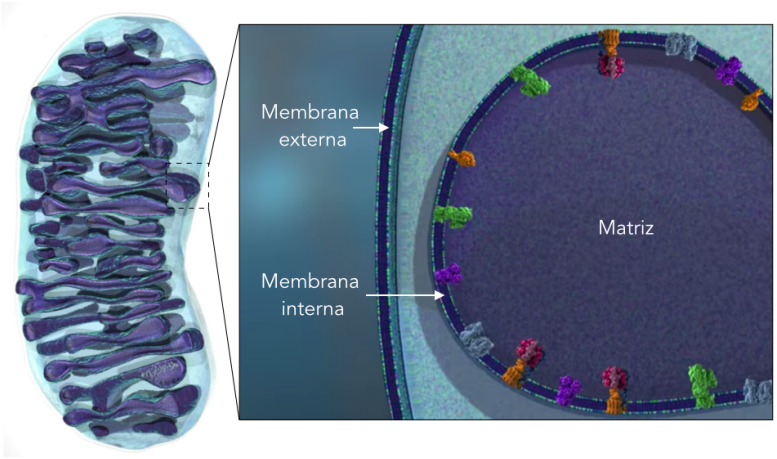

Figura 1. La mitocondria. Las mitocondrias son organelos formados por dos membranas, la membrana externa y la interna que delimitan el espacio intermembranal (azul). La membrana interna forma a las crestas mitocondriales (morado). Imagen modificada de Edx, HarvardX: MCB64.1x Cell Biology: Mitochondria, 2017.

Las mitocondrias no se encuentran flotando en el citosol de la célula, sino que se mueven en caminos definidos gracias a la interacción de estos organelos con el citoesqueleto que constantemente se está remodelando como respuesta a cambios metabólicos o estrés (Saxton & Hollenbeck, 2012). La co-localización de microtúbulos con las mitocondrias está bien documentada y el tratamiento de agentes que despolimerizan los microtúbulos causan un desalineamiento y re-distribución de las mitocondrias (Ball y Singer 1982). Las proteínas motoras, como las cinesinas, transportan mitocondrias a través de los microtúbulos. Las cinesinas KIF5 y KIFB1-α se ha reportado están encargadas de transportar mitocondrias de manera anterógrada en neuronas (Sheng y Cai.,2012).

El origen de la mitocondria.

Las mitocondrias se originaron hace 2 mil millones de años por la endocitosis de una α-proteobacteria por una arqueobacteria. La identidad del huésped fue recientemente esclarecido gracias al descubrimiento de las Lockiarcheotas (Asgard superfilum), un clado de las arqueas que se encontró en sedimentos acuíferos en el Castillo de Loki, sitio ubicado entre Groenlandia y Noruega. Estudios filogenéticos posicionaron a las arqueas Asgard como el grupo con mayor cercanía a eucariontes, ya que codifican para proteínas que se creía específicas de eucariontes, tal es el caso de

componentes del citoesqueleto, proteínas involucradas en tráfico vesicular y de secreción, así como GTPasas involucradas en tráfico y remodelado del citoesqueleto (Zaremba y colaboradores, 2017).

Una de las hipótesis metabólicas aceptadas de cómo se dió la endosimbiosis es la hipótesis del H_2 (Muller y Martin, 1998). La hipótesis consiste en que los eucariontes surgen a través de una asociación simbiótica metabólica (sintrofía), entre una α-proteobacteria metabólicamente versátil que generaba H_2/CO_2 y una arquea anaerobia dependiente de H_2, posiblemente metanógena. Ambos simbiontes se encontraron en un ambiente anaerobio rico en H_2 y CO_2, en donde el hospedero cambio la fuente exógena de H_2 y CO_2 por los desechos que el simbionte ofrecía. La arquea incrementó el contacto con el simbionte hasta importar sistemas de transporte y metabolismo de carbohidratos. Finalmente, el resultado fue un organismo irreversiblemente heterótrofo que contiene una mitocondria ancestral e independencia del H_2 (López García y David Moreira, 1999).

Enfermedades mitocondriales. Herencia y heterogeneidad.

Nuestras mitocondrias las heredamos de nuestra madre. El mecansimo por el cual las mitocondrias paternas son eliminadas posterior a la fertilización se encontró por Sato y Sato, (2011) en el nematodo *Caenorhabditis elegans,* en este estudio se encontró que las mitocondrias paternas desaparecen por autofagia. Por medio de los animales transgénicos LGG-1::GFP (homólogo a LC3/ Atg8, requerido en la degradación de componentes celulares durante la autofagia) se observó la formación del autofagosoma alrededor del pronúcleo paterno, que co-localiza con las mitocondrias después de la fertilización. La inhibición de la formación del autofagosoma, causa la retención de las mitocondrias paternas y como consecuencia un aumento en la letalidad embrionaria. Además, mutantes deficientes en la función lisosomal, fallan en desaparecer a las mitocondrias paternas, demostrando que la degradación de las mitocondrias paternas es dependiente del lisosoma (Sato y Sato, 2011). En un estudio relacionado, Rawi y colaboradores (2011) examinaron ovocitos recién fertilizados de *Mus musculus* y *C. elegans* demostrando que la autofagia de las mitocondrias paternas es un evento evolutivamente conservado.

Más de 150 enfermedades mitocondriales se han ligado a la herencia de mutaciones en el mtDNA, afectando a 1 de cada 5,000-10,000 personas en los Estados Unidos (Skladal y colaboradores, 2003). Estas enfermedades se pueden presentar en la infancia o en la adultez y por lo general afectan la síntesis de ATP, debido a mutaciones en los genes que codifican para la cadena

transportadora de electrones. Las enfermedades mitocondriales generalmente afectan a tejidos que son metabólicamente muy activos, tal es el caso del músculo esquelético, músculo del corazón y el cerebro, por ende algunos síntomas característicos de las enfermedades son: acidosis láctica, debilidad muscular, defectos en habilidades cognitivas, neurodegeneración, sordera y ceguera (Vafai y Mootha, 2012).

Para entender un poco mejor a las enfermedades mitocondriales, es importante tener en cuenta que las mitocondrias muestran heterogeneidad entre las mitocondrias de una célula y entre los tejidos de un organismo. La heterogeneidad que se observa en una célula, se debe a que la población de mitocondrias (10-20 mitocondrias/célula) no está compuesta de mitocondrias con el mismo genoma, p.ej. si 2-3 mitocondrias tienen mutaciones en el genoma que afectan su función y el resto de las mitocondrias en la célula se encuentran sanas, el resultado del estado de la célula dependerá del número de mitocondrias sanas (Edx, HarvardX: MCB64.1x Cell Biology: Mitochondria, 2017). Dos genomas mitocondriales con diferentes mutaciones pueden complementarse genéticamente entre ellas por medio de la fusión mitocondrial y codificar lo que a la otra mitocondria le haga falta, generando todos los componentes para la fucnción mitocondrial. La heterogeneidad entre tejidos se refiere al uso distinto de sustratos y capacidad de biosíntesis, así como la morfología que exhiben las mitocondrias entre los distintos tejidos. Se calcula que aproximadamente el 25% de los componentes mitocondriales no se comparten entre tejidos (Pagliarini y colaboradores, 2008), teniendo consecuencias funcionales, p. ej. la mayoría de las mitocondrias comparten los mismos complejos de la cadena transportadora de electrones, sin embargo, en mamíferos se han observado diferentes isoformas del complejo IV en diferentes tejidos teniendo consecuencias en la respuesta a hipoxia (Pierron y colaboradores, 2012).

Metabolismo celular de organismos aerobios. Generalidades.

Podemos dividir la síntesis de ATP en tres pasos:

1) La glucólisis. La glucólisis es una serie de 10 reacciones que ocurren en el citoplasma y no requiere de oxígeno para llevarse acabo. En esta vía, una molécula de glucosa se oxida a dos moléculas de piruvato y como resultado se generan 2 moléculas de ATP totales y se donan los electrones de la glucosa al aceptor universal de electrones NAD+ que se reduce a NADH. Posterior a la glucólisis, el piruvato se transporta a la matriz de la mitocondria en donde por una

descarboxilación oxidativa el piruvato pierde un grupo carboxilo en forma de CO_2 y el resto de la molécula forma parte del grupo acetil del acetil-CoA (Nelson y Cox, 2017).

2) Ciclo del ácido cítrico. El acetil-CoA alimenta al ciclo del ácido cítrico, en el cual el grupo acetil (2C) es donado al oxaloacetato (4C) para formar citrato (6C), el cual pasa por una serie de reacciones en donde es descarboxilado dos veces hasta formar una molécula de succinato (4C), que se convierte finalmente en oxaloacetato (4C) para regenerar el ciclo. Durante el ciclo del ácido cítrico se producen 3 moléculas de NADH y 1 de $FADH_2$ por molécula de acetil-CoA (Nelson y Cox, 2017).
3) Fosforilación oxidativa. En la membrana interna mitocondrial se encuentran el complejo I (NADH/ubiquinona oxidoreductasa), complejo III (citocoromo *c* reductasa) y el complejo IV (citocromo *c* oxidasa), responsables de la generación del gradiente electroquímico, $\Delta\mu_{H+}$ (en bioenergética se convierte el $\Delta\mu_{H+}$ en unidades de potencial eléctrico y se refiere como fuerza protonmotriz, Δp) (Figura 2, A). El complejo I se alimenta de los electrones de la molécula NADH (generado en el ciclo del ácido cítrico) y los transfiere al quinol de la membrana. La energía liberada por la transferencia de los electrones se utiliza para bombear 4 protones de la matriz al espacio intermembranal. El complejo III toma los electrones del quinol reducido y los transfiere a la proteína soluble citocromo *c*, bombeando un H^+ en el proceso. Finalmente, el complejo IV transfiere los electrones del cyt *c* a la molécula del O_2 que se reduce a H_2O. El complejo II (succinato deshidrogenasa) transfiere los electrones del $FADH_2$ (generado en el ciclo del ácido cítrico) del succinato directamente al quinol y no contribuye en el gradiente de protones. La Δp lleva a la síntesis de ATP conforme los protones fluyen de regreso a la matriz a través de la ATP sintasa (Mitchell, 1967).

Los complejos que forman la cadena transportadora de electrones se ensamblan en supercomplejos o respirosomas (Figura 2, B-C). Los respirosomas pueden ayudar a evitar interacciones proteína-proteína no favorables en el ambiente aglomerado de la membrana interna mitocondrial. Por estudios de criomicroscopía electrónica se pudo determinar que los respirosomas de corazón de bovino consisten en un complejo I, un dímero del complejo III y un monómero del complejo IV en donde se pudo identificar el camino de los electrones a partir del NADH (Figura 2, C; Althoff y colaboradores, 2011).

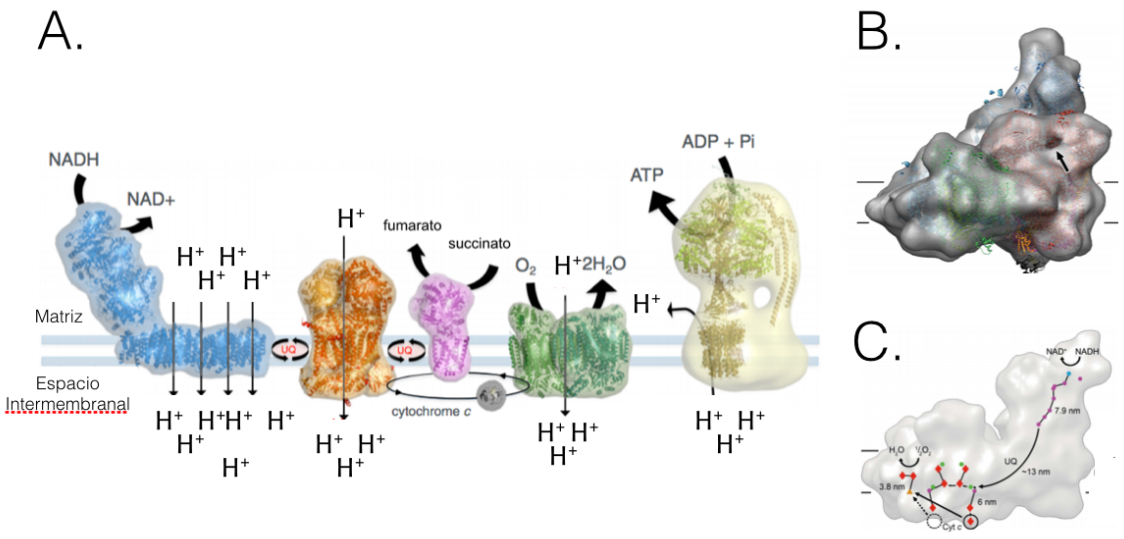

Figura 2. La cadena transportadora de electrones. (A) Los electrones se donan del complejo I y II a la UQ en su forma reducida (QH_2), la UQ dona los electrones al complejo III que los pasa al cyt *c*. El complejo IV finalmente dona los electrones del cyt *c* al O_2 el cual se reduce a H_2O. Se muestran los complejos I (azul), complejo II (violeta); complejo III (naranja); complejo IV (verde); complejo V (amarillo). Imagen modificada de Kühlbrandt, 2015. (B) Mapa realizado por criomicroscopia electrónica 3D del respirosoma superpuesta con la estructura por cristalografía de rayos X de los complejos I, III y IV. Se muestran los complejos I (azul), complejo III (naranja); complejo IV (verde) y cyt *c* (negro y flecha punteada). (C) Mapa de la ruta de electrones en el respirosoma. Imagen modificada de Althoff y colaboradores, 2013.

Características generales de las ATPasas que rotan.

Las ATPasas que rotan son nano-máquinas convertidoras de energía, que acoplan la translocación de protones a través de la membrana a la síntesis o hidrólisis de ATP y se encuentran en todos los organismos vivos. Las ATPasas de tipo F sintetizan el ATP en bacterias, mitocondrias y cloroplastos y utilizan el gradiente electroquímico transmembranal para producir ATP a partir de ADP y P_i (Boyer, 1997). Las V-ATPasas (vacuolas) trabajan en reversa, utilizando la energía liberada por la hidrólisis de ATP para bombear protones a través de la membrana para acidificar componentes celulares (Forgac y colaboradores, 2007), mientras que las A-ATPasas al igual que las F-ATPasas sintetizan ATP en arqueas y bacterias extremófilas (Figura 3, A-C). En condiciones fisiológicas, la F-ATP sintasa mitocondrial sintetiza ATP a partir del ADP+P_i, utilizando Δp generado por la respiración o la fotosíntesis. Algunas bacterias anaerobias y arqueas utilizan la fuerza motriz del Na^+ y lo acopla a la síntesis de ATP (Dimroth y colaboradores, 1999; revisado en Kühlbrandt y Davies, 2016).

Las ATPasas de tipo F están formadas de dos complejos, el complejo globular F_1 que está formado por las subunidades catalíticas y el complejo F_o que consiste en un anillo rotor, las subunidades a, b y otras subunidades hidrofóbicas (Figura 3, A). Las ATPasas V_1 y A_1 también están formadas de una cabeza catalítica y del complejo V_o y A_o con un rotor en forma de anillo en la membrana. En todas las ATPasas un tallo central conecta la cabeza con el rotor en forma de anillo que está formado a su vez de varias subunidades conformadas de dos α hélices hidrofóbicas en forma de pasador. Además, las ATPasas están formadas de un tallo periférico que conecta el complejo catalítico con el estator en la membrana para estabilizar a la ATPasa mientras rota. Las V-ATPasas tienen tres tallos periféricos mientras las A-ATPasas tienen dos tallos (Figura 3, B-C). A diferencia de las ATPasas de cloroplasto, bacterias, las V o A ATPasas, las F-ATPasas de la mitocondria forman dímeros en la membrana (Shagger y colaboradores, 2000; Minauro-Sanmiguel y colaboradores, 2005; Kühlbrandt y Davies, 2016; Figura 3, A).

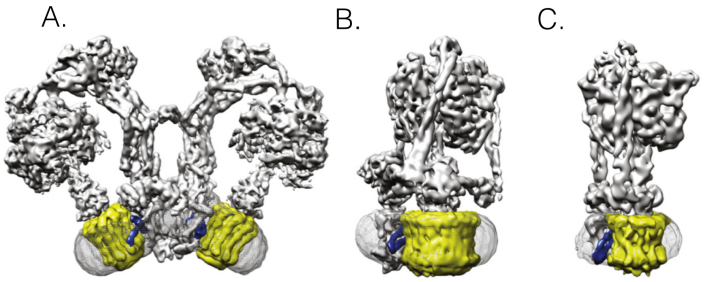

Figura 3. Criomicroscopía electrónica de 3 diferentes ATPasas. (A) F-ATPasas mitocondriales. (B) V-ATPasas vacuolares. (C) A-ATPasas de arqueas. Imagen modificada de Kühlbrandt y Davies, 2016.

La F_oF_1-ATP sintasa.

Estructura de la F_oF_1-ATP sintasa.

El mecanismo y la estructura de la F_oF_1-ATP sintasa fueron descubiertas por Paul Boyer, un bioquímico de la Universidad de California en Los Angeles (UCLA) y John Walker, un biólogo estructural del Laboratorio de Biología Molecular de Cambridge, dicha colaboración entre bioquímicos y biólogos estructurales es una de las más importantes colaboraciones que ha habido en tiempos recientes (Gresser y colaboradores, 1982; Abrahams y colaboradores, 1994). Por sus esfuerzos Boyer y Walker ganaron el premio Nobel de Química en 1997, junto con Jenz Skou, que se dedicó al estudio de la estructura y función de la ATPasa Na^+/K^+.

La F_oF_1-ATP sintasa está formada de dos dominios funcionales, una porción extrínseca de la membrana llamado F_1 y una porción intrínseca de membrana llamado F_o, unido por un tallo central y periférico (Figura 4, A-B).

F_1 es el dominio catalítico de la enzima donde el ATP es formado a partir de ADP y P_i y está formada de 5 subunidades (bovino): α, β, γ, δ, ε con la estequiometría α_3, β_3, γ_1, δ_1, ε_1 (Walker y colaboradores, 1985). Las subunidades $\alpha_3\beta_3$ forman una estructura esférica, con las subunidades α y β alternadas alrededor de la subunidad γ que es el eje giratorio del complejo; el resto de la subunidad γ se extiende 30 Å fuera del hexámero ($\alpha_3\beta_3$) y forma el ancla que fija a las subunidades $\alpha_3\beta_3\gamma_1$ al complejo F_o; la interacción entre γ y F_o es reforzada por la subunidad ε en bacterias y cloroplastos, mientras que en mitocondria está dada por la subunidad δ la cual estabiliza al hexámero y previene que rote. Además de la subunidad δ existe otra proteína que fija la subunidad γ a F_o y recibe el nombre de ε (no confundir con la ε bacteriana) (Figura 4, A-B). El complejo F_o es

un motor, que genera rotación utilizando el Δ*p* y está compuesta de las subunidades *a, b* y *c*. Las subunidades *c* que forman el anillo-*c* se arreglan en una estructura de anillo formado de 8-12 subunidades que atraviesa la membrana interna y el canal de protones se encuentra en la interfase entre el anillo-*c* y las subunidad *a* (Figura 4, C).

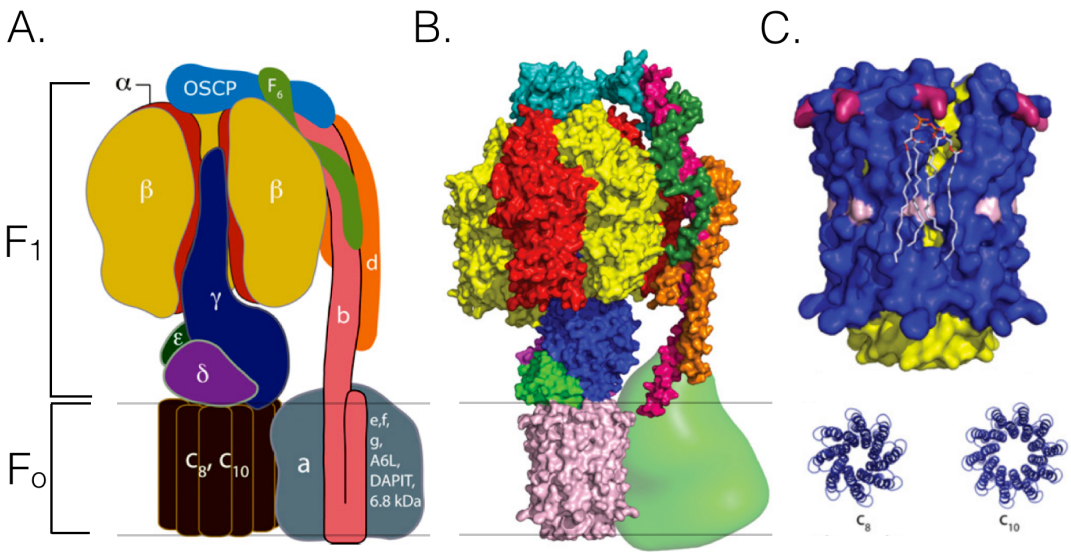

Figura 4. La F_oF_1-ATP sintasa mitocondrial. (A) Esquema de las subunidades que componen a la ATP sintasa mitocondrial de bovino. La parte superior de la enzima está compuesta por el domino catalítico F_1. La subunidad γ (azul) se encuentra en el eje central del dominio $\alpha_3\beta_3$. La subunidad γ y subunidades anexas, están en contacto con F_o que contiene a las subunidades *c* (café) y a la subunidad *a* (gris). El número de subunidades *c* que componen el anillo-*c*, varía con la especie. El rotor de la enzima consiste en el anillo-*c*, la subunidad γ y subunidades accesorias. El paso de protones en el dominio F_o se encuentra entre el anillo-c y la subunidad a. El cuello periférico formado por las subunidades *b* (rosa), *d* (naranja), F6 (verde) y OSCP (azul). (B) Estructura molecular de la ATP sintasa de mitocondria de bovino. (C) (Arriba) El anillo rotor externo y central formado por las subunidades *c* (azul y amarillo). (Abajo) Anillo rotor formado de subunidades *c*, c_8 mitocondria de bovino y c_{10} mitocondrias de *Saccharomyces cerevisiae.* Imágenes modificadas de Walker, 2013.

El mecanismo de la F_oF_1-ATP sintasa.

El rotor de la ATP sintasa esta formado de subunidades *c*, que a su vez están formadas por dos α-hélices transmembranales unidas por un asa, la cual interactúa con el pie del tallo central (γ) (Figura 4, A-B). Gracias a estudios de entrecruzamiento se encontró que la subunidad *a* está cercana al anillo de subunidades *c* (Moore y colaboradores, 2008). Sin embargo fue hasta que se perfeccionó la técnica de criomicroscopía electrónica que se encontró que 4 α-hélices de la subunidad *a* se encuentran horizontales al anillo de subunidades *c*, estas observaciones se realizaron en *Polytomella sp.*, *Yarrowia lipolytica* y en bovino (revisado en Kühlbrandt y Davies, 2016) (Figura 5, A-C). En una de estas α-hélices de la subunidad *a* se encuentra una arginina (Arg) muy conservada, que cuando se muta se elimina la síntesis de ATP acoplado al transporte de protones, esta Arg se encuentra muy cercana al aminoácido aceptor de protones (glutamato, Glu) que se encuentra en las subunidades *c* (Figura 5, B-C). Las largas α-hélices horizontales de la subunidad *a* se dirigen hacia la matriz (Figura 5, A) formando un canal que, visto desde la matriz, se hace cada vez más estrecho en donde interaccionan las α-hélices horizontales de la subunidad *a* con las subunidades *c* y termina hasta la Arg. Del otro lado de la membrana se encuentra otra cavidad por donde los protones entran al anillo rotor de subunidades *c* (Figura 5, C).

El glutamato de la subunidad *c* (cadena ácida) puede adquirir dos diferentes conformaciones dependiendo del ambiente en el que se encuentre, cuando se encuentra en un ambiente hidrofílico la cadena se encuentra posicionada hacia afuera de la subunidad *c* permitiendo la unión con el H^+, una vez unido el glutamato adquiere una conformación cerrada que atrapa al protón (Pogoryelov y colaboradores, 2010), dicha posición la adquiere al estar en el ambiente hidrofóbico de la membrana (Figura 5, C). La Arg conservada de la subunidad *a* participa como una barrera electrostática, previniendo la rotación reversa y la pérdida del H^+. Cuando la subunidad *c* da la vuelta completa y llega a un ambiente hidrofílico la cadena protonada cambia a la conformación abierta y el H^+ escapa a la matriz.

El Δp da lugar a la rotación del anillo de subunidades *c*, si la concentración de protones es más alto en el lado del lumen (pH 7-7.4) que en la matriz mitocondrial (pH 8), el anillo *c* rota a favor de las manecillas de reloj (visto de F_o a F_1). Las ATPasas de tipo F también pueden actuar de modo reverso (Simoni y Postma, 1975). En el modo reverso la hidrólisis de ATP en F_1 lleva a las

cadenas de glutamato a tomar los protones de la matriz a través de la membrana hasta el residuo de Arg, al llegar a este punto los protones escapan por el canal del lumen generando un gradiente electroquímico.

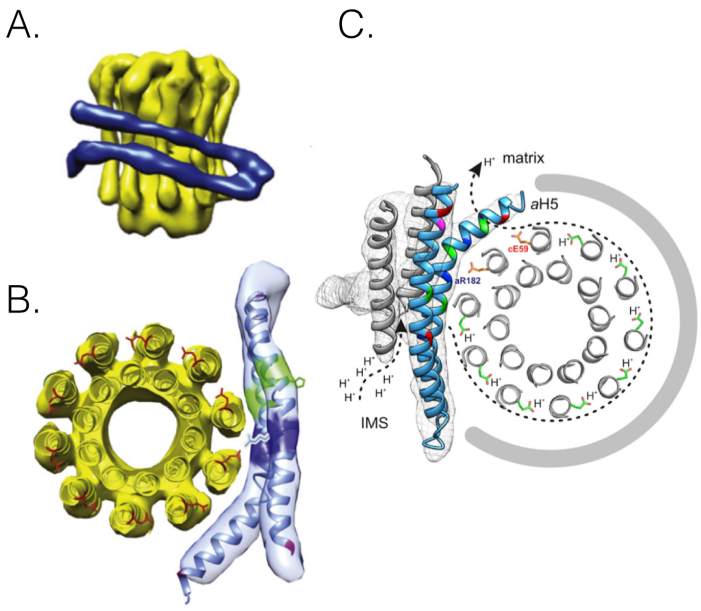

Figura 5. Estructura y mecanismo de rotación de F_o. (A) Anillo rotor (amarillo) y hélices horizontales de la subunidad *a*. (B) Localizacion de residuos importantes indicados en color. En rojo se muestran los glutamatos en las subunidades *c*; en azul la Arg conservada de la subunidad *a*; en verde la histidina y glutamato que se encuentran en la cavidad por donde entran los H^+. Las imágenes A y B fueron obtenidas por criomicroscopia electrónica de *Polytomella sp* (Kühlbrandt y Davies, 2016). (C) Anillo rotor de *Yarrowia lipolytica* formado de 10 subunidades *c* en gris, el glutamato de las subunidades *c,* se muestra en verde (forma cerrada) y en naranja (forma abierta). Las hélices horizontales de la subunidad *a* se muestran en azul. La línea punteada muestra el camino por donde entra el protón, la dirección de la rotación y la salida de este. Imagen modificada de Hahn y colaboradores, 2016.

Debido a que la subunidad γ tiene una estructura asimétrica, obliga que las tres subunidades catalíticas β adopten 3 diferentes conformaciones con una diferente afinidad por la unión de nucleótidos: “tight (apretado; T)”, "loose (suelto; L)” y "open (abierto; O)” y que tengan diferentes propiedades catalíticas (Figura 6, A-B). Una subunidad β, designada β_{DP} tiene unido MgADP, otra subunidad designada β_{TP} tiene unido MgATP, la tercera subunidad se llama β_E (empty; vacío) y no contiene ningún nucleótido. La subunidad γ por cada 360º de rotación lleva a las subunidad β por los tres estados β_{TP}, β_{DP} y β_E dando lugar a la síntesis o hidrólisis de 3 moléculas de ATP. Las 3

subunidades α se encuentran en un estado cerrado unidas a Mg^{2+} y nucleótidos sin embargo no participan en la síntesis de ATP (Walker J., 2013).

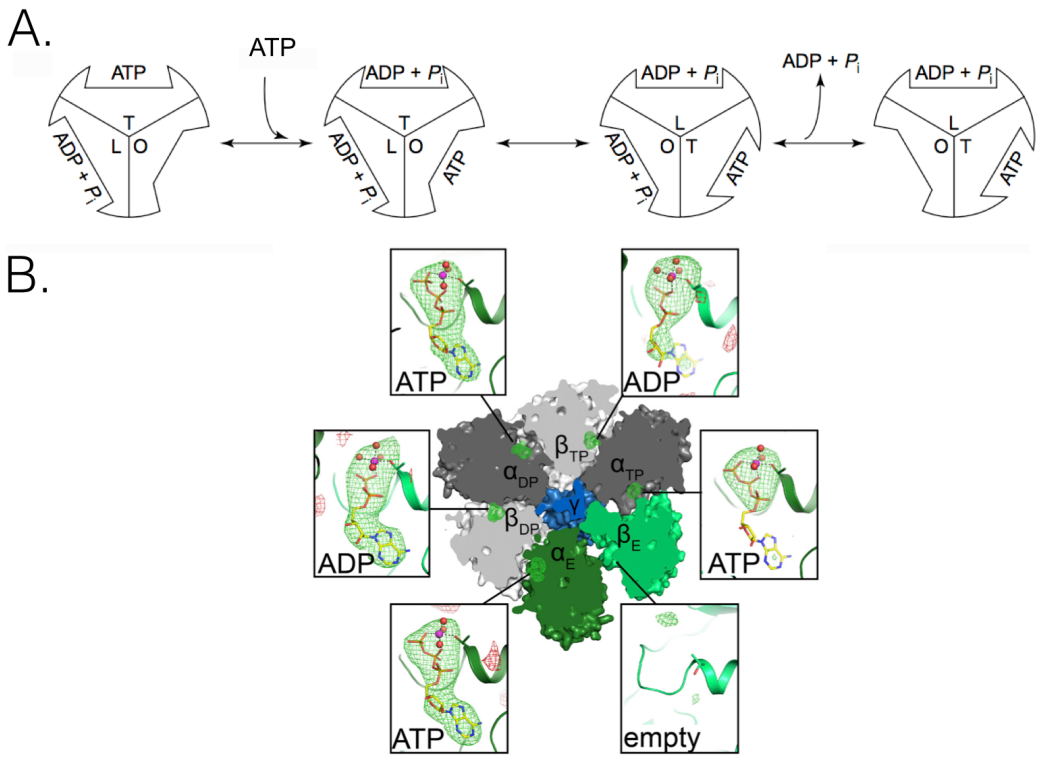

Figura 6. Modelo de la síntesis/hidrólisis de ATP de acuerdo con el modelo de sitios alternantes de Paul Boyer. (A) El ATP se une a un sitio "O" ("open" abierto; sitio vacío) para convertirse en T ("tight" apretado; ocupado por ATP), posteriormente se rompe el enlace fosfodiéster del ATP y el sitio T se convierte en L ("loose" suelto; ocupado por ADP+Pi), el ADP+P_i sale de este sitio y la conformación O se recupera. En un determinado tiempo los 3 sitios catalíticos están en las conformaciones O,T y L. El cambio continuo de estos estados resulta en la hidrólisis (o síntesis) de una molécula de ATP (Modificado de Capaldi y Aggeler, 2002). (B) Corte de la estructura por rayos X de la F_1. Se muestra los seis sitios de unión a nucleótidos en las interfaces de las subunidades α/β vistos desde la matriz. Las subunidades α (verde intenso, y gris intenso) y β (verde débil y gris débil) se arreglan alrededor de la subunided γ (azul). En las cajas se muestran los motivos de unión a nucleótidos y los nucleótidos. Los iones Mg^{2+} se muestran con moléculas de agua coordinadas. Los átomos C, N, O, P y Mg se muestran en los colores amarillo, azul, rojo, naranja y magenta respectivamente. En todos los sitios α se encuentra unido Mg-ATP[3 H_2O] y Mg-ADP[4 H_2O] se encuentra en β_{DP} y β_{TP}, mientras que β_E se encuentra vacío. Imagen tomada de Hahn y colaboradores, 2016.

Las F-ATPasa forman dímeros.

En comparación con las ATPasas de cloroplastos, bacterias, V-ATPasas o A-ATPasas, todas las ATPasas mitocondriales son capaces de formar dímeros. Los dímeros se acomodan en largas filas en las crestas de la membrana interna mitocondrial y son el instrumento para la creación de las mismas. Las filas de dímeros tienen impacto en la actividad respiratoria y en la morfología mitocondrial (Paumard y colaboradores, 2002). El lumen de la cresta puede considerarse un sub-compartimento mitocondrial que asiste la producción de ATP a través de variaciones en la concentración de protones (Strauss y colaboradores, 2008).

En la levadura se propuso que las subunidades *h, i, 6, e, g* y *4* están involucradas en la formación de dímeros. Estas subunidades se encuentran en la membrana entre el tallo periférico de los protómeros. Davies y colaboradores (2012) mutaron las subunidades *e, g* y su4TM1 y encontraron que las mitocondrias de las mutantes carecen de las crestas típicas observadas en la cepa silvestre. Las membranas extraídas de las mutantes, se observaron en forma de esfera o en forma de disco, en lugar de crestas tubulares como la cepa silvestre (Figura 7, A). Además, la ATP sintasa de las cepas mutantes se encontró como monómero en vez de como un dímero (Figura 7, B). También encontraron que dímeros individuales causan una curvatura convexa en el plano *x* (que se extiende una distancia de 15-20 nm), sin embargo, el dímero también provoca una curvatura en el plano perpendicular *y*. Ellos consideraron que cuando dos dímeros de ATP sintasas se acercan uno a otro por difusión lateral en la membrana, la curvatura de deformación en el plano *y* disminuye cuando dos ATP sintasas se alinean en paralelo estabilizando el arreglo.

Las subunidades *e* y *g* forman un heterodímero a través de sus motivos GxxxG, es por medio de estos motivos que se propuso ocurre la interacción entre dos monómeros y así la formación del dímero de ATP sintasas (Arselin y colaboradores, 2003). Gracias a estudios con criomicroscopía electrónica en *Y. lypolitica,* se encontró que no existe contacto entre las subunidades *e/g* entre los monómeros de las ATP sintasas, sin embargo, se encontró que cada heterodímero de subunidades *e/g* dobla la membrana aproximadamente 50º, resultando en un ángulo total de quiebre de la membrana de 100º. El contacto más directo que existe entre las subunidades de los dímeros está dado por la subunidad *f,* que pueden interactuar gracias al quiebre de la membrana dada por *e/g* (Hahn y colaboradores, 2016; Figura 7, C).

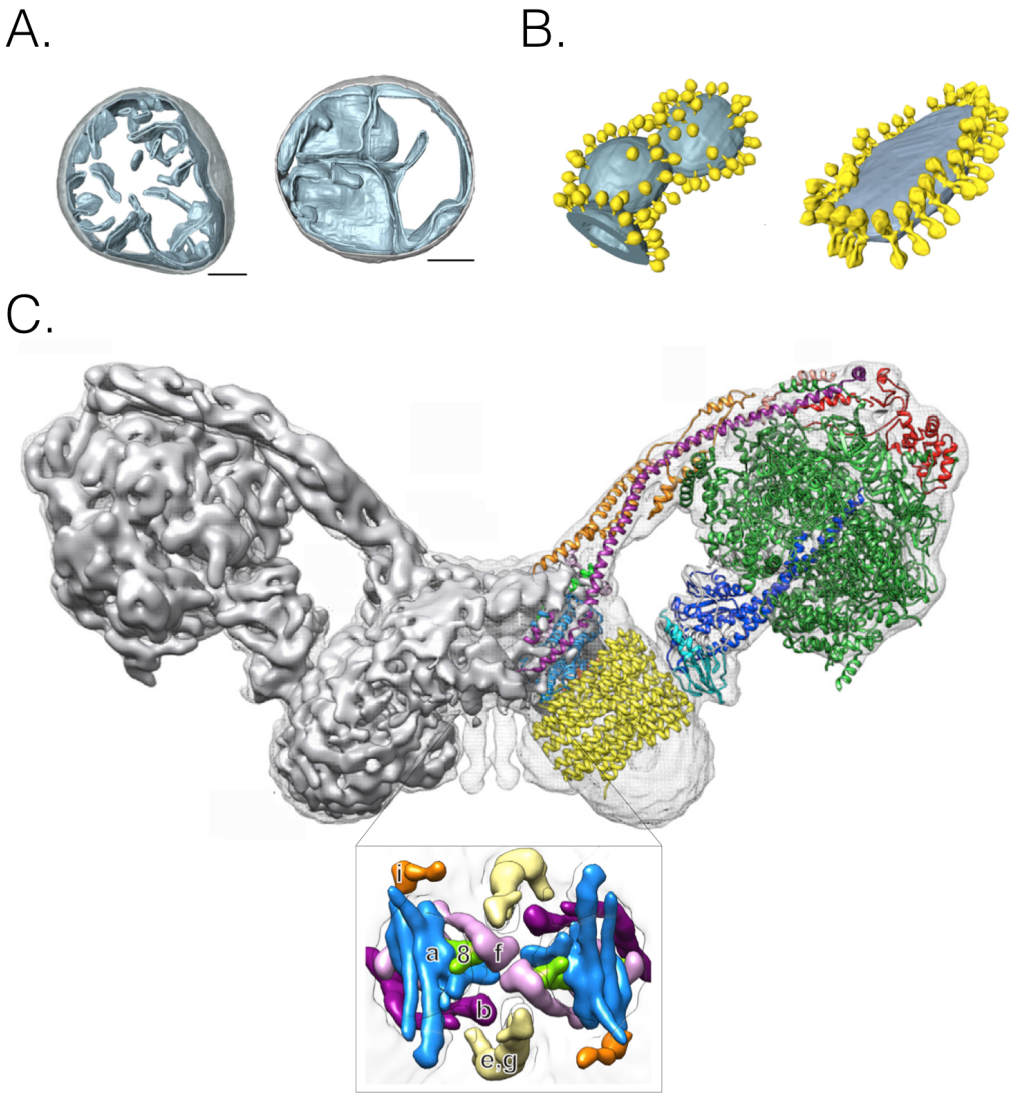

Figura 7. La ATP sintasa dimérica. (A) Morfología de la mitocondria de una cepa de levadura silvestre (izquierda) y mutante en su4TM1 (derecha). En la cepa silvestre las crestas de las mitocondrias son lamelares con ejes curvos, mientras que las crestas de las mutantes en *e, g* y su4TM1 parecen vesículas con pocas o ninguna cresta. (B) Distribución de las ATP sintasas en membranas de mitocondrias aisladas. Las ATP sintasas de la cepa silvestre se acomodan en filas de dímeros sobre los bordes curvos de las crestas en forma de disco, en las mutantes las ATP sintasas se acomodan como monómeros de forma regular en toda la cresta que tiene forma esférica (Modificado de Davies y colaboradores, 2012). (C) Criomicroscopía electrónica del dímero de la ATP sintasa de *Y. lipolyitica*, en la derecha está la estructura en rayos X del monómero. En el cuadrado una imagen desde el espacio intermembranal, las subunidades *f* hacen contacto entre los dos monómeros en el dímero (Modificado de Hahn y colaboradores, 2016).

Regulación de la F_oF_1-ATP sintasa por la proteína inhibidora (IF_1).

La proteína inhibidora de la ATPasa es codificada por el gen *ATPIF1* localizado en los cromosomas 1 y 4 de humano y ratón respectivamente. IF_1 fue encontrada por Pullman y Monroy en los años 60s en el músculo cardiaco de corazón de bovino (Pullman & Monroy 1963). Los homólogos de IF_1 han sido aislados a partir de otros mamíferos (rata y humano), la levadura (*Saccharomyces cerevisiae* y *Candida utilis*), el nematodo *Caenorhabditis elegans,* el crustáceo *Litopenaeus vannamei* y en diferentes plantas (revisado en Faccenda y Campanella, 2012). En la levadura el gen *INH1* codifica para el homólogo de IF_1, sin embargo, dos proteínas adicionales Stf1 y Stf2 cooperan en su función (Hashimoto y colaboradores, 1990).

IF_1 es una proteína pequeña (10 kDa), en su forma madura tiene 81 aa (humano) y 84 aa (bovino), es básica y estable al calor. Se encuentra predominantemente en la matriz mitocondrial, sin embrago, también se ha encontrado en el citosol y en la membrana plasmática de las células (Cortés-Hernández y colaboradores, 2005). La IF_1 también es secretada al espacio extracelular donde modula la actividad de células endoteliales (Burwick y colaboradores, 2005) y en su forma extracelular también se ha visto involucrada en el metabolismo de colesterol HDL y de triglicéridos (Genoux y colaboradores, 2011), sin embargo, la función de IF_1 afuera de la mitocondria aún no se tiene clara.

Cuando el pH de la matriz mitocondrial disminuye, IF_1 interactúa con el sector F_1 inhibiendo la hidrólisis de ATP en condiciones que favorecen la reversibilidad de la actividad de la enzima (p.ej. hipoxia, inhibidores de la cadena respiratoria y desacoplantes), de esta manera IF_1 protege a la célula de la hidrólisis de ATP a expensas del $\Delta\psi_m$ (Pullman y Monroy, 1963; Rouslin y colaboradores, 1993) (Figura 8). IF_1 se ha considerado un inhibidor uni-direccional que actúa únicamente durante la hidrólisis de ATP, sin embargo, existen estudios en donde se ha visto que IF_1 al estar unida a F_oF_1-ATP sintasa inhibe tanto la hidrólisis como la síntesis de ATP (Husain y Harris, 1983). Por ejemplo, en animales transgénicos que sobre-expresan a la IF_1 H49K (una mutante dominante positiva, en donde la IF_1 se encuentra constitutivamente activa) se promueve la inhibición de la actividad de ATP sintasa (Formentini y colaboradores, 2014). El mismo grupo, observó en células NRK (fibroblasto de hígado de rata) y células HeLa que cuando se sobre-expresa la IF_1 aumenta el metabolismo glucolítico y disminuye el fosforilativo, sugiriendo que la sobre-expresión de IF_1 actúa como un "switch" metabólico inhibiendo la síntesis de ATP (Sanchez Cenizo

y colaboradores, 2010; Formentini y colaboradores, 2012; Sánchez Aragó y colaboradores, 2013; Shen y colaboradores, 2009). Recientemente, se confirmó en cultivos celulares de humano que la inhibición de la hidrólisis y síntesis de ATP depende del estado fosforilado de la S39 de la IF_1 que actúa como un switch para la unión de la IF_1 a la enzima, en mitocondrias aisladas se encontró que cuando IF_1 está en su forma de-fosforilada la producción de ATP se ve disminuída y se observa una mayor capacidad de producción de ATP cuando IF_1 está fosforilada (García-Bermúdez y colaboradores, 2015).

En contraste, cuando la enzima purificada se re-constituyó en vesículas de fosfolípidos y se generó un Δp gracias a la proteína bacteriorodopsina, IF_1 no tuvo efecto en la síntesis de ATP, mientras que la hidrólisis de ATP fue inhibida (Runswick y colaboradores, 2013). Además, el grupo del profesor Yoshida demostró que al disminuir la expresión de IF_1 en células HeLa ("knock down", KD), la síntesis de ATP no se afecta con respecto al control (Fujikawa y colaboradores, 2012) y ratones mutantes en IF_1 ("knock out", KO) presentaron prácticamente el mismo fenotipo que los ratones silvestres (Nakamura y colaboradores, 2013), sugiriendo que la IF_1 no afecta la síntesis de ATP.

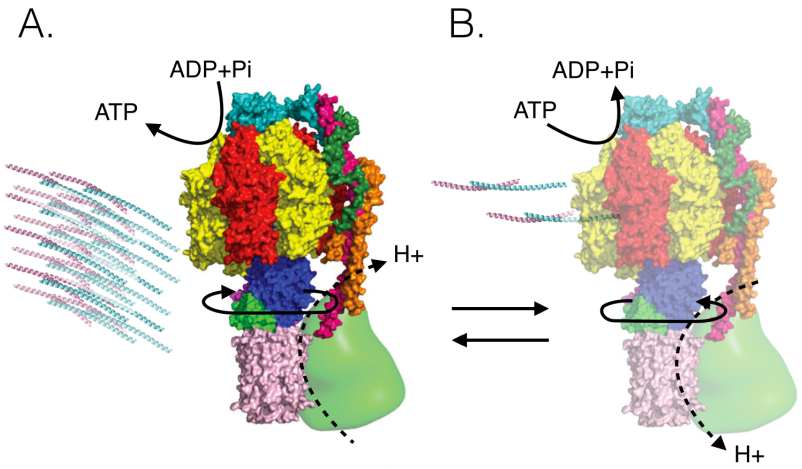

Figura 8. Interacción de la IF_1 con la F_oF_1-ATP sintasa. (A) La F_oF_1-ATP sintasa sintetiza ATP gracias a la presencia de $\Delta\psi_m$, en esta situación el pH de la matriz es ligeramente básico y la IF1 (rosa y cyan) está presente en su forma inactiva. (B) Cuando el $\Delta\psi_m$ se pierde la F_oF_1-ATPasa hidroliza el ATP que se importa desde el citosol y se bombea H^+ de regreso al espacio intermembranal re-estableciendo el $\Delta\psi_m$, la IF_1 se muestra en unida a la F_1. Imagen modificada de Walker, 2013.

Secuencia mínima de inhibición y estructura de la IF_1.

La proteína IF_1 de humano exhibe 75% de identidad con la IF_1 de bovino, 90% de identidad con la de murino y entre la de bovino y murino se observa 65% de identidad. Incluso hay una correlación entre la conservación de secuencia y función, debido a que la IF_1 de una determinada especie es capaz de inhibir la ATPasa de otra especie, incluyendo la IF_1 de levadura, la cual carece del C- terminal (63 aa) y necesita de proteínas accesorias que estabilicen su actividad de inhibidora. Hay dos regiones en las que se han basado los estudios de IF_1: la primera es la que comprende a los aminoácidos 20-50 que tiene el 80% de identidad entre bovino-humano y 90% entre humano-bovino y la segunda región, es la rica en histidinas (RRH; ver figura 10) que abarca los residuos 48-70 aa que se ha vinculado a cambios conformacionales y actividad dependiente de pH (revisado en Green y Grover, 2000).

La secuencia mínima de inhibición ha sido un tema de estudio controversial, sin embargo, uno de los trabajos más influyentes en el campo fue el de Van Raaj y colaboradores (2006) que encontraron que una IF_1 de bovino que carece de los residuos del N-terminal (1-9 o 1-13) tenía la actividad indistinguible a la IF_1 intacta, mientras que la deleción de los residuos 57-84 en el C-terminal tampoco presentaron defectos en la inhibición, sin embargo, se pierde 130 veces la capacidad de inhibición, al eliminar los residuos 46-84. Por lo tanto, se concluyó que la secuencia mínima de inhibición debía estar entre los residuos 9-13 y 46-57 (Figura 9). Posteriormente, se usaron péptidos de los aa 10-47 y no se encontraron diferencias en la inhibición con respecto a la IF_1 intacta, concluyendo que la secuencia mínima de inhibición se encuentra entre estos residuos. En contraste, Papa y colaboradores (1996) encontraron que un péptido que incluía los residuos 42-58 era tan potente como la IF_1 silvestre.

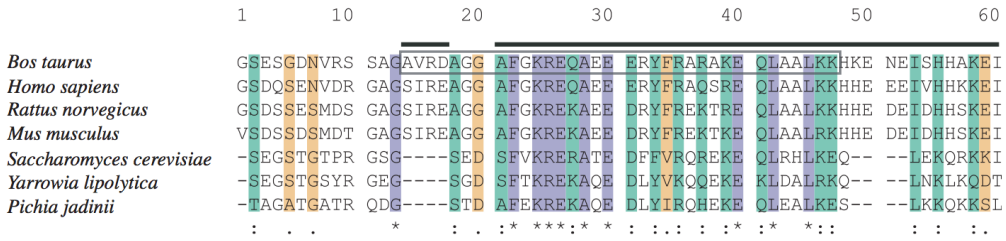

Figura 9. Alineamiento de los residuos 1-60 de la IF_1 madura de bovino y sus regiones equivalentes en levadura y otras especies. En morado, verde y naranja muestran residuos idénticos, conservados y pobremente conservados, respectivamente. La barra de arriba representa una α-hélice en la secuencia de bovino y en cuadrado se encuentra la región mínima de inhibición. La numeración se refiere a la secuencia de bovino. Imagen tomada de Graham C. Robinson y colaboradores, 2013.

La estructura de la IF_1 de bovino fue caracterizada por cristalografía de rayos X (resolución de 2.2Å) por Cabezón y colaboradores (2001). Está formada en su mayoría por una α-hélice (90 Å en longitud) y es activa como un homodímero a un pH <6.7. La dimerización ocurre en el C-terminal de ambas proteínas formando una estructura anti-paralela estabilizada por los residuos hidrofóbicos que se localizan entre los residuos 49 y 81 (Cabezón y colaboradores, 2001) (Figura 10, A). En el dímero, la región mínima de inhibición se encuentra en el extremo contrario al sitio de dimerización y pueden inhibir dos dominios F_1 simultáneamente, sin embargo la IF_1 puede también inhibir también como monómero (Gledhill y colaboradores, 2007). Cuando el pH está por arriba de 7, los dímeros pueden ensamblarse como tetrámeros inactivos u oligómeros más complejos ocultando el N-terminal que se une al dominio F_1 (Cabezón y colaboradores, 2000; Figura 8, A).

La IF_1 contiene 5 histidinas conservadas (en las posiciones 48, 49, 55, 56 y 70) que son importantes para detectar cambios en el pH y dar cambios conformacionales que dictan la actividad de IF_1 (Figura 10, B). La histidina 49 es crítica para la interconversión de dímero a tetrámero y se ha observado que la sustitución de ésta histidina por una lisina activa de manera constitutiva a la IF_1 a un pH de 8.

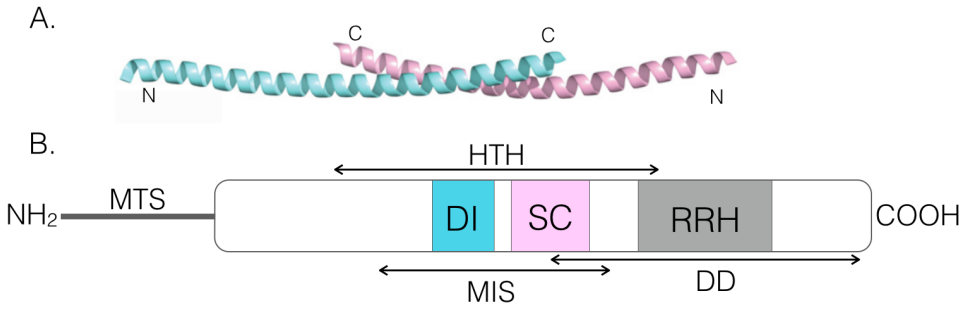

Figura 10. Estructura de la IF_1 de bovino. (A) Dímero de IF_1. Imagen tomada de Walker, (2013). (B) En el amino-terminal (N) se encuentra la secuencia de localización mitocondrial (MTS, por sus siglas en inglés), en gris el dominio de inhibición (ID) localizado en la secuencia mínima de inhibición (SMI, residuos 14-47), en rosa una región de unión a calmodulina (SC), seguido de una región rica en histidinas (RRH, residuos 48-70). La dimerización de IF_1 depende del carboxilo terminal (C, DD).

Un artículo importante en el estudio de la IF_1 fue realizado por Gledhill y colaboradores (2007). El primer hallazgo interesante de este trabajo, es que por primera vez se pudo tener la estructura del amino-terminal de la IF_1 de bovino, el cual consiste de una estructura extendida

(residuos 8-13) seguido de dos α-hélices (residuos 14-18 y 21-50) unidas por un asa (Figura 11, A). El segundo hallazgo fue que por primera vez se determinó el sitio de unión de la IF_1 al dominio F_1 de la ATP sintasa. Se encontró a la IF_1 en la interfase β_{DP} y α_{DP} con contribución de 5 diferentes subunidades que forman una cavidad (β_{DP}, α_{DP}, β_{TP}, α_E), por donde la IF_1 se adentra hasta la subunidad γ (Figura 11, B-C). Gracias a este hallazgo, los autores propusieron un mecanismo por el cual la IF_1 puede adentrarse tan profundamente hasta interactuar con γ y α_E, este mecanismo consiste en que IF_1 se une a β_E y conforme 2 moléculas de ATP se hidrolizan, la interfase β_E-α_E se convierte a β_{DP}-α_{DP} (vía β_{TP}-α_{TP}), atrapando a la IF_1 y a un nucleótido en β_{DP} (Figura 11, D).

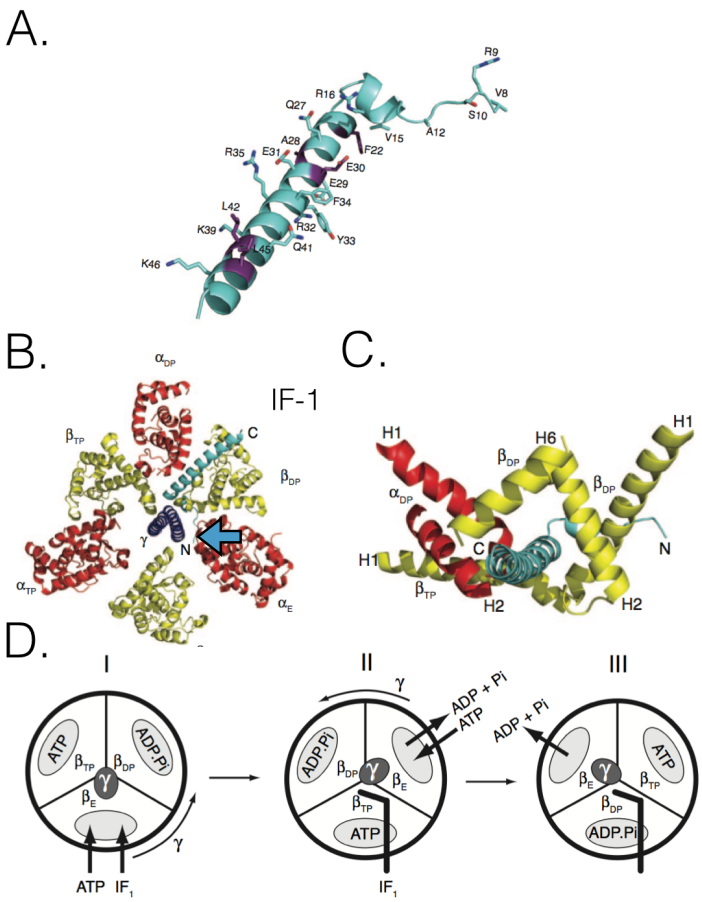

Figura 11. Estructura y mecanismo de unión de la IF_1 de bovino. (A) Se indican todos los residuos que interactúan con la F_1-ATPasa; en morado se muestran residuos estrictamente conservados. (B) Se muestra a la IF_1 (monómerica; cyan) en la interfase de las subunidades αβ y la α-hélice extendida interactuando con α_E (flecha azul). (C) Cavidad formada por α-hélices y asas del C-terminal de β_{DP}-α_{DP} y β_{TP} en donde se une la IF_1. (D) Para que la IF_1 pueda adentrarse en la interfase de la subunidad αβ e inhibir la hidrólisis de ATP se requieren dos rotaciones de γ de 120º (I y II). Figura tomada de Gledhill y colaboradores, 2007

Dimerización de la IF_1 y su efecto en la ultra-estructura mitocondrial.

Debido a que la forma activa de la IF_1 es como dímero, la idea de que IF_1 puede intervenir en la dimerización de dos ATP sintasas parece atractiva. Existe evidencia de que la IF_1 afecta la dimerización de la ATP sintasa. El grupo de Walker (Cabezón y colaboradores, 2000), por medio de cromatografía de filtración en gel, ultracentrifugación analítica y microscopía electrónica, encontraron que IF_1 dimeriza al complejo F_1 (Cabezón y colaboradores, 2000). Para indagar hasta qué grado IF_1 contribuye en la formación del dímero de ATP sintasas, Dienhart y colaboradores (2002) encontraron por medio de geles azul nativos, (técnica diferente a la utilizada por Cabezón y colaboradores en el año 2000 y que ha sido de las más utilizadas para estudiar la formación de dímeros de ATP sintasa) que no se afecta el dímero de F_oF_1-ATP sintasas en levaduras mutantes carentes del gen que codifica para Inh1 y las proteínas accesorias Stf1 y Stf2. En contraste, el grupo de García-Trejo y colaboradores (2006) removieron a la IF_1 de partículas sub-mitocondriales de hígado de rata y corazón de bovino y observaron un incremento en la actividad de F_oF_1-ATPasa y una disminución en la proporción de dímero/monómero de la ATP sintasa. Cuando se reconstituyó la IF_1 en estas partículas submitocondriales, se restableció la inhibición de ATPasa (90%) y la formación de dímeros. El mismo grupo encontró por microscopia electrónica de transmisión que el dímero de ATP sintasas de corazón de bovino tiene una apariencia cónica y propusieron que tiene un efecto en promover la curvatura de la membrana interna mitocondrial; además, los complejos F_1 en el lado de la matriz se unen por un puente proteico que se atribuyó a la IF_1 (Minauro-Sanmiguel y colaboradores, 2005) (Figura 12).

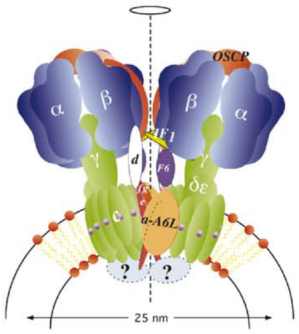

Figura 12. Modelo del dímerización de ATP sintasas por IF_1 de bovino. La asociación del complejo F_1 está dado por una estructura de baja densidad que sirve de puente entre dímeros de F_1 que podría corresponder a la IF_1. Imagen tomada de Minauro-Sanmiguel y colaboradores, 2005.

En el 2008, Campanella y colaboradores confirmaron la hipótesis hecha por el grupo de García-Trejo y encontraron que al sobre-expresar a IF_1 en células HeLa se promueve la dimerización de F_oF_1-ATP sintasa, incrementando la proporción entre el dímero/monómero, además por primera vez al aumentar o disminuir la expresión de IF_1 se observó un efecto en el número de crestas mitocondriales, las cuales aumentan o disminuyen dramáticamente, respectivamente

(Campanella y colaboradores, 2008; Faccenda y colaboradores, 2017). En contraste, Fujikawa y colaboradores (2012) disminuyeron de manera estable la expresión de IF_1 por transducción retroviral en células HeLa y al observar de manera extensiva las mitocondrias, no encontraron cambios en la morfología mitocondrial, ni en el número de crestas mitocondriales. Igualmente, Nakamura y colaboradores estudiaron en ratones mutantes en IF_1 la proporción de dímero/ monómero y la morfología de las mitocondrias y no encontraron cambios al comparar con el control (Nakamura y colaboradores, 2013). Otros grupos también disminuyeron la expresión IF_1 en células de eritroleucemia de ratón (células MEL) (Shah y colaboradores, 2012) y en células haploides de humano KBM7 (Chen y Biroy, 2014) y no encontraron defectos en el número o morfología de las crestas mitocondriales. Estas discrepancias, pueden deberse a las técnicas de disminución o sobre-expresión de IF_1 y a las diferentes líneas celulares utilizadas.

Otro tema que aún está en debate es si la dimerización de ATP sintasas modula la síntesis o hidrólisis de ATP, algunos dicen que la dimerización aumenta la actividad de la enzima (Campanella y colaboradores, 2008), mientras que otros reportan una disminución o falta de efecto en la actividad (García-Trejo y colaboradores, 2006; Wittig y Schagger, 2008)

La función de la IF_1 en la regulación de la sobrevivencia y muerte celular.

El grupo de Campanella encontró que en ausencia de glucosa y oxígeno las células C2C12 (células inmortalizadas de mioblasto de ratón) y HeLa con IF_1 sobre-expresada mostraron estar protegidas de la muerte celular, mientras que la reducción en la expresión de IF_1 aumentó la muerte celular (Campanella y colaboradores, 2008). Posteriormente, el mismo grupo exploró cómo la ultra-estructura mitocondrial afecta la ejecución de la apoptosis al sobre-expresar o disminuir a IF_1 en presencia de estaurosporina (STS; que inhibe a las proteínas cinasas, impidiendo la unión de ATP) y encontraron que la sobre-expresión de IF_1 preserva la morfología de las crestas y de ésta manera limita la liberación de cyt *c,* atrasando la cascada de apoptosis que involucra: (i) la liberación de Ca^{2+} del retículo endoplásmico vía cyt *c;* (ii) el reclutamiento y activación de Drp1 a la membrana externa mitocondrial; (iii) la inserción de Bax a la membrana externa mitocondrial; y (iv) una mayor liberación de cyt *c* y activación del apoptosoma. Este trabajo propuso que IF_1 es un punto de control que limita la progresión de la cascada apoptótica y protege a las células de muerte celular por apoptosis (Faccenda y colaboradores, 2013).

Consistente con Campanella y colaboradores (2008), Fujikawa y colaboradores (2012) encontraron que la disminución de IF_1 tiene un efecto en la viabilidad de las células al someterlas a condiciones de estrés, las células que tienen disminuída la expresión de IF_1 murieron más rápido que las células control, en presencia de 2-deoxiglucosa y cianuro o al ser incubadas con paraquat. En contraste, Chen y Birsoy (2014) encontraron que células carentes en IF_1 sobreviven más al tratamiento con antimicina A, un inhibidor del complejo III, debido al mantenimiento del $\Delta\psi_m$, señal de viabilidad y sobrevivencia celular, dado por la reacción reversa de la ATPasa. Chen y Birsoy sugieren a la IF_1 como un blanco para el diseño de fármacos para tratar enfermedades mitocondriales.

Por otro lado, se ha estudiado ampliamente que células cancerosas tienen sobre-expresada a IF_1 (Bravo y colaboradores, 2004; Sánchez-Cenizo y colaboradores, 2010; Sánchez Arago y colaboradores, 2013). Formentini y colaboradores (2012) encontraron que en células HCT116 (cáncer de colon) la sobre-expresión de IF_1 causa la inhibición de la ATP sintasa y desata un aumento en la proliferación celular y una disminución en la muerte celular. Estos fenotipos se deben a que las mitocondrias se encuentran hiperpolarizadas debido a la inhibición de la ATP sintasa por IF_1, lo que impide el regreso de los protones a la matriz mitocondrial y como consecuencia un aumento en ROS, que promueve la activación de NFkB que activa una respuesta adaptativa que induce la resistencia a la muerte celular y un aumento en la proliferación.

Mantenimiento del potencial de membrana de la mitocondria por IF_1 y su efecto en la mitocondria.

El potencia de membrana de la mitocondria ($\Delta\psi_m$) es esencial en la función mitocondrial, la pérdida de este es letal debido a que se detiene la síntesis de ATP por la F_oF_1-ATP sintasa, la dinámica mitocondrial y el transporte de proteínas nucleares a la mitocondria dependiente de $\Delta\psi_m$ (Twig y colaboradores, 2008). Aunque aún no se entiende cómo la pérdida del $\Delta\psi_m$ participa en la ejecución de la apoptosis (revisado en Ly y colaboradores, 2003), se ha propuesto que al disminuir el $\Delta\psi_m$, se facilita la apertura del poro de transición (PTP) que permite la liberación de cyt *c* de la mitocondria y la formación del apoptosoma. Por otro lado, se ha observado que una vez iniciada la apoptosis el complejo I es proteolizado por caspasas en la subunidad p75 exacerbando la pérdida del $\Delta\psi_m$ (Tait y Green 2010).

La hidrólisis de ATP por la ATPasa mantiene el $\Delta\psi_m$, por lo tanto, la inhibición de la actividad de ATPasa por IF_1 preservará los niveles de ATP pero perderá el $\Delta\psi_m$. En condiciones fisiológicas, Fujikawa y colaboradores, (2012) y Shah y colaboradores, (2013) encontraron que al silenciar a IF_1 en células HeLa y MEL respectivamente, el $\Delta\psi_m$ de las células se encuentra incrementado y los niveles de ATP disminuídos, sugiriendo que al disminuir la expresión de IF_1 la ATPasa hidroliza el ATP. Por otro lado, Barbato y colaboradores (2015) encontraron un aumento en el $\Delta\psi_m$ en células de osteosarcoma, sin observar alteraciones en los niveles de ATP. En este trabajo se discute que esto puede deberse a algunas de las siguientes opciones: (i) IF_1 se une a otra proteína diferente de β lo cual incrementa el $\Delta\psi_m$, (ii) recientemente se ha propuesto que los dímeros de ATP sintasas forman el PTP y que en ausencia de IF_1 el poro se desregula resultando en un aumento constante de $\Delta\psi_m$ y (iii) la falta de IF_1 disminuye el dímero de ATP sintasas que causa una disminución en la actividad y un aumento en el $\Delta\psi_m$.

La pérdida del $\Delta\psi_m$ de la mitocondria también es importante para llevar acabo la mitofagia. La mitofagia es una forma de macro-autofagia de mitocondrias dañadas que se fusionan con autofagosomas y encapsulan a las mitocondrias completas o selectivamente a zonas dañadas de las mismas. Este proceso depende de dos proteínas: la proteína de membrana externa PINK1 y la E3-ubiquitín ligasa Parkin (PARK2), ambas llevan acabo la mitofagia en respuesta a la pérdida prolongada del $\Delta\psi_m$. En un escrutinio hecho con RNAi en células HeLa, se encontró que células tratadas con un desacoplante requieren de la presencia de IF_1 para llevar acabo la mitofagia (Lefevre y colaboradores, 2013), debido a que IF_1 promueve la pérdida de $\Delta\psi_m$ y la activación de la mitofagia.

Efecto de la sobre-expresión de IF_1 en el cáncer.

Se ha descrito que IF_1 se encuentra sobre-expresada en diferentes tipos de cáncer como el de colon, pulmón, seno y ovario entre otros carcinomas (Bravo y colaboradores, 2004; Sánchez-Cenizo y colaboradores, 2010; Sánchez Arago y colaboradores, 2013). La sobre-expresión de IF_1 se ha descrito como el "switch" entre el metabolismo fosforilativo y el glucolítico en células cancerosas, neuronas *in vivo* y en hepatocitos. La disminución de OXPHOS a su vez promueve la activación de la cinasa AMPK y otras cinasas que ayudan a contender la limitación energética. Además, se encontró que en células de cáncer de colon, la sobre-expresión de IF_1 inhibe la síntesis de ATP promoviendo la hiperpolarización de la mitocondria y el aumento en la producción de ROS

mitocondrial que señaliza al núcleo en donde se activa la vía de sobrevivencia NFκB promoviendo a través de Bcl-xL la protección contra la muerte celular y el aumento en la proliferación (Formentini y colaboradores, 2012).

Recientemente se ha encontrado que la sobre-expresión de IF_1 es señal de una mala prognosis en cáncer de hígado, vejiga, estómago y pacientes con glioma. En hígado, IF_1 promueve la metástasis y angiogénesis a través de la vía no canónica de NFκB, mientras que en el cáncer gástrico y de colon se observó un incremento en la proliferación y resistencia a la muerte también a través de la misma vía. Sin embargo, en cáncer de seno y colón la sobre-expresión de IF_1 predice una buena prognosis, sugiriendo que cada tejido tiene diferente fisiología mitocondrial. En contraste a las células cancerígenas, las células diferenciadas dependen de OXPHOS y la re-programación de células somáticas a células troncales pluripotenciales induce la disminución de OXPHOS con la activación de la glucólisis. Al disminuir a IF_1, se acelera la diferenciación de las células hMCS a osteocitos, debido al cambio metabólico de la glucólisis a un metabolismo fosforilativo (revisado en García Bermudez y Cuezva, 2016).

ii. Características y fisiología de *Caenorhabditis elegans.*

Generalidades de *Caenorhabditis elegans*

El *Caenorhabditis elegans* es un nematodo de vida libre, que habita en muchas partes del mundo y se alimenta de microorganismos, principalmente de bacterias. Es un buen modelo de estudio en múltiples campos como la biología celular y del desarrollo, la genética, la neurobiología y el envejecimiento. Este organismo presenta muchas ventajas que facilitan su estudio como: un ciclo de vida corto, genoma completamente secuenciado, propagación sencilla y tamaño pequeño (1 mm de largo en estado adulto). El animal puede mantenerse en el laboratorio en placas de agar o medio líquido, cultivados con bacteria *Escherichia coli* de la cepa OP50*,* como fuente de alimento. Su ciclo de vida tiene una duración de tres días en condiciones ideales y también puede sobrevivir en condiciones no favorables, cambiando a un estado de diapausa conocido como la larva dauer, estadio que le permite sobrevivir de 4 a 8 veces más de lo normal (Cassada & Russell 1975). Debido a que el animal es transparente, sus células pueden visualizarse con facilidad por medio de microscopía diferencial de interfase (DIC). La descripción anatómica del animal entero se ha completado por microscopía electrónica y su linaje celular, el cual es constante entre individuos ha sido descrito con detalle, la descripción del linaje celular dió a Sydeny Brenner, Robert Horvitz y John E. Sulston el Premio Nobel en Medicina en el 2002 (Sulston y colaboradores, 1983; Byerly y colaboradores, 1976; Brenner 1973; Wood 1988).

Una ventaja adicional de este organismo es que existe un gran número de mutantes accesibles para la investigación. Las mutantes pueden generarse por: i) mutagénesis al azar utilizando p.ej. mutagénesis química o ii) mutagénesis dirigida utilizando p.ej. la técnica de CRISPR/Cas-9 (Friedland y colaboradores, 2013; Paix y colaboradores, 2014; Kim y colaboradores, 2014). Las cepas mutantes generadas por la comunidad científica de todo el mundo son conservadas y mantenidas en el *Caenorhabditis* Genetics Center (CGC) y están disponibles al público bajo petición.

Las poblaciones de *C. elegans* están compuestas por dos tipos sexuales: hermafroditas, con 5 pares de autosomas más un par de cromosomas sexuales (XX) y machos con 5 pares de autosomas más un sólo cromosoma sexual (X) (Figura 13, A). Los machos inciden de manera espontánea en la

población en baja frecuencia (0.1-0.2%) debido a la no-disyunción de los cromosomas y en una incidencia de más del 50% por apareamiento entre un animal hermafrodita y un macho.

Ciclo de vida de *C. elegans.*

Un embrión recién fertilizado toma aproximadamente 14 horas a una temperatura de 20°C para completar la embriogénesis y que una larva eclosione del huevo. Durante el proceso de fertilización, un ovocito maduro pasa a través de la espermateca (tubo que contiene espermatozoides) y es fertilizado, ya sea por los espermas del hermafrodita o por los espermas de un macho. Después de 30 minutos post-fertilización, el cigoto desarrolla una membrana vitelina y otras dos de quitina y colágena, haciéndolo impermeable y permitiendo el desarrollo afuera del útero.

La embriogénesis se puede dividir en dos fases: (i) proliferación celular y (ii) organogénesis/ morfogénesis (Sulston y colaboradores, 1983). La etapa de proliferación (0-350 min) se divide a su vez en dos fases: la primera fase (0-150 min) abarca la formación del cigoto hasta la generación de 6 células fundadoras (AB, MS, E, C, D y P_4), mientras que en la segunda etapa (150-350 min) ocurren divisiones celulares seguidas de la gastrulación y concluye con el comienzo de la organogénesis (Bucher y Seydoux, 1994).

Al término de la etapa de proliferación, el embrión es un esferoide de 671 células, organizado en tres capas germinales: el ectodermo que da lugar a la hipodermis y neuronas; el mesodermo, que genera la faringe y la pared muscular; y el endodermo que da lugar a la línea germinal e intestino. Durante la organogénesis/morfogénesis (6-14 hrs) ocurre la diferenciación de las células sin que ocurran divisiones adicionales, el embrión se elonga y toma la forma de un animal con tejidos y órganos diferenciados (Sulston y colaboradores,1983; Bird y Bird, 1991).

El desarrollo post-embrionario comienza en cuanto la larva comienza a alimentarse, si la larva L1 no se alimenta su crecimiento se arresta de 6-10 días y muere. En presencia de comida, el 10% de las células continúan dividiéndose dando lugar a células de la hipodermis, sistema nervioso y del músculo. Las células germinales también comienzan a dividirse y continúan proliferando hasta la etapa de adulto. Posteriormente, en condiciones normales el animal pasa por cuatro estadios larvarios (L1, L2, L3 y L4) hasta llegar al estadio de adulto, los cuatro estadios larvarios se definen

por la muda de cutícula, en la cual se detiene el bombeo de la faringe y entra a un estado de letargo (Figura 13B).

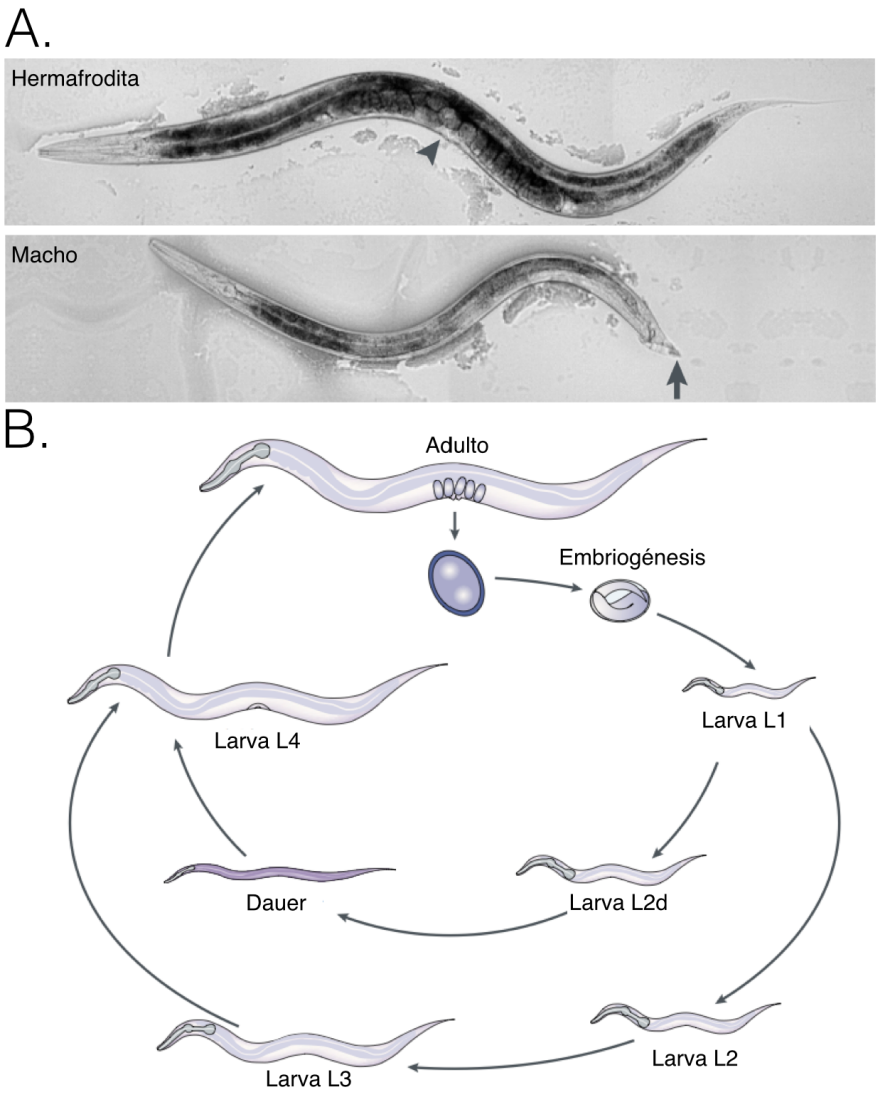

Figura 13. Ciclo de vida del *C. elegans*. (A) El nematodo *C. elegans* puede ser mantenido como hermafrodita (XX, panel de arriba) que tiene una vulva (flecha) y como macho (X0, panel de abajo) que tiene una cola en forma de abanico. (B) Después de 14 h de desarrollo embrionario, una larva eclosiona del huevo y pasa a través de cuatro estadios larvarios (L1-L4) que se separan por un periodo de letargo en la cual el animal cambia de cutícula. En condiciones de aglomeración o escasez de comida el L1 puede entrar en un desarrollo alterno llamado estado dauer, en la cual los animales pueden sobrevivir por meses. Imagen modificada de Jorgensen y Mango, 2002.

El sistema reproductor del *C. elegans.*

El sistema reproductor del nematodo hermafrodita produce gametos, así como la estructura y el ambiente para que ocurra la fertilización y se depositen los embriones. Se puede dividir en dos secciones: (i) la gónada somática, el aparato para depositar embriones y (ii) la línea germinal. La gónada somática y la línea germinal forman dos brazos en forma de U unidos a un útero.

La gónada somática se refiere a la gónada que no comprende a la línea germinal. Comprende 5 tejidos, cada uno con una función específica y características anatómicas particulares: (i) la célula de la punta distal (CPD), (ii) las células de la vaina; (iii) la espermateca; (iv) la válvula espermateca-útero y (v) el útero. Todas las células de la gónada somática se derivan de las células fundadoras Z1 y Z4 presentes en la gónada primordial en el estadío L1.

La línea germinal se establece en el embrión temprano a partir de la primera célula germinal primordial llamada célula P_4. A partir de la célula P_4, se originan las células Z2 y Z3 que darán origen a todas las células germinales del organismo. Durante los dos primeros estadios larvarios, las células germinales proliferan exponencialmente y al comienzo del estadio L3 las células entran en meiosis, estableciendo polaridad a la gónada. En el estadio de L4, las primeras 40 células germinales de cada brazo se diferencían a 160 espermatozoides que se almacenan en cada espermateca y posteriormente la gónada inicia la producción de ovocitos que continúa durante el resto del periodo reproductivo del animal.

En el animal adulto, la célula CPD (célula de la punta distal) por medio de la señalización GLP-1/Notch promueve el mantenimiento de las células troncales germinales (Seydoux y Schedl, 2001), adyacente a ésta célula se encuentra la región mitótica que comprende alrededor de 225-250 células germinales y abarca 20 células de diámetro en eje distal-proximal (Crittenden y colaboradores, 1994). Posterior a la zona de mitosis inicia la "zona de transición", zona en la que se inicia la meiosis (profase 1, leptoteno y zigoteno) en esta zona los cromosomas se aparean y la envoltura nuclear adquiere la morfología de luna creciente (Dernburg y colaboradores, 1998). Conforme las células se alejan de la zona de transición, las células entran en paquíteno y aumentan su tamaño, los núcleos en esta etapa lucen como un "plato de spaguetti". Posteriormente, las células entran en diploteno en el asa de la gónada y las células se organizan en una fila y entran en el brazo proximal de la gónada, es aquí en donde las células entran en diaquinesis hasta la maduración del

ovocito. El ovocito más próximo a la espermateca (llamado -1) progresa a la metafase de la meiosis y ocurre un re-arreglo del cortex y del citoplasma, posteriormente es ovulado y fertilizado (McCarter y colaboradores, 1999) (Figura 14).

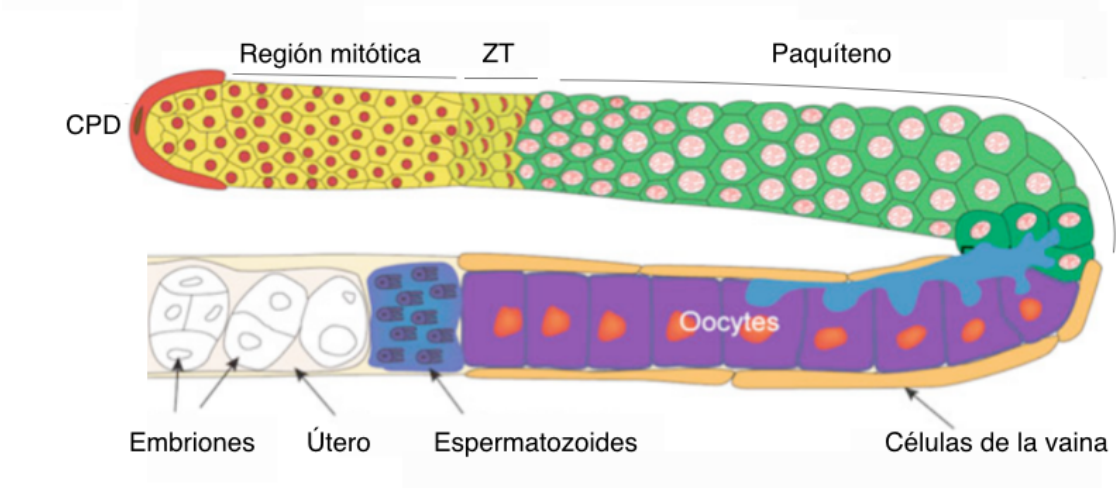

Figura 14. La gónada de *C. elegans*. El hermafrodita de *C. elegans* tiene dos brazos en forma de U, conectados por un útero. Se muestra uno de los brazos de las gónadas del nematodo, en rojo se muestra la célula de la punta distal (CPD), en amarillo está la zona de mitosis, en verde claro la zona de transición, las células en verde representan células en paquíteno y las células en morado representan ovocitos en maduración. Las células en azul obscuro representan la espermateca y los embriones se ven en el útero. Imagen modificada de Pazdernick y Schedl, 2013.

La apoptosis fisiológica de las células germinales del *C. elegans.*

La apoptosis fisiológica de las células germinales en *C. elegans* ocurre con frecuencia en condiciones óptimas de crecimiento (en ausencia de estrés). Se ha observado que se lleva acabo durante la producción de ovocitos en organismos hermafroditas, y que ocurre en el asa de la gónada, cuando las células dejan el paquíteno e inician el diploteno. Cuando la célula muere, el núcleo se celulariza y se rodea de un poco de citoplasma. Finalmente, se produce un cuerpo apoptótico que es fagocitado por las células de la vaina (Figura 14, células naranjas).

El mecanismo y la razón por la cual las células germinales mueren por apoptosis aún es desconocida. El modelo más atractivo del por qué las células mueren, es que las células que mueren en paquíteno sirven de células nodrizas para los ovocitos que están madurando, y las células al morir dan los componentes citoplásmicos (mRNA, proteínas y organelos) esenciales para el crecimiento de los ovocitos. La evidencia experimental que apoya este modelo es que los ovocitos

de mutantes en *ced-4*/APAF-1 y *ced-3*/caspasa-3 no muestran diferencias evidentes, sin embargo, cuando estos animales envejecen sus ovocitos son más pequeños que el de los animales silvestres (Gumienny y colaboradores, 1999).

Los cuerpos apoptóticos pueden ser observados como discos refráctiles utilizando microscopía DIC Nomarski (Gumienny y colaboradores, 1999), aunque también es posible identificarlos por medio de la cepa transgénica CED-1::GFP (Schumacher y colaboradores, 2005), que expresa una proteína de fusión localizada en las células de la vaina encargadas de fagocitar al cuerpo apoptótico. Estos animales transgénicos se utilizan para detectar cuerpos apoptóticos tempranos que muchas veces no se alcanzan a ver por microscopía DIC, sin embargo, presenta la desventaja de que cuando hay muchos cuerpos apoptóticos la señal se diluye dificultando el conteo de cuerpos apoptóticos (Wormbook, Anton Gartner, Peter R. Boag, and T. Keith Blackwell).

Mecanismo por el cual se lleva acabo la apoptosis de las células germinales en *C. elegans.*

La apoptosis de las células germinales requieren, al igual que la apoptosis de las células somáticas, a las proteínas de la maquinaria central de apoptosis: CED-9/BCL-2, CED-4/APAF-1 y CED-3/Caspasa-3 y Caspasa-9. EGL-1 es otra proteína importante en la apoptosis somática, sin embargo, no se requiere en la apoptosis fisiológica de las células germinales, salvo en la respuesta apoptótica ante ciertos tipos de estrés.

Los genes que codifican para dichas proteínas se aislaron por medio de un escrutinio de mutantes con defectos en la muerte celular (CED). Mutantes pérdida de función en *egl-1*, *ced-4* y *ced-3* tienen aproximadamente 131 células más que un organismo silvestre, sugiriendo una función pro-apoptótica, mientras que una mutante ganancia de función en *ced-9* bloquea la apoptosis (Parrish y colaboradores, 2000; Yan y colaboradores, 2004). Estudios epistáticos revelaron que *egl-1* regula negativamente a *ced-9* y que *ced-9* a su vez regula negativamente a *ced-4* y a *ced-3*.

CED-9 es una proteína similar a Bcl-2 de mamíferos (linfoma de células B, tipo 2) (Hengartner y Horvitz, 1994) y tiene actividad anti-apoptótica, es decir protege a las células de la muerte celular por apoptosis. Mutaciones por pérdida de función en *ced-9* causan letalidad embrionaria como consecuencia de las muertes ectópicas de las células que normalmente viven. *ced-4* codifica para una proteína adaptadora pro-apoptótica, que en su ausencia promueve que las

células sobrevivan a la señal de apoptosis y es similar al factor activador de la proteasa apoptótica 1 (Apaf-1) en mamíferos. *ced-3* codifica para una caspasa del tipo cisteína-aspartato (posee en su sitio activo una cisteína y corta después de un aspartato), que al igual que para otras caspasas se sintetiza como una pro-enzima y se activa por medio de proteólisis para generar una proteasa cuya actividad es esencial para llevar acabo la apoptosis en *C. elegans* (revisado en Lettre y Hengartner, 2006).

En las células somáticas, CED-9 interactúa con el dímero de CED-4, este complejo se encuentra anclado a la membrana externa de la mitocondria, impidiendo la activación de CED-3. Cuando EGL-1 interactúa con CED-9, induce un cambio conformacional en CED-9 permitiendo la liberación de CED-4 (Yan y colaboradores, 2004), dos dímeros de CED-4 se oligomerizan para formar un tetrámero que es la forma activa para la activación de CED-3 (Revisado en Lettre y Hengartner, 2006).

Una vez que el programa de apoptosis se ha activado, se inicia el proceso de desensamblar a la célula, como la fragmentación del DNA nuclear, la reducción del citoplasma y exposición de señales para que la célula sea fagocitada por sus células vecinas. Hasta el momento se han identificado 10 genes involucrados en la fragmentación del DNA nuclear que incluyen a *nuc-1, cps-6, wah-1, crn-1 a crn-6* y *cyp-13*. La pérdida de alguno de estos genes resulta en la acumulación de células positivas para TUNEL en el embrión (Parrish y colaboradores, 2001; Parrish y Xue, 2003; Sulston, 1976; Wang y colaboradores, 2002; Wu y colaboradores, 2000). Además, la reducción en alguno de estos genes causa un incremento en el tiempo de aparición de los cuerpos apoptóticos sugiriendo que la degradación del DNA nuclear es importante para la correcta progresión de la apoptosis.

Cuando la célula muere por apoptosis expone señales en la superficie de las células que son reconocidas por células encargadas de la fagocitosis. Los genes encargados de la fagocitosis son *ced-1, ced-2, ced-5, ced-6, ced-7, ced-10, ced-12 y psr-1*. Estos genes se encuentran en dos vías diferentes: *ced-1, ced-6* y *ced-7* se encuentran en una vía y *ced-2, ced-5, ced-10, ced-12* y *psr-1* en otra. La primera de estas vías se encarga del reconocimiento del cuerpo apoptótico, mientras que el segundo grupo de genes codifica componentes de la señalización Rac GTPasa involucrados en la re-organización del citoesqueleto, esenciales para la migración celular y la fagocitosis del cuerpo (Revisado en Programmed Cell Death, Wormbook).

Participación de la mitocondria en la apoptosis de *C. elegans.*

En mamíferos, la activación de la apoptosis por la vía intrínseca depende de la permeabilización de la membrana externa mitocondrial, que promueve la liberación de cyt *c* de la mitocondria, el cyt *c* interactúa con APAF-1 promoviendo su oligomerización y así forma el apoptosoma, el cual activa a la caspasa-9, que a su vez activa a la caspasa-3 y a la caspasa-7 dando lugar a la apoptosis (Figura 15, B). Sin embargo, en *C. elegans* el papel de la mitocondria en la activación de la apoptosis no parece ser indispensable y aún no se entiende por completo. Varios estudios sustentan que CED-9 se encuentra secuestrando a CED-4 en la superficie de la mitocondria y cuando la célula está programada para morir, EGL-1 se une a CED-9 promoviendo cambios conformacionales que liberan a CED-4 de la mitocondria. Aunque la mitocondria es el sitio de anclaje de la maquinaria de apoptosis en *C. elegans*, el papel directo de la mitocondria en la activación de la apoptosis aún no se entiende (revisado en Seervi y Xue, 2015; Figura 15, A).

Existe evidencia de que hay factores que son liberados de la mitocondria y juegan un papel importante en la ejecución de la muerte celular en *C. elegans,* sin embargo aún no se entiende como son liberados de la mitocondria. WAH-1 es el homólogo de AIF y se libera durante la apoptosis para promover la fragmentación cromosomal y la externalización de fosfatidilserina (Wang y colaboradores, 2002). WAH-1 actúa en la misma vía que CPS-6 (homóloga a la proteína EndoG), otra proteína mitocondrial que es liberada y migra al núcleo para promover la degradación del DNA en la apoptosis (Parrish y colaboradores, 2001).

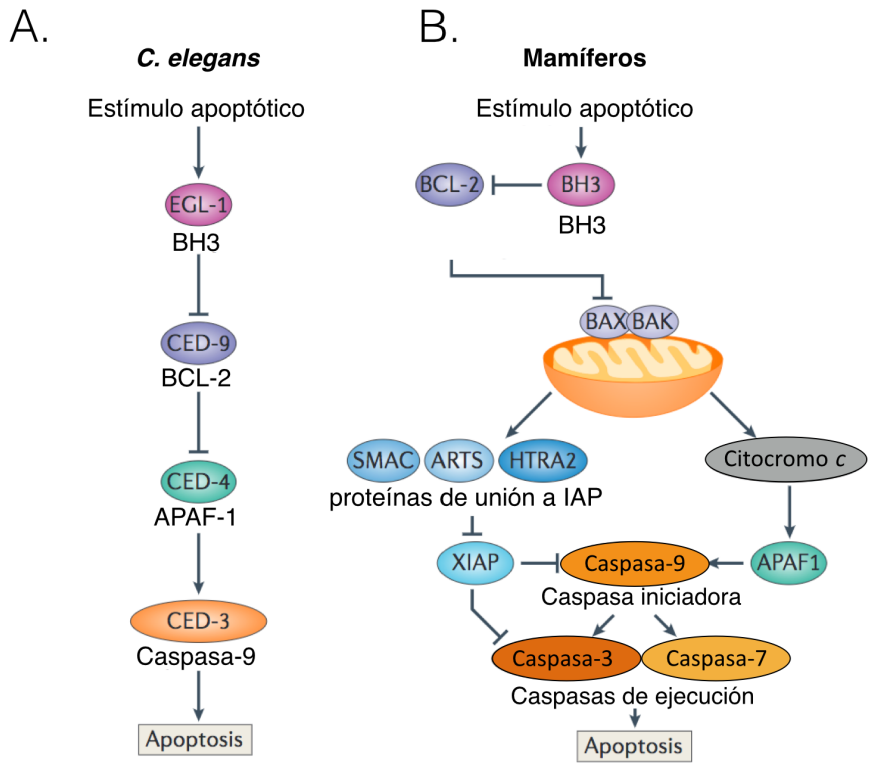

Figura 15. La maquinaria de apoptosis se encuentra conservada entre organismos. (A) En *C. elegans*, la apoptosis somática EGL-1 (homólogo a BH3-only) se une e inhibe a CED-9 (homólogo a BCL-2), resultando en la liberación de CED-4 (homólogo a APAF-1) que lleva a la eliminación de la célula por CED-3 (caspasa). (B) En mamíferos, durante la apoptosis la familia de proteínas BH3-only facilitan a BAX y BAK para la liberación de cyt *c* de la mitocondria, el cyt *c* interactúa con APAF-1 y se da lugar a la formación del apoptosoma. En paralelo, antagonistas de IAP se liberan de la mitocondria y liberan a las caspasas de la regulación negativa por IAPs. La caspasa-9 se libera de las IAPs y es activada por el apoptosoma, ésto estimula a las caspasas 3 y 7. Imagen modificada de Fuchs y Steller, 2014.

Inducción de la apoptosis de las células germinales por estrés.

Además de la apoptosis fisiológica que ocurre en condiciones normales, se ha descrito otro tipo de apoptosis en respuesta a estrés. Se han observado cuatro diferentes condiciones que inducen apoptosis a través de vías independientes (revisado en Lascarez-Lagunas y Navarro RE., 2015), dichas vías convergen en la maquinaria central de apoptosis descrita anteriormente.

Las condiciones de estrés que causan la apoptosis de las células germinales son: (i) infecciones por bacterias patógenas para el *C. elegans* como son la *Salmonella typhimurium* y *Salmonella entérica*, este tipo de apoptosis es dependiente de la proteína EGL-1. El mecanismo de

inducción de apoptosis ante una infección se desconoce, sin embargo, se ha observado que los animales mutantes en *ced-4* y *ced-3* (en los cuales no hay apoptosis) mueren más rápido que los organismos silvestres sometidos a este tipo de infección.

La apoptosis inducida por daño a DNA por agentes genotóxicos, como son la radiación ionizante, la radiación UV y los agentes alquilantes, depende de la proteína CEP-1(el homólogo de p53 en mamíferos) que activa a la maquinaria central de apoptosis (CED-9, CED-4 y CED-3). CEP-1 promueve la transcripción de *egl-1* y posiblemente al igual que en las células somáticas EGL-1 y CED-9 interactúen liberando al activador de la apoptosis CED-4 (Horvitz y Conradt, 1998).

La apoptosis por choque de calor, estrés osmótico y oxidativo no afecta posiblemente el DNA pero afecta vías de señalización. En *C. elegans* la exposición a estos tipos de estrés induce un aumento en la apoptosis de las células germinales, la cual es independiente de CEP-1/p53 como de EGL-1 y es dependiente de la vía de las MAP cinasas (MAPKKs) que regulan a cinasas tipo Jun y Fos (JNK y p38; Salinas y colaboradores, 2006). Animales mutantes en las cinasas tipo MAPKK (*mek-1* y *sek-1*), así como en la cinasa antagonista de p53 (ABL-1) no inducen apoptosis en respuesta a estos tipos de estrés.

La apoptosis por estrés por ayuno, se induce independiente de los genes *egl-1, cep-1, mek-1, sek-1 o abl-1*. Láscarez-Lagunas y colaboradores (2014) encontraron que el mecanismo de inducción de apoptosis por ayuno requiere de las proteínas LIN-35, el cual regula negativamente a *ced-9*. Este dato junto con la traducción ineficiente del mRNA de *ced-9* genera una reducción importante de CED-9. DPL-1 también se induce durante el ayuno, el mRNA de *dpl-1* también se acumula y genera una regulación positiva en la expresión de *ced-4* reforzando el desencadenamiento de la muerte celular por apoptosis (revisado en Lázcarez Lagunas LA y Navarro González RE, 2015).

II. Antecedentes

En el 2006, Ichikawa y colaboradores, encontraron que en *C. elegans* existen dos proteínas que son similares a la proteína inhibidora de la ATPasa mitocondrial (IF_1) (36.36% de identidad entre la IF_1 de *Bos taurus* y MAI-1; 37.14% de identidad entre la IF_1 *Bos taurus* y MAI-2) reciben el nombre de MAI-1 y MAI-2 (48.86% de identidad entre ellas) (Mitochondrial ATPase Inhibitor). Por dicroísmo circular se encontró que MAI-1 y MAI-2 tienen una estructura que consiste principalmente de hojas β y estructura al azar, dicha estructura contrasta con la estructura de las IF_1s de mamífero compuestas principalmente de α-hélices. Ambas proteínas, MAI-1 y MAI-2, inhiben a las ATPasa de levadura, sin embargo, la inhibición de MAI-1 resultó ser pH independiente. Finalmente, Ichikawa y colaboradores estudiaron la localización de ambas proteínas en la levadura por medio de proteínas de fusión. MAI-2-GFP se localizó en mitocondrias mientras que MAI-1-GFP se localizó en el citoplasma de la levadura.

Estudios previos que realicé en la maestría en Ciencias Bioquímicas, UNAM (2013), ayudaron a conocer la localización de las proteínas MAI-1 y MAI-2 mediante la generación de nematodos transgénicos. Los transgenes se incorporaron a los nematodos mediante el método de bio-balística. MAI-2::GFP se encontró en las mitocondrias de *C. elegans* de manera ubicua a lo largo de todo el desarrollo del nematodo, mientras que mCherry::MAI-1 se expresa principalmente en las neuronas de la cabeza y cola, en la hipodermis y en el intestino. Por otra parte, los animales MAI-1::mCherry no mostraron una segregación del transgen con herencia mendeliana, lo que sugiere que el transgen es un arreglo extracromosomal, la presencia de arreglos extracromosomales puede generar animales mosaico que dificultan el estudio de la localización de proteínas.

Finalmente, se disminuyó la expresión de *mai-1* y *mai-2* mediante RNAi, sin embargo, mediante esta técnica no fue posible observar ningún fenotipo, posiblemente debido a la eficiencia del silenciamiento o a que los animales *mai-1(RNAi)* y *mai-2(RNAi)* no presentan un fenotipo aparente en condiciones normales.

III. Planteamiento del Problema e Hipótesis

En un válido intento por estudiar la expresión de estas proteínas, el grupo de Ichikawa y colaboradores (2006) estudió la localización de las proteínas MAI-1 y MAI-2, de *C. elegans* en *S. cerevisiae* (ver antecedentes, pág 50). Sin embargo, este estudio no refleja la localización real de las proteínas en el nematodo. Ichikawa y colaboradores al analizar la secuencia de MAI-1 encontraron que no cuenta con una secuencia de transporte a mitocondria predecible, además MAI-1-GFP se encontró distribuida en el citoplasma de la levadura. Aún con este antecedente, no puede descartarse que MAI-1 tenga una secuencia de transporte mitocondrial que no sea reconocida en sistemas heterólogos o incluso pueda ser transportada a otro organelo en *C. elegans.*

Además de la función canónica que es la de regular a la ATPasa mitocondrial, a la IF_1 se le han atribuido a la IF_1 diferentes funciones como: i) la dimerización de ATPasas, ii) la formación de crestas mitocondriales, iii) la regulación del volumen mitocondria, iv) la regulación de la apoptosis v) y la mitofagia entre otras funciones. Sin embargo, algunos de estos estudios son contradictorios y no han sido de ayuda para entender el papel de IF_1 en un organismo entero. Algunos de estos papeles podrían deberse al uso de diferentes líneas celulares o a los métodos utilizados para disminuir o sobre-expresar a IF_1.

Hipótesis:

Esperamos encontrar a MAI-2::GFP en las mitocondrias de *C. elegans*, mientras que al reportero de MAI-1::GFP en el citoplasma. Se espera que los animales mutantes en *mai-2* presenten un fenotipo con alteraciones evidentes, con defectos en los parámetros mitocondriales y con mayor susceptibilidad a diferentes tipos de estrés.

IV. Objetivos

Objetivo General:

Este trabajo tiene como objetivo general estudiar la localización de MAI-1 en *C. elegans,* así como estudiar la función de MAI-2.

Objetivos Particulares:

1. Determinar la localización de la proteína MAI-1 en el nematodo.

Generar animales transgénicos estables y con inserciones monocopia que expresen al reportero en el extremo amino y extremo carboxilo de MAI-1. Determinar la localización de las proteínas de fusión a nivel subcelular y tisular.

2. Generar mutantes pérdida de función para el gen *mai-2.*

Hacer una mutante en *mai-2* por el método de edición del genoma CRISPR-Cas9.

3. Evaluar los fenotipos producidos en los animales mutantes en *mai-2* en condiciones fisiológicas y en condiciones de estrés.

a) Analizar si los animales mutantes en *mai-2* muestran un fenotipo evidente, p.ej. cambios en el número de progenie, letalidad embrionaria, tiempo de vida, defectos en la movilidad, etc.

b) Evaluar parámetros mitocondriales (que sean realizables en el modelo de estudio) como medir el potencial de membrana mitocondrial ($\Delta\psi_m$), el consumo de oxígeno, las cantidades de ATP y morfología de redes mitocondriales en los animales mutantes en *mai-2.* Además se quiere evaluar la proporción del dímero y monómero de la ATP sintasa mitocondrial.

c) Determinar si los animales mutantes en *mai-2*, presentan una sobrevivencia afectada ante una situación de estrés, p. ej. estrés por choque de calor, estrés oxidativo o un estrés que afecte directamente la funcionalidad mitocondrial.

d) Analizar si las mutantes en *mai-2,* presentan defectos en la apoptosis en condiciones fisiológicas y en condiciones de estrés.

V. Materiales y Métodos

Mantenimiento de cepas.

Las cepas y temperatura de crecimiento que se usaron en este trabajo se indican en la Tabla 1. Las cepas se mantuvieron en medio NGM-lite sembradas con *Escherichia coli* OP50 (Brenner 1974; Sun y Lambie 1997). Las bacterias OP50 se cultivaron durante toda la noche en medio Luria Bertani (LB) (abajo) con 250 µl del antibiótico Estreptomicina (stock de 50 mg/ml).

Los animales se observaron y manipularon en un microscopio estereoscópico Nikon SMZ745. La manipulación de los animales se realizó con un alambre de platino (99.95% Platino, 0.05% Iridium, 3 ft/pk) acoplado a una pipeta Pasteur de vidrio.

A continuación se indican las cepas utilizadas en este trabajo.

Tabla 1. Cepas

Cepa	Genotipo	Temperatura de Crecimiento
N2	Wild type, Bristol isolate	20°C
HT1593	*unc-119(ed3)* III	15°C
RN057	*mai-2(xm18)* IV	20°C
RN058	*mai-2(xm19)* IV	20°C
RN069	*[Pmai-2::mai-2::GFP::mai-2 3′*UTR*; unc-119(+)]**	24°C
RN078	*[Pmai-2::mai-2::GFP::mai-2 3′UTR; unc-119(+)];xmSi01*	24°C
EG6699	*[ttTi5605 II; unc-119(ed3) III oxEx1578]*	15°C
RN037	*xmSi31[Pmai-1::mai-1::mCherry::mai-1 3′*UTR*, Cbr unc-119(+)]* II	24°C
RN038	*xmSi32[Pmai-1::GFP::mai-1::mai-1 3′*UTR*, Cbr unc-119(+)]* II	24°C
RN015	*xmSi01[Pmex-5::tomm-20::mcherry::tbb-2 3′*UTR*; Cbr unc-119 (+)]* II	24°C
MD701	*bcIs39[Plim-7::ced-1::GFP; lin-15(+)]* V	24°C
RN070	*mai-2(xm18)* IV*; bcIs39* V	24°C
RN071	*mai-2(xm19)* IV*; bcIs39* V	24°C
SD1347	*ccIs4251[Pmyo-3::GFP::LacZ + Pmyo-3::mitochondrial GFP + dpy-20(+)]* I	20°C
RN079	*mai-2(xm18) IV; ccIs4251* I	20°C

* El locus no se ha definido.

Generación de los reporteros traduccionales *mai-1::gfp, mCherry::mai-1* y *tomm-20::mCherry* por MosSCI.

a) Descripción de la técnica MosSCI.

La técnica MosSCI (Mos1 mediated Single Copy Insertion) permite la integración de un transgen en un sitio específico y único en el genoma de *C. elegans,* dicha integración puede ocurrir gracias a la inserción experimental del transposón Mos1 de *Drosophila sp.* (Roberts y Bessereau, 2007) en el genoma de *C. elegans* (Frøkjaer-Jensen *C.* y colaboradores, 2008; Frøkjaer-Jensen C. y colaboradores, 2012). Mosl está insertado en un sitio en el genoma donde la transposición se cree no afecta genes o promotores. El transposon Mos1 puede ser movilizado en la línea germinal del animal posterior a la inyección de una transposa Mos1, que deja un corte de doble hebra en el DNA, el cual por recombinación homóloga puede ser reparado con un templado de reparación (Figura 16). La técnica MosSCI tiene las siguientes ventajas: permite la expresión de un transgen en niveles similares a la expresión endógena del gen de estudio, permite la expresión del transgen en la línea germinal y es estable.

Para que esta técnica sea exitosa se requiere de una cepa de *C. elegans* que contenga insertado el transposón Mos1 y que sea mutante en el gen *unc-119, unc-119* es necesario para el correcto desarrollo del sistema nervioso en *C. elegans* y mutantes en este gen son severamente no-coordinados (inmotiles).

Para generar el templado de reparación (transgen), se utilizó el plásmido pCFJ150 que contiene sitios homólogos a las secuencias que flanquean al transposón Mos1 y además cuenta con el gen de rescate *Cb-unc-119.* Se inyectaron en los animales de la cepa EG6699 (ver Tabla 1) los siguientes plásmidos: el templado de reparación, el plásmido que codifica para la transposasa Mos1, tres plásmidos de co-inyección que codifican proteínas fluorescentes y un plásmido que contiene el gen *peel-1* que expresa un canal de K^+ en la pared del músculo que al activarse por choque de calor (34ºC) causa parálisis en los animales.

Las inserciones monocopia en el genoma se distinguieron de arreglos extracromosomales identificando en la filial 1 (F1), animales que presentaron: i) rescate del gen *unc-119,* ii) motilidad después del choque de calor y iii) ausencia de marcadores de co-inyección (generalmente se

inyectan tres plásmidos que codifican para proteínas GFP o mCherry, cuyos genes están fusionados a promotores que inducen la expresión fuerte en tejidos como el músculo o sistema nervioso; Frokjaer-Jensen y colaboradores, 2008).

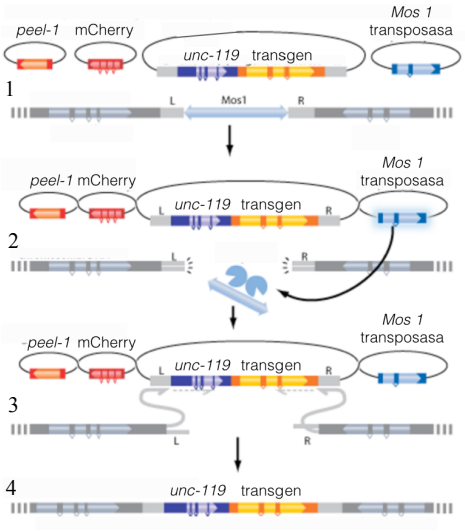

Figura 16. Representación de MosSCI. El transposon Mos1 puede movilizarse por la expresión de la transposasa Mos1 dando lugar a un corte de doble hebra en el cromosoma (1 y 2). Los 3' de las secuencias homólogas L y R del cromosoma invaden y se unen a las regiones homólogas en el arreglo extracromosomal (3) El arreglo extracromosomal comprende a la transposasa y los marcadores de selección negativa *peel-1* y marcadores fluorescentes. Seguido de la pérdida de los arreglos (4), los animales candidatos con inserción monocopia se aislan. L y R son regiones homólogas. Modificado de (Frokjaer-Jensen y colaboradores, 2012)

b) Generación de los animales transgénicos.

La construcción de los transgenes se realizó por MultiSite Gateway (Thermo Fisher Scientific) y todos los insertos se amplificaron a partir de DNA genómico. Para el transgen *Pmai-1::GFP::mai-1 3'-UTR* se amplificó un fragmento de 2000 pb de la región intergénica río arriba de *mai-1,* para la región codificante se amplificó un fragmento de 932 pb del ATG a la región 3'-UTR más larga de *mai-1* (Wormbase WS224). Los productos de PCR se purificaron por extracción de gel (QIAquick Gel Extraction, Quiagen). La región del promotor se clonó por recombinación en el plásmido pDONRP4-P1R (Gateway), mientras que la región codificante se clocó en el pDONRP2R-P3 (Gateway). Para la secuencia de *GFP* se usó el plásmido donador pCM1.53 (#17250).

Para generar el transgen *Pmai-1::mai-1::mCherry-mai-1-3'-UTR*, se utilizó el mismo promotor descrito anteriormente y un fragmento de *mai-1* de 567 pb desde el ATG hasta el final de la secuencia codificante sin codón de paro. Además, se amplificó a partir del vector pCFJ104 (#19328) un fragmento de 864 pb para el gen de la mCherry, el cual se sobrelapó con el 3'-UTR de *mai-1* mediante PCR (Heckman y Pease, 2007). Los fragmentos de PCR se purificaron por extracción de gel. El promotor de *mai-1* se clonó en el vector donador pDONRP4-P1R (Gateway),

mai-1 se clonó en el pDONR221 (Gateway) y el fragmento de *mCherry-mai-1-3'-UTR* se clonó en el pDONRP2R-P3 (Gateway).

Para la construcción del transgen de *Pmex-5::tomm-20::mCherry tbb-2 3'-UTR* se amplificó un fragmento de 225 pb del gen *tomm-20*, la secuencia de mCherry se amplificó a partir del vector pGH8 (#19359) y se sobrelapó con el fragmento de *tbb-2 3'-UTR* por PCR, dicha fusión se clonó el pDON221. Finalmente, se utilizó el plásmido donador pCFJ183-*Pmex-5* (donado por el doctor Frokjaer-Jensen), el pDONR221-*tomm-20::mCherry* y pCm1.36 (#17249) como plásmidos donadores.

Los plásmidos donadores con los insertos respectivos se purificaron con el kit QIAprep Miniprep, Quiagen. Los insertos se secuenciaron posterior a ser clonados en los plásmidos donadores y una vez confirmados se clonaron en el plásmido destino pCFJ150 (#19329) (Frøkjaer-Jensen y colaboradores, 2008). Los oligonucleótidos utilizados se muestran en la Tabla 2.

Tabla 2. Oligonucleótidos utilizados en este trabajo.

Uso	Oligo	Secuencia
Pmai-2::mai-2::GFP::mai-2 3'UTR	*Pmai-2* F	5'-GGGGACAACTTTGTATAGAAAAGTTGATTTCGTTTGGTAGACGAGG-3'
	Pmai-2 R	5'-GGGGACTGCTTTTTTGTACAAACTTGATTCTGAAAATTGAGTGAATTAGAGAG-3'
	mai-2 F	5'-GGGGACAAGTTTGTACAAAAAAGCAGGCTCAATGCTCAGCGTTTCAAGAGCCG-3'
	mai-2 R	5'-GGGGACCACTTTGTACAAGAAAGCTGGGTTTCCTTCCTTTCCGAGGGCACGC-3'
	gfp F	5'-GGGGACAGCTTTCTTGTACAAAGTGGGAATGAGTAAAGGAGAAGAACTTTTCACTG-3'
	gfp R	5'-GACTAGCTCGCGTTCTTGTACTGCAAATTATTTGTATAGTTCGTCCATGCCATG-3'
	*mai-2 3'*UTR F	5'-CATGGCATGGACGAACTATACAAATAA TTTGCAGTACAAGAACGCGAGCTAGTC-3'
	*mai-2 3'*UTR R	5'-GGGGACAACTTTGTATAATAAAGTTG CCTCTATAATTTTCCTCTATAAAGCTTGTC-3'
Pmai-1::GFP::mai-1::mai-1 3'UTR	*Pmai-1* F	5'-GGGGACAACTTTGTATAGAAAAGTTGTTTGTTTTGATGTGCTTT-3'
	Pmai-1 R	5'-GGGGACTGCTTTTTTGTACAAACTTGTCATCTGTTTTGATTTCCTG-3'
	mai-1 F	5'-GGGGACAAGTTTGTACAAAAAAGCAGGCTCAATGTCAGGATCTGGAAGTG-3'
	mai-1 R	5'-GGGGACAACTTTGTATAATAAAGTTGGGACAAGACGTCCGATTC-3'
Pmai-1::mai-1::mCherry::mai-1 3'UTR	*Pmai-1* F	5'-GGGGACAACTTTGTATAGAAAAGTTG TTTGTTTTGATGTGCTTT-3'
	Pmai-1 R	5'-GGGGACTGCTTTTTTGTACAAACTTGTCATCTGTTTTGATTTCCTG-3'
	mai-1 F	5'-GGGGACAAGTTTGTACAAAAAAGCAGGCTCAATGTCAGGATCTGGAAGTG-3'
	mai-1 R	5'-GGGGACCACTTTGTACAAGAAAGCTGGGTTTCCTGTTCCGTGTCCTTTCTCGA-3'
	mCherry F	5'-GGGGACAGCTTTCTTGTACAAAGTGGGAATGGTCTCAAAGGGTGAAGAA-3'
	mCherry R	5' AGAGCCGTTTGAAAAGCCCTCTATTTTTTACTTATACAATTCATCCATGCCACC-3'
	*mai-1-3'*UTR F	5'-GGTGGCATGGATGAATTGTATAAGTAAAAAATAGAGGGCTTTTCAAACGGCTCT-3'
	*mai-1-3'*UTR R	5'-GGGGACAAC TTTGTATAATAAAGTTGGGACAAGACGTCCGATTC-3'
Pmex-5::tomm-20::mcherry::tbb-2 3'UTR	*tomm-20* F	5'-GGGGACAAGTTTGTACAAAAAAGCAGGCTTAAAAATGTCGGACACAATTCTTG-3'
	tomm-20 R	5'-TTCTTCACCCTTTGAGACCATTCCAGCCTGGGCACG-3'
	mCherry F	5'-AGAGACGTGCCCAGGCTGGAATGGTCTCAAAGGGTGAAGAAG-3'
	mCherry R	5'-GGGGACCACTTTGTACAAGAAAGCTGGGTACTTATACAATTCATCCATGCCACC-3'.
Edición de *mai-2* por CRISPR/Cas9	*mai-2 sgRNA* F	5'-GGATCGATCCGCGACGCCGGGTTTTAGAGCTAGAAATAGCAAGTTAAAATAAG-3
	mai-2 sgRNA R	5'-CCCGGCGTCGCGGATCGATCCAAACATTTAGATTTGCAATTCAATTATATAGG-3'.
	mai-2 ssDNA1	5'GGAATGGTCGCCCGCTTCTCCGCCGGAGGACACGGAGACGGAGCCGGACGCGGAGGA GGCTCCGGTGGATCGATCCGCGACGCCGGCAGCTGAGGTGCGTTCGGAAAGATGGAGGC CGCCCGCGAGGACGAGTACTTCTACAAGAAGCAGAAGGCTCAACT-3'
	mai-2 ssDNA2	5'CGGAATGGTCGCCCGCTTCTCCGCCGGAGGACACGGAGACGGAGCCGGACGCGGAGG AGGCTCCGGTTAATAATTTGCAGTACAAGAACGCGAGCTAGTCGTCTTCTGAAATTTTCTT CATTTTTC-3'
Detección de *mai-2(xm18)* y *mai-2(xm19)*	*mai-2* F	5'-TTTCGCAAGTTTCAGGCAG-3'
	*mai-2(xm*18) R	5'-ATTGTTCAGCTCCCGCAC-3'
	*mai-2(xm19)*R	5'-GGTCTCGAAGTGGAAGAAA-3'
rt-PCR	*mai-2* F	5'-GCTCTAGAATGCTCAGCGTTTCAAGA-3'
	mai-2(xm18) R	5'-GCGGATCCTTATTCCTTTCCGAGGGC-3'
	mai-2(xm19) R	5'-CACGTGGCGAAAATAGAGAGAG-3'

Los fragmentos *Pmai-1::GFP::mai-1::mai-1-3'-UTR, Pmai-1::mai-1::mCherry-3'-UTR* y *Pmex-5::tomm-20::mCherry-3'-UTR* clonados cada uno en el pCFJ150 se inyectaron junto con los

plásmidos de co-inyección en la cepa EG6699 (ver Tabla 1). Las mezclas de DNA que se inyectaron fueron las siguientes: pCFJ150 con *Pmai-1::gfp::mai-1::mai-1 3'-UTR* (30 ng/µl), pMA122 (10 ng/µl) (#34873), pCFJ601 (50 ng/µl) (#34874), pCFJ104 (5 ng/µl), pGH8 (#19359) y pCFJ90 (2 ng/µl) (#19327); pCFJ150 con *Pmai-1::mai-1::mCherry::mai-1 3'-UTR* (30 ng/µl), pMA122 (10 ng/µl), pCFJ601 (50 ng/µl), pCFJ421 (2.5 ng/µl) (#34876), pCFJ420 (5 ng/µl) (#34877), pCFJ66 (10 ng/µl) (#24981); pCFJ150 con *Pmex-5::tomm-20::mCherry::tbb-2 3'-UTR* (10 ng/µl), pCFJ601 (10 ng/µl), pCFJ104 (10 ng/µl), pGH8 (10 ng/µl), pCFJ90 (2 ng/µl).

Se inyectaron aproximadamente 50 animales por construcción, 3 animales inyectados se colocaron en una caja Petri (60 mm) y se incubaron a 25ºC durante aproximadamente una semana hasta que los animales (F0 y F1) se ayunaron completamente. Algunos animales ya podían observarse con una recuperación de la coordinación (rescate del fenotipo Unc). Posteriormente, los animales se sometieron a choque de calor por 2 h a 34ºC (se introdujeron las cajas Petri en una incubadora de aire) y después de 4 h de recuperación a 20ºC los animales coordinados que no fueron paralizados (perdieron arreglos extracromosomales) se aislaron y separaron. Finalmente, aquellos animales fluorescentes para GFP::MAI-1, TOMM-20::mCherry y MAI-1::mCherry pero que no tuvieron la fluorescencia de los marcadores de co-inyección se seleccionaron y segregaron en líneas.

Adquisición de imágenes y procesamiento de los animales transgénicos.

Los animales *mai-2::gfp* se observaron por microscopía de fluorescencia en un microscopio equipado con una cámara AxioCam MRc (Zeiss). Las imágenes se tomaron utilizando el software AxioVision (Zeiss) y las imágenes fueron deconvolucionadas con el software ImageJ con el plugin Parallel Spectral Deconvolution and Diffraction PSF 3D. Las larvas y adultos que expresan las proteínas de fusión MAI-2::GFP, TOMM-20::mCherry, GFP::MAI-1 y MAI-1::mCherry se observaron por microscopia confocal utilizando el microscopio Olympus FluoView FV10i (Olympus), tamaño 1024 x1024 con apertura confocal 2x y las imágenes se procesaron en ImageJ.

Generación de los alelos de *mai-2* por CRISPR-Cas9.

Para generar mutantes en *mai-2* se utilizó la técnica de CRISPR-Cas-9. CRISPR-Cas9 es una técnica utilizada para editar el genoma que consiste en que la endonucleasa Cas9 genera cortes

de doble hebra en el genoma, el investigador puede aprovechar la maquinaria endógena de reparación del DNA para realizar modificaciones deseadas. Existen dos vías por las que la célula puede reparar el genoma: i) unión de extremos sujeto a error y ii) la reparación dirigida por recombinación homóloga. En la primera vía, tras el corte de doble hebra, la maquinaria de reparación introduce un pequeño número de inserciones o deleciones al azar (INDELS); mientras que en la segunda se introduce una secuencia exógena que tras el corte de doble hebra por Cas9 sirve de templado de reparación. En nuestro proyecto se utilizó la segunda estrategia para generar los alelos *mai-2(xm18)* y *mai-2(xm19).*

Se eligió un sgRNA localizado en el exón 1 del gen *mai-2* con la secuencia GGATCGATCCGCGACGCCGG para ser reconocida por Cas-9. El sitio PAM (Protospacer Associated Motif) se localiza en la posición 3, 386, 025 (Wormbase WS224). Para clonar el sgRNA de *mai-2* se reemplazó por PCR el sgRNA *unc-119* del plásmido *pU6::unc-119* (#46169) con el sgRNA de *mai-2*. Utilizando los oligonucleótidos indicados en la Tabla 2. El producto de PCR se digirió con DpnI durante 4 h, se purificó con el kit QIAquick PCR Purification Kit y se confirmó por secuenciación. Se diseñaron dos ssDNA que sirvieron como templado de reparación (Tabla 2) (Paix y colaboradores, 2014). El ssDNA1 se diseñó con un brazo de homología río arriba del sitio PAM de 83 nt con la inserción de un sitio PvuII que introduce un codón de paro temprano y un brazo río abajo del sitio PAM compuesto de 78 nt. Para generar una deleción, el ssDNA2 se diseñó con un brazo de homología río arriba del sitio PAM de 67 nt y un brazo de río abajo del sitio PAM de de 71 nt que comprende el 3'-UTR del gen *mai-2* (Tabla 2). Se microinyectaron los plásmidos previamente purificados con el kit QIAprep Miniprep, Quiagen: *Peft-3::cas-9-SV40-NLS::tbb-2 3'-UTR* (50 ng/µl) (#46168), pU6::*mai-2* sgRNA (45 ng/µl), pCFJ104 (5 ng/µl) y los templados de reparación ssDNA 1 o 2 (30 ng/µl) a 30-50 adultos jóvenes (con pocos embriones) de la cepa silvestre N2. La F1 de los gusanos inyectados (P0) se observó en un microscopio estereoscópico con fluorescencia Nikon SZ1500 con un accesorio de fluorescencia P-Fla-2, los animales con expresión de la proteína mCherry (marcador de co-inyección) se aislaron en cajas Petri (35 mm) individuales y se dejaron tener progenie (F2).

Las mutaciones se identificaron por medio de la lisis de gusano individual de la F1,(abajo) del cual se obtuvo el DNA cromosomal y se utilizó de templado para amplificar por PCR a *mai-2,* los oligonucleótidos utilizados se indican en la Tabla 2. Para detectar la inserción de el sitio de restricción PvuII que introduce un codón de paro, se incubó la mezcla de reacción posterior al PCR

(20 µl) con 2 µl de PvuII diluida (1:10) en un amortiguador para diluir enzimas de restricción (Apéndice I) y se incubó durante 2 horas a 37ºC o a TA toda la noche. Para observar la deleción de *mai-2* se detectó por peso molecular (Figura 17). Las mutantes *mai-2(xm18)* y *mai-2(xm19)* se retrocruzaron 3 veces para eliminar mutaciones fuera de rango.

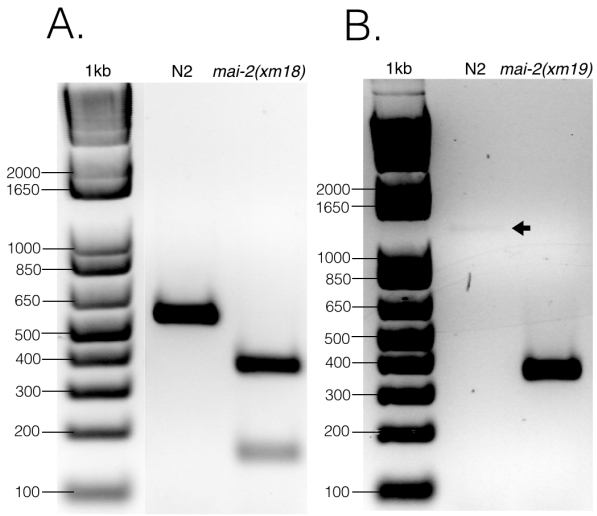

Figura 17. Identificación de las mutaciones en mutantes *mai-2(xm18)* y *mai-2(xm19)* por digestión y PCR. (A) A partir de DNA cromosomal de los animales de la cepa N2 y mutantes en *mai-2,* se amplificó por PCR a *mai-2* y el amplificado se digirió con la enzima de restricción PvuII, únicamente los animales mutantes podrán ser digeridos con PvuII. (B) Se amplificó a partir de DNA cromosomal a *mai-2*, la forma silvestre tiene un peso de 1157 bp mientras que la mutante *mai-2(xm19)* tiene una deleción de 794 pb.

Extracción de RNA.

Aproximadamente 6,000 gusanos sincronizados en estadio de L4 a adulto joven de las cepas N2, *mai-2(xm18)* y *mai-2(xm19)* se lavaron 3 veces con medio M9 1X (ver Apéndice I) para retirar la bacteria. La pastilla de animales se resuspendió con 500 µl-1000 µl del reactivo TRIZOL (Invitrogen) y se congelaron a -70ºC con ayuda de N_2 líquido. El día de la extracción, las muestras se descongelaron y se agregaron a un mortero con pistilo para fragmentar a los gusanos, se hicieron 4 repeticiones de congelación, descongelación y molienda. Posteriormente, las muestras se recuperaron en un tubo tipo Eppendorf, se agregaron 100 µl de cloroformo, se incubararon por 3 min a temperatura ambiente (TA) y se centrifugaron a 13,400 rpm durante 15 min a 4ºC en una microcentrífuga Eppendorf Minispin Plus. Delicadamente se recuperó la fase superior en donde y se separó a un tubo tipo Eppendorf nuevo. El RNA se precipitó con 250 µl de isopropanol a TA

durante 10 min y se centrifugó a 13,400 rpm durante 10 min a 4ºC en una microcentrífuga Eppendorf Minispin Plus. La pastilla se lavó con alcohol etílico al 70% para retirar sales y se centrifugó a 7500 rpm durante 5 min a 4ºC en una microcentrífuga Eppendorf Minispin Plus. El etanol se decantó, se extrajo el residual con ayuda de un pipeta y se dejaron secar por 5 min. La pastilla se resuspendió con 30 µl de agua DEPC y se incubó a 60ºC por 10 min. Finalmente, se cuantificó la cantidad de RNA de cada muestra en un NanoDrop. La pureza y calidad de la preparación de RNA se determinó a partir de la relación A_{260nm}/A_{280nm}.

Cuantificación de la expresión del mRNA de *mai-2* por RT-PCR semicuantitativo.

0.5-1 µg/µl de RNA se utilizó para la síntesis de cDNA, se utilizó el kit de la retrotranscriptasa ImProm II de Promega. El RNA junto con 1 µl de oligonucleótido dT (0.5 µg/µl) se llevaron a 5 µl con agua DEPC y se incubaron 5 min a 70ºC, posteriormente se incubaron 5 min en hielo. Posteriormente, se agregaron 15 µl de la mezcla que contenía 4µl del amortiguador de reacción ImProm II 5x, 2.4 µl de $MgCl_2$ 25 mM, 1 µl de dNTPs 10 mM, 1 µl de la enzima ImProm-II y se llevaron a 15 µl de agua milliQ estéril. La mezcla se agregó al RNA y se incubaron durante 25ºC por 5 min, 42ºC por 60 min y 70ºC por 15 min. Generalmente, a partir de 1 µl de cDNA sintetizado se amplificó a *mai-2* utilizando los oligonucleótidos de la Tabla 2.

Tiempo de Vida.

50 animales N2 y *mai-2(xm18)* se sincronizaron y crecieron a 20ºC. Los animales perdidos o que hayan muerto prematuramente se reemplazaron por animales reserva que se crecieron en las mismas condiciones. Los animales muertos se contaron aproximadamente cada dos días a lo largo de la vida de los animales.

Conteo de progenie y letalidad embrionaria.

Se colocaron 10 animales en estadio de L4 de las cepas N2, *mai-2(xm18)* y *mai-2(xm19)* individualmente en cajas Petri de 35 mm con medio NGM-lite sembradas con OP50. El animal se cambio de caja Petri aproximadamente cada 24 horas durante 4 días, al término de este periodo los animales ya no depositan embriones debido a que se dejan de producir los espermatozoides del animal. A las 24 h post cambio se contaron los embriones que no eclosionaron y las 48 h post

cambio se contaron el número de larvas eclosionadas. La progenie total incluye a los animales que lograron eclosionar y así como los embriones muertos.

Visualización de las mitocondrias.

Para visualizar las mitocondrias se utilizó MitoTracker Red CMXROS (#M7512; Molecular Probes) el cual se diluyó con DMSO a una concentración final de 1 mM (stock). Antes de la tinción se diluyó el MitoTracker Red CMXROS a 5 µM con medio M9 y se colocó en cajas Petri de vidrio (60 mm). 20-30 animales adultos de un día se incubaron durante 20 minutos a 20ºC. Los animales se inmobilizaron con tetramisol 10 mM/M9 1X y se montaron en placas de agarosa al 2% para examinarlos por microscopia de fluorescencia (Yee y colaboradores, 2014).

Para la tinción con TMRM, el TMRM se diluyó en DMSO a 0.1 M (stock) y se añadió al medio NGM-lite a una concentración de 30 µM, las cajas Petri (35 mm) se dejaron secar toda la noche. Posteriormente, las cajas se sembraron con OP50 y se dejaron secar en la obscuridad durante 24 h. Se transfirieron 30 animales adultos de un día de cada cepa a las cajas y se incubaron por 15 h. A los animales de 2 días de adulto se les extrajo los embriones y se inmobilizaron con tetramisol 10 mM/M9 1X y se montaron en placas de agarosa al 2%. Para visualizar la acumulación de TMRM en el animal completo se usó las mismas condiciones previamente descritas pero se visualizaron animales adulto de un día. Los animales se visualizaron con un microscopio de fluorescencia y se capturaron las imágenes al mismo tiempo de exposición.

Para visualizar la redes mitocondriales de las células de la pared del músculo, se utilizaron animales sincronizados en estadio de L4 de la cepa SD1347 *ccIs4251* [*Pmyo3::GFP::LacZ* + *Pmyo3::mitoGFP* + *dpy-20* (+)] como control y cruzados con la cepa *mai-2(xm18)*. Los animales se montaron en tetramisol/M91X 10 mM en un colchón de agarosa 2% y después de colocar el cubreobjetos, se rodó para voltear los gusanos y visualizar las mitocondrias del músculo. Se cuantificó el número de células musculares de la pared del nematodo que presentaron morfología tubular (silvestre), agregación, mitocondrias fusionadas/elongadas o fisionadas.

Las mitocondrias se visualizaron en un microscopio de fluorescencia Nikon Eclipse E600 equipado con una cámara AxioCam MRc (Zeiss). Las imágenes se capturaron utilizando un software AxioVision Zeiss. Para cuantificar la fluorescencia del TMRM se utilizó el programa Fiji (ImageJ). A partir de las imágenes obtenidas se delineó el contorno de la célula P_1 de los embriones

(2 células) y el de los animales enteros además del fondo para obtener la densidad integrada del área seleccionada. La fluorescencia total (FT) se calculó con la siguiente fórmula: FT=(densidad integrada-(área seleccionada x promedio de la fluorescencia del fondo) y se normalizó con el control.

Consumo de oxígeno.

Aproximadamente 10,000 animales/ml en estadio de L4-adulto joven se colectaron, se lavaron 3 veces en M9 1X seguido de una incubación de 30 min en agitación constante para lavar el intestino y remover las bacterias. Previo a agregar los animales se incubaron 100 µl de medio M9 en una cámara Mitocell con cubierta de agua en agitación constante, previamente calibrada a 20ºC, al cual se agregó 15 µl de la pastilla de animales. Para medir la velocidad del consumo de oxígeno se utilizó un electrodo tipo Clark conectado a un oxímetro Strathkelvin Instruments modelo 782 (North Lanarkshire, Escocia) acoplado a una computadora para registro de datos. El consumo de oxígeno se midió hasta que el trazo fue lineal y se detuvo con 5 µl de NaCN (1M). Los animales se recuperaron de la cámara y se realizó la precipitación de proteína por TCA y cuantificación por el método de Lowry que se explican a continuación (Bollag y Edelstein 1991; Markwell y colaboradores, 1978).

Los nematodos recuperados de la cámara Mitocell se diluyeron en 1 ml de agua destilada, posteriormente se agregó 0.15 ml de NaOH 1.85M, 7.4% de β-Mercaptoetanol. El tubo se mezcló por inversión y se incubó en hielo durante 10 min. Las muestras se centrifugaron a 14,000 *g* durante 12 min y los sobrenadantes se removieron cuidadosamente. La pastilla se lavó en 1 ml de acetona, se re-centrifugó y dejó secar por 5 min. La pastilla se solubilizó en agitación durante 20-30 min en 50 µl de 5% de SDS, Tris-HCl, pH 6.8.

Para realizar la cuantificación de proteína por el método de Lowry (para más detalle ver Apéndice I) se llevó la muestra a 0.5 ml de agua destilada y se añadió 2.5 ml de solución C, se agitó y se dejó a TA por 10 minutos. Posteriormente, se añadió 0.25 ml se solución D, se agitó y se incubó por 30 min. Se incluyó una curva estándar con BSA (1 mg/ml) y se leyeron la curva y las muestras de nematodos a una A_{750}.

Cuantificación de ATP.

La cuantificación de ATP se determinó por medio de bioluminiscencia, utilizando la dependencia de ATP de la enzima lucíferasa que cataliza la oxidación de luciferin. La extracción de ATP se realizó como previamente descrito con modificaciones (Palikaras y colaboradores, 2015). 50 animales adultos de 1 día se colectaron en 50 µl de M9 y se congelaron en N_2 líquido. Los animales se descongelaron, se hirvieron durante 15 min, se dejaron enfriar y se centrifugaron a 2,000 rpm por 5 min en una centrifuga Eppendorf 5418R. El sobrenadante se pasó a un tubo nuevo y se diluyó 5 veces. El contenido de ATP se determinó por medio de Roche ATP Bioluminescent Assay Kit CLS II (Roche Applied Science) y se midió con un luminómetro POLARstar Omega (BMG LABTECH). Los niveles de ATP se normalizaron con el contenido de proteína.

Purificación de mitocondrias, electroforesis de 1D y SDS-PAGE.

50, 000-100,000 animales sincronizados en estadio de L4 y adulto joven se molieron 10 veces en un mortero con ayuda de N_2 líquido y la mezcla se resusendió en 100 µl de amortiguador para aislar mitocondrias (ver Apéndice I). Los animales homogenizados se centrifugaron en 2,700 rpm por 5 min y el sobrenadante se colectó en un tubo tipo Eppendorf por separado. Este procedimiento se repitió 2 veces. El sobrenadante se centrifugó a 10,500 rpm por 5 min para obtener la pastilla de mitocondrias, las cuales fueron resuspendidas en 250 mM de sacarosa y 1mM de $MgCl_2$. La ATP sintasa se extrajo con digitonina (0.66 mg/ml), se incubó durante 10 min y se centrifugó por 5 min a 75,000 rpm en una centrifuga Airfuge Ultracentrifuge, Beckman Coulter. El sobrendante se usó para determinar proteína y 100 µg de proteína se incorporaron en un gel azul nativo (1D) seguido de una 2D SDS-PAGE.

Para el gel BN-PAGE la proteína extraída se combinó con 10 µl amortiguador 3X (ver Apéndice I) y se cargó en un BN-PAGE 3.5%-11% y la electroforesis se efectuó a 70V por 30 min y 100 V por 2h a 4ºC. La 1D se tiñó con solución Coomassie y se agitó a temperatura ambiente por 2 h y se decoloró con solución para decolorar (ver Apéndice I). Para cuantificar la proporción de dímero y monómero se realizó un análisis densitométrico en el programa Fiji (Image J). Para la 2D SDS-PAGE, el gel Coomassie desnaturalizó en una solución que contenía SDS 1% y 5mM de DTT durante 1 h. La banda que corresponde al dímero y monómero se cortó del gel Coomassie y se roto 90º en un gel 15% de SDS-PAGE von Jagow y la electroforesis se realizó por 30 minutos a 70V y a 100V durante 2h a 4ºC (Yoshida y colaboradores, 1975). El gel fue escaneado y analizado. La actividad de ATPasa se identificó incubando el gel de 1D en una solución de pre-incubación que contenía 35 mM de Tris, 250 mM de glicina, pH 8.3. Posteriormente, se incubó el gel en agitación

y se incubó 2 h a 37ºC con 5mM de ATP, 5 mM de MgCl2, 0.15% (m/v) de acetato y 150 mM de glicina, pH 8.3. El gel se agitó y se incubó a TA por 24 h. El monómero y dímero se visualizaron en un fondo obscuro y se escaneó a las 2h.

Ensayos de sobrevivencia.

Para analizar la sobrevivencia de los animales a choque calor, 30 gusanos sincronizados de 4 días de adulto se crecieron a 20ºC y se transfirieron a cajas Petri (35 mm) con medio NGM-lite sembradas con OP50. Los animales se incubaron a 35ºC durante 12 h en una incubadora de aire y cada 2 horas se retiraron las cajas de la incubadora para medir la sobrevivencia.

Para analizar la sobrevivencia de los animales a cianuro de sodio (NaCN) y carbonil-m-clorofenil hidrazone (CCCP), se probaron diferentes concentraciones de cianuro de sodio (50-100 mM) y CCCP (50-125 μM) diluidos en M9. Aproximadamente 30-50 adultos de un día se pusieron a nadar en 200 μl de M9 como control, NaCN y CCCP en cajas Petri de vidrio (60 mm). Se dejaron incubando durante 1 h a 20ºC, al término de la incubación se agregaron 2 ml de medio M9, los animales se recuperaron con ayuda de una pipeta y puntas de baja retención y se pusieron en cajas Petri con medio NGM-lite sembradas con OP50. Los animales se dejaron recuperar durante 1 hora y posteriormente se evaluó la sobrevivencia

Para el estrés oxidativo, los animales se incubaron en tubos tipo Eppendorf de baja retención con 200 mM de paraquat con OP50 (Labbadia y Marimoto, 2015). Posteriormente, se incubaron los animales durante 4, 8 y 12 h, se colocaron en cajas Petri con medio NGM-lite para realizar el conteo de animales sobrevivientes.

Los experimentos de sobrevivencia se cuantificaron en un microscopio estereoscópico Nikon SMZ745, los animales que no respondieron al toque del asa de platino se evaluaron como muertos.

Ensayos de apoptosis.

Los ensayos de apoptosis fisiológica y en respuesta a estrés se realizaron como previamente descrito (García-Silva y Navarro RE, 2013; Salinas y colaboradores, 2006). Se cruzaron las cepas

mai-2(xm18) y *mai-2(xm19)* con MD701 *bcIs39* [*Plim-7::ced-1::GFP; lin-15*(+)]. Se seleccionaron gusanos L4 de cada cepa y aproximadamente 24 h después se montaron en placas de agarosa al 2% y los cuerpos apoptóticos se visualizaron con un microscopio de fluorescencia. Para cuantificar la respuesta apoptótica en condiciones de estrés se sometieron los animales adultos de 1 día a las siguientes condiciones:

- Ayuno. Los animales se incubaron 6 h en medio NGM-lite sin bacterias.
- Choque de calor. Los animales se incubaron en cajas Petri (35 mm) con medio NGM-lite sembradas con OP50 y se incubaron durante 3 h a 31ºC en una incubadora de agua seguido de 4.5 h de recuperación a 24ºC.
- Irradiación por UV-C. Los animales se sometieron a 1000 J/m^2 (Stratalinker, 1800) y se dejaron recuperar durante 3 h a 24 ºC.
- Estrés oxidativo. Los animales se incubaron en 10 mM de paraquat disuelto en M9 (200 µl) durante 1 h en una caja Petri de vidrio (60mm), posterior a la incubación, se diluyó el paraquat con 2 ml de M9 y al término los animales se dejaron recuperar 1 h en cajas Petri con medio NGM-lite a 24ºC.

VI. Resultados

Para estudiar la función de *mai-2* en *C. elegans* se generaron animales transgénicos para estudiar la localización de MAI-1 y MAI-2 (de las siglas en inglés Mitochondrial ATPase Inhibitor). Para MAI-2 se generó una proteína transgénica que tiene la proteína MAI-2 fusionada con GFP (Figura 18, C*5*). Además para entender la localización de la proteína MAI-1 realizamos dos proteínas transgénicas que tienen a la proteína GFP y mCherry fusionadas en el amino y carboxilo terminal respectivamente (Figura 18, C*6,7*).

Se contruyeron dos alelos distintos para *mai-2,* el alelo *mai-2(xm18)* que tiene insertado un codón de paro temprano (ópalo) y el alelo *mai-2(xm19)* que tiene una deleción de 794 bp (Figura 18, A*1,2*). Los alelos *mai-2(xm18)* y *mai-2(xm19)* se consideran alelos pérdida-de-función puesto que ambos alelos codifican para proteínas MAI-2 que carecen de un dominio de inhibición (DI) íntegro (Figura 18, B*3,4*); que es el dominio funcional y conservado en *C. elegans* que permite la inhibición de la ATPasa mitocondrial (Ichikawa y colaboradores, 2006).

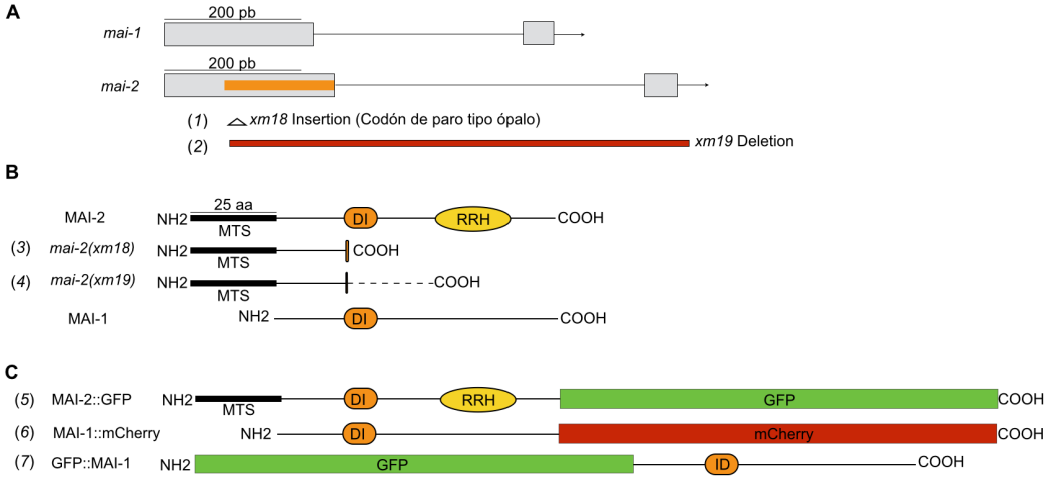

Figura 18. Alelos y reporteros traduccionales utilizados para el estudio de la función de la proteína inhibidora de la ATPasa mitocondrial en *C. elegans.* Los genes *mai-1* y *mai-2* están compuestos de dos exones (rectángulos grises) y un intrón (línea delgada). (B) Se generaron dos alelos mutantes llamados *mai-2(xm18)* y *mai-2(xm19)*. Ambos alelos codifican para dos proteínas truncas que conservan la secuencia de transporte a mitocondria pero carecen de un dominio de inhibición (naranja, DI) y región RRH indispensables en la función y regulación de la dimerización de la proteína. (C) Para estudiar la localización de MAI-1 y MAI-2 se generaron reporteros traduccionales (*5-7*). Se insertó una GFP en el carboxilo de MAI-2 (*5*) y para MAI-1 se insertó una mCherry en el carboxilo (*6*) y una GFP en el amino (*7*).

MAI-1 no se expresa en la mitocondria.

Para estudiar la expresión de MAI-1, se generaron animales transgénicos por MosSCI (ver Materiales y Métodos). Brevemente, se fusionaron en el N-terminal de MAI-1 la proteína GFP y en el C-terminal se fusionó una mCherry. Para los animales transgénicos con la GFP en el N-terminal, se clonó el promotor putativo de *mai-1* (1966 pb) y la región codificante de *mai-1* del ATG al 3'-UTR de *mai-1* (924 pb). Se obtuvo una línea transgénica a la cual se llamó *xmSi32*[*Pmai-1::GFP::mai-1 3'-UTR; Cbr-unc-119* (+)]II. Para la generación de MAI-1::mCherry, se clonó el promotor de *mai-1* (1966 pb) seguido de la región codificante de *mai-1* del ATG al final del gen sin codón de paro (546 pb). Posteriormente, se fusionó una quimera de mCherry con el gen *mai-1 3'-UTR* (1217 pb). Se obtuvieron dos líneas independientes con el mismo patrón de expresión, se eligió trabajar con *xmSi29*[*Pmai-1::mai-1::mCherry::mai-1-3'UTR; Cbr-unc-119* (+)]II.

La localización de MAI-1 en los animales transgénicos que expresan a GFP::MAI-1 (Figura 19, A-F) y a MAI-1::mCherry (Figura 19, G-J) se observó en los mismos tejidos, en el citoplasma y en el núcleo de células de tejidos específicos del animal incluyendo la cutícula, celomocitos, hipodermis, el recto, la vulva y en las neuronas. Sin embargo, los animales GFP::MAI-1 mostraron a diferencia de los animales MAI-1::mCherry una mayor expresión de la MAI-1 en la cutícula (Figura 19, A-J).

De acuerdo con que MAI-1 no cuenta con una secuencia de transporte mitocondrial, GFP::MAI-1 no mostró un patrón de distribución que sugiriera redes mitocondriales. Se estudió si GFP::MAI-1 se expresa en las mitocondrias incubando los animales con Mitotracker Red CMXRos se encontró que no existe co-localización entre la sonda y GFP::MAI-1, esto al observar tejidos que se tiñen con Mitotracker Red CMXRos, como es la hipodermis del animal. Estos resultados sugieren que GFP::MAI-1 no se expresa en la mitocondria, pero si en el citoplasma y el núcleo del nematodo (Figura 19, K-P). Debido a que MAI-1 no parece tener la función canónica de IF_1 se decidió continuar con el estudio de MAI-2.

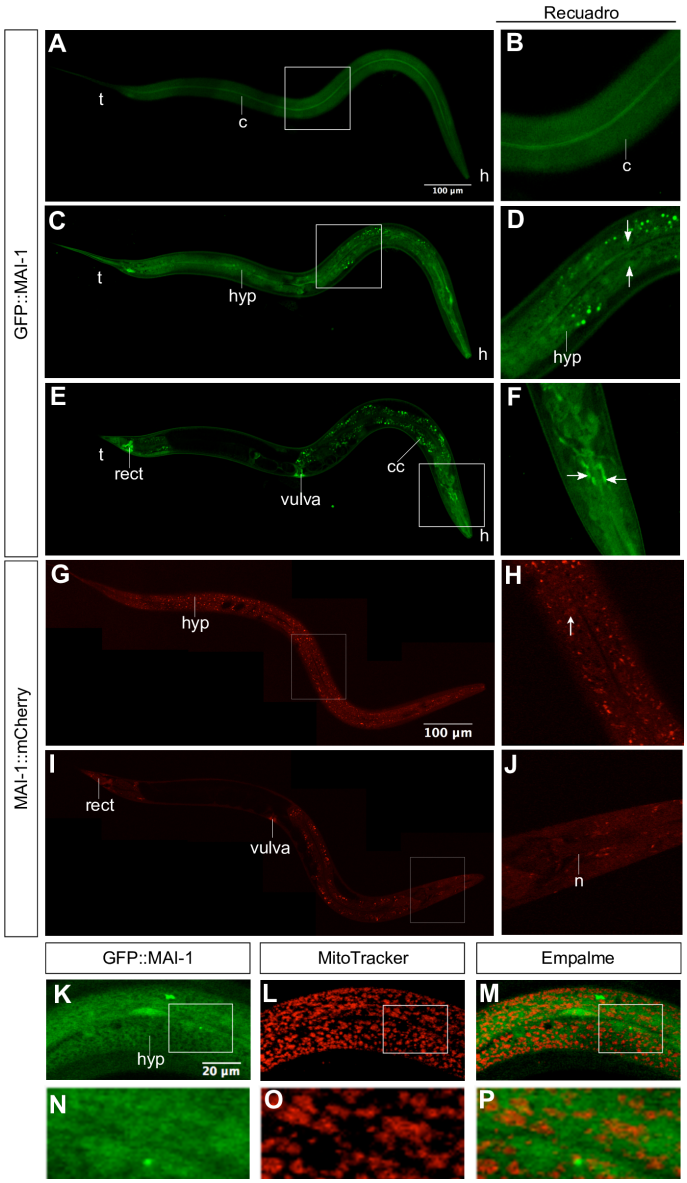

Figura 19. GFP::MAI-1 y MAI-1::mCherry se expresa en el citoplasma y no en la mitocondria. Se montaron adultos de un día que expresan los transgenes: *Pmai-1::gfp::mai-1 3'-UTR* y *Pmai-1::mai-1::mCherry::mai-1-3'UTR* se observaron en el microscopio confocal. Se observó expresión de GFP::MAI-1 en la cutícula (c) (A-B). GFP::MAI-1 y MAI-1::mCherry se expresaron en el citoplasma y en el núcleo (flecha) de la hipodermis (hyp) (C-D, G-H), en el recto (rect), la vulva, los celomocitos (cc) (E,I) y en las neuronas de la cabeza del animal (E,F,J). Los detalles de cada imagen se muestra en el recuadro. Se realizaron tinciones de los animales GFP::MAI-1 con MitoTracker CMX Ros y no se observó co-localización entre ellos (K-P). Los detalles de cada imagen se encuentran en la parte inferior (N-P). MAI-2 se expresa en la mitocondria de *C. elegans*.

MAI-2 se expresa en la mitocondria de *C. elegans.*

Durante la maestría se generaron animales transgénicos que expresan la proteína GFP en el C-terminal de la proteína MAI-2 (Figura 18, B*5*). Para esta construcción, se clonaron en tándem el promotor putativo de *mai-2* (1796 pb), seguido de la región codificante de *mai-2,* del ATG sin el codón de paro (852 pb) y una química del gen que codifica para la GFP (con intrones) fusionado al 3'-UTR de *mai-2* (1093 pb; para más detalles ver Materiales y Métodos). La construcción *Pmai-2::mai-2::GFP::mai-2-3'-UTR* se clonó en el plásmido pCFJ150 y se introdujo a los animales por biobalística (Praitis y colaboradores, 2001). Se obtuvieron 12 líneas transgénicas independientes, 3 de ellas mostraron expresión en el soma y la línea germinal. Se decidió estudiar el patrón de expresión en una línea transgénica que mostrara expresión en ambos tejidos. Para una descripción más detallada de la técnica y resultados revisar Fernández-Cárdenas, 2013.

Un conjunto no sincronizado de embriones que expresan a MAI-2::GFP se observaron en el microscopio de fluorescencia. Se observó la expresión de MAI-2::GFP en el citoplasma en todos los estadios embrionarios (Figura 20, A-L) y estadios post-embrionarios en un patrón que sugiere redes mitocondriales. Además, la expresión de MAI-2::GFP se observó en todos los estadios larvarios (L1-L4) (Figura 20, M-P), en el adulto hermafrodita y adulto macho así como en la larva dauer (Figura 20, Q-S). MAI-2 está presente en todos los tejidos del animal como es en las neuronas, faringe, intestino, el músculo de la pared y la hipodermis. Para una análisis más detallado de la expresión de MAI-2::GFP en los diferentes tejidos del nematodo revisar Fernández-Cárdenas, (2013).

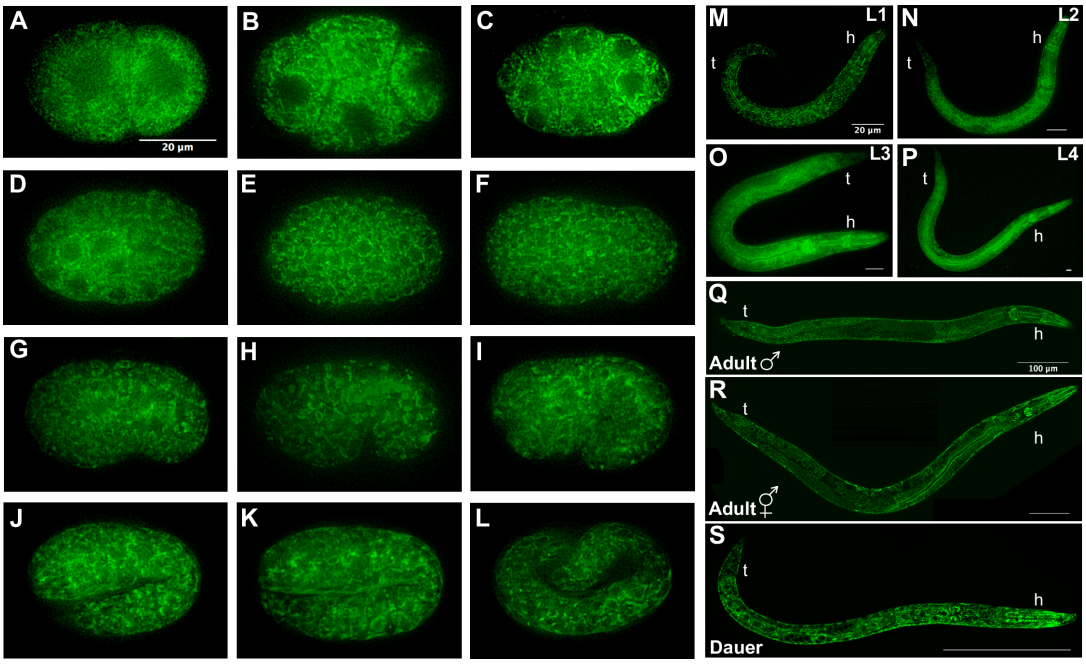

Figura 20. MAI-2::GFP se expresa en el soma y la línea germinal. Embriones, larvas y adultos que expresan el transgen *Pmai-2::mai-2::GFP::mai-2-3'UTR* se observaron en el microscopio de fluorescencia. (A-L) Embriónes, 2 células (A), 4 células (B), ~26-células (C), ~44-células (D), estadio de frijol (G), estadio de coma (H), 1.5-vueltas (I), 2-vueltas (K), 3-vueltas (L). (M-P) Larvas, L1 (M), L2 (N), L3 (O), L4 (P). Machos adultos (Q), hermafroditas adultos (R), larva dauer (S).

Para corroborar que MAI-2 tiene localización mitocondrial en *C. elegans*, se cruzó el transgénico que expresa MAI-2::GFP con los animales transgénicos *xmSi01* [*Pmex-5::tomm-20::mCherry::tbb-2 3'-UTR; Cbr-unc-119(+)*]II (elaborado por A. Emmanuel Villanueva-Chimal) y se buscó co-localización en condiciones fisiológicas. La cepa *xmSi01* expresa únicamente el fragmento amino de la proteína TOMM-20 regulado por el promotor *mex-5* que favorece su expresión únicamente en la células germinales y en embriones (Merritt y colaboradores, 2008). Encontramos que MAI-2::GFP co-localiza con la mitocondria en la gónada (Figura 21, A-C) y en los embriones (Figura 21, D-F).

Para corroborar la expresión de MAI-2::GFP en la mitocondria por medio de otra técnica, se realizó la tinción de los animales transgénicos que expresan MAI-2::GFP con la sonda mitocondrial MitoTracker Red CMXRos (Figura 21, G-O). Para este propósito, animales adultos de un día se incubaron en M9 con MitoTracker se montaron y observaron en el microscopio de fluorescencia. El Mitotracker Red CMXRos tiñe varios tejidos del animal, pero principalmente en las condiciones utilizadas pueden observarse adecuadamente las mitocondrias del músculo (Rolland, 2014) e

hipodermis (Yang y Hekimi, 2010), en donde se encontró co-localización (Figura 21, G-O). Estos resultados apoyan que MAI-2::GFP es una proteína mitocondrial.

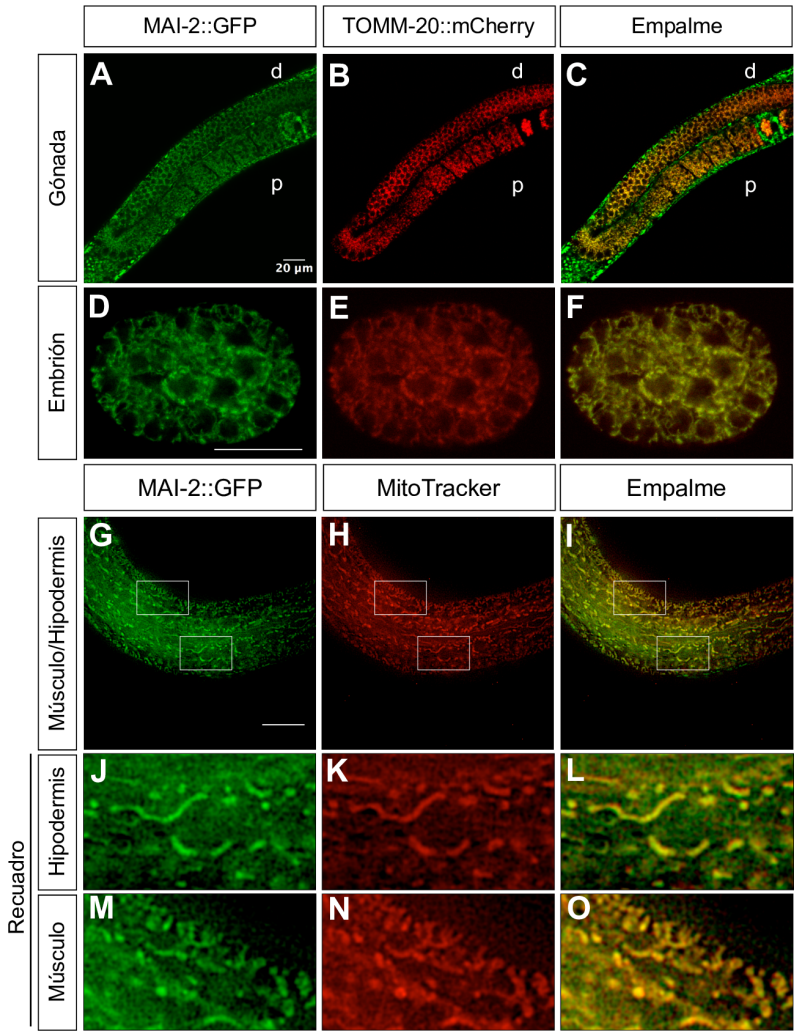

Figura 21. El reportero MAI-2::GFP se expresa en la mitocondria de *C. elegans.* (A-F) Se cruzó TOMM-20::mCherry con MAI-2::GFP. Se montaron y observaron animales adultos de un día en un microscopio confocal y se observó colocalización en las células germinales (A-C) y en embriones (D-F). Se tiñeron animales MAI-2::GFP con MitoTracker Red CMXRos se montaron y observaron en el microscopio de fluorescencia (G-O) se observó co-localización en la hipodermis (J-L) y en el músculo (M-O).

Las mutantes en *mai-2* no muestran fenotipo en condiciones fisiológicas.

Para estudiar los fenotipos generados por mutantes en *mai-2*, se generaron mutantes por CRISPR/Cas-9 en este gen (Friedland y colaboradores, 2013; Paix y colaboradores, 2014) (Figura 18, A*3,4*). El alelo *mai-2(xm18)* cuenta con la inserción del sito de restricción PvuII, que resulta en un codón de paro prematuro que ocasiona una proteína truncada de 41 amino ácidos. El alelo *mai-2(xm19)* cuenta con una deleción de 794 pb: 151 pb (de 261 pb) del primer exón, todo el intrón (525pb), exón 2 (69 pb) y 49 pb del UTR de *mai-2* que promueve una proteína truncada de 37 amino ácidos (Figura 22, A).

Para ver la abundancia de *mai-2* se usó RT-PCR semi-cuantitativo en las mutantes *mai-2(xm18)* y *mai-2(xm19)*. Se encontró que el mensajero en ambas mutantes se encuentra disminuído en un 90% (Figura 22, B). Estos resultados muestran que el mRNA que codifica para las proteínas truncas es poco abundante, posiblemente debido a que puede ser degradada por la maquinaria de decaimiento de "non-sense mediated RNA decay" (Baker y Parker 2004).

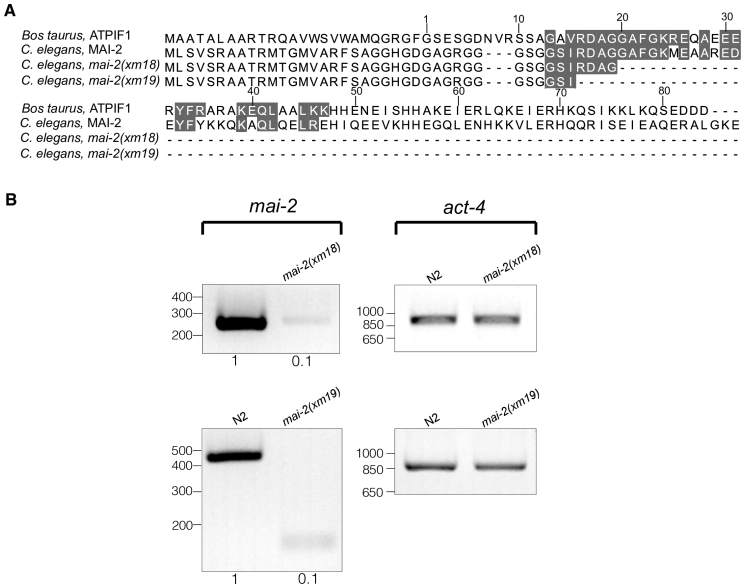

Figura 22. El mRNA de *mai-2* es poco abundante en las mutantes de *mai-2*.(A) Secuencia de aminoácidos de IF_1 de bovino (*Bos taurus*) y MAI-2 de *C. elegans* silvestre. Los residuos que forman la secuencia mínima de inhibición se muestran en gris. (B) RT-PCR semi-cuantitativo utilizando cDNA obtenido de extractos de animales adulto de 1 día N2 (control) y mutantes en *mai-2* (alelos *xm18* y *xm19*). Se realizó un análisis densitométrico analizando la banda que corresponde a *mai-2* con respecto a la banda control (*act-4*), los valores se muestran abajo de cada panel.

Las mutantes en *mai-2* fueron incubados a 20ºC y a simple vista no mostraron tener alteraciones en el fenotipo de manera evidente en tamaño, movilidad ni en el desarrollo. Para caracterizar con mayor detalle se cuantificó la progenie y la letalidad embrionaria de los animales mutantes y no se encontraron diferencias entre las mutantes en *mai-2* y la cepa silvestre N2 (Figura 23, A-B). Además se evaluó el tiempo de vida de los animales *mai-2(xm18)* y no se encontraron diferencias cuando se compararon con la cepa silvestre (Figura 23, C).

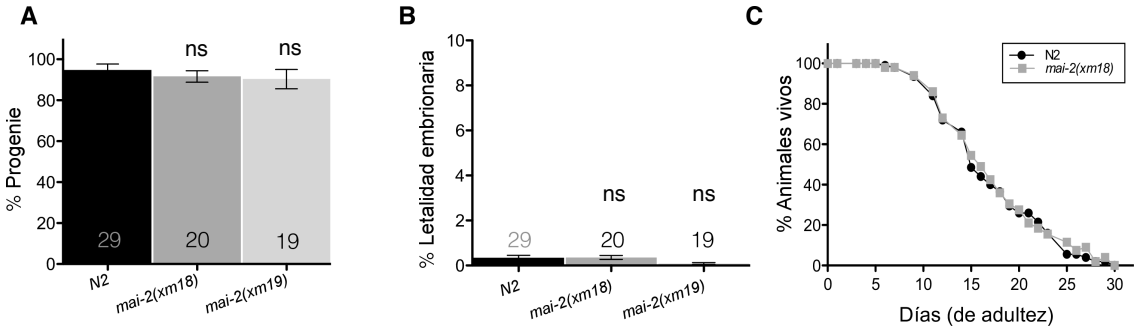

Figura 23. Los animales mutantes en *mai-2* no muestran defectos en el número de progenie ni en el tiempo de vida. (A-B) Los animales en estadio de L4 de la cepas N2 (control), *mai-2(xm18)* y *mai-2(xm19)* se transfirieron a nuevas cajas Petri cada 24 h durante el transcurso de 4 días a 20ºC. Los platos se cuantificaron para progenie (A) y letalidad embrionaria (B). Para la cepa N2, se muestra un promedio de 3 experimentos independientes, mientras que para *mai-2(xm18)* y *mai-2(xm19)* se muestran el promedio de dos (promedio±SEM). Se realizó una ANOVA de una vía seguido de una prueba Tukey, los animales mutantes para *mai-2* se compararon con los animales control (N2) y no resultó ser significativo (ns). El número de animales utilizados se muestra en cada barra. (C) Para la cuantificación del tiempo de vida, se midió el número de animales vivos cada dos días aproximadamente de las cepas N2 (control) y *mai-2(xm18)* hasta que todos los animales murieran. La interacción entre la cepa N2 y *mai-2(xm18)* se calculó por una ANOVA de dos vías y no fueron significativas. Se cuantificó el tiempo de vida de 50 animales por cada experimento.

Los animales mutantes en *mai-2* no muestran defectos en las redes mitocondriales, en el consumo de consumo, en la cantidad de ATP, ni en la dimerización de ATP sintasa, pero si muestran un $\Delta\psi_m$ incrementado.

A continuación se estudiaron los efectos de la mutación de *mai-2* en el $\Delta\psi_m$. Para medir el $\Delta\psi_m$ se incubaron a los animales control (N2) y a los animales *mai-2(xm18)* y *mai-2(xm19)* en medio NGM-lite con TMRM, una tinción fluorescente que puede permear a la célula y acumularse en la mitocondria y su brillantez es proporcional al $\Delta\psi_m$ (Andreux y colaboradores, 2014). La

fluorescencia del TMRM se cuantificó en la célula P_1 en embriones de dos células y en los animales adultos de un día (Palikaras y colaboradores, 2015). Se encontró que los animales *mai-2(xm18)* y *mai-2(xm19)* generaron un $\Delta\psi_m$ mayor que los animales control (N2) (Figura 24, A-B).

Para estudiar si la pérdida de MAI-2 tiene un efecto en la respiración, aproximadamente 10,000 animales en estadio de L4 a adultos jóvenes (animales adultos pero que aún no tienen embriones) se colectaron, lavaron durante 30 min para vaciar el intestino, se introdujeron a un oxímetro con temperatura regulada (20ºC) y se midió el consumo de oxígeno hasta que el trazo fue lineal (estado estacionario). Finalmente, se agregó cianuro de sodio (NaCN), un inhibidor del complejo IV de la cadena respiratoria, para comprobar que el consumo de oxígeno registrado proviniera de los complejos respiratorios mitocondriales. Los animales *mai-2(xm18)* y *mai-2(xm19)* no mostraron diferencias en el consumo de oxígeno cuando se compararon con los animales control (N2) (Figura 24, C) y se observó la inhibición del consumo de oxígeno en los animales control y mutantes posterior al NaCN.

También se determinó la cantidad de ATP total en los animales *mai-2* mutantes por medio de ensayos de bioluminiscencia y se observó una disminución del 15% en los animales *mai-2(xm18),* sin embargo, esta diferencia no fue significativa (Figura 24, D) , mientras que los animales *mai-2(xm19)* no presentaron diferencias al compararse con los animales control. Estos resultados indican que en ausencia de MAI-2, la cadena transportadora de electrones y la hidrólisis de ATP parecen no estar afectadas y que el defecto en el $\Delta\psi_m$ tiene otro origen.

Para determinar si en *C. elegans* la ausencia de *mai-2* afecta la morfología mitocondrial, se cruzó la mutante *mai-2(xm18)* con la cepa SD1347 *ccIs4251* I. Este transgen tiene una secuencia de importación mitocondrial fusionada al gen que codifica para la proteína GFP bajo el promotor de *myo-3* que expresa a la proteína GFP en las células musculares de la pared del animal (Liu y colaboradores, 2009). Los animales en L4 se anestesiaron, montaron y se determinó si las redes mitocondriales de las células musculares tenían un aspecto tubular (silvestre), fragmentadas, elongadas o agregadas. Se encontró que los animales control (*ccIs4251 I*) mostraron un 99.1% de células con redes tubulares, mientras que en los animales *ccIs4251*;*mai-2(xm18)* no se observaron defectos evidentes en la morfología de las redes mitocondriales y presentaron un 99.8% de células musculares con redes tubulares (Figura 24, E).

También se estudió la dimerización de la F_oF_1-ATP sintasa en la mutante *mai-2(xm18),* estos experimentos fueron realizados con ayuda de la Dr. Marietta Tuena de Gómez Puyou y José Concepción Nuñez. Por medio de geles azules nativos encontramos que las mutante en *mai-2* no mostraron diferencias en la proporción de dímero/monómero cuando se comparó con el control (N2). Estos resultados demuestran que en *C. elegans,* MAI-2 no es indispensable para la formación del dímero de ATP sintasa (Figura 24, F). Para verificar que las bandas del dímero y monómero correspondieran a la F_oF_1-ATP sintasa mitocondrial, se realizó una segunda dimensión a partir del dímero y monómero de los animales N2 y *mai-2(xm18)* y se observó a las subunidades α,β (~55 y ~50 kDa) y γ (~30 kDa) de la ATP sintasa, lo que nos confirmó que estábamos trabajando con el complejo adecuado. También se verificó la identidad de la F_oF_1-ATP sintasa por medio de geles de la actividad de la hidrólisis de ATP .

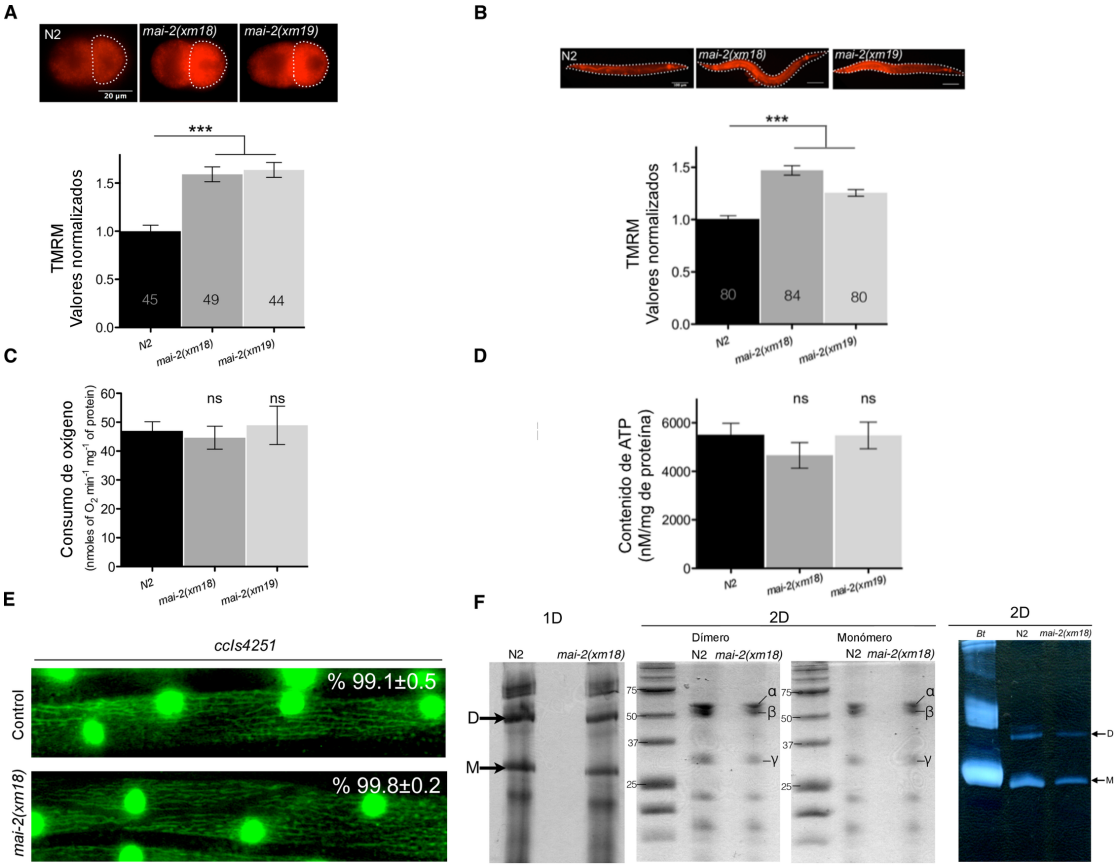

Figura 24. Las mutantes en *mai-2* tienen un $\Delta\psi_m$ más elevado y no se observaron alteraciones en el consumo de oxígeno, en la cantidad de ATP, morfología de las redes mitocondriales, ni en la proporción dímero/monómero de ATPasa. (A-B) Para evaluar el $\Delta\psi_m$, animales adultos de un día se incubaron en medio NGM-lite con TMRM por aproximadamente 15 h y se evaluó la fluorescencia de la célula P_1 en embriones de dos células y en el animal entero. Para los embriones N2 se mostró el promedio de 4 experimentos independientes, 4 para *mai-2(xm18)* y 2 para *mai-2(xm19)*. Para los animales enteros, se indica el promedio de seis experimentos independientes. Las barras muestran el promedio±SEM y adentro de cada barra se muestra el número de gusanos totales a los que se midió la fluorescencia. Los símbolos ***(P<0.0001) son la comparación entre el las mutantes en *mai-2* y la cepa N2. Los resultados se determinaron con una prueba Dunn´s ***P<0.0001. (C) Para cuantificar el consumo de oxígeno, animales en estadio de L4-adulto joven se introdujeron a un oxímetro y el consumo de O_2 se midió hasta que el trazo fue lineal. El consumo de oxígeno se normalizó con la cantidad de proteína. Un promedio de 4 experimentos independientes se muestran para N2 y *mai-2(xm18),* mientras que para *mai-2(xm19)* se muestran 2 experimentos. (D) Para la cuantificación de ATP, se extrajo y cuantificó el ATP de 50 animales adultos de un día por medio de un ensayo de bioluminiscencia, la cantidad de ATP se normalizó con la cantidad de proteína. Se muestra el promedio±SEM de 4 experimentos independientes. (E) Los animales de la cepa SD1347 *ccIs4251 I* [*Pmyo-3::gfp::LacZ+Pmyo-3::mitoGFP+dpy-20(+)*]I se cruzaron con los animales *mai-2(xm18),* se montaron y observaron en un microscopio de fluorescencia. Se analizaron las células musculares de la pared y las redes mitocondriales con apariencia tubular se cuantificaron. Se muestra el promedio±SEM de 2 experimentos independientes. (F) Se realizó un 1D BN-PAGE y un 2D SDS-PAGE de la F_oF_1-ATP sintasa purificada de *C. elegans* de los animales control y *mai-2(xm18).* Las flechas en el gel de 1D indican el dímero (D) y monómero (M). La 2D muestra las subunidades α,β y γ de la F_oF_1-ATP sintasa , además de un gel de actividad de hidrólisis de ATP.

MAI-2 se requiere para que los animales resistan al estrés.

Para examinar el papel de MAI-2 durante el estrés en el animal entero, se expusieron animales hermafroditas adultos de 1 día a diferentes concentraciones de NaCN y del desacoplante mitocondrial CCCP y se cuantificó la sobrevivencia de los animales. Se encontró que a concentraciones bajas de NaCN y CCCP los animales *mai-2(xm18)* y *mai-2(xm19)* no resultaron ser sensibles comparados con el control (concentraciones menores a los 75 mM o 75 uM respectivamente), pero en concentraciones mayores a 75 mM o 75 μM respectivamente, las mutantes de *mai-2* fueron más sensibles y murieron en un porcentaje mayor que el control (Figura 25, A y B).

Se ha reportado que a una alta temperatura se incrementa la hidrólisis de ATP en *C. elegans* (Yee y colaboradores, 2014), por lo que quisimos evaluar la sobrevivencia de los animales en ausencia de MAI-2. Se incubaron animales hermafroditas N2, mutantes *mai-2(xm18)* y *mai-2(xm19)* durante 12 h a 35ºC y se analizó la mortalidad de los animales cada 2 h. Durante las primeras 8 h de incubación no se observó una diferencia significativa entre los animales control y las mutantes *mai-2(xm18)*. Sin embargo, a las 12 h de choque de calor se observó que 60% de los animales mutantes se encontraban muertos con respecto a los animales control (Figura 25, C).

Para determinar sí MAI-2 participa en la resistencia a estrés oxidativo, se incubaron los animales control y mutantes en *mai-2* en presencia de 200 mM de paraquat, un compuesto que causa la producción de ROS mitocondrial. Se observó que los animales mutantes se murieron un 30% más que los animales control a las 12 h de incubación con paraquat, demostrando que los animales mutantes son más vulnerables en estrés oxidativo (Figura 25, D).

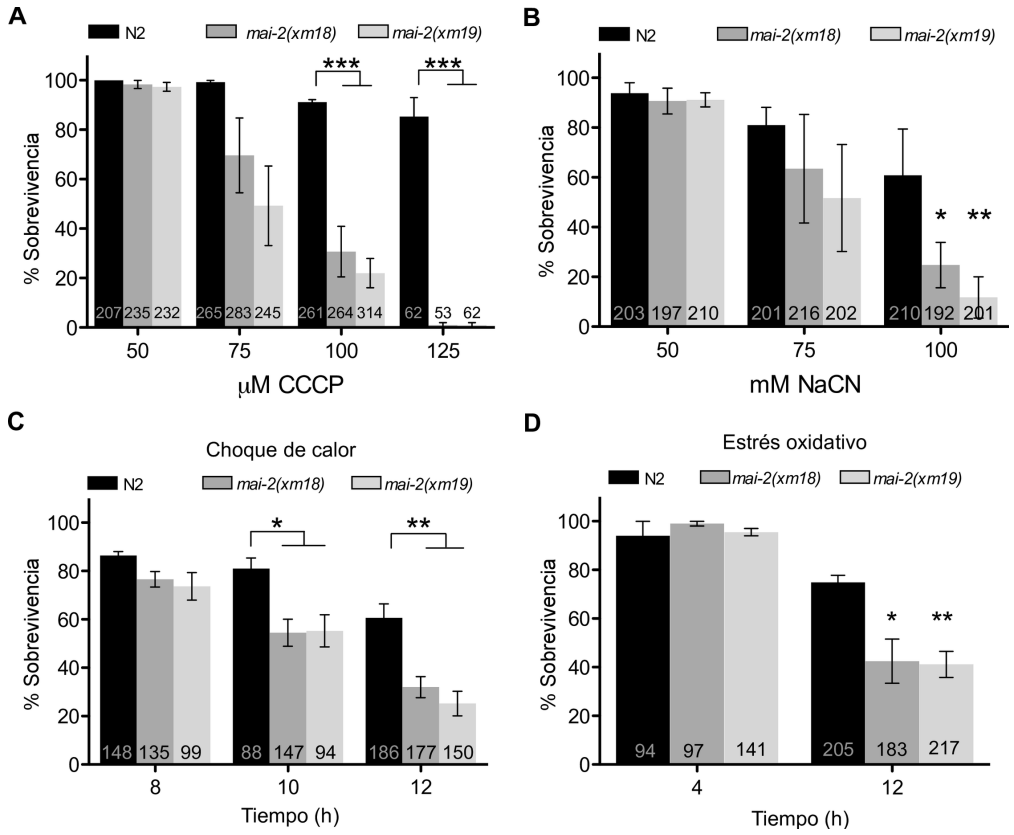

Figura 25 MAI-2 se requiere para la sobrevivencia en condiciones de estrés. (A-B) Se expuso durante 1 h a animales sincronizados adultos de un día N2, *mai-2(xm18)* y *mai-2(xm19)* a diferentes concentraciones de CCCP (A) y NaCN (B) y se recuperaron durante 1 h en medio NGM-lite sembradas con bacterias OP50. Para los experimentos con CCCP se realizó un promedio de 4 experimentos, mientras que para NaCN se muestra un promedio de 3 experimentos. (C) Se realizó choque de calor a 35ºC a 4 días de adulto del genotipo indicado durante 12 h y cada 2 horas se evaluó la sobrevivencia. Para los animales N2 y *mai-2(xm18)* se muestra un promedio de cuatro experimentos, mientras que para *mai-2(xm19)* se muestra un promedio de dos experimentos. (D) Se incubaron animales adultos de un día en 200 mM de paraquat y se midió la sobrevivencia cada 4 horas en un intervalo de 12 h. Se muestra un promedio de 3 experimentos. (A-D) Los animales se cuantificaron por la pérdida de movimiento después de ser tocados con el asa de platino. Los datos representan promedio±SEM. El número de animales observados se expresa adentro de cada barra. Se realizó una ANOVA de dos vías (prueba de Bonferroni) para comparar cada condición con el control. ****P*=0.001, ***P*=0.01, **P*=0.05.

MAI-2 se requiere para inducir apoptosis por estrés.

Se examinó la apoptosis somática durante la embriogénesis, en los estadios embrionarios de coma, pretzel y en las larvas L1. No observamos diferencias en la apoptosis somática entre los animales control y animales mutantes en *mai-2* (Tabla 3). Estos experimentos fueron realizados por la M. en C. Laura Silvia Salinas.

Tabla 3. Los animales mutantes en *mai-2* no muestran diferencias significativas en la apoptosis somática.

Estadío	Genotipo		
	N2	*mai-2(xm18);ced-1(RNAi)*	*mai-2(xm19);ced-1(RNAi)*
Embrión (frijol)	1.67±0.1	1.63±0.1	1.66±0.1
Embrión (pretzel)	2.61±0.2	2.48±0.1	2.64±0.1
Larva L1	1.37±0.1	1.38±0.1	1.34±0.1

También se examinó la apoptosis de las células germinales en el animal adulto en los organismos control, *mai-2(xm18)* y *mai-2(xm19)*. Para cuantificar la apoptosis de las células germinales se cruzaron las mutantes en *mai-2(xm18) y mai-2(xm19)* con la cepa MD701 que se utilizó para cuantificar cuerpos apoptóticos por medio de microscopía de fluorescencia. Los animales *ced-1:gfp*, *ced-1::gfp;mai-2(xm18)* y *ced-1::gfp;mai-2(xm19)* se crecieron a 24ºC y 24 h post-L4 se montaron en placas de agarosa para el conteo de cuerpos apoptóticos. Se encontró que los animales mutantes en *mai-2* presentaron una menor apoptosis comparada con el control (Figura 26, A).

En el caso del estrés oxidativo, se evaluó el papel de MAI-2 en la apoptosis de células germinales inducida por estrés como el ayuno, choque de calor, estrés a UV-C y estrés oxidativo (Salinas y colaboradores, 2006). Los animales control de la cepa *ced-1::gfp* mostrararon un incremento en la apoptosis después del ayuno, choque de calor e irradiación con rayos UV-C. Los animales *ced-1::gfp;mai-2(xm18)* mostraron un incremento en condiciones de ayuno, sin embargo, para el choque de calor y radiación UV-C se observó una inducción parcial (Figura 26, B).

Para inducir estrés oxidativo, se incubaron las cepas *ced-1::gfp* y *ced-1::gfp;mai-2(xm18)* durante 1 h en paraquat (10mM), se dejaron recuperar durante 1 h y después del periodo de recuperación se montaron los animales y se contaron los cuerpos apoptóticos en un microscopio de fluorescencia. Se encontró que los animales *ced-1::gfp* mostraron un incremento en el número de cuerpos apoptóticos, pero los animales *ced-1::gfp;mai-2(xm18)* y *ced-1::gfp;mai-2(xm19)* no mostraron un incremento significativo o mostraron un incremento parcial respectivamente (Figura 26, C). Nuestros resultados muestran que MAI-2 es necesaria para inducir la apoptosis en la gónada en condiciones fisiológicas, estrés oxidativo, choque de calor y UV-C. Sin embargo, MAI-2 no muestra tener un rol en la apoptosis somática que ocurre en la embriogénesis tardía y en estadios

larvarios.

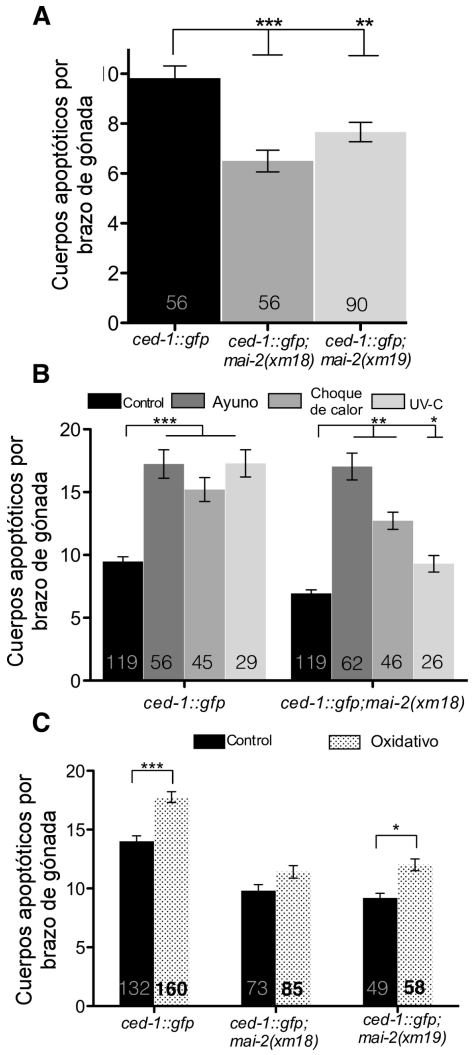

Figura 26. MAI-2 es importante para inducir apoptosis en condiciones fisiológicas o en condiciones de estrés. La apoptosis de las células germinales en mutantes *mai-2* se cuantificó utilizando la cepa MD701 *bcIs39*[*Plim-7::ced-1::gfp; lin-15*(+)] en la cual los cuerpos apoptóticos pueden visualizarse bajo un microscopio de fluorescencia. Los cuerpos apoptóticos por brazo de gónada se contaron en adultos de 1 día del genotipo indicado en condiciones fisiológicas (A) y en condiciones de estrés (B-C). Los animales se sometieron a ayuno, choque de calor, irradiación UV-C (B) y paraquat (C). Se muestra el promedio de 3 experimentos independientes para la apoptosis fisiológica, mientras que para la apoptosis por estrés se muestra el promedio de dos experimentos independientes. Las barras representan promedio±SEM y adentro de cada barra se indica el número de animales analizados. Se realizó una prueba de Dunn´s para comparar cada condición con el control. ***P<0.0001, ** P<0.001, *P<0.01. El número de animales analizados se muestra en cada barra.

VII. Discusión

MAI-1 y MAI-2 se expresan diferencialmente.

En este estudio, mostramos la expresión de MAI-1 y MAI-2 mediante proteínas de fusión y durante el desarrollo de *C. elegans.* Encontramos que MAI-2::GFP se expresa en la mitocondria de todos los tejidos del nematodo a través del desarrollo embrionario y larvario (Figura 20). Ichikawa y colaboradores, encontraron que MAI-1 no tiene una secuencia de transporte predecible a la mitocondria, y que en la levadura MAI-1 no se asocia a la mitocondria, sin embargo, no podemos descartar que ciertas interacciones proteína-proteína podrían dirigir MAI-1 a la mitocondria en el nematodo. Por otro lado, encontramos que la proteína de fusión GFP::MAI-1 no está asociada a la mitocondria y se expresa en el citoplasma de tejidos específicos tales como la cutícula, hipodermis, neuronas de la cabeza, recto, celomocitos y vulva (Figura 19, A-J). Inesperadamente, MAI-1 también fue encontrada en el núcleo de ciertas células aunque carece de una secuencia NES típica (Figura 19, D). Por la localización tejido-específico observada y su localización nuclear, MAI-1 permanece como un blanco interesante para la investigación futura.

En condiciones normales las mutantes en *mai-2* mostraron incremento en el $\Delta\psi_m$ y una menor apoptosis de las células germinales.

En condiciones fisiológicas, no observamos una alteración en el fenotipo en las mutantes de *mai-2* cuando evaluamos el tiempo de vida, fertilidad y letalidad embrionaria (Figura 23). Este trabajo respalda las observaciones hechas por Nakamura y colaboradores, en el cual en condiciones fisiológicas no se observaron alteraciones en el crecimiento y fertilidad de ratones mutantes en IF_1. Además, no observamos defectos en la morfología de las redes mitocondriales del músculo de la pared del nematodo (Figura 24, E), ni en la proporción dímero/monómero de la ATP sintasa (Figura 24, F). Recientemente, los grupos de Campanella y Yoshida colaboraron para observar defectos en las mitocondrias en células HeLa con la expresión disminuída de IF_1 y encontraron mitocondrias con crestas anormales y una menor cantidad de las mismas (Faccenda y colaboradores, 2017). Sería interesante estudiar con mayor detalle la ultra-estructura de las mitocondrias y la dinámica de redes mitocondriales en la mutante *mai-2* en condiciones fisiológicas y estrés.

El $\Delta\psi_m$ es importante para la función mitocondrial y cuando se pierde resulta letal para la mitocondria, debido a que se detiene la producción de ATP por la F_oF_1-ATP sintasa, al igual que la dinámica mitocondrial y el transporte de proteínas dependiente de $\Delta\psi_m$ (Mootha y colaboradores,

2001; Waterhouse, 2001). En nuestro trabajo demostramos que las mutantes en *mai-2* tienen un $\Delta\psi_m$. mayor al control. De manera similar a lo reportado por Fujikawa y colaboradores (2012) y Shah y colaboradores (2013) en cultivos celulares que tienen disminuída la expresión de IF_1 (Figura 24, A y B). En estos trabajos, también observaron una menor cantidad de ATP total, ellos explican que el incremento en el $\Delta\psi_m$ se puede deber a un incremento en la actividad hidrolítica del ATP por la F_oF_1-ATPasa. Sin embargo, nosotros no observamos diferencias significativas en la cantidad de ATP en animales mutantes en *mai-2,* posiblemente debido a vías compensatorias productoras de ATP, como la glucólisis. Barbato y colaboradores (2015) disminuyeron la expresión de IF_1 en células de osteosarcoma y encontraron un $\Delta\psi_m$ elevado con respecto al control sin diferencias en la cantidad de ATP, como lo observamos nosotros. Para mejorar nuestras observaciones proponemos medir la cantidad de ATP de los animales mutantes en *mai-2*, en condiciones fisiológicas, en presencia de CCCP e inhibidores de la glucólisis (p.ej. 2-deoxiglucosa). Adicionalmente, al igual que Fujikawa y colaboradores, 2012; Shah y colaboradores, 2013; Barbato y colaboradores, (2015) nosotros cuantificamos la cantidad de $\Delta\psi_m$ por medio de TMRM, el cual se usa ampliamente para medir el $\Delta\psi_m$ en cultivos celulares y en *C. elegans;* sin embargo, sabemos la importancia de mejorar la técnica para cuantificar la cantidad de $\Delta\psi_m$, por lo que proponemos probar otras tinciones (p.ej. rodamina B hexil ester, HRB, HRB101 y rodamina 6G) que aunque no han sido usadas para medir $\Delta\psi_m$ en *C. elegans* sino para observar redes mitocondriales podrían ser de utilidad para mejorar nuestros resultados (revisado en Rolland, 2014).

Aunque su relación aún no se entiende del todo, la pérdida del $\Delta\psi_m$ está asociado a la apoptosis (Ly y colaboradores, 2003; Tait y colaboradores, 2010). Se piensa que el poro de transición (PTP) libera ciertos factores mitocondriales apoptogénicos y su apertura se favorece con una disminución o pérdida del $\Delta\psi_m$ (Ly y colaboradores, 2003). En nuestro trabajo encontramos que las mutantes en *mai-2* tienen un apoptosis fisiológica significativamente más baja (Figura 26, A). Además, observamos que mutantes en *mai-2* tienen una respuesta apoptótica parcial al estrés como en el caso del choque de calor, exposición a UV-C y estrés oxidativo (Figura 26, B-C). En contraste, los animales mutantes en *mai-2* no muestran cambios en la apoptosis somática. La apoptosis somática se regula de manera diferente a la apoptosis de la línea germinal. La apoptosis en el soma (embriónes y larvas L1) es regulada por la proteína apoptótica EGL-1 (proteína con dominio BH-3-only), mientras que la apoptosis fisiológica de las células germinales es inducida parcialmente en el nematodo por la proteína homóloga al Retinoblastoma LIN-35 e independiente de EGL-1. Diferentes vías inducen la apoptosis de células germinales durante estrés en *C. elegans*

(Salinas y colaboradores, 2006), la apoptosis inducida por daño a DNA se regula en el nematodo por el homólogo de p53, CEP-1 (Schumacher y colaboradores, 2001). El choque de calor y estrés oxidativo induce la apoptosis de las células germinales por la vía de MAPK (Salinas y colaboradores, 2006). Por otro lado, mientras que la apoptosis de las células germinales por ayuno es inducida por la disminución de la expresión de CED-9/BCL-2 (Lascarez-Lagunas y colaboradores,, 2014).

Nosotros hipotetizamos que puede haber una co-relación entre la menor apoptosis de células germinales observada y el alto $\Delta\psi_m$ observado en mutantes de *mai-2*. Chen y colaboradores (2014) propusieron que la deficiencia de IF_1 en células KBM7 induce el mantenimiento del $\Delta\psi_m$ cuando el complejo III de la cadena transportadora de electrones es inhibido, promoviendo la sobrevivencia celular y la salud mitocondrial. IF_1 también ha sido propuesta como una proteína anti-apoptótica directamente relacionado con el mantenimiento de las crestas mitocondriales y la integridad de la red mitocondrial (Faccenda y colaboradores, 2013). Faccenda y colaboradores (2013) demostraron en células que la disminución de IF_1, provoca defectos en las crestas mitocondriales, propiciando la liberación de cyt *c* y la cascada apoptótica al ser tratadas con estaurosporina.

Aunque en *C. elegans* no existe evidencia de la permeabilización de la membrana externa mitocondrial o la liberación de cyt *c* durante la apoptosis, la redes mitocondriales sí se afectan y las mitocondrias tubulares se vuelven fisionadas (Jagasia y colaboradores, 2005), también existe evidencia de que factores como WAH-1 (Wang y colaboradores, 2002) y CPS-6 (Parrish y colaboradores, 2001) se liberan de la mitocondria y son importantes para su ejecución (Seervi y colaboradores, 2015). Estos cambios estructurales que ocurren en la mitocondria durante la apoptosis, nos llevó a hipotetizar que un $\Delta\psi_m$ elevado podría conservar una configuración ortodoxa de la morfología mitocondrial que cause la disminución de los eventos apoptóticos (Gottlieb y colaboradores, 2003). Dicha hipótesis podría probarse analizando la dinámica mitocondrial de las mutantes en *mai-2* al ser sometidos a un estrés, analizando las redes mitocondriales principalmente en la zona de paquíteno (asa de la gónada), zona en donde ocurre la aparición de cuerpos apoptóticos. Nuestro trabajo sugiere que cambios en el $\Delta\psi_m$ podrían jugar un papel menos importante en la apoptosis somática en *C. elegans* pero es importante para la protección de células germinales de la muerte por apoptosis.

MAI-2 protege a *C. elegans* del estrés.

En nuestro trabajo, estudiamos la sobrevivencia de mutantes deficientes en IF_1 (MAI-2), cuando se trataron con cianuro (un inhibidor del complejo IV), CCCP (un desacoplante), choque de calor y paraquat (un generador de ROS mitocondrial). Encontramos que las mutantes en *mai-2* fueron más sensibles al cianuro o al CCCP (Figura 25 A y B) y de manera menos dramática pero consistente, al choque de calor o al estrés oxidativo (Figura 25, C y D). Los nematodos pueden estar expuestos a diferentes tipos de estrés en su medio ambiente silvestre, como a cambios en la temperatura, distribución desigual del oxígeno en la tierra o puede estar expuesto a patógenos como la bacteria *Pseudomonas aeruginosa* que produce cianuro como factor tóxico principal que mata al nematodo (Saldanha y colaboradores, 2013). Por todo esto, nosotros proponemos que MAI-2 es necesario para la protección de los animales del estrés. Similarmente, Fujikawa y colaboradores, (2012) y Campanella y colaboradores, 2008 observaron que células con la expresión de IF_1 disminuida mueren con mayor rapidez comparados con las células control. En contraste, Chen y colaboradores (2014) demostraron que la ausencia de IF_1 incrementó la sobrevivencia de las células cuando se trataron con un inhibidor del complejo III. Estas diferencias pueden deberse a las diferentes líneas celulares utilizadas entre grupos, así como a los distintos métodos utilizados para disminuir la expresión de IF_1.

En este trabajo demostramos que MAI-2 juega un rol importante en la apoptosis probablemente por la regulación del $\Delta\psi_m$. Adicionalmente, demostramos que la función de MAI-2 se observa principalmente durante el estrés.

VIII. Conclusiones

1. MAI-2::GFP se expresan en redes mitocondriales de forma ubicua durante la embriogénesis y en todos los estadios larvarios/adulto (hermafrodita, macho) y en la larva dauer.

2. GFP::MAI-1 y MAI-1::mCherry se expresan en el citoplasma y en los núcleos de la hipodermis, células de la vulva, neuronas y en el recto, pero no se expresa en la mitocondria.

4. Los animales mutantes en el gen *mai-2* no mostraron un fenotipo evidente.

Los animales mutantes en *mai-2* no mostraron a simple vista tener alteraciones en el fenotipo, además no presentaron diferencias en el número de progenie, en la letalidad embrionaria o en el tiempo de vida.

5. Los animales mutantes en el gen *mai-2* presentaron un elevado $\Delta\psi_m$ en embriones y en el animal completo.

6. Los animales mutantes en el gen *mai-2* no mostraron diferencias en el consumo de oxígeno, en la morfología de las redes mitocondriales, proporción dímero/monómero de ATP sintasa, ni en las cantidades de ATP total.

7. Los animales mutantes en *mai-2* tuvieron una menor sobrevivencia ante el estrés.

Se encontró que los animales mutantes en *mai-2* sobrevivieron menos que los animales control en condiciones de choque de calor, CCCP, cianuro y paraquat.

8. Los animales mutantes en *mai-2* presentaron menor apoptosis fisiológica.

9. Los animales mutantes en *mai-2* presentaron respuesta apoptótica parcial ante el estrés.

Los animales mutantes en *mai-2* presentaron una respuesta apoptótica parcial ante el estrés por choque de calor, UV-C y estrés oxidativo, sin embargo, sí respondieron de igual manera que el control ante el estrés por ayuno.

IX. Perspectivas

1. **Continuar con el estudio de la falta de *mai-2* en parámetros mitocondriales, sobrevivencia y muerte celular.**

- Evaluar diferentes sondas que midan el $\Delta\psi_m$ en las mutantes en *mai-2*. En nuestro trabajo usamos la sonda TMRM para cuantificar el $\Delta\psi_m$, el TMRM ha sido ampliamente utilizado en el estudio de la IF_1 en cultivos celulares (Campanella y colaboradores, 2008; Fujikawa y colaboradores, 2013; Shah y colaboradores, 2012; Chen y Birsoy, 2014; Formentini y colaboradores, 2012; Barbato y colaboradores, 2015). Además, su uso en el animal entero y embriones ha sido utilizado en *C. elegans* para la cuantificación del $\Delta\psi_m$ y en la visualización de redes mitocondriales (Palikaras y colaboradores, 2015; Green y colaboradores, 2014, respectivamente). Sin embargo, consideramos que el uso de otras tinciones como la rodamina B hexil ester, rodamina 6G, DiS-C3(3), HRB y HR101 que se han utilizado previamente en la visualización de redes mitocondriales (Green y colaboradores) podría hacer más robusto nuestro dato.

Además consideramos importante encontrar las condiciones en donde pueda visualizarse en el animal entero, embrión o tejido, la pérdida o el mantenimiento del $\Delta\psi_m$ en presencia de un desacoplante o inhibidor de la cadena respiratoria.

- Evaluar cambios en la cantidad de ATP en los animales mutantes en *mai-2* en presencia de un desacoplante o inhibidor de la cadena respiratoria. En nuestro trabajo se estudió la cantidad de ATP en la cepa silvestre y mutante en *mai-2* en condiciones fisiológicas, sin embargo resulta interesante conocer la cantidad de ATP en presencia de un desacoplante o inhibidor de la cadena.

- Analizar la ultra-estructura de las mitocondrias de los animales mutantes en *mai-2*. Campanella y colaboradores (2008), encontraron por medio de microscopia electrónica que células con la expresión de IF_1 disminuida tenían menos crestas mitocondriales que las células control. Para evaluar la estructura de las crestas mitocondriales, así como su abundancia y distribución celular en las mutantes de *mai-2* proponemos hacer microscopia electrónica del músculo del animal.

- Determinar el mecanismo por el cual los animales mutantes en *mai-2* son más sensibles al estrés. Previamente, se encontró que la sobre-expresión de IF_1 incrementa ROS mitocondrial y esto activa la vía de NFkB incrementando BcL-xL que protege de la muerte celular. Además Nrf-2 también se induce incrementando la protección con la el estrés oxidativo. En esta perspectiva, se busca encontrar vías de señalización que en condiciones fisiológicas o en estrés se encuentren alteradas en los animales *mai-2* mutantes.

- Estudiar si existe relación entre la apoptosis de las células germinales y cambios en el $\Delta\psi_m$ en *C. elegans* y cómo la dinámica mitocondrial se relaciona con estos cambios. Proponemos estudiar en *C. elegans* cómo el aumento en el $\Delta\psi_m$ afecta la apoptosis de las células germinales y vincular esta hipótesis con la dinámica mitocondrial, la cual se ha visto afectada tanto la apoptosis de *C. elegans* como en la pérdida o mantenimiento del $\Delta\psi_m$.

2. Estudiar los efectos de la falta de expresión de MAI-1 en *C. elegans.*

- Explorar cambios en la expresión de GFP::MAI-1 en condiciones de estrés (p.ej. en choque de calor).

- Explorar cambios en la expresión de GFP::MAI-1 en condiciones fisiológicas y de estrés (p.ej. en choque de calor) en un fondo genético de *mai-2(xm18)*.

- Determinar las neuronas en las que se expresa GFP::MAI-1 y estudiar el posible papel que desempeña MAI-1 desde un enfoque neurobiológico.

- Realizar una mutación nula para el gen *mai-1* y evaluar los fenotipos generados por la ausencia de *mai-1*.

- Realizar una doble mutante para los genes *mai-1* y *mai-2* y evaluar los fenotipos.

X. Referencias Bibliográficas

Abrahams, J. P., Leslie, A. G., Lutter, R. and Walker, J. E. (1994) "Structure at 2.8 A resolution of F_1-ATPase from bovine heart mitochondria" *Nature*, 370(6491), pp. 621–628.

Althoff, T., Mills, D. J., Popot, J.-L. and Kühlbrandt, W. (2011) "Arrangement of electron transport chain components in bovine mitochondrial supercomplex $I_1 III_2 IV_1$" *The EMBO Journal*, 30(22), pp. 4652–4664.

Andreux, P. A., Mouchiroud, L., Wang, X., Jovaisaite, V., Mottis, A., Bichet, S., Moullan, N., Houtkooper, R. H. and Auwerx, J. (2014) "A method to identify and validate mitochondrial modulators using mammalian cells and the worm *C. elegans*" *Sci Rep*, 4, p. 5285.

Arselin, G., Giraud, M.F., Dautant, A., Vaillier, J., Bre` thes, D., Coulary-Salin, B., Schaeffer, J., and Velours, J. (2003). "The GxxxG motif of the transmembrane domain of subunit e is involved in the dimerization/oligomerization of the yeast ATP synthase complex in the mitochondrial membrane." *Eur. J. Biochem. 270*, 1875–1884.

Baker, K. E. and Parker, R. (2004) "Nonsense-mediated mRNA decay: Terminating erroneous gene expression" *Current Opinion in Cell Biology*, 16(3), pp. 293–299.

Ball, E. H. and Singer, S. J. (1982) "Mitochondria are associated with microtubules and not with intermediate filaments in cultured fibroblasts." *Proceedings of the National Academy of Sciences of the United States of America*, 79, pp. 123–126.

Barbato, S., Sgarbi, G., Gorini, G., Baracca, A. and Solaini, G. (2015) "The Inhibitor Protein (IF_1) of the F_1F_0-ATPase Modulates Human Osteosarcoma Cell Bioenergetics" *The Journal of biological chemistry*, 290(10), pp. 6338–48.

Bird A.F. and Bird J. (1991). "The structure of nematodes". Academic Press, California.

Bollag, D. M. and Edelstein, S. J. (1991) Protein methods in *ISBN 0471568716*, p. 230.

Boyer, P. D. (1997) "The ATP synthase-a splendid molecular machine" *Annual review of biochemistry*, 66, pp. 717–49.

Bravo, C. y colaboradores. (2004). "Overexpression of the inhibitor protein IF_1 in AS-30D hepatoma produces a higher association with mitochondrial F_1F_0 ATP synthase compared to normal rat liver: Functional and cross-linking studies." *Journal of Bioenergetics and Biomembranes*, 36(3), pp.257–264.

Brenner, S. (1973) "The genetics of behaviour," *British Medical Bulletin*, 29(3), pp. 269–271.

Brenner, S. (1974) "The genetics of *Caenorhabditis elegans*" *Genetics*, 77(1), pp. 71–94.

Buchner y Seydoux (1994) "Gastrulation in the nematode *Caenorhabditis elegans*" *Seminars in Developmental Biology*, 5, pp. 121–130.

Burwick, M. L. Wahl, J. Fang y colaboradores, “An inhibitor of the F_1 subunit of ATP synthase (IF_1) modulates the activity of angiostatin on the endothelial cell surface” *The Journal of Biological Chemistry*, vol. 280, no. 3, pp. 1740–1745, 2005.

Byerly, L., Cassada, R. C. and Russell, R. L. (1976) “The life cycle of the nematode *Caenorhabditis elegans*” *Developmental Biology*, 51(1), pp. 23–33.

Cabezón, E., Arechaga, I., Butler, P. J. G. and Walker, J. E. (2000) “Dimerization of bovine F1-ATPase by binding the inhibitor protein, IF_1” *Journal of Biological Chemistry*, 275(37), pp. 28353–28355.

Cabezón, E., Runswick, M. J., Leslie, a G. and Walker, J. E. (2001) “The structure of bovine IF(1), the regulatory subunit of mitochondrial F-ATPase.,” *The EMBO journal*, 20(24), pp. 6990–6.

Campanella, M., Casswell, E., Chong, S., Farah, Z., Wieckowski, M. R., Abramov, A. Y., Tinker, A. and Duchen, M. R. (2008) “Regulation of Mitochondrial Structure and Function by the F1Fo-ATPase Inhibitor Protein, IF_1,” *Cell Metabolism*, 8(1), pp. 13–25.

Campanella, M., Seraphim, A., Abeti, R., Casswell, E., Echave, P. and Duchen, M. R. (2009) “IF1, the endogenous regulator of the F_1F_o-ATPsynthase, defines mitochondrial volume fraction in HeLa cells by regulating autophagy” *Biochimica et Biophysica Acta - Bioenergetics*, 1787(5), pp. 393–401.

Capaldi, R. A. and Aggeler, R. (2002) “Mechanism of the F_1F_0-type ATP synthase, a biological rotary motor” *Trends in Biochemical Sciences*, 27(3), pp. 154–160.

Carlos Giovanni, S. G. and Rosa, E. N. (2013) “The *C. elegans* TIA-1/TIAR homolog TIAR-1 is required to induce germ cell apoptosis” *Genesis*, 51(10), pp. 690–707.

Cassada, R. C. and Russell, R. L. (1975) “The dauer larva, a post-embryonic developmental variant of the nematode *Caenorhabditis elegans*” *Developmental Biology*, 46(2), pp. 326–342.

Chen, W. W., Birsoy, K., Mihaylova, M. M., Snitkin, H., Stasinski, I., Yucel, B., Bayraktar, E. C., Carette, J. E., Clish, C. B., Brummelkamp, T. R., Sabatini, D. D. and Sabatini, D. M. (2014) “Inhibition of ATPIF1 ameliorates severe mitochondrial respiratory chain dysfunction in mammalian cells” *Cell Reports*, 7(1), pp. 27–34.

Conradt B, Horvitz HR. “The *C. elegans* Protein EGL-1 is required for programmed cell death and interacts with the Bcl-2-like protein CED-9.” *Cell*. 1998;93: 519–529.

Cortes-Hernandez, L. Dominguez-Ramirez, A. Estrada- Bernal y colaboradores, “The inhibitor protein of the F_1F_0-ATP synthase is associated to the external surface of endothelial cells” *Biochemical and Biophysical Research Communications*, vol. 330, no. 3, pp. 844–849, 2005.

Crittenden, S. L., Troemel, E. R., Evans, T. C. and Kimble, J. (1994) “GLP-1 is localized to the mitotic region of the *C. elegans* germ line” *Development*, 120, pp. 2901–2911.

Davies, K. M., Anselmi, C., Wittig, I., Faraldo-Gomez, J. D. and Kuhlbrandt, W. (2012) "Structure of the yeast F_1F_0-ATP synthase dimer and its role in shaping the mitochondrial cristae" *Proceedings of the National Academy of Sciences*, 109(34), pp. 13602–13607.

Dernburg, A. F., McDonald, K., Moulder, G., Barstead, R., Dresser, M. and Villeneuve, A. M. (1998) "Meiotic recombination in *C. elegans* initiates by a conserved mechanism and is dispensable for homologous chromosome synapsis" *Cell*, 94(3), pp. 387–398.

Derry, W. B., Putzke, A. P. and Rothman, J. H. (2001) "*Caenorhabditis elegans* p53: role in apoptosis, meiosis, and stress resistance" *Science*, 294(5542), pp. 591–595.

Dienhart, M., Pfeiffer, K., Schagger, H. and Stuart, R. a (2002) "Formation of the yeast F_1F_0-ATP synthase dimeric complex does not require the ATPase inhibitor protein, Inh1.," *The Journal of biological chemistry*, 277(42), pp. 39289–95.

Dimroth, P., Wang, H., Grabe, M. and Oster, G. (1999) "Energy transduction in the sodium F-ATPase of Propionigenium modestum" *Proceedings of the National Academy of Sciences of the United States of America*, 96(April), pp. 4924–4929.

Eckmann, C. R., Crittenden, S. L., Suh, N. and Kimble, J. (2004) "GLD-3 and control of the mitosis/meiosis decision in the germline of *Caenorhabditis elegans*" *Genetics*, 168(1), pp. 147–160.

Esteve, J., Champagne, E., Pineauk, T., Rolland, C., Cabezo, E., Walker, J. E., Perret, B. and Barbaras, R. (2003) "Ectopic β-chain of ATP synthase is an apolipoprotein A-I receptor in hepatic HDL endocytosis," *Public Health*, 1, pp. 75–79.

Evans, T. C., Crittenden, S. L., Kodoyianni, V. and Kimble, J. (1994) "Translational control of maternal *glp-1* mRNA establishes an asymmetry in the *C. elegans* embryo," *Cell*, 77(2), pp. 183–194.

Faccenda, D. and Campanella, M. (2012) "Molecular Regulation of the Mitochondrial F1Fo-ATPsynthase: Physiological and Pathological Significance of the Inhibitory Factor 1 (IF1)," *International Journal of Cell Biology*, 2012, pp. 1–12.

Faccenda, D., Tan, C. H., Seraphim, a, Duchen, M. R. and Campanella, M. (2013) "IF_1 limits the apoptotic-signalling cascade by preventing mitochondrial remodelling.," *Cell death and differentiation*, 20(5), pp. 686–97.

Faccenda, D., Nakamura, J., Gorini, G., Dhoot, G. K., Faccenda, D., Nakamura, J., Gorini, G., Dhoot, G. K., Piacentini, M. and Yoshida, M. (2017) "Control of Mitochondrial Remodeling by the ATPase Inhibitory Factor 1 Unveils a Pro-survival Relay Report Control of Mitochondrial Remodeling by the ATPase Inhibitory Factor 1 Unveils a Pro-survival Relay via OPA1" *CellReports*. Elsevier Company., 18(8), pp. 1869–1883.

Fernández-Cárdenas L. Paulette (2013). La función de las proteínas MAI-1 y MAI-2 en el desarrollo de *Caenorhabditis elegans*. Tesis para obtener el grado de Maestra en Ciencias.

Formentini, L., Pereira, M. P., Sanchez-Cenizo, L., Santacatterina, F., Lucas, J. J., Navarro, C., Martinez-Serrano, a and Cuezva, J. M. (2014) "*In vivo* inhibition of the mitochondrial H+-ATP synthase in neurons promotes metabolic preconditioning" *The Embo Journal*, 33(7), pp. 762–778.

Formentini, L., Sánchez-Aragó, M., Sánchez-Cenizo, L. and Cuezva, J. M. (2012) "The Mitochondrial ATPase Inhibitory Factor 1 Triggers a ROS-Mediated Retrograde Prosurvival and Proliferative Response" *Molecular Cell*, 45(6), pp. 731–742.

Formentini, L., Pereira, M. P., Sanchez-Cenizo, L., Santacatterina, F., Lucas, J. J., Navarro, C., Martinez-Serrano, a and Cuezva, J. M. (2014) "In vivo inhibition of the mitochondrial H+-ATP synthase in neurons promotes metabolic preconditioning" *The Embo Journal*, 33(7), pp. 762–778.

Forgac, M. (2007) "Vacuolar ATPases: rotary proton pumps in physiology and pathophysiology" *Nature Reviews Molecular Cell Biology*, 8(11), pp. 917–929.

Friedland, A. E., Tzur, Y. B., Esvelt, K. M., Colaiácovo, M. P., Church, G. M. and Calarco, J. a (2013) "Heritable genome editing in *C. elegans* via a CRISPR-Cas9 system" *Nature methods*, 10(8), pp. 741–3.

Frøkjaer-Jensen, C., Davis, M. W., Hopkins, C. E., Newman, B. J., Thummel, J. M., Olesen, S.-P., Grunnet, M. and Jorgensen, E. M. (2008) "Single-copy insertion of transgenes in *Caenorhabditis elegans*" *Nature genetics*, 40(11), pp. 1375–1383.

Fujikawa, M., Imamura, H., Nakamura, J. and Yoshida, M. (2012) "Assessing actual contribution of IF_1, inhibitor of mitochondrial F_oF_1, to ATP homeostasis, cell growth, mitochondrial morphology, and cell viability" *The Journal of biological chemistry*, 287(22), pp. 18781–7.

Fuchs, Y. and Steller, H. (2015) "Live to die another way: modes of programmed cell death and the signals emanating from dying cells" *Nature Reviews Molecular Cell Biology*, 16(6), pp. 329–344. doi: 10.1038/nrm3999.

García-Bermúdez, J., Sánchez-Aragó, M., Soldevilla, B., del Arco, A., Nuevo-Tapioles, C. and Cuezva, J. M. (2015) "PKA Phosphorylates the ATPase Inhibitory Factor 1 and Inactivates Its Capacity to Bind and Inhibit the Mitochondrial H^+-ATP Synthase" *Cell Reports*, pp. 1–13.

García-Bermúdez, J. and Cuezva, J. M. (2016) "The ATPase Inhibitory Factor 1 (IF_1): A master regulator of energy metabolism and of cell survival" *Biochimica et biophysica acta.*

Garcia, J. J., Morales-Rios, E., Cortes-Hernandez, P. and Rodriguez-Zavala, J. S. (2006) "The inhibitor protein (IF_1) promotes dimerization of the mitochondrial F1F0-ATP synthase" *Biochemistry*, 45(42), pp. 12695–12703.

Gartner, A., Milstein, S., Ahmed, S., Hodgkin, J. and Hengartner, M. O. (2000) "A conserved checkpoint pathway mediates DNA damage--induced apoptosis and cell cycle arrest in *C. elegans*" *Molecular cell*, 5(3), pp. 435–43.

Genoux, A., Pons, V., Radojkovic, C., Roux-Dalvai, F., Combes, G., Rolland, C., Malet, N., Monsarrat, B., Lopez, F., Ruidavets, J. B., Perret, B. and Martinez, L. O. (2011) "Mitochondrial

inhibitory factor 1 (IF1) is present in human serum and is positively correlated with HDL-cholesterol" *PLoS ONE*, 6(9).

Gledhill, J. R., Montgomery, M. G., Leslie, A. G. W. and Walker, J. E. (2007) "How the regulatory protein, IF(1), inhibits F(1)-ATPase from bovine mitochondria" *Proceedings of the National Academy of Sciences of the United States of America*, 104(40), pp. 15671–6.

Gottlieb, E., Armour, S., Harris, M. and Thompson, C. (2003) "Mitochondrial membrane potential regulates matrix configuration and cytochrome *c* release during apoptosis" *Cell Death and Differentiation*, 10, pp. 709–717.

Green, D. W. and Grover, G. J. (2000) "The IF(1) inhibitor protein of the mitochondrial F(1)F(0)-ATPase" *Biochimica et biophysica acta*, 1458(2–3), pp. 343–55.

Gresser, M. J., Myers, J. A. and Boyer, P. D. (1982) "Catalytic site cooperativity of beef heart mitochondrial F_1 adenosine triphosphatase. Correlations of initial velocity, bound intermediate, and oxygen exchange measurements with an alternating three-site model" *Journal of Biological Chemistry*, 257(20), pp. 12030–12038.

Gumienny, T. L., Lambie, E., Hartwieg, E., Horvitz, H. R. and Hengartner, M. O. (1999) "Genetic control of programmed cell death in the *Caenorhabditis elegans* hermaphrodite germline" *Development (Cambridge, England)*, 126(5), pp. 1011–1022.

Guo, X., Macleod, G. T., Wellington, A., Hu, F., Panchumarthi, S., Schoenfield, M., Marin, L., Charlton, M. P., Atwood, H. L. and Zinsmaier, K. E. (2005) "The GTPase dMiro is required for axonal transport of mitochondria to drosophila synapses" *Neuron*, 47(3), pp. 379–393.

Hahn, A., Parey, K., Bublitz, M., Mills, D. J., Zickermann, V., Vonck, J., Kühlbrandt, W. and Meier, T. (2016) "Structure of a Complete ATP Synthase Dimer Reveals the Molecular Basis of Inner Mitochondrial Membrane Morphology" *Molecular Cell*, 63(3), pp. 445–456.

Hashimoto, T., Yoshida, Y. and Tagawa, K. (1990) "Simultaneous bindings of ATPase inhibitor and 9K protein to F_1F_0-ATPase in the presence of 15K protein in yeast mitochondria" *Journal of biochemistry*, 108(1), pp. 17–20.

Heckman, K. L. and Pease, L. R. (2007) "Gene splicing and mutagenesis by PCR-driven overlap extension" *Nature protocols*, 2(4), pp. 924–932.

Hengartner, M. O. and Horvitz, H. R. (1994) "*C. elegans* cell survival gene ced-9 encodes a functional homolog of the mammalian proto-oncogene bcl-2" *Cell*, 76(4), pp. 665–676.

Huang, L. J., Chuang, I. C., Dong, H. P. and Yang, R. C. (2011) "Hypoxia-Inducible Factor-1 alpha Regulates the Expression of the Mitochondrial ATPase Inhibitor Protein (IF1) in Rat Liver" *Shock*.

Husain, I. and Harris, D. A. (1983) "ATP synthesis and hydrolysis in submitochondrial particles subjected to an acid-base transition. Effects of the ATPase inhibitor protein" *FEBS Letters*, 160(1–2), pp. 110–114.

Ichikawa, N., Ando, C. and Fumino, M. (2006) "*Caenorhabditis elegans* MAI-1 protein, which is similar to mitochondrial ATPase inhibitor (IF_1), can inhibit yeast F_1F_0-ATPase but cannot be transported to yeast mitochondria" *Journal of bioenergetics and biomembranes*, 38(2), pp. 93–9.

Jagasia, R., Grote, P., Westermann, B. and Conradt, B. (2005) "DRP-1-mediated mitochondrial fragmentation during EGL-1-induced cell death in *C. elegans*" *Human Performance*, 433(February).

Jorgensen, E. M. and Mango, S. E. (2002) "The art and design of genetic screens: *Caenorhabditis elegans*" *Nature Reviews Genetics*, 3(5), pp. 356–369.

Kang, J. S., Tian, J. H., Pan, P. Y., Zald, P., Li, C., Deng, C. and Sheng, Z. H. (2008) "Docking of Axonal Mitochondria by Syntaphilin Controls Their Mobility and Affects Short-Term Facilitation" *Cell*, 132(1), pp. 137–148.

Kim, H., Ishidate, T., Ghanta, K. S., Seth, M., Conte, D., Shirayama, M. and Mello, C. C. (2014) "A Co-CRISPR strategy for efficient genome editing in *Caenorhabditis elegans*" *Genetics*, 197(4), pp. 1069–1080.

Kühlbrandt, W. (2015) "Structure and function of mitochondrial membrane protein complexes" *BMC Biology*, 13(1), p. 89.

Kühlbrandt, W. and Davies, K. M. (2016) "Rotary ATPases: A New Twist to an Ancient Machine," *Trends in Biochemical Sciences*, pp. 106–116.

Labbadia, J. and Morimoto, R. I. (2015) "Repression of the Heat Shock Response Is a Programmed Event at the Onset of Reproduction" *Molecular Cell*. Elsevier Inc., 59(4), pp. 1–12.

Lamont, L. B., Crittenden, S. L., Bernstein, D., Wickens, M. and Kimble, J. (2004) "FBF-1 and FBF-2 regulate the size of the mitotic region in the *C. elegans* germline" *Developmental Cell*, 7(5), pp. 697–707.

Láscarez-Lagunas, L. I., Silva-García, C. G., Dinkova, T. D. and Navarro, R. E. (2014) "LIN-35/Rb causes starvation-induced germ cell apoptosis via CED-9/Bcl2 downregulation in *C. elegans*" *Molecular and cellular biology*, 34(13), pp. 2499–2516.

Láscarez-Lagunas, L. I., Navarro, R. E. (2015). "La regulación de la apoptosis de las células germinales del nematodo *Caenorhabditis elegans".* Mensaje Bioquímico, Vol. XLII.

Lefebvre, V., Du, Q., Baird, S., Ng, A. C. H., Nascimento, M., Campanella, M., McBride, H. M. and Screaton, R. a. (2013) "Genome-wide RNAi screen identifies ATPase inhibitory factor 1 (ATPIF1) as essential for PARK2 recruitment and mitophagy" *Autophagy*, 9(11), pp. 1770–1779.

Lettre, G. and Hengartner, M. O. (2006) "Developmental apoptosis in *C. elegans:* a complex CEDnario" *Nature Reviews Molecular Cell Biology*, 7(2), pp. 97–108.

Lippe, G., Sorgato, M. C. and Harris, D. A. (1988) "Kinetics of the release of the mitochondrial inhibitor protein. Correlation with synthesis and hydrolysis of ATP," *BBA - Bioenergetics*, 933(1), pp. 1–11.

Liu, X., Long, F., Peng, H., Aerni, S. J., Jiang, M., Sánchez-Blanco, A., Murray, J. I., Preston, E., Mericle, B., Batzoglou, S., Myers, E. W. and Kim, S. K. (2009) "Analysis of Cell Fate from Single-Cell Gene Expression Profiles in *C. elegans*" *Cell*, 139(3), pp. 623–633.

López-García, P. and Moreira, D. (1999) "Metabolic symbiosis at the origin of eukaryotes" *Trends in Biochemical Sciences*, pp. 88–93.

Ly, J.D., Grubb, D.R. & Lawen, (2003). "The mitochondrial membrane potential (deltapsi(m)) in apoptosis; an update". *Apoptosis : an international journal on programmed cell death*, 8(2), pp. 115–128.

Markwell, M. A., Haas, S. M., Bieber, L. L. and Tolbert, N. E. (1978) "A modification of the Lowry procedure to simplify protein determination in membrane and lipoprotein samples" *Analytical biochemistry*, 87, pp. 206–210.

Matic, I., Cocco, S., Ferraina, C., Martin-Jimenez, R., Florenzano, F., Crosby, J., Lupi, R., Amadoro, G., Russell, C., Pignataro, G., Annunziato, L., Abramov, A. Y. and Campanella, M. (2016) "Neuroprotective coordination of cell mitophagy by the ATPase Inhibitory Factor 1," *Pharmacological Research*, 103, pp. 56–68.

Martin, W. and Müller, M. (1998) "The hydrogen hypothesis for the first eukaryote" *Nature*, 392(6671), pp. 37–41.

Minauro-Sanmiguel, F., Wilkens, S. and García, J. J. (2005) "Structure of dimeric mitochondrial ATP synthase: novel F_0 bridging features and the structural basis of mitochondrial cristae biogenesis" *Proceedings of the National Academy of Sciences of the United States of America*, 102(35), pp. 12356–12358.

Mccarter, J., Bartlett, B., Dang, T. and Schedl, T. (1999) "On the Control of Oocyte Meiotic Maturation and Ovulation in *Caenorhabditis elegans*" *Developmental Biology*, 205, pp. 111–128.

Merritt, C., Rasoloson, D., Ko, D. and Seydoux, G. (2008) "Report 3 0 UTRs Are the Primary Regulators of Gene Expression in the *C. elegans* Germline" pp. 1476–1482.
Minauro-Sanmiguel, F., Wilkens, S. and García, J.J. (2005) "Structure of dimeric mitochondrial ATP synthase: novel F_0 bridging features and the structural basis of mitochondrial cristae biogenesis" *Proceedings of the National Academy of Sciences of the United States of America*, 102(35), pp. 12356–12358.

Mitchell, P. and Moyle, J. (1967) "Chemiosmotic hypothesis of oxidative phosphorylation," *Nature*, 213(5072), pp. 137–139.

Moore, K. J. and Fillingame, R. H. (2008) "Structural interactions between transmembrane helices 4 and 5 of subunit *a* and the subunit *c* ring of *Escherichia coli* ATP synthase" *Journal of Biological Chemistry*, 283(46), pp. 31726–31735.

Mootha, V. K. y colaboradores, A reversible component of mitochondrial respiratory dysfunction in apoptosis can be rescued by exogenous cytochrome *c*. EMBO J. 20, 661–671 (2001).

Mootha, V. K., Bunkenborg, J., Olsen, J. V, Hjerrild, M., Wisniewski, J. R., Stahl, E., Bolouri, M. S., Ray, H. N., Sihag, S., Kamal, M., Patterson, N., Lander, E. S. and Mann, M. (2003) "Integrated analysis of protein composition, tissue diversity, and gene regulation in mouse mitochondria" *Cell*, 115(5), pp. 629–640.

Nakamura, J., Fujikawa, M. and Yoshida, M. (2013) "IF1, a natural inhibitor of mitochondrial ATP synthase, is not essential for the normal growth and breeding of mice" *Bioscience reports*, 33(5), pp. 10–12.

Nelson y Cox. (2017) Lehninger Principles of Biochemistry. 7th. Ed. Cap 19 págs 711-749 W.H. Freeman.

Paix, A., Wang, Y., Smith, H. E., Lee, C.-Y. S., Calidas, D., Lu, T., Smith, J., Schmidt, H., Krause, M. W. and Seydoux, G. (2014) "Scalable and Versatile Genome Editing Using Linear DNAs with Micro-Homology to Cas9 Sites in Caenorhabditis elegans.," *Genetics*, 198(December), pp. 1347–1356.

Pagliarini, D. J., Calvo, S. E., Chang, B., Sheth, S. A., Vafai, S. B., Ong, S. E., Walford, G. A., Sugiana, C., Boneh, A., Chen, W. K., Hill, D. E., Vidal, M., Evans, J. G., Thorburn, D. R., Carr, S. A. and Mootha, V. K. (2008) "A Mitochondrial Protein Compendium Elucidates Complex I Disease Biology," *Cell*, 134(1), pp. 112–123.

Palikaras, K., Lionaki, E. and Tavernarakis, N. (2015) "Coordination of mitophagy and mitochondrial biogenesis during ageing in *C. elegans*" *Nature*, 521(7553), pp. 525–528.

Papa, S., Zanotti, F., Cocco, T., Perrucci, C., Candita, C. and Minuto, M. (1996) "Identification of functional domains and critical residues in the adenosinetriphosphatase inhibitor protein of mitochondrial F_1F_0 ATP synthase" *Eur J Biochem*, 240(2), pp. 461–467.

Parrish, J., Li, L., Klotz, K., Ledwich, D., Wang, X. and Xue, D. (2001) "Mitochondrial endonuclease G is important for apoptosis in *C . elegans*" *Nature*, 412(July), pp. 0–4.

Parrish, J. Z. and Xue, D. (2003) "Functional genomic analysis of apoptotic DNA degradation in C. elegans," *Mol Cell*, 11, pp. 987–996.

Paumard, P., Vaillier, J., Coulary, Â., Schaeffer, J., Soubannier, V., Mueller, D. M., Rago, J. and Velours, J. (2002) "The ATP synthase is involved in generating mitochondrial cristae morphology" *The EMBO Journal*, 21(3), pp. 221–230.

Pazdernik, N. and Schedl, T. (2013) "Introduction to germ cell development in *Caenorhabditis elegans*" *Advances in Experimental Medicine and Biology*, pp. 1–16.

Pierron, D. y colaboradores, "Cytochrome *c* oxidase:evolution of control *via* nuclear subunit addition". *Biochim. Biophys. Acta* 1817, 590–597 (2012).

Pogoryelov, D., Krah, A., Langer, J. D., Yildiz, Ö., Faraldo-Gómez, J. D. and Meier, T. (2010) "Microscopic rotary mechanism of ion translocation in the Fo complex of ATP synthases" *Nature Chemical Biology*, 6(12), pp. 891–899.

Praitis, V., Casey, E., Collar, D. and Austin, J. (2001) "Creation of low-copy integrated transgenic lines in *Caenorhabditis elegans*" *Genetics*, 157, pp. 1217–1226.

Pullman, M. E. and Monroy, G. C. (1963) "A Naturally Occurring Inhibitor of Mitochondrial Adenosine Triphosphatase" *The Journal of biological chemistry*, 238(11), pp. 3762–9.

Rouslin, W. (1991) "Regulation of the mitochondrial ATPase in situ in cardiac muscle: Role of the inhibitor subunit" *Journal of Bioenergetics and Biomembranes*, 23(6), pp. 873–888.

Rardin, M. J., Newman, J. C., Held, J. M., Cusack, M. P., Sorensen, D. J., Li, B., Schilling, B., Mooney, S. D., Kahn, C. R., Verdin, E. and Gibson, B. W. (2013) "Label-free quantitative proteomics of the lysine acetylome in mitochondria identifies substrates of SIRT3 in metabolic pathways," *Proceedings of the National Academy of Sciences* , 110(16), pp. 6601–6606.

Robert, V. J. P., Katic, I. and Bessereau, J. L. (2009) "Mos1 transposition as a tool to engineer the *Caenorhabditis elegans* genome by homologous recombination" *Methods*, 49(3), pp. 263–269.

Rolland, S. G. (2014) "How to Analyze Mitochondrial Morphology in Healthy Cells and Apoptotic Cells in *Caenorhabditis elegans"* 544, pp. 75–98.

Rouslin, W. and Broge, C. W. (1996) "IF1 function in situ in uncoupler-challenged ischemic rabbit, rat, and pigeon hearts" *Journal of Biological Chemistry*, 271(39), pp. 23638–23641.

Rouslin, W., Frank, G. D. and Broge, C. W. (1995) "Content and binding characteristics of the mitochondrial ATPase inhibitor, IF_1 in the tissues of several slow and fast heart-rate homeothermic species and in two poikilotherms," *Journal of Bioenergetics and Biomembranes*, 27(1), pp. 117–125.

Runswick, M. J., Bason, J. V., Montgomery, M. G., Robinson, G. C., Fearnley, I. M. and Walker, J. E. (2013) "The affinity purification and characterization of ATP synthase complexes from mitochondria" *Open Biology*, 3(2), pp. 120160–120160.

Saldanha, J. N., Parashar, A., Pandey, S. and Powell-Coffman, J. A. (2013) "Multiparameter behavioral analyses provide insights to mechanisms of cyanide resistance in caenorhabditis elegans" *Toxicological Sciences*, 135(1), pp. 156–168.

Salinas, L. S., Maldonado, E. and Navarro, R. E. (2006) "Stress-induced germ cell apoptosis by a p53 independent pathway in Caenorhabditis elegans.," C1. Salinas LS, Maldonado E, Navarro RE. Stress-induced germ cell apoptosis by a p53 independent pathway in *Caenorhabditis elegans. Cell Death Differ*. 2006;13(12):2129–39. Available from: http://www.ncbi.nlm.nih.gov/pubmed/16729024ell death and, 13(12), pp. 2129–39.

Sánchez-Cenizo y colaboradores, 2010)Sánchez-Cenizo, L., Formentini, L., Aldea, M., Ortega, Á. D., García-Huerta, P., Sánchez-Aragó, M. and Cuezva, J. M. (2010) "Up-regulation of the ATPase

Inhibitory Factor 1 (IF_1) of the mitochondrial H+-ATP synthase in human tumors mediates the metabolic shift of cancer cells to a warburg phenotype," *Journal of Biological Chemistry*, 285(33), pp. 25308–25313.

Sánchez-Aragó, M., García-Bermúdez, J., Martínez-Reyes, I., Santacatterina, F. and Cuezva, J. M. (2013) "Degradation of IF_1 controls energy metabolism during osteogenic differentiation of stem cells.," *EMBO reports*, 14(7), pp. 638–44.

Sánchez-Aragó, M. y colaboradores, 2013. Expression, regulation and clinical relevance of the ATPase inhibitory factor 1 in human cancers. *Oncogenesis*, 2(October 2012), p.e46.

Santacatterina, F., Sánchez-Cenizo, L., Formentini, L., Mobasher, M. A., Casas, E., Rueda, C. B., Martínez-Reyes, I., Núñez de Arenas, C., García-Bermúdez, J., Zapata, J. M., Sánchez-Aragó, M., Satrústegui, J., Valverde, Á. M. and Cuezva, J. M. (2016) "Down-regulation of oxidative phosphorylation in the liver by expression of the ATPase inhibitory factor 1 induces a tumor-promoter metabolic state.," *Oncotarget*, 7(1), pp. 490–508.

Sato, M. and Sato, K. (2011) "Degradation of paternal mitochondria by fertilization-triggered autophagy in *C. elegans* embryos.," *Science*, 334(6059), pp. 1141–1144.

Saxton, W. M. and Hollenbeck, P. J. (2012) "The axonal transport of mitochondria.," *Journal of cell science*, 125(Pt 9), pp. 2095–104.

Schumacher, B., Hofmann, K., Boulton, S. and Gartner, A. (2001) "The C. elegans homolog of the p53 tumor suppressor is required for DNA damage-induced apoptosis," *Curr. Biol*, 11(21), pp. 1722–1727.

Schumacher, B., Schertel, C., Wittenburg, N., Tuck, S., Mitani, S., Gartner, a, Conradt, B. and Shaham, S. (2005) "C. elegans ced-13 can promote apoptosis and is induced in response to DNA damage.," *Cell death and differentiation*, 12(2), pp. 153–61.

Shah, D. I., Takahashi-Makise, N., Cooney, J. D., Li, L., Schultz, I. J., Pierce, E. L., Narla, A., Seguin, A., Hattangadi, S. M., Medlock, A. E., Langer, N. B., Dailey, T. a, Hurst, S. N.,
Faccenda, D., Wiwczar, J. M., Heggers, S. K., Vogin, G., Chen, W., Chen, C., Campagna, D. R., Brugnara, C., Zhou, Y., Ebert, B. L., Danial, N. N., Fleming, M. D., Ward, D. M., Campanella, M., Dailey, H. a, Kaplan, J. and Paw, B. H. (2012) "Mitochondrial Atpif1 regulates haem synthesis in developing erythroblasts.," *Nature*. Nature Publishing Group, 491(7425), pp. 608–12.

Schagger, H. (2000) "Supercomplexes in the respiratory chains of yeast and mammalian mitochondria," *The EMBO Journal*, 19(8), pp. 1777–1783.

Seervi, M. and Xue, D. (2015) *Mitochondrial Cell Death Pathways in Caenorhabiditis elegans*. 1st ed, *Apoptosis and Development*. 1st ed. Elsevier Inc.

Seydoux, G. and Schedl, T. (2001) "The germline in *C. elegans*: origins, proliferation, and silencing," *Int.Rev.Cytol.*, 203, pp. 139–185.

Simoni and Postma (1975). The energetics of bacterial active transport. A*nnu. Rev. Biochem.* 44, 523-554.

Sheng, Z.-H. and Cai, Q. (2012) "Mitochondrial transport in neurons: impact on synaptic homeostasis and neurodegeneration.," *Nature reviews Neuroscience*, 13(2), pp. 77–93.

Skladal, D., Halliday, J. and Thorburn, D. R. (2003) "Minimum birth prevalence of mitochondrial respiratory chain disorders in children," *Brain*, 126(8), pp. 1905–1912.

Strauss, M., Hofhaus, G., Schröder, R. R. and Kühlbrandt, W. (2008) "Dimer ribbons of ATP synthase shape the inner mitochondrial membrane.," *The EMBO journal*, 27(7), pp. 1154–60.

Sulston, J. E. (1976) "Post-Embryonic Development in the Ventral Cord of *Caenorhabditis elegans*," *Philosophical Transactions of the Royal Society B: Biological Sciences*, 275(938), pp. 287–297.

Sulston, J. E., Schierenberg, E., White, J. G. and Thomson, J. N. (1983) "The embryonic cell lineage of the nematode *Caenorhabditis elegans,*" *Developmental Biology*, pp. 64–119.

Sulston, J.E. y colaboradores (1983). "The embryonic cell lineage of the nematode *Caenorhabditis elegans". Developmental Biology*, 100(1), pp.64–119.

Sun, A. Y. and Lambie, E. J. (1997) "gon-2, a gene required for gonadogenesis in *Caenorhabditis elegans*" *Genetics*, 147(3), pp. 1077–1089.

Tait, S. W. G. and Green, D. R. (2010) "Mitochondria and cell death : outer membrane permeabilization and beyond," *Nature Publishing Group*. Nature Publishing Group, 11(9), pp. 621–632.

Twig, G., Elorza, A., Molina, A. J. A., Mohamed, H., Wikstrom, J. D., Walzer, G., Stiles, L., Haigh, S. E., Katz, S., Las, G., Alroy, J., Wu, M., Py, B. F., Yuan, J., Deeney, J. T., Corkey, B. E. and Shirihai, O. S. (2008) "Fission and selective fusion govern mitochondrial segregation and elimination by autophagy," *The EMBO Journal*, 27(2), pp. 433–446.

Vafai, S. B. and Mootha, V. K. (2012) "Mitochondrial disorders as windows into an ancient organelle.," *Nature*, 491(7424), pp. 374–83.

Van Raaij, M.J. y colaboradores, 1996. The ATPase inhibitor protein from bovine heart mitochondria: The minimal inhibitory sequence. *Biochemistry*, 35(49), pp.15618–15625.

Vafai, S. B. and Mootha, V. K. (2012) "Mitochondrial disorders as windows into an ancient organelle" *Nature*, 491(7424), pp. 374–83.

Van Raaij, M. J., Orriss, G. L., Montgomery, M. G., Runswick, M. J., Fearnley, I. M., Skehel, J. M. and Walker, J. E. (1996) "The ATPase inhibitor protein from bovine heart mitochondria: The minimal inhibitory sequence" *Biochemistry*, 35(49), pp. 15618–15625.

Wang, X., Yang, C., Chai, J., Shi, Y., & Xue, D. (2002). Mechanisms of AIF-mediated apoptotic DNA degradation in *Caenorhabditis elegans. Science*, 298, 1587–1592.

Walker, J. E., Fearnley, I. M., Gay, N. J., Gibson, B. W., Northrop, F. D., Powell, S. J., Runswick, M. J., Saraste, M. and Tybulewicz, V. L. J. (1985) "Primary structure and subunit stoichiometry of F1-ATPase from bovine mitochondria," *Journal of Molecular Biology*, 184(4), pp. 677–701.

Walker, J.E. (1998) "ATP synthesis by rotary catalysis (Nobel lecture)" C*hemie-International Edition*, pp. 2308–2319.

Walker J.E. (2013). "The ATP synthase: the understood, the uncertain and the unknown" *Biochem. Soc. Trans,* 41, 1–16.

Waterhouse, N. J. y colaboradores (2001). "Cytochrome *c* maintains mitochondrial transmembrane potential and ATP generation after outer mitochondrial membrane permeabilization during the apoptotic process." *J. Cell Biol*. 153, 319–328

Wittig, I. and Schägger, H. (2008) "Structural organization of mitochondrial ATP synthase" *Biochimica et biophysica acta*, 1777(7–8), pp. 592–8.

Wood, W. B. (1988) "Introduction to *C. elegans* Biology" *The Nematode Caenorhabditis elegans*, pp. 1–16.

Wu, Y. C., Stanfield, G. M. and Horvitz, H. R. (2000) "*Nuc-1*, a *Caenorhabditis elegans* DNase II homolog, functions in an intermediate step of DNA degradation during apoptosis" *Genes and Development*, 14(5), pp. 536–548.

Yan, N., Gu, L., Kokel, D., Chai, J., Li, W., Han, A., Chen, L., Xue, D. and Shi, Y. (2004) "Structural, biochemical, and functional analyses of CED-9 recognition by the proapoptotic proteins EGL-1 and CED-4" *Molecular Cell*, 15(6), pp. 999–1006.

Yang, W. and Hekimi, S. (2010) "A Mitochondrial Superoxide Signal Triggers Increased Longevity in *Caenorhabditis elegans*" *PLoS Biology*, 8(12), p. e1000556.

Yee, C., Yang, W. and Hekimi, S. (2014) "The intrinsic apoptosis pathway mediates the pro-longevity response to mitochondrial ROS in *C. elegans" Cell*, 157(4), pp. 897–909.

Yoshida M, Sone N, Hirata H, Kagawa Y. A highly stable adenosine triphosphatase from a thermophillie bacterium. Purification, properties, and reconstitution. *J Biol Chem*. 1975;250: 7910–6.

Zaremba-Niedzwiedzka, K., Caceres, E. F., Saw, J. H., Bäckström, D., Juzokaite, L., Vancaester, E., Seitz, K. W., Anantharaman, K., Starnawski, P., Kjeldsen, K. U., Stott, M. B., Nunoura, T., Banfield, J. F., Schramm, A., Baker, B. J., Spang, A. and Ettema, T. J. G. (2017) "Asgard archaea illuminate the origin of eukaryotic cellular complexity" *Nature*, 541(7637), pp. 353–358.

Referencia de sitio web:

https://www.edx.org/course/cell-biology-mitochondria-harvardx-mcb64-1x

http://www.wormbook.org/chapters/www_programcelldeath/programcelldeath.html

XI. Apéndice I

Medio NGM-lite:

NaCl	1.5 g/l
Bactotriptona	4 g/l
KH_2PO_4	3 g/l
K_2HPO_4	0.5 g/l
Colesterol	8 mg/l
Agar	20 g/l

Medio Luria Bertani (LB) para crecer OP50:

Triptona	10 g/l
Extracto de levadura	5 g/l
NaCl	5 g/l
Estreptomicina	50 ug/ml

Medio M9 10x para *C. elegans.*

Na_2HPO_4 $7H_2O$	60 g
KH_2PO_4	30 g
NaCl	50g
$MgSO_4$	2.5 g

Se filtra la solución 10X y se disuelve a 1X, posteriormente se esteriliza.

Amortiguador para lisar *C. elegans.*

Tris-HCl (pH 8.3)	10 mM
KCl	50 mM
$MgCl_2$	2.5 mM
NP-40	0.45%
Tween-20	0.45%
Gelatin	0.01%

Se esteriliza posterior a la preparación.

Se realizó una mezcla de 30 µl de amortiguador de lisis con 0.5 µl de Proteinasa K y se añaden 2.5 µl por tubo de PCR (0.2 ml). Posteriormente con ayuda del asa de platino se introducen de 1-5 gusanos.

Amortiguador para diluir enzimas de restricción

Tris-HCl	10 mM
NaCl	100 mM
DTT	1 mM
EDTA	0.1 mM
BSA	200 µg/ml
Glicerol	50%
pH 7.4	

La enzima de restricción (PvuII) se diluyó en una proporción 1:10.

Cuantificación de proteína por el Método de Lowry

Solución A (100 ml)

$CuSO_4$ $5H_2O$	0.5 g
$Na_3C_6H_5O_7$	1 g

Solución B (100 ml)

Na_2CO_3	20 g
NaOH	4 g
SDS	1%

Solución C (51 ml)

Solución A	1 ml
Solución B	50 ml

Solución D (20 ml)

Fenol Folin	10 ml
Agua destilada	10 ml

Ensayo:

1. Se lleva la muestra a 0.5ml con agua destilada.
2. Se añade 2.5ml de Solución C.
3. Se agita y se deja reposar por 10 minutos.
4. Se añade 0.5ml de Solución D y se agita.
5. Después de 30 minutos se mide a una $A_{750.}$

Amortiguador para aislar mitocondrias.

Manitol	220 mM
Sacarosa	70 mM
MOPS	5 mM
EGTA	2 mM
BSA	0.4% BSA
pH 7.4	

Amortiguador 3X

Ácido-6-aminocapróico	1.5 M
Bis-Tris	150 mM
Serva Blue G (7 µg/µl)	30 ng/µg de proteína.

Solución Coomasie

Coomassie Blue R5-250	0.1%
Metanol	45%
Ácido acético	10%

Solución para Desteñir

Metanol	30%
Ácido acético	10%

Apéndice II

Producción científica

PLOS ONE

RESEARCH ARTICLE

Caenorhabditis elegans ATPase inhibitor factor 1 (IF_1) MAI-2 preserves the mitochondrial membrane potential ($\Delta\psi_m$) and is important to induce germ cell apoptosis

L. P. Fernández-Cárdenas[1], E. Villanueva-Chimal[1], L. S. Salinas[1], C. José-Nuñez[2], M. Tuena de Gómez Puyou[2]*, R. E. Navarro[1]*

1 Departamento de Biología Celular y Desarrollo, Instituto de Fisiología Celular, Universidad Nacional Autónoma de México, Ciudad de México, México, **2** Departamento de Bioquímica y Biología Estructural, Instituto de Fisiología Celular, Universidad Nacional Autónoma de México, Ciudad de México, México

* rnavarro@ifc.unam.mx (REN); mtuena@ifc.unam.mx (MTdeGP)

Citation: Fernández-Cárdenas LP, Villanueva-Chimal E, Salinas LS, José-Nuñez C, Tuena de Gómez Puyou M, Navarro RE (2017) *Caenorhabditis elegans* ATPase inhibitor factor 1 (IF_1) MAI-2 preserves the mitochondrial membrane potential ($\Delta\psi_m$) and is important to induce germ cell apoptosis. PLoS ONE 12(8): e0181984. https://doi.org/10.1371/journal.pone.0181984

Editor: Janine Santos, National Institute of Environmental Health Sciences, UNITED STATES

Received: May 11, 2017

Accepted: July 10, 2017

Published: August 22, 2017

Data Availability Statement: All relevant data are within the paper and its Supporting Information files.

Funding: This work was supported by grants from Dirección General de Asuntos del Personal Académico PAPIIT-UNAM (IN207412 and IN207415) and Consejo Nacional de Ciencia y

Abstract

When the electrochemical proton gradient is disrupted in the mitochondria, IF_1 (Inhibitor Factor-1) inhibits the reverse hydrolytic activity of the F_1F_o-ATP synthase, thereby allowing cells to conserve ATP at the expense of losing the mitochondrial membrane potential ($\Delta\psi_m$). The function of IF_1 has been studied mainly in different cell lines, but these studies have generated contrasting results, which have not been helpful to understand the real role of this protein in a whole organism. In this work, we studied IF_1 function in *Caenorhabditis elegans* to understand IF_1´s role *in vivo*. *C. elegans* has two inhibitor proteins of the F_1F_o-ATPase, MAI-1 and MAI-2. To determine their protein localization in *C. elegans*, we generated translational reporters and found that MAI-2 is expressed ubiquitously in the mitochondria; conversely, MAI-1 was found in the cytoplasm and nuclei of certain tissues. By CRISPR/Cas9 genome editing, we generated *mai-2* mutant alleles. Here, we showed that *mai-2* mutant animals have normal progeny, embryonic development and lifespan. Contrasting with the results previously obtained in cell lines, we found no evident defects in the mitochondrial network, dimer/monomer ATP synthase ratio, ATP concentration or respiration. Our results suggest that some of the roles previously attributed to IF_1 in cell lines could not reflect the function of this protein in a whole organism and could be attributed to specific cell lines or methods used to silence, knockout or overexpress this protein. However, we did observe that animals lacking IF_1 had an enhanced $\Delta\psi_m$ and lower physiological germ cell apoptosis. Importantly, we found that *mai-2* mutant animals must be under stress to observe the role of IF_1. Accordingly, we observed that *mai-2* mutant animals were more sensitive to heat shock, oxidative stress and electron transport chain blockade. Furthermore, we observed that IF_1 is important to induce germ cell apoptosis under certain types of stress. Here, we propose that MAI-2 might play a role in apoptosis by regulating $\Delta\psi_m$. Additionally, we suggest that IF_1 function is mainly observed under stress and that, under physiological conditions, this protein does not play an essential role.

Tecnología-MEXICO (103856-Q and 220987) to R. E.N. L.P.F.C. is a doctoral student from Programa de Doctorado en Ciencias Bioquímicas, Universidad Nacional Autónoma de México (UNAM) and received fellowships from CONACyT and PAPIIT-UNAM. Fundación Miguel Alemán/ UNAM. The funders had no role in study design, data collection and analysis, decision to publish, or preparation of the manuscript.

Competing interests: The authors have declared that no competing interests exist.

Introduction

F_1F_o-ATP synthase is an evolutionarily conserved enzyme that synthesizes ATP from ADP and P_i using a H^+ gradient that the electron transport chain complexes generate [1,2]. When the electrochemical proton gradient that spans the mitochondrial inner membrane collapses—for example, during ischemia—ATP synthase catalyzes the back reaction and hydrolyzes ATP (F_1F_o-ATPase) to conserve the mitochondrial membrane potential ($\Delta\psi_m$) [3–5]. Therefore, ATPase Inhibitor Factor 1 (IF_1) regulates F_1F_o-ATPase hydrolyzing activity and maintains cellular ATP [3,6,7]. Several groups have attributed different roles to IF_1 apart from its canonical function in regulating F_1F_o-ATPase; however, some of them are contradictory. For example, some studies have proposed that IF_1 regulates the mitochondria volume through autophagy [8] and promotes the dimeric form of F_1F_o-ATP synthase complexes [4,9,10] that may influence mitochondria cristae formation [4]. Furthermore, Faccenda *et al*. observed that the disruption of mitochondria cristae, due to the down-regulation of IF_1, increased cytochrome *c* liberation and apoptosis [11]. By contrast, Fujikawa *et al*. (2012) from the Yoshida group found that IF_1 knockdown (KD) HeLa cells were neither affected in mitochondria volume nor in diminished cristae formation [12]; the same observation was made by other groups [13–15]. Fujikawa *et al*. explained that these differences might be due to the methods used for silencing IF_1 expression [12]. While Campanella and Faccenda [4,11] used transient knockdown, Fujikawa *et al*. suppressed IF_1 permanently [12]. Recently, the Campanella and Yoshida groups performed a more extensive analysis of mitochondria in the permanent KD cells and observed that, indeed, mitochondria cristae and volume are affected when IF_1 is silenced [16].

It has also been observed that IF_1 protects cultivated cells from stress. Campanella *et al*. (2008) found that IF_1 down-regulated cells showed increased cell death when cultivated in glucose-free medium and exposed to anoxia [4]. Similarly, Fujikawa *et al*. (2012) exposed IF_1-KD cells to 2-deoxyglucose (glycolysis inhibitor) and cyanide (respiratory inhibitor) and observed that these cells died faster than control cells and were more sensitive to paraquat [12]. By contrast, Chen *et al*. found that the loss of IF_1 increased cell survival against complex III inhibition, proposing that IF_1 inhibition might help ameliorate severe mitochondrial respiratory chain disorders [14]. To explain IF_1-KD susceptibility to stressful conditions, Campanella *et al*. and Fujikawa *et al*. [4,12] suggested that IF_1-KD cells continue depleting ATP, and the lack of ATP makes cells more sensitive to stress. Additionally, Chen *et al*. [14] proposed that IF_1 knockout (KO) boosts $\Delta\psi_m$ with the loss of ATP, improving mitochondria health and promoting cell survival.

One way to conciliate these results is to study IF_1 function in model organisms. In zebrafish, *atpif1a* loss-of-function mutants and morpholino KD fish lack hemoglobinized cells, resulting in anemia [13]. The mechanism that leads to the anemic phenotype was elucidated by silencing *atpif1* in mouse erythroleukemia cells (MELs). *atpif1* KD cells showed an increase in $\Delta\psi_m$, leading to an alkaline pH in the mitochondria and altering the activity of the mitochondrial FECH enzyme, which synthesizes the heme group [13]. Surprisingly, IF_1-KO mice showed no evident phenotype and had no differences compared with wild-type animals in ATP synthesis or hydrolysis, F_1F_o-ATPase dimer content or autophagy [17]. Recently, a more extensive analysis of the mitochondria ultra-structure in the KO mice showed fewer cristae formation and scarcer mitochondria per field [16].

To study additional IF_1 function *in vivo*, we used the nematode *Caenorhabditis elegans*. The *C. elegans* genome encodes two ATPase inhibitor proteins MAI-1 and MAI-2 [18]. Previously, Ichikawa *et al*. (2006) characterized *C. elegans* MAI-1 and MAI-2 proteins localization and biochemical parameters in yeast and found that both proteins had inhibitory activity for the ATPase. However, MAI-1 is localized in the yeast´s cytoplasm, while MAI-2 is localized in the

yeast´s mitochondria [19]. To corroborate whether MAI-1 and MAI-2 localization in yeast was conserved in *C. elegans*, we generated GFP::MAI-1 and MAI-2::GFP transgenic animals and observed that MAI-2::GFP is localized in the mitochondria and is expressed ubiquitously, whereas GFP::MAI-1 is expressed in specific tissues of the nematode in a non-mitochondrial pattern. Our work confirms that MAI-1 is not a mitochondrial protein and, because MAI-2 has a more conventional expression pattern and role for IF-1, we studied *mai-2* function.

We generated, by CRISPR/Cas9 genome editing, two different mutant alleles for *mai-2*. In contrast to previous phenotypes described in KD cell lines, we found that *mai-2* mutants displayed no significant differences in the oxygen consumption rate, total ATP concentration, mitochondrial network and F_1F_o-ATP synthase dimerization. Interestingly, we found that *mai-2* mutant animals had hyperpolarized mitochondria and showed decreased physiological germ cell apoptosis. When the mutants were exposed to different stresses, we found that the germ cell apoptosis response was decreased compared with that of the control, suggesting that MAI-2 affects the germ cell response to stress. Furthermore, when we exposed *mai-2* mutants to heat shock, oxidative stress and mitochondria-disturbing agents such as cyanide, an electron transport chain inhibitor and a CCCP uncoupler, we observed that *mai-2* mutant animals were more vulnerable than wild-type. Our results showed that, in an organism such as *C. elegans*, MAI-2 appears to be non-essential under physiological conditions; however, when animals encounter stress, the survival of the whole organism seem to be affected.

Materials and methods

Strains

C. elegans strains were maintained on NGM-lite agar plates seeded with *Escherichia coli* (*E. coli*) strain OP50 bacteria [20,21]. Strains are indicated in Table 1.

Generation of translational reporters

The cloning of *mai-1* and *mai-2* were done using MultiSite Gateway (Thermo Fisher Scientific) and all inserts were amplified from genomic DNA. For the transgene carrying *Pmai-2*::*mai-2*::*gfp*::*mai-2* 3'-UTR (Fig 1C, line 5), we amplified a 1796 bp fragment upstream of *mai-2*, for the coding region a 852 bp fragment from the ATG start codon until the end of the gene without a stop codon, a 910 bp fragment of *gfp* from template pCM1.53 (Addgene #17250) was fused

Table 1. Strains. List of strains that were used in this study, their genotype, and optimal temperatures is shown.

Strains	Genotype	Growth Tempertaure	References
RN69	[*Pmai-2*::*mai-2*::*GFP*::*mai-2 3*'UTR*; unc-119*(+)]*	24˚C	This work
RN80	[*Pmai-2*::*mai-2*::*GFP*::*mai-2 3'UTR; unc-119*(+)];*xmSi01*	24˚C	This work
EG6699	*ttTi5605 II; unc-119(ed3) III oxEx1578*	15˚C	[26]
RN37	*xmSi31*[*Pmai-1*::*mai-1*::*mCherry*::*mai-1 3*'UTR, *Cbr unc-119*(+)]II	24˚C	This work
RN38	*xmSi32*[*Pmai-1*::*GFP*::*mai-1*::*mai-1 3*'UTR, *Cbr unc-119*(+)]II	24˚C	This work
RN15	*xmSi01*[*Pmex-5*::*tomm-20*::*mcherry*::*tbb-2 3*'UTR*; Cbr unc-119*(+)]II	24˚C	This work
MD701	*bcIs39*[*Plim-7*::*ced-1*::*GFP; lin-15*(*+*)]V	24˚C	[51]
RN70	*mai-2(xm18)* IV*; bcIs39* V	24˚C	This work
RN71	*mai-2(xm19)* IV*; bcIs39* V	24˚C	This work
SD1347	*ccIs4251*[*Pmyo-3*::*GFP*::*LacZ+Pmyo-3*::*mitoGFP+dpy-20*(*+*)]I	20˚C	[52]
RN79	*mai-2(xm18) IV; ccIs4251* I	20˚C	This work

* The LG for the insertion has not been defined.

https://doi.org/10.1371/journal.pone.0181984.t001

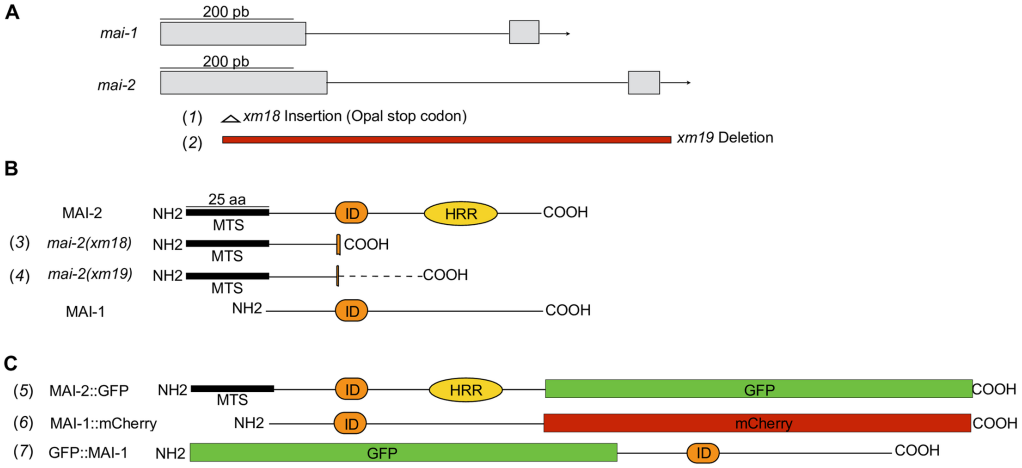

Fig 1. Alleles and translational reporters used to study the function of mitochondria ATPase inhibitors in *C. elegans*. (A) The *mai-1* and *mai-2* genes are composed of 2 exons (gray rectangles) and one intron (thin line). (B) We generated two mutant alleles, *mai-2(xm18)* and *mai-2(xm19)*, by CRISPR/Cas9 genome editing. Both mutant alleles encode two truncated MAI-2 proteins that conserve the mitochondrial targeting sequence (MTS) but lack the inhibitory domain (ID) and histidine-rich region (HRR), which are essential for MAI-2 function and regulation (3,4). The dotted line (—) in the *mai-2 (xm19)* product represents a randomly formed sequence of amino acids (4). (C) To study protein localization, we generated translational reporters for MAI-1 and MAI-2 (5–7). We inserted, in the carboxyl-terminal, a GFP construct for MAI-2 (5); for MAI-1, we inserted a carboxy-terminal mCherry (6) and an amino-terminal GFP (7).

https://doi.org/10.1371/journal.pone.0181984.g001

with a 182 bp *mai-2* 3'-UTR by PCR overlap extension [22]. The PCR products were gel-purified, *mai-2* promoter was cloned in the donor vector pDONRP4-P1R (Gateway vector), *mai-2* coding region was cloned in the donor vector pDONR221 (Gateway vector) and the chimera *gfp-mai-2* 3'-UTR was cloned in pDONRP2R-P3 (Gateway vector). The construct *Pmai-2*::*mai-2*::*gfp*::*mai-2* 3´-UTR was cloned into the pCFJ150 vector and were bombarded into HT1593 *unc-119(ed3)* animals [23] using standard procedures [24,25]. To study the expression pattern, we chose to study a transgenic line that showed high expression in both tissues. For *Pmai-2*::*mai-2*::*gfp*::*mai-2* 3´-UTR we obtained twelve independent transgenic lines, three of which showed expression in the soma and germline.

For the transgene carrying *Pmai-1*::*gfp*::*mai-1*::*mai-1* 3'-UTR (Fig 1C, line 7) we amplified a 2002 bp fragment from the intergenic region upstream *mai-1* and for the coding region containing the 3'-UTR we amplified a 932 bp fragment from the ATG start codon until the end of the longest 3'-UTR reported (Wormbase release WS224). The PCR products were gel-purified, and the promoter region was cloned by recombination into the pDONRP4-P1R, while the coding region was cloned into pDONRP2R-P3. For the *gfp* sequence we used the donor vector pCM1.53. For the transgene carrying *Pmai-1*::*mai-1*::*mCherry*::*mai-1* 3'-UTR (Fig 1C, line 6) we used the same *mai-1* promoter described above, for *mai-1* coding region we amplified a 567 bp fragment from the ATG start codon until the end of the gene without stop codon. A *mCherry* fragment of 864 bp was amplified using as template pCFJ104 (Addgene #19328) and for *mai-1* 3'-UTR we amplified a fragment of 356 bp. We fused *mCherry* fragment with *mai-1* 3'-UTR by PCR overlap extension. The PCR products were purified, and the promoter was cloned through recombination in the donor vector pDONRP4-P1R, *mai-1* coding region was

cloned in donor vector pDONR221, while *mCherry*::*mai-1* 3'-UTR chimera was cloned in pDONRP2R-P3. Inserts were sequenced after cloned in the donor vectors, and the desired fragments in each donor vector were cloned in tandem into the pCFJ150 (Addgene #19329) [26].

For the generation of *Pmex-5*::*tomm-20*::*tbb-2* 3'-UTR, we amplified a fragment of 225 bp of *tomm-20* gene, *mCherry* sequence was amplified from the vector pGH8 (Addgene #19359). The PCR products were gel-purified and fused by PCR overlap extension. The fused PCR product was cloned into the pDONR221. Finally, the donor vector pCFJ183-*Pmex-5* (kindly donated by Frøkjaer-Jensen), pDONR221-*tomm-20*::*mcherry* and pCm1.36 (Addgene #17249) were mixed and cloned in tandem through recombination into the destination vector pCFJ150 vector. Primer sequences are listed in S1 Table.

For *Pmai-1*::*gfp*::*mai-1*::*mai-1* 3'-UTR, *Pmai-1*::*mai-1*::*mCherry*::*mai-1 3*'UTR and *Pmex-5*::*tomm-20*::*mCherry*::*tbb-2* 3'-UTR transgenes were inserted by single copy insertion methodology [26,27]. DNA mixtures were microinjected into the strain EG6699 and selection of the transgenic animals was done a previously reported with modified microinjection mixtures [25]. The microinjection mixtures used were: target vector pCFJ150 with *Pmai-1*::*gfp*::*mai-1*::*mai-1* 3'-UTR (30 ng/ μl), pMA122 (10 ng/μl) (Addgene #34873), pCFJ601 (50 ng/μl) (Addgene #34874), pCFJ104 (5 ng/μl), pGH8 (Addgene #19359) and pCFJ90 (2 ng/μl) (Addgene #19327); pCFJ150 with *Pmai-1*::*mai-1*::*mCherry*::*mai-1* 3'-UTR transgene (30 ng/μl), pMA122 (10 ng/μl), pCFJ601 (50 ng/μl), pCFJ421 (2.5 ng/μl) (Addgene #34876), pCFJ420 (5 ng/μl) (Addgene #34877), pCFJ66 (10 ng/μl) (Addgene #24981); pCFJ150 with *Pmex-5*::*tomm-20*::*mcherry*::*tbb-2* 3'-UTR (10 ng/μl), pCFJ601 (10 ng/μl), pCFJ104 (10 ng/μl), pGH8 (10 ng/μl), pCFJ90 (2 ng/μl).

For *Pmai-1*::*gfp*::*mai-1*::*mai-1* 3'-UTR we obtained one transgenic line named *xmSi32* [*Pmai-1*::*gfp*::*mai-1-3*'-UTR; *Cbr-unc-119* (+)]II and for *Pmai-1*::*mai-1*::*mCherry*::*mai-1 3*'UTR we obtained two independent lines with the same expression pattern, and we chose to work with *xmSi31*[*Pmai-1*::*mai-1*::*mCherry*::*mai-1-3*'-UTR; *Cbr-unc-119* (+)]II.

Image acquisition and processing of translational reporters

The embryos expressing MAI-2::GFP were observed by fluorescence microscopy to detect GFP expression using a Nikon Eclipse E600 microscope equipped with an AxioCam MRc camera (Zeiss). The pictures were captured using AxioVision software (Zeiss) and deconvolved using ImageJ software [28] with Parallel Spectral Deconvolution and Diffraction PSF 3D plugins. Larvae and adult animals expressing MAI-2::GFP and TOMM-20::mCherry, GFP::MAI-1 and MAI-1::mCherry were observed by confocal imaging using an Olympus Fluoview Confocal microscope FV10i (Olympus) and images were processed with ImageJ software.

Generation of *mai-2* alleles

CRISPR/Cas9 genome editing was used to generate *mai-2(xm18)* and *mai-2(xm19)* alleles [29,30]. We targeted a site localized in the first exon of *mai-2* with a single guide (sgRNA) to be cut by Cas9 with the sequence `GGATCGATCCGCGACGCCGG`. The protospacer-associated motif (PAM) is at position 3,386,025 (Wormbase release WS224). To generate the *mai-2* sgRNA we replaced by PCR the *unc-119* in the pU6::*unc-119* sgRNA vector (Addgene #46169) with the desired *mai-2* sequence using primers listed in S1 Table. The PCR product was digested with DpnI, purified pU6::*mai-2* sgRNA was confirmed by sequencing. Single-strand oligonucleotides (ssDNA) were used as repair templates [30]. *mai-2* ssDNA1 repair template consisted of a 5' upstream homology arm of 83 nt before the modification site which consisted

in the insertion of a PvuII restriction enzyme site that introduced an opal stop codon, and a 78 nt 3' downstream homology arm. To generate a deletion of *mai-2* gene we used ssDNA2 that consisted of a 67 nt 5´upstream homology arm and a 71 nt downstream homology arm of *mai-2* 3'-UTR. We microinjected the following vectors: *Peft-3*::*cas-9-SV40-NLS*::*tbb-2* 3'-UTR (50 ng/μl) (Addgene #46168), pU6::*mai-2* sgRNA (45 ng/μl), pCFJ104 (5 ng/μl) and repair templates ssDNA 1 or 2 (30 ng/μl) in 30–50 young adults of N2 strain. F_1 with mCherry expression were picked individually to plates and allowed to lay eggs for one day, then F1 were transfered into lysis buffer and were screened by PCR followed in the case of allele *mai-2 (xm18)* by restriction enzyme digestion to detect insertion. Primer sequences are listed in S1 Table.

RT-PCR

The RNA purification and cDNA synthesis was done as previously reported [25]. The total RNA was isolated from approximately 7,000 one-day-old adult animal hermaphrodites using TRIzol (Life Technologies) and purified via chloroform and isopropanol precipitation. 0.5–1 μg of RNA was reverse transcribed into cDNA using Im-Prom II reverse transcriptase (Promega) and oligo(dT) primers. Semi-quantitative reverse transcriptase-PCR was performed with primers designed specifically for *mai-2* (listed in S1 Table) and normalized with *act-4*. Densitometric analysis was done using Fiji (ImageJ) software.

Lifespan, fertility and embryonic lethality

Lifespan was done as previously described [31]. An experimental pool of synchronized 50 animals from N2 and *mai-2(xm18)* strains were used, and lost or animals that died prematurely were replaced from a back-up pool. Lifespan measurements were done al 20˚C.

The fertility assay and embryonic lethality were done as previously described [32]. N2 and *mai-2* mutants were grown at 20˚C and were individually selected as L4 larvae and then transferred to new plate every 24 h over the course of 4 days. Embryos that did not hatch within 24 h after being laid were considered dead.

Mitochondria imaging

MitoTracker Red CMX ROS (#M7512; Molecular Probes) was diluted in DMSO (1 mM stock solution). Before staining, stocks were diluted in M9 buffer at 5 μM and one-day-old adult animals were incubated for 20 min at 20˚C [33]. Animals were immobilized with tetramisol 10 mM and mounted on 2% agarose pads for microscopic examination. For TMRM (#T-668; Molecular Probes) we modified procedure from previous method [34,35]. We diluted TMRM in DMSO (0.1 M stock solution) and added to NGM-lite agar medium at a final concentration of 30 μM, we left the plates to dry overnight and seeded *E. coli* OP50 for 24 h in the dark. For embryo imaging we transferred approximately 30 one-day-old adults of each strain to the TMRM plates, incubated at 20˚C for 15 h, and dissected animals for embryo extraction. For complete animal staining we incubated L4 animals in TMRM plates for 15 h. Stained embryos and animals were mounted on 2% agar pads for microscopy. Images were acquired under the same exposure and to calculate the level of fluorescence its integrated density was measured in ImageJ software by selecting the whole area of P_1 cell (embryos) and the whole animal. The corrected total fluorescence was calculated as CTCF = (integrated density-(selected area x mean fluorescence of background readings). For visualizing the mitochondria network in the body wall muscle cells we used synchronized L4 larvae from the transgenic strain SD1347 crossed with *mai-2(xm18)*. Animals were anesthetized with tetramisol diluted in M9 (10 mM), and mounted on an agarose pad (2%). A cover slide was put on top of the agarose pads and to

rotate worms for muscle cells visualization, the cover slide was push carefully. We quantified all mitochondria per muscle cell as tubular (wild-type), fragmented, elongated/highly connected or aggregated mitochondria. Mitochondria visualization we performed using a Nikon Eclipse E600 microscope equipped with an AxioCam MRc camera (Zeiss).

Oxygen consumption

Oxygen consumption rates were measured as previously described [36], with modifications using a Strathkelvin Instruments 782 Oxygen Meter (North Lanarkshire, Scotland, UK) interfaced to a computer. Approximately, 10,000 animals/ml in L4 to young adults were collected, washed 3 times in M9 and incubated for 30 min in constant agitation to empty the digestive system. 15 μl of slurry pellet of worms were delivered into a water-jacketed chamber Mitocell (MT200) at 20˚C with 100 μl of M9 on it. Oxygen consumption was recorded until linear and stopped with NaCN to abolish oxygen consumption. Worms were recovered after respiration measurements and collected for protein quantification by Lowry assay [37,38]. Rates were normalized to protein content.

ATP quantification

ATP quantification was done as previously described with slight modifications [35]. 50 one-day-old adult hermaphrodites were collected in 50 μl of M9 buffer and frozen in liquid N_2. Frozen worms were immersed in boiling water for 15 min, cooled and centrifuged at 2000 rpm for 5 min to pellet insoluble debris. The supernatant was moved to a fresh tube and diluted 5-fold before measurement. ATP content was determined using the Roche ATP bioluminescent assay kit HS II (Roche Applied Science) and a POLARstar Omega luminometer (BMG LABTECH). ATP levels were normalized to total protein content.

Mitochondria isolation, blue native electrophoresis and SDS-PAGE

About 50,000–100,000 synchronized animals in L4 to young adult stages were crushed approximately 10 times with liquid N_2 on a mortar with pestle and resuspended (100 μl) in a buffer that contained 220 mM of manitol, 70 mM of sucrose, 5 mM of MOPS, 2 mM of EGTA and 0.4% BSA, pH 7.4. The homogenized animals were centrifuged at 2,700 rpm for 5 min, supernatant was collected in a separate tube, the pellet was resuspended in previously described buffer and centrifuged again. This procedure was repeated two more times. Collected supernatant was centrifuged at 10,500 rpm for 5 min to obtain the mitochondrial pellet. Mitochondria were resuspended in 250 mM of sucrose and 1 mM of $MgCl_2$. We extracted F_1F_o-ATP synthase with digitonin 0.66mg/mg of protein, incubate on ice for 10 min and centrifuge for 5 min at 75,000 rpm (Airfuge Ultracentrifuge, Beckman Coulter). The supernatant was used for protein determination and 100 μg of protein was loaded into a first dimension (1D) blue native PAGE [39] followed by a second dimension (2D) SDS-PAGE [40]. For BN-PAGE the digitonin extracted protein was combined with 10 μl buffer 3X (1.5M 6-aminocaproic acid, 150 mM Bis-Tris) plus serva blue G (7 μg/μl stock serva blue G in 0.5M 6-aminocaproic acid) (final concentration, 30 ng of serva Blue G/1 μg of protein), the samples were charged into a BN-PAGE 3.5–11%, and the electrophoresis was performed at 70V for 30 min and 100V for 2h at 4˚C. 1D gel was stained with Coomassie solution (0.1% Coomassie Blue R5-250, 45% of methanol and 10% of glacial acetic acid) and stirred at room temperature for 2 h and discolored with a solution containing 30% methanol, 10% glacial acetic acid. Densitometric analysis of dimeric and monomeric bands of each genotype was performed using Fiji (Image J) software. ATPase activity was identified by incubating the first dimension gel in a pre-incubation solution containing 35 mM Tris, 250 mM glycine, pH 8.3. Then, the gel was stirred and incubated for 2 h at

37˚C with 5 mM ATP, 5 mM $MgCl_2$, 0.15% (w/v) lead acetate, and 150 mM glycine, pH 8.3. After that, the gel was stirred and incubated at room temperature for 24 h. Monomer and dimer bands with dark background were scanned at 2 h.

For 2D SDS-PAGE, the Coomassie gel was denatured with a solution containing 1% SDS, 5 mM DTT for 1 h. The band that corresponds to the dimer and monomer were cut out of the Coomasie gel. The band was rotated 90˚ on a 15% SDS-PAGE Von Jagow and the electrophoresis was performed at 70V for 30 min and 100V for 2h at 4˚C with slight modifications to the described in [41]. The gel was scanned and analyzed.

Survival assays

Heat shock experiments were performed as previously described [25], with some modifications. Synchronized animals (30–40 animals per plate) were grown at 20˚C until animals reached a 4-day-old adult stage, and transferred to several (35 mm) NGM plates seeded with *E. coli* OP50 for heat shock. The plates were incubated for up to 12 h at 35˚C, and every 2 h the plates were taken from the incubator to observe animals under the stereoscopic microscope. Animals that did not respond to touch were scored as dead.

We tested different concentrations for sodium cyanide (NaCN, 50–100 mM) and carbonyl cyanide m-chlorophenyl hydrazone (CCCP, 50–125 μM). We chose CCCP concentrations that did not affect considerably wild-type nematodes survival but did affect *mai-2* mutant animals. Incubations and recovery were done as previously described [42], with some modifications. One-day-old adult animals (approximately 30) were placed in 200 μl of M9 (control) and M9-containing freshly diluted NaCN or CCCP at indicated concentrations for 1 h at 20˚C on a crystal Petri dish. Cyanide when diluted in a buffered solution at pH 7 is known to outgas to hydrogen cyanide (HCN) [43], it has also shown that HCN contributes to the survival of the animal [44]. After the incubation period, 2 ml of M9 were added to dilute the solutions; animals were then recovered by pipetting and placed on *E. coli* seeded NGM plates. After the plates were drained from excess liquid for approximately 5 min, the animals were allowed to recover for another 55 min more at 20˚C. Finally, the animals were observed under the stereoscopic microscope. Animals that did not respond to touch were scored as dead.

Oxidative stress experiments were performed as previously described [45], with some modifications. Previously, it has been recommended to use a paraquat concentration between 100 mM and 400 mM due to variation in batch potency [46]. We used paraquat at a concentration of 200 mM [45] diluted in M9 with *E. coli* OP50. We incubated animals in agitation a 20˚C, at indicated time animals were recovered by pipetting and placed on *E. coli*-seeded NGM plates. The plates were drained for excess liquid for approximately 5 min and animals were observed under the stereoscopic microscope. Animals that did not respond to touch or showed movement when exposed to a drop of M9 were scored as dead.

Apoptosis assays

We crossed *mai-2(xm18)* and *mai-2(xm19)* with MD701 *bcIs39*[*Plim-7*::*ced-1*::*gfp*; *lin-15*(+)] strain. We selected L4 animals of each strain and approximately 24 h later we mounted on slides using 2% agarose pads; the cell corpses were then visualized by fluorescence microscopy using a Nikon Eclipse E600 microscope equipped with an AxioCam MRc camera (Zeiss). For stress conditions, such as starvation, oxidative stress, heat shock and UV irradiation (DNA damage) we performed experiments as previously described [32,42]. To quantify apoptosis in the soma, synchronized L1 animals of N2, *mai-2(xm18)* and *mai-2(xm19)* strains grown at 20˚C were fed *ced-1* dsRNA until they had offspring as previously described [42]. Late stage

embryos and L1 larvae were mounted on agarose pads and cell corpses were quantify under Nomarski microscopy.

Statistical analysis

Brood size, embryonic lethality, TMRM fluorescence (embryos and whole animal), oxygen consumption rates, ATP quantification and germ cell apoptosis (physiological conditions and stress) were tested for equality of group variance. One-way ANOVA followed by Tukey method were performed for those datasets that had the same variance, while for unequal variances, non-parametric comparisons were performed using Dunn's method, with wild-type as a control. *t*-test was used to analyze dimer/monomer F_1F_oATPase ratio. For survival assays two-way ANOVA analysis with Bonferroni test was used to compare each condition to the control. Data was analyzed using GraphPad Prism Statistical Software.

Results

MAI-2 is expressed in the mitochondria of *C. elegans*

Ichikawa *et al*. previously showed MAI-1 and MAI-2 sub-cellular localization using yeast and demonstrated that MAI-2 is associated with yeast mitochondria, while MAI-1 is not [19]. Because these proteins were not expressed in their natural environment, we determined MAI-1 and MAI-2 expression in *C. elegans* and tested whether, in the nematode, MAI-1 could indeed associate with mitochondria. To test this hypothesis, we generated transgenic animals that express Green Fluorescent Protein (GFP) in the C-terminus of the MAI-2 protein (Fig 1C, line 5) (see Materials and methods).

A mix of MAI-2::GFP embryos, synchronized hermaphrodite larvae (L1-L4), one-day-old hermaphrodite and male adults, and dauer larvae were mounted and observed under the fluorescence microscope. We observed the expression of the transgene in the cytoplasm at all the embryonic (Fig 2A–2L) and post-embryonic stages (Fig 2M–2S) in what seems to be a mitochondrial pattern. The expression of MAI-2::GFP was observed in the germline and all somatic tissues, including neurons, pharynx, the intestine, body wall muscle and the hypodermis, during *C. elegans* development.

To corroborate MAI-2::GFP mitochondrial localization in *C. elegans*, we crossed the MAI-2::GFP transgenic with mitochondrial protein reporter transgenic animals *xmSi01*[*Pmex-5*::*tomm-20*::*mCherry*::*tbb-2* 3'-UTR; *Cbr-unc-119* (+)]II and looked for co-localization under normal conditions (Fig 3). The *mex-5* promoter region drives TOMM-20::mCherry expression in the germ cells and embryo [47]. We found that MAI-2::GFP co-localized with mitochondria in the gonad (Fig 3A–3C) and embryos (Fig 3D–3F). To further corroborate MAI-2::GFP expression in mitochondria, we also stained the transgenic MAI-2::GFP animals with the mitochondrial probe MitoTracker Red CMXRos (Fig 3G–3O). For this purpose, one-day-old adult worms were incubated in M9 with MitoTracker Red CMXRos and were observed under a fluorescence microscope. Mitotracker Red CMXRos has been used to stain mitochondria however works better in mitochondria of the body muscle cells [34] and the hypodermis [33]. We found a clear co-localization of MAI-2::GFP with the mitochondrial probe in the hypodermis (Fig 3J–3L) and muscle (Fig 3M–3O). These results demonstrate that MAI-2::GFP is a mitochondrial protein.

To study MAI-1 expression in *C. elegans*, we generated by MosSCI, N-terminal GFP and C-terminal mCherry protein reporter transgenes (Fig 1C, line 6 and 7) (see Materials and methods). GFP::MAI-1 (*xmSi32*) and MAI-1::mCherry (*xmSi31*) showed the same tissue localization (Fig 4; S1 Fig). GFP::MAI-1 is expressed in specific somatic tissues in the nuclei and in the cytoplasm through specific tissues, including the cuticle (Fig 4A and 4B), hypodermis (Fig 4C

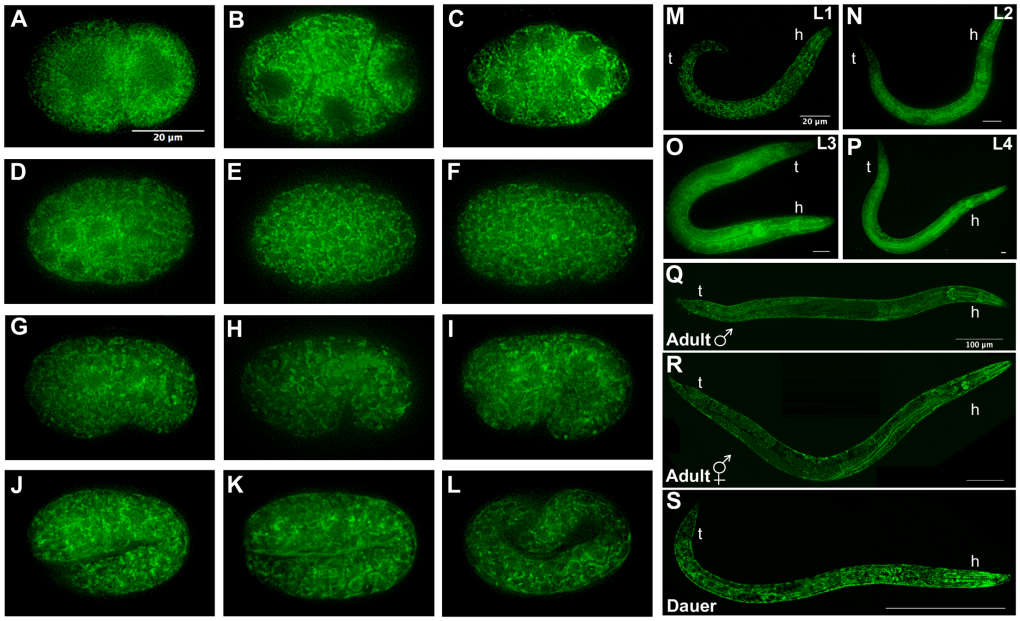

Fig 2. MAI-2::GFP is expressed in the soma and germline. Embryos, larvae and adults expressing the transgene *Pmai-2*::*mai-2*::*gfp*::*mai-2*-3'UTR were observed under a fluorescence microscope. Embryos (A-L), 2-cell (A), 4-cell (B), ~26-cell (C), ~44-cell (D), bean stage (G), comma stage (H), 1.5-fold (I), 2-fold (K), 3-fold (L). Indicate larval stages (M-P). Male adult (Q). Hermaphrodite adult (R). Dauer larva (S). h: head, t: tail.

https://doi.org/10.1371/journal.pone.0181984.g002

and 4D), rectum, vulva and neurons (Fig 4E and 4F). Although the expression pattern did not suggest a mitochondria network and MAI-1 does not carry a mitochondrial transport sequence, we tested whether MAI-1 was expressed in the mitochondria by incubating GFP::MAI-1 with Mitotracker Red CMXRos and found no co-localization between the mitochondrial probe and GFP::MAI-1 (Fig 4G–4L). These results demonstrate that MAI-1 is indeed not expressed in mitochondria but in the cytoplasm, as previously suggested Ichikawa *et al*. Additionally, we observed that GFP::MAI-1 is expressed in the nuclei. Because MAI-1 does not seem to be a canonical IF_1, we studied only MAI-2.

mai-2 mutant animals show no defects under physiological conditions

To study the function of *mai-2*, we generated mutants by CRISPR/Cas9 genome editing (Fig 1A, line 1 and 2) [29,30], see Materials and methods). Allele *mai-2(xm18)* contains an insertion of a PvuII restriction enzyme site, resulting in a premature stop codon that produces a truncated MAI-2 protein of 41 amino acids (Fig 1A and 1B, line 1 and 3; Fig 5A). The allele *mai-2(xm19)* carries a 794-bp deletion consisting of the following: 151 bp (from 261 bp) of the first exon, the entire intron (525 bp), exon 2 (69 bp) and 49 bp from the *mai-2* 3'-UTR, resulting in a putative truncated MAI-2 protein of 37 amino acids (Fig 1A and 1B, line 2 and 4; Fig 5A). We tested the abundance of the *mai-2* mRNA by semi-quantitative RT-PCR in *mai-2*

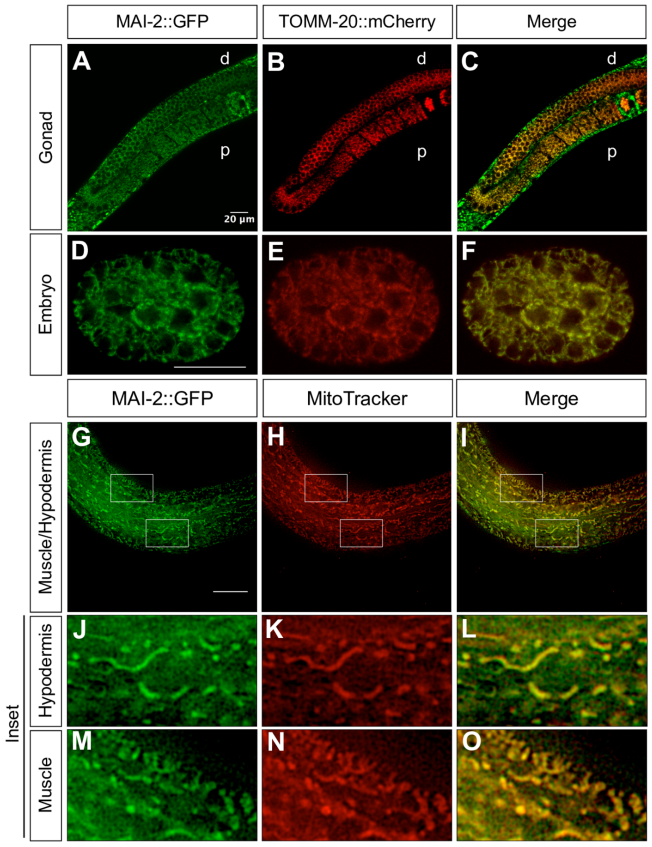

Fig 3. MAI-2::GFP is localized in the mitochondria. We crossed MAI-2::GFP animals with mitochondria expressing transgenic TOMM-20::mCherry animals (A-F). We mounted and observed one-day-old adult animals under a confocal microscopy and observed co-localization in germ cells (A-C) and embryos (D-F). Stained MAI-2::GFP animals with MitoTracker Red CMXRos were mounted and observed under a fluorescence microscope (G-O). We observed the co-localization of signals in tissues such as the hypodermis (J-L) and muscle (M-O), shown in the inset. d: distal, p: proximal.

https://doi.org/10.1371/journal.pone.0181984.g003

(xm18) and *mai-2(xm19)* mutant backgrounds. We found that the mRNA in both mutants was down-regulated by 90% (Fig 5B). These results confirmed that the mRNA encoding the predicted truncated proteins in both *mai-2* mutants are present in low abundance because it might be degraded by the nonsense-mediated decay machinery [48]. *mai-2* mutant animals showed no evident phenotype under normal conditions, had normal fertility (tested in *xm18* and *xm19* strains) (Fig 6A), no embryonic lethality (tested in *xm18* and *xm19* strains) (Fig 6B), and normal lifespan (tested only in *xm18*) (Fig 6C).

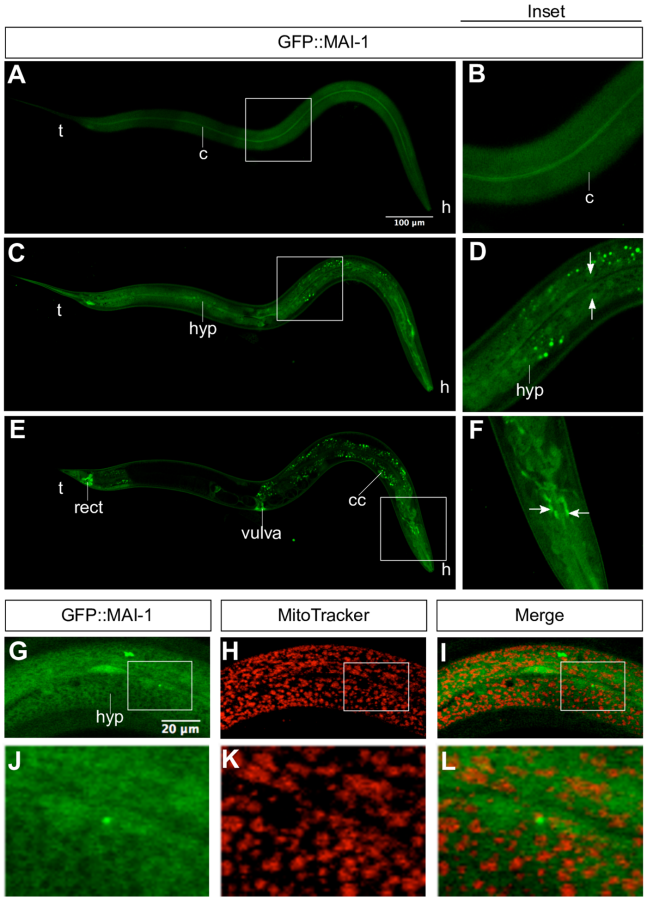

Fig 4. GFP::MAI-1 is diffusely expressed in the cytoplasm and some nuclei. We mounted one-day-old adult animals expressing the transgene *Pmai-1*::*gfp*::*mai-1*-3´UTR and observed them under a confocal microscope. We observed the expression of GFP::MAI-1 in the cuticle (A-B), cytoplasm and nuclei (arrow) of the hypodermis (C-D), in the rectum, vulva, and coelomocytes (E) and in some neurons of the animal´s head (E,F). Details of each picture are shown in the right (inset). We stained GFP::MAI-1 animals with MitoTracker CMXRos and observed no co-localization between them (G-I). Details of each picture are shown on the bottom (J-L). h: head, t: tail, c: cuticle, hyp: hypodermis, rect: rectum, coelomocytes: cc.

https://doi.org/10.1371/journal.pone.0181984.g004

mai-2 mutants animals show no defect in the mitochondria network and ATP synthase dimerization but show higher $\Delta\psi_m$

We studied the effect of *mai-2* mutation in the $\Delta\psi_m$ of the mitochondria of *C. elegans* by incubating animals in NGM-lite plates with the TMRM fluorescent probe. These compounds

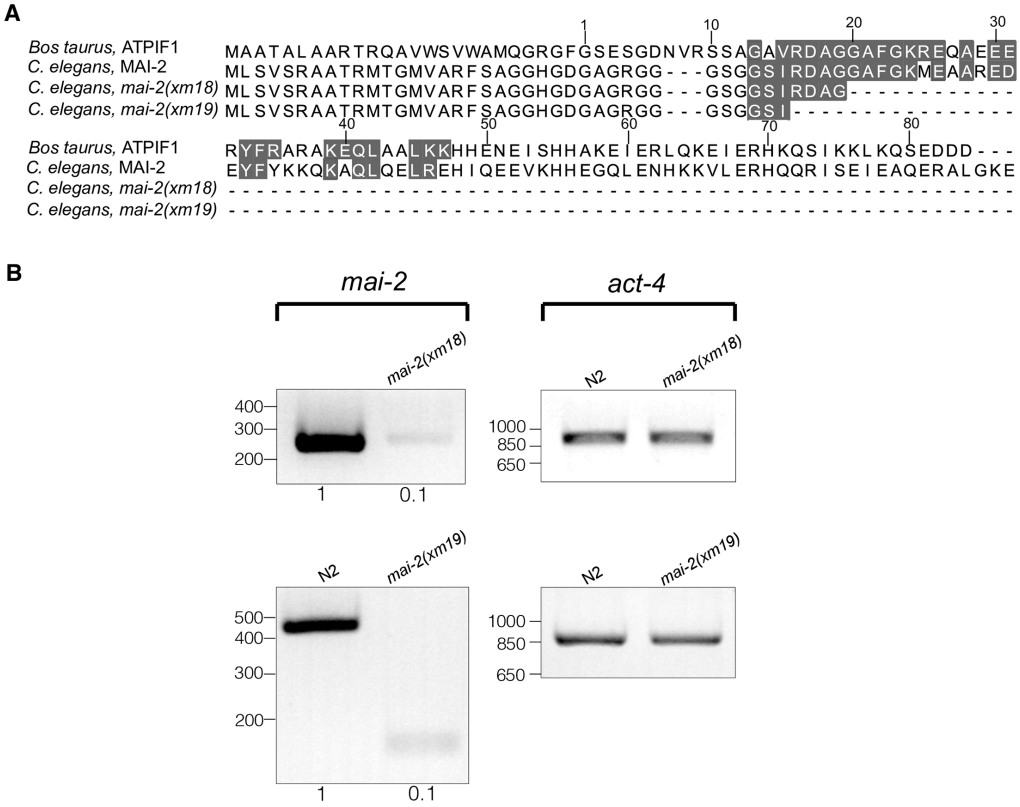

Fig 5. *mai-2* mRNA is barely detectable in *mai-2* mutants. (A) The amino acid sequences of wild-type and putative MAI-2 mutant proteins (alleles *xm18* and *xm19*) of *C. elegans* are compared with the amino acid sequence of *Bos taurus*. The residues that form the minimal inhibitory sequence are shaded in gray [19]. (B) Semi-quantitative RT-PCR analysis using cDNA synthesized from RNA extracts obtained from one-day-old control animals (N2) and *mai-2* mutant animals (alleles *xm18* and *xm19*). Specific primers for *mai-2* and *act-4* were used; *act-4* was used as a loading control. Densitometry analysis was performed, normalizing each band with its corresponding *act-4* band using ImageJ software.

https://doi.org/10.1371/journal.pone.0181984.g005

accumulate inside the mitochondria of the embryo proportionally to the mitochondrial $\Delta\psi_m$ [49]. We measured the intensity of TMRM fluorescence on the P_1 cell of 2-cell embryos and in the complete animal under normal conditions (Fig 7A and 7B). We found that *mai-2(xm18)* and *mai-2(xm19)* animals generated higher $\Delta\psi_m$ than wild-type animals.

Due to the high $\Delta\psi_m$ observed in our experiments, we evaluated the animal respiration of the wild-type and *mai-2* mutants. Synchronized L4 to early adult animals grown in NGM-lite and *E. coli* OP50 bacteria were collected, washed and introduced into a water-jacketed chamber, and the oxygen consumption rate was recorded until the trend was linear (resting state) [50]. Despite the high $\Delta\psi_m$ previously observed, we found that *mai-2(xm18)* and *mai-2(xm19)* showed no differences in oxygen consumption compared with wild-type animals (Fig 7C). To

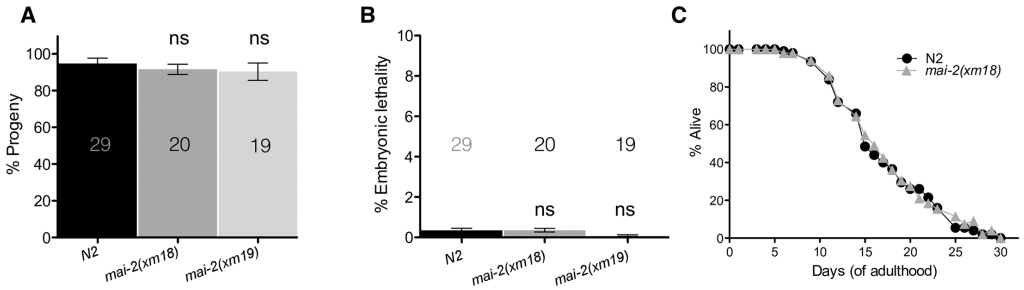

Fig 6. *mai-2* mutants show no defects in fertility or lifespan. To quantify the offspring and embryonic development, L4 wild-type (control), *mai-2(xm18)* and *mai-2(xm19)* animals were transferred to new plates every 24 h over the course of 4 days at 20˚C. The plates were scored for offspring (A) and dead embryos (B). Total progeny included all the offspring that developed (as larvae) or died as embryos. Embryos not hatching after 24 h after being laid were considered dead. For N2, the average of three independent experiments is shown, for *mai-2(xm18)* and *(xm19)* the average of two independent experiments is shown (means±SEM). Statistical significance was determined by one-way ANOVA followed by Tukey post-test and was not significant (ns). The number of analyzed animals (N) is indicated in each graph. (C) For the lifespan assay, wild-type and *mai-2(xm18)* animals were scored every other day until all of them were found death (aprox. 30 days) at 20˚C. The data represent the mean of two independent replicates in which 50 worms per group were assayed. The interaction effect of wild-type and *mai-2(xm18)* was calculated by two-way ANOVA and were not significant (not shown).

https://doi.org/10.1371/journal.pone.0181984.g006

evaluate whether the increase in $\Delta\psi_m$ was a consequence of an increase in hydrolysis, we analyzed the total [ATP] of whole animals and observed a decrease of ~15% in *mai-2(xm18)* (Fig 7D); however, this difference was non-significant. These results indicate that, in the absence of MAI-2 protein, the electron transport chain may not be disturbed and $\Delta\psi_m$ could be affected by another mechanism.

To determine whether, in *C. elegans*, the absence of *mai-2* may promote changes in mitochondrial morphology, we crossed *mai-2(xm18)* animals with SD1347 *ccIs4251* I. This transgene expresses GFP in the mitochondria networks of the body wall muscle, which carry a nuclear- and mitochondria-targeted GFP under the control of the *myo-3* promoter [51]. We observed that L4 control animals displayed mostly tubular mitochondria (99.1%). *ccIs4251* I; *mai-2(xm18)* revealed no evident defects in the mitochondria network and showed mostly tubular mitochondria (99.8%) (Fig 7E). For N2 animals, 555 cells of 22 animals were visualized while 612 cells of 27 animals were visualized for *mai-2(xm18)*. Furthermore, we studied in *mai-2(xm18)* ATP synthase dimerization using blue native gels. We observed that, in *mai-2 (xm18)*, ATP synthase dimers, with respect to the monomer content of ATP synthase dimers, were unmodified when compared with control animals [N2 = 0.95±0.12, *mai-2(xm18)* = 0.99 ±0.07. Data represents means±SEM and comparisons were non-significant after *t*-test analysis] (Fig 7F). To demonstrate that the dimer and monomer bands corresponds to F_1F_o-ATP synthase, we analyzed by a 2D SDS-PAGE F_1F_o-ATP synthase subunits content [40] and we clearly distinguished the (α, β and γ) subunits. We further corroborated that we were observing the dimer and monomer forms of the F_1F_o-ATP synthase by a blue native gel to detect ATPase activity (S2 Fig).

MAI-2 is required for stress survival

To examine the role of MAI-2 in the whole animal survival under stress conditions that affect the mitochondria, we exposed control and *mai-2* mutant one-day-old hermaphrodite adults to different concentrations of the respiratory chain inhibitor sodium cyanide (NaCN) and the uncoupler carbonyl cyanide *m*-chlorophenyl hydrazone (CCCP) for 1 h and then quantified

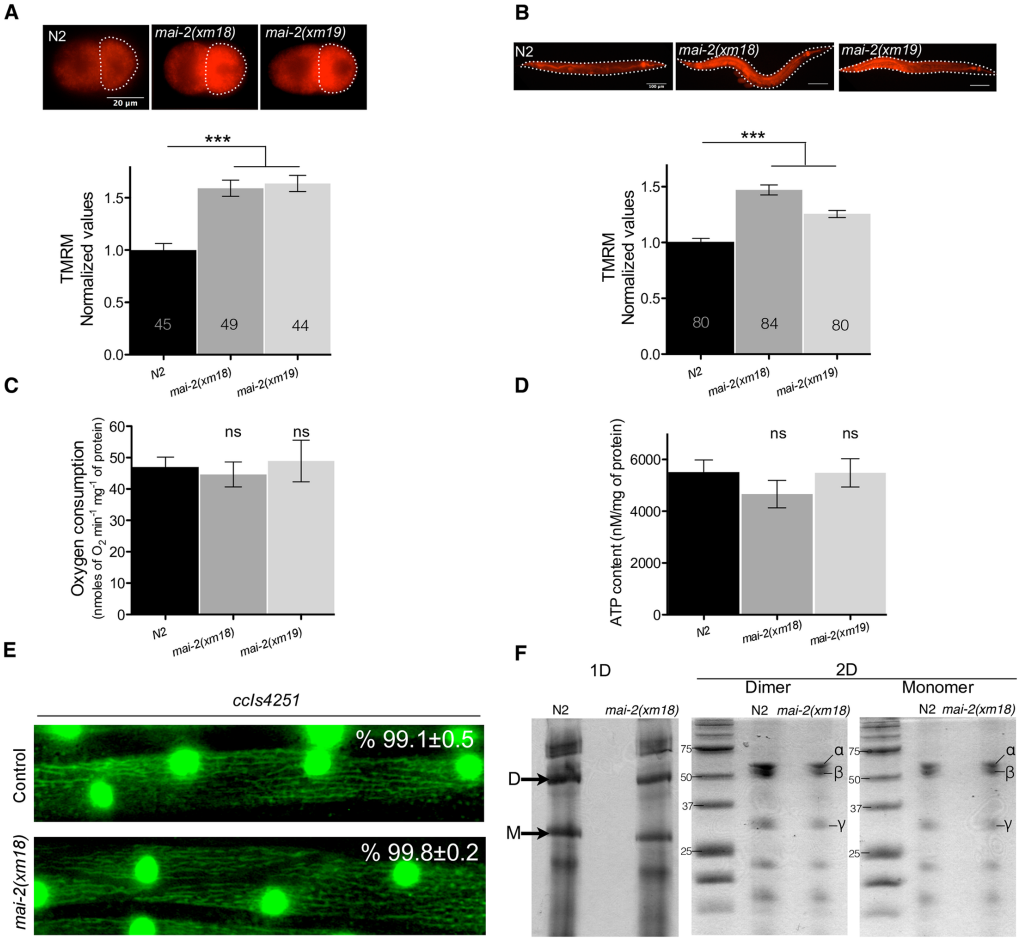

Fig 7. $\Delta\psi_m$ is elevated in *mai-2* mutants. (A-B) To test the $\Delta\psi_m$ of one-day-old N2, *mai-2(xm18)* and *mai-2(xm19)* synchronized adults were grown in NGM with TMRM for approximately 15 h, after incubation animals were dissected for embryo extraction. 2-cell embryos and the whole animal were observed under a fluorescence microscope. The fluorescence of TMRM (arbitrary units) was quantified for each of the genotypes and conditions. The values were normalized relative to the fluorescence of wild-type animals, grown at 20˚C in normal conditions. For N2 embryos, the average of four independent experiments is shown, four for *mai-2(xm18)* and two for *mai-2(xm19)*. For whole animals, the average of six independent experiments for each indicated background is shown. The bars show mean±SEM and inside each bar the number of animals tested is indicated. The *** ($P<0.0001$) symbols placed on top of the bars are comparisons between wild-type and *mai-2* mutants, statistical significance was determined by Dunn´s method. (C) To quantify oxygen consumption, a pool of L4 to early adults was introduced in a water-jacketed chamber and oxygen consumption rate was recorded until linear. Oxygen consumption was normalized with protein concentration. Average of four independent experiments for N2, four for *mai-2(xm18)* and two for *mai-2(xm19)* is shown. (D) For ATP quantification, ATP was extracted from 50 one-day-old adult animals and was quantified with a bioluminescent assay. ATP content was normalized by protein concentration. The average of four independent experiments of each indicated background is shown. (C-D) The bars indicate mean±SEM. The ns (non-significant) symbols placed on top of the bars are comparisons between wild-type and *mai-2* mutants, statistical significance was determined by one-way ANOVA followed by Tukey post-test. (E) L4 animals of the strain SD1347 *ccIs4251*[*myo-3p*::GFP(NLS)::LacZ (pSAK2)+*myo-3p*::GFP (mitochondrially targeted) (pSAK4)+dpy-20(+)] and SD1347 crossed with *mai-2(xm18)* were mounted on agarose pads and observed under a fluorescence microscope. The mitochondria network morphology was assessed in the body wall muscle and the percentage of cells with

tubular mitochondria was determined from two independent experiments. A representative picture of each condition is shown. The percentage of tubular mitochondria and SEM are shown. (F) Purified F_1F_o-ATP synthase from *C. elegans* control and *mai-2(xm18)* animals were subjected to 1D BN-PAGE and 2D SDS-PAGE. The arrows in 1D gel indicate the dimeric (D) and monomeric (M) bands. The 2D gel shows the F_1F_o-ATP synthase subunits (α, β, γ) which constitutes, among other subunits, the dimer and the monomer of N2 and *mai-2(xm18)* animals. The data of one of three independent experiments are shown.

https://doi.org/10.1371/journal.pone.0181984.g007

the animals' survival. We found that *mai-2(xm18)* and *mai-2(xm19)* were not sensitive to NaCN or CCCP compared with control animals at concentrations less than 75 mM or 75 μM, respectively; however, at higher concentrations, *mai-2* mutants were more sensitive and died at a higher percentage than wild-type animals (Fig 8A and 8B).

High temperatures increased ATP depletion [31]; therefore, we heat shocked 4-day-old control and *mai-2* hermaphrodite animals for 12 h at 35˚C. We analyzed the mortality every 2 h. During the first 8 h of incubation, we observed no significant difference between control and *mai-2* mutant animals (Fig 8C). However, at 12 h of heat shock, we observed that 60% of *mai-2* mutants were dead compared with control animals (Fig 8C).

To determine whether MAI-2 participates in oxidative stress resistance, we incubated *mai-2* mutants and control adult animals in the presence of 200 mM paraquat, a poison that promotes ROS production for 12 h. We observed that *mai-2* mutants died 30% more than control animals at 12 h of incubation with paraquat (Fig 8D), demonstrating that they are more vulnerable to oxidative stress. These data support that *mai-2* mutants are less resistant to stress.

MAI-2 is required for stress-induced germ cell apoptosis

To explore the effect of *mai-2* mutation over apoptosis on *C. elegans*, we examined somatic (embryogenesis), physiological and stress-induced germ cell apoptosis (gonads) in wild-type and *mai-2* mutants. For apoptosis quantification, we crossed the strain MD701, which is commonly used to quantify apoptotic corpses using fluorescence microscopy [52], with *mai-2 (xm18)* and *mai-2(xm19)* animals. *ced-1*::*gfp* control animals, and *ced-1*::*gfp;mai-2(xm18)* and *ced-1*::*gfp;mai-2(xm19)* mutant animals were grown at 24˚C and were observed under a fluorescence microscope to quantify cell corpses at 24 h post L4. We found that *ced-1*::*gfp;mai-2 (xm18)* and *ced-1*::*gfp;mai-2(xm19)* showed a significant decrease in physiological germ cell apoptosis (Fig 9A). By contrast, we found no differences in somatic apoptosis between wild-type and *mai-2* mutant animals when we quantified cell corpses during the late stages of embryogenesis and early larval stages [Bean embryo stage: *ced-1(RNAi)* = 1.8±0.1 cell corpses; *mai-2(xm18); ced-1(RNAi)* = 1.6±0.1 cell corpses; *mai-2(xm19); ced-1(RNAi)* = 1.6±0.1 cell corpses. Pretzel embryo stage: *ced-1(RNAi)* = 2.7±0.1 cell corpses; *mai-2(xm18); ced-1(RNAi)* = 2.5±0.1 cell corpses; *mai-2(xm19); ced-1(RNAi)* = 2.6±0.1 cell corpses. L1 larval stage: *ced-1 (RNAi)* = 1.4±0.1 cell corpses; *mai-2(xm18); ced-1(RNAi)* = 1.4±0.1 cell corpses; *mai-2(xm19); ced-1(RNAi)* = 1.4±0.1 cell corpses].

We tested the role of MAI-2 in germ cell apoptosis induced by stress, including starvation, heat shock, UV-C stress and oxidative stress [42]. *ced-1*::*gfp* control animals showed an increase in germ cell apoptosis after starvation (1.8-fold), heat shock (1.6-fold) and UV-C irradiation (1.8-fold) (Fig 9B) of the animals. *mai-2(xm18);ced-1*::*gfp* also showed a significant increase in apoptotic corpses under starvation (2.4-fold), heat shock (1.8-fold) and UV-C stress (1.3-fold) (Fig 9B). Although we observed a significant induction of apoptosis under these stressors, we did not observe the same induction levels, only a partial response, for heat shock and UV-C stress.

To induce oxidative stress, we incubated *ced-1*::*gfp* and *ced-1*::*gfp;mai-2(xm18)* for 1 h in paraquat and allowed them to recover in NGM plates seeded with bacteria for 1 h. After the

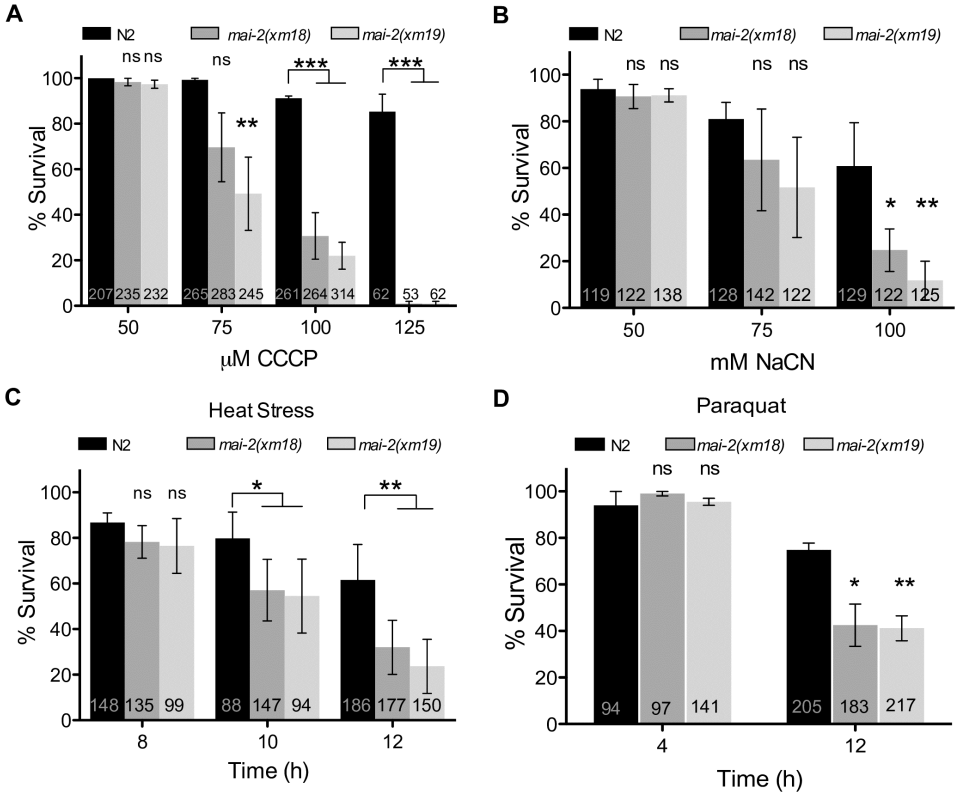

Fig 8. MAI-2 is required for stress survival. We exposed synchronized one-day-old adults N2, *mai-2(xm18)* and *mai-2(xm19)* to different concentrations of CCCP (A) and NaCN (B) for 1 h and recover them on NGM plates seeded with bacteria for 1 h. For CCCP experiments the average of four independent experiments is shown, while for NaCN experiments we show the average of three independent experiments. (C) We heat shocked synchronized 4-day-old adults of the indicated background at 35˚C for 12 h; every 2 h animals were observed under the dissecting scope for animal survival. For N2 and *mai-2(xm18)* we show the average of four independent experiments, while for *mai-2(xm19)* we show the average of two independent experiments. (D) We incubated one-day-old adults of the indicated background in 200 mM paraquat and scored for survival every 4 h through an interval of 12 h. We show the average of three independent experiments. (A-D) Animal survival was quantified by the lack of movement when touched. The data represent means±SEM and inside each bar the number of animals tested is indicated. Two-way ANOVA followed by Bonferroni post-test was used to compare each condition with the control, ns represents non-significant. ***P<0.001, **P<0.01, *P<0.05.

https://doi.org/10.1371/journal.pone.0181984.g008

recovery period, we mounted animals and counted apoptotic corpses under a fluorescence microscope. We found that control *ced-1*::*gfp* animals showed a slight but significant increase in apoptotic corpses, but *mai-2(xm18)* and *mai-2(xm19)* did not show a significant increase or show a partial response in germ cell apoptosis (Fig 9C). Our data showed that MAI-2 is necessary to induce apoptosis in the gonad under physiological conditions and under oxidative stress, heat shock, and UV-C. However, MAI-2 does not play a role during the somatic apoptosis, which occurs during late embryogenesis and the early larval stages.

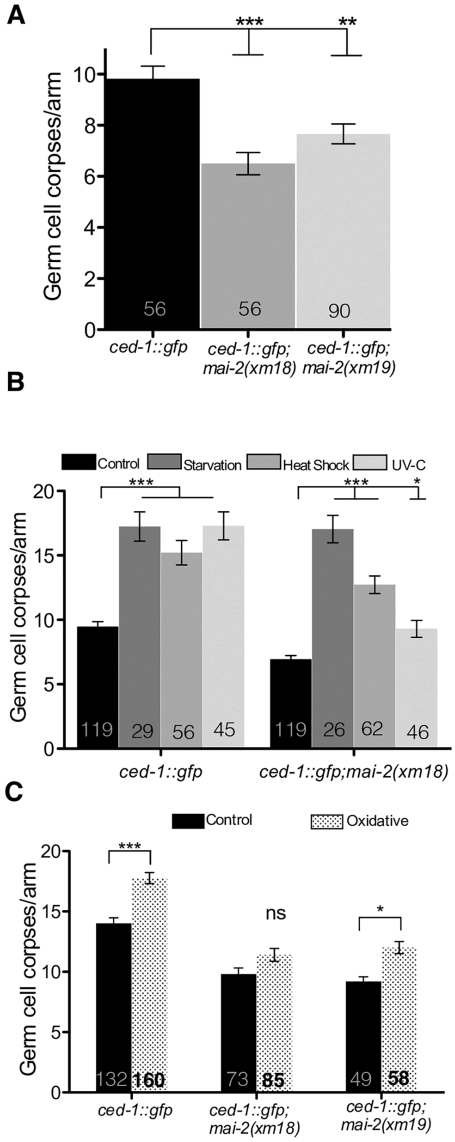

Fig 9. MAI-2 is important to induce apoptosis under physiological and stress conditions. Germ cell apoptosis was assessed in *mai-2* mutants using the strain MD701 *bcIs39*[*Plim-7*::*ced-1*::*gfp; lin-15*(+)] in which apoptotic cell corpses can be easily visualized under a fluorescence microscope. Germ cell corpses per gonad arm were counted in one-day-old adults of the indicated backgrounds under physiological (A) and

stress conditions (B-C). Animals were exposed to starvation, heat shock, UV-C irradiation (B) and paraquat (C), as indicated in the materials and methods section. We show the average of three independent experiments for physiological apoptosis (A). For apoptosis induced by starvation, heat shock and UV-C irradiation we show the average of two independent experiments (B), while for apoptosis induced by oxidative stress we show the average of three independent experiments for *ced-1::gfp* and *ced-1::gfp;mai-2(xm18)* mutant, while the average of two independent experiments are shown for *ced-1::gfp;mai-2(xm19)* (C). (A-C) The data represent means±SEM and the number of animals analyzed in each condition is shown in each bar. Dunn´s test was used to compare each condition with the control and ns represents non-significant. ***P<0.0001, **P<0.001, *P<0.01.

https://doi.org/10.1371/journal.pone.0181984.g009

Discussion

MAI-1 and MAI-2 is expressed differentially

In this study, we showed the expression of MAI-1 and MAI-2 in their natural environment and during development. We found that MAI-2::GFP is expressed in the mitochondria of all *C. elegans* tissues (Fig 2) through all embryonic and larval stages of development. Although MAI-1 does not have a predictable mitochondrial import signal sequence and Ichikawa *et al.* previously observed that, in yeast, this protein does not associate with mitochondria [19], we could not rule out that certain protein-protein interactions could direct MAI-1 to the mitochondria in the nematode. We found that GFP::MAI-1 fusion protein is indeed not associated with mitochondria and, instead, is expressed in the cytoplasm of specific tissues such as the cuticle, hypodermis, neurons of the head, rectum, coelomocytes and vulva (Fig 4A–4F). Unexpectedly, MAI-1 was also found in the nuclei of certain cells, although it lacks an obvious NES sequence (Fig 4D and S1 Fig), which was not observed when MAI-1 was expressed in yeast [19]. However, we cannot rule out that the endogenous MAI-1 protein might have a different localization because MAI-1 specific antibodies are yet not available. Because of its specific tissue localization and nuclear and cytoplasmic expression, MAI-1 remains an interesting target for future research.

Under normal conditions, *mai-2* mutants display an increased $\Delta\psi_m$ and less germ cell apoptosis

We found no evident alterations in the phenotype of *C. elegans* mutants under normal conditions when we tested the lifespan, fertility and embryonic lethality (Fig 6A–6C). Our work supports observations made by Nakamura *et al.* in which no evident phenotype was observed in IF_1 mutant mice grown under normal conditions [17]. Furthermore, we observed no defects in the mitochondrial network when we used muscle expressing transgenes in a *mai-2* mutant background (Fig 7E) or any changes in the ATP synthase dimer/monomer ratio (Fig 7F). Although we observed that, in *C. elegans*, MAI-2 is not necessary for F_1F_o dimer assembly, it was observed recently that IF_1-KO mice indeed have abnormal cristae formation and scarcer mitochondria [16].

$\Delta\psi_m$ is important for mitochondria function, and when lost, it affects mitochondria in a lethal way due to the halt of ATP production by F_1F_o-ATP synthase, mitochondria dynamics [53] and $\Delta\psi_m$-dependent transport activities [54]. Here, we show that *mai-2* mutants had increase $\Delta\psi_m$. Similarly, Fujikawa *et al.* [12] and Shah *et al.* [13] found higher $\Delta\psi_m$ in IF_1-KD cells than in control cells. In these studies, they also observed lower ATP levels; therefore, they explained that the increase in $\Delta\psi_m$ was probably due to the high hydrolyzing activity of F_1F_o-ATPase. We did not observe any difference in the ATP concentration in MAI-2 deficient nematodes. Our results are related to previous observations in which IF_1-silenced osteosarcoma cells show higher $\Delta\psi_m$ but no significant decrease in the ATP concentration [15].

$\Delta\psi_m$ loss is associated with apoptosis, although their relationship is not entirely yet understood [55,56]. It is believed that the mitochondrial permeability transition pore (PTP) releases certain mitochondrial apoptogenic factors, which, in turn, trigger apoptosis. The probability of PTP opening increases with a decrease in $\Delta\psi_m$ [55,57]. In our work, we found that *mai-2* mutants had a significantly lowered physiological germ cell apoptosis (Fig 9A). In addition, we observed that *mai-2* mutants had a partial apoptotic response to stresses like heat shock, exposure to UV-C and oxidative stress (Fig 9B and 9C). By contrast *mai-2* mutant animals show no changes in somatic apoptosis. Apoptosis in *C. elegans* soma and germline is regulated differentially. Apoptosis in the soma (embryo and larval stages) is regulated by the pro-apoptotic protein EGL-1 (a BH3-only domain protein) [42], while physiological germ cell apoptosis (in the gonad) is induced partially by the nematode Retinoblastome homologue protein LIN-35 [58] independently of EGL-1 [59]. Different pathways induce germ cell apoptosis under stress in *C. elegans* [42]. Germ cell apoptosis induced by DNA damage is regulated by the p53 worm homologue CEP-1 [60], which induces EGL-1 expression. Heat shock and oxidative stress induce germ cell apoptosis through the MAPK pathway and independently of EGL-1 [42]. Germ cell apoptosis induced by starvation is regulated by CED-9/BCL-2 down-regulation via LIN-35/RB [61].

We hypothesized that there might be a correlation between the lower germ cell apoptosis and high $\Delta\psi_m$ observed in MAI-2 deficient nematodes. Chen *et al*. proposed that IF_1 deficiency maintains $\Delta\psi_m$ when complex III is inhibited, promoting cell survival and mitochondrial health [14]. Interestingly, IF_1 has also been proposed to play an anti-apoptotic role, directly linked to IF_1's role in regulating mitochondria cristae structure and the mitochondrial network integrity. Faccenda *et al*. showed that IF_1-KD have cristae defects that enhanced cytochrome *c* liberation and the apoptotic cascade when treated with staurosporine [11].

Although, in *C. elegans*, there is no evidence of mitochondria outer membrane permeabilization by PTP and cytochrome *c* liberation during apoptosis, the mitochondrial network does seem affected and tubular mitochondria become fissioned [62]. There is also evidence that factors like WAH-1 [63] and CPS-6 [64] are released from the mitochondria and are important for cell apoptosis execution [65]. This structural change enables the hypothesis that high $\Delta\psi_m$ might conserve an orthodox configuration that decreases apoptotic events [66]. Our data suggest that $\Delta\psi_m$ might play a less important role during somatic apoptosis in *C. elegans*, but it is important to protect germ cells from this type of cell death.

MAI-2 protects *C. elegans* from stress

In our work, we studied the impact on the survival of whole organisms deficient in IF_1 (MAI-2) when threatened with cyanide (a mitochondrial complex IV inhibitor), CCCP (an uncoupler), heat stress and paraquat, a mitochondrial ROS generator. We found that *mai-2* mutants were more sensitive to cyanide or CCCP (Fig 8A and 8B), and less, but consistently, sensitive to heat shock or oxidative stress (Fig 8C and 8D). *C. elegans* is prone to encounter different stressors in the wild such as changes in temperature, unevenly distribution of oxygen in the soil or microbial pathogens such as *Pseudomona aeruginosa* that produce cyanide as a primary toxic factor that kills the nematode [44]. Due to these circumstances, we hypothesized that MAI-2 is necessary to protect whole animals from stress. Similarly, Fujikawa *et al*. and Campanella *et al*. observed that IF_1-KD cells died at a higher rate than wild-type under fatal conditions such as paraquat and cyanide [4,17]. By contrast, Chen *et al*. [14] showed that, in the absence of IF_1, cells showed increased survival when treated with antimycin, a complex III inhibitor.

Our work showed that MAI-2 plays an important role in apoptosis, probably by regulating $\Delta\psi_m$. Additionally, we demonstrated that IF_1 function is mainly observed under stress

conditions and that, under physiological conditions, this protein apparently does not play an essential role. Our work urges the relevance of studying the role of IF_1 under stress conditions in organism models like zebrafish and mice in which mutants are available. Although we focused on the study of MAI-2, due to the lack of an MAI-1 mutant, it will be interesting to study the function of MAI-1 because its expression is unusual.

Supporting information

S1 Fig. MAI-1::mCherry localizes in the hypodermis, rectum, vulva, neurons and coelomocytes. One-day-old adult animals expressing the transgene *Pmai-1*::*mai-1*::*mCherry-mai-1 3'UTR* were observed under a confocal microscope. We observed the expression of mCherry:: MAI-1 in the cytoplasm and nuclei of the hypodermis (hyp, shown with arrows) (A-B), in the rectum (rect), vulva, coelomocytes (cc) and neurons (C-D).
(TIF)

S2 Fig. F_1F_oATPase activity of the monomeric and dimeric F_1F_o ATPase complex in *C. elegans* mitochondria. F_1F_oATPase purified extracts from a mix population of L4/young adult animals of the indicated background were loaded into blue native gels and ATPase activity was assessed after 2 h of incubation. Bt = *Bos taurus* F_1F_oATPase was used as loading control.
(TIF)

S1 Table. Primers used for the construction of transgenes and CRISPR-Cas-9 genome editing.
(PDF)

Acknowledgments

Some strains were provided by CGC, which is funded by NIH Office of Research Infrastructure Programs (P40 OD010440). We thank WormBase release WS224 for gathering information and making it available. We also thank T. Keith Blackwell and members of the Navarro lab for their insightful comments on the development of this project as well to Salvador Uribe Carvajal, Emilio Espinoza and Alfredo Cabrera Oréfice for kindly advising us and borrowing us the equipment and/or materials for respiratory experiments and ATP quantifications. We are grateful Erik M. Jorgensen, C. Frøkjær-Jensen for kindly providing reagents for MosSCI experiments. We thank Rachel Beltzhoover for reading and kindly editing our manuscript.

L.P.F.C. is a doctoral student from Programa de Doctorado en Ciencias Bioquímicas, Universidad Nacional Autónoma de México (UNAM) and received fellowships from CONACyT and PAPIIT-UNAM.

Author Contributions

Conceptualization: L. P. Fernández-Cárdenas, M. Tuena de Gómez Puyou, R. E. Navarro.

Formal analysis: L. P. Fernández-Cárdenas, M. Tuena de Gómez Puyou, R. E. Navarro.

Funding acquisition: R. E. Navarro.

Investigation: L. P. Fernández-Cárdenas, E. Villanueva-Chimal, L. S. Salinas, C. José-Nuñez, M. Tuena de Gómez Puyou, R. E. Navarro.

Methodology: L. P. Fernández-Cárdenas, E. Villanueva-Chimal, L. S. Salinas, C. José-Nuñez, M. Tuena de Gómez Puyou.

Project administration: R. E. Navarro.

Resources: R. E. Navarro.

Supervision: E. Villanueva-Chimal, M. Tuena de Gómez Puyou, R. E. Navarro.

Visualization: L. P. Fernández-Cárdenas, M. Tuena de Gómez Puyou, R. E. Navarro.

Writing – original draft: L. P. Fernández-Cárdenas, M. Tuena de Gómez Puyou, R. E. Navarro.

Writing – review & editing: L. P. Fernández-Cárdenas, M. Tuena de Gómez Puyou, R. E. Navarro.

References

1. Mitchell P, Moyle J. Chemiosmotic hypothesis of oxidative phosphorylation. Nature. 1967; 213: 137–139. https://doi.org/10.1038/213137a0 PMID: 4291593
2. Boyer PD. The ATP synthase—a splendid molecular machine. Annu Rev Biochem. 1997; 66: 717–49. https://doi.org/10.1146/annurev.biochem.66.1.717 PMID: 9242922
3. Pullman ME, Monroy GC. a Naturally Occurring Inhibitor of Mitochondrial Adenosine Triphosphatase. J Biol Chem. 1963; 238: 3762–9. Available: http://www.ncbi.nlm.nih.gov/pubmed/14109217 PMID: 14109217
4. Campanella M, Casswell E, Chong S, Farah Z, Wieckowski MR, Abramov AY, et al. Regulation of Mitochondrial Structure and Function by the F1Fo-ATPase Inhibitor Protein, IF1. Cell Metab. 2008; 8: 13–25. https://doi.org/10.1016/j.cmet.2008.06.001 PMID: 18590689
5. Lefebvre V, Du Q, Baird S, Ng ACH, Nascimento M, Campanella M, et al. Genome-wide RNAi screen identifies ATPase inhibitory factor 1 (ATPIF1) as essential for PARK2 recruitment and mitophagy. Autophagy. 2013; 9: 1770–1779. https://doi.org/10.4161/auto.25413 PMID: 24005319
6. Faccenda D, Campanella M. Molecular Regulation of the Mitochondrial F1Fo-ATPsynthase: Physiological and Pathological Significance of the Inhibitory Factor 1 (IF1). Int J Cell Biol. 2012; 2012: 1–12. https://doi.org/10.1155/2012/367934 PMID: 22966230
7. García-Bermúdez J, Cuezva JM. The ATPase Inhibitory Factor 1 (IF1): A master regulator of energy metabolism and of cell survival. Biochim Biophys Acta. 2016; https://doi.org/10.1016/j.bbabio.2016.02.004 PMID: 26876430
8. Campanella M, Seraphim A, Abeti R, Casswell E, Echave P, Duchen MR. IF1, the endogenous regulator of the F1Fo-ATPsynthase, defines mitochondrial volume fraction in HeLa cells by regulating autophagy. Biochim Biophys Acta—Bioenerg. 2009; 1787: 393–401. https://doi.org/10.1016/j.bbabio.2009.02.023 PMID: 19269273
9. Garcia JJ, Morales-Rios E, Cortes-Hernandez P, Rodriguez-Zavala JS. The inhibitor protein (IF1) promotes dimerization of the mitochondrial F1F0-ATP synthase. Biochemistry. 2006; 45: 12695–12703. https://doi.org/10.1021/bi060339j PMID: 17042487
10. Buzhynskyy N, Sens P, Prima V, Sturgis JN, Scheuring S. Rows of ATP synthase dimers in native mitochondrial inner membranes. Biophys J. 2007; 93: 2870–6. https://doi.org/10.1529/biophysj.107.109728 PMID: 17557793
11. Faccenda D, Tan CH, Seraphim a, Duchen MR, Campanella M. IF1 limits the apoptotic-signalling cascade by preventing mitochondrial remodelling. Cell Death Differ. 2013; 20: 686–97. https://doi.org/10.1038/cdd.2012.163 PMID: 23348567
12. Fujikawa M, Imamura H, Nakamura J, Yoshida M. Assessing actual contribution of IF1, inhibitor of mitochondrial FoF1, to ATP homeostasis, cell growth, mitochondrial morphology, and cell viability. J Biol Chem. 2012; 287: 18781–7. https://doi.org/10.1074/jbc.M112.345793 PMID: 22493494
13. Shah DI, Takahashi-Makise N, Cooney JD, Li L, Schultz IJ, Pierce EL, et al. Mitochondrial Atpif1 regulates haem synthesis in developing erythroblasts. Nature Publishing Group; 2012; 491: 608–12. https://doi.org/10.1038/nature11536 PMID: 23135403
14. Chen WW, Birsoy K, Mihaylova MM, Snitkin H, Stasinski I, Yucel B, et al. Inhibition of ATPIF1 ameliorates severe mitochondrial respiratory chain dysfunction in mammalian cells. Cell Rep. 2014; 7: 27–34. https://doi.org/10.1016/j.celrep.2014.02.046 PMID: 24685140
15. Barbato S, Sgarbi G, Gorini G, Baracca A, Solaini G. The Inhibitor Protein (IF1) of the F1F0-ATPase Modulates Human Osteosarcoma Cell Bioenergetics. J Biol Chem. 2015; 290: 6338–48. https://doi.org/10.1074/jbc.M114.631788 PMID: 25605724
16. Faccenda D, Nakamura J, Gorini G, Dhoot GK, Faccenda D, Nakamura J, et al. Control of Mitochondrial Remodeling by the ATPase Inhibitory Factor 1 Unveils a Pro-survival Relay Report Control of

Mitochondrial Remodeling by the ATPase Inhibitory Factor 1 Unveils a Pro-survival Relay via OPA1. CellReports. ElsevierCompany.; 2017; 18: 1869–1883. https://doi.org/10.1016/j.celrep.2017.01.070 PMID: 28228254

17. Nakamura J, Fujikawa M, Yoshida M. IF1, a natural inhibitor of mitochondrial ATP synthase, is not essential for the normal growth and breeding of mice. Biosci Rep. 2013; 33: 10–12. https://doi.org/10.1042/BSR20130078 PMID: 23889209

18. Spieth J, Brooke G, Kuersten S, Lea K, Blumenthal T. Operons in *C. elegans*: Polycistronic mRNA precursors are processed by trans-splicing of SL2 to downstream coding regions. Cell. 1993; 73: 521–532. https://doi.org/10.1016/0092-8674(93)90139-H PMID: 8098272

19. Ichikawa N, Ando C, Fumino M. *Caenorhabditis elegans* MAI-1 protein, which is similar to mitochondrial ATPase inhibitor (IF1), can inhibit yeast F0F1-ATPase but cannot be transported to yeast mitochondria. J Bioenerg Biomembr. 2006; 38: 93–9. https://doi.org/10.1007/s10863-006-9009-2 PMID: 16897438

20. Brenner S. The genetics of *Caenorhabditis elegans*. Genetics. 1974; 77: 71–94.

21. Sun AY, Lambie EJ. gon-2, a gene required for gonadogenesis in *Caenorhabditis elegans*. Genetics. 1997; 147: 1077–1089. PMID: 9383054

22. Heckman KL, Pease LR. Gene splicing and mutagenesis by PCR-driven overlap extension. Nat Protoc. 2007; 2: 924–932. https://doi.org/10.1038/nprot.2007.132 PMID: 17446874

23. Maduro M, Pilgrim D. Identification and cloning of unc-119, a gene expressed in the *Caenorhabditis elegans* nervous system. Genetics. 1995; 141: 977–988. PMID: 8582641

24. Praitis V, Casey E, Collar D, Austin J. Creation of low-copy integrated transgenic lines in *Caenorhabditis elegans*. Genetics. 2001; 157: 1217–1226. PMID: 11238406

25. Paz-Gómez D, Villanueva-Chimal E, Navarro RE. The DEAD Box RNA helicase VBH-1 is a new player in the stress response in *C. elegans*. PLoS One. 2014; 9: e97924. https://doi.org/10.1371/journal.pone.0097924 PMID: 24844228

26. Frøkjaer-Jensen C, Davis MW, Hopkins CE, Newman BJ, Thummel JM, Olesen S-P, et al. Single-copy insertion of transgenes in *Caenorhabditis elegans*. Nat Genet. 2008; 40: 1375–1383. https://doi.org/10.1038/ng.248 PMID: 18953339

27. Frøkjær-Jensen C, Davis MW, Ailion M, Jorgensen EM. Improved Mos1-mediated transgenesis in *C. elegans*. Nat Methods. 2012; 9: 117–118. https://doi.org/10.1038/nmeth.1865 PMID: 22290181

28. Schneider C a, Rasband WS, Eliceiri KW. NIH Image to ImageJ: 25 years of image analysis. Nat Methods. 2012; 9: 671–675. https://doi.org/10.1038/nmeth.2089 PMID: 22930834

29. Friedland AE, Tzur YB, Esvelt KM, Colaiácovo MP, Church GM, Calarco J a. Heritable genome editing in *C. elegans* via a CRISPR-Cas9 system. Nat Methods. 2013; 10: 741–3. https://doi.org/10.1038/nmeth.2532 PMID: 23817069

30. Paix A, Wang Y, Smith HE, Lee C-YS, Calidas D, Lu T, et al. Scalable and Versatile Genome Editing Using Linear DNAs with Micro-Homology to Cas9 Sites in *Caenorhabditis elegans*. Genetics. 2014; 198: 1347–1356. https://doi.org/10.1534/genetics.114.170423 PMID: 25249454

31. Yee C, Yang W, Hekimi S. The intrinsic apoptosis pathway mediates the pro-longevity response to mitochondrial ROS in *C elegans*. Cell. 2014; 157: 897–909. https://doi.org/10.1016/j.cell.2014.02.055 PMID: 24813612

32. Carlos Giovanni SG, Rosa EN. The *C. elegans* TIA-1/TIAR homolog TIAR-1 is required to induce germ cell apoptosis. Genesis. 2013; 51: 690–707. https://doi.org/10.1002/dvg.22418 PMID: 23913578

33. Yang W, Hekimi S. A Mitochondrial Superoxide Signal Triggers Increased Longevity in *Caenorhabditis elegans*. PLoS Biol. 2010; 8: e1000556. https://doi.org/10.1371/journal.pbio.1000556 PMID: 21151885

34. Rolland SG. How to Analyze Mitochondrial Morphology in Healthy Cells and Apoptotic Cells in *Caenorhabditis elegans*. 2014; 544: 75–98. https://doi.org/10.1016/B978-0-12-417158-9.00004-2

35. Palikaras K, Lionaki E, Tavernarakis N. Coordination of mitophagy and mitochondrial biogenesis during ageing in *C. elegans*. Nature. 2015; 521: 525–528. https://doi.org/10.1038/nature14300 PMID: 25896323

36. Grad LI, Sayles LC, Lemire BD. Isolation and functional analysis of mitochondria from the nematode *Caenorhabditis elegans*. Methods Mol Biol. 2007; 372: 51–66. https://doi.org/10.1007/978-1-59745-365-3_4 PMID: 18314717

37. Bollag DM, Edelstein SJ. Protein methods. 2Ed, Wiley-Liss, Inc, New York, 1996.

38. Markwell MA, Haas SM, Bieber LL, Tolbert NE. A modification of the Lowry procedure to simplify protein determination in membrane and lipoprotein samples. Anal Biochem. 1978; 87: 206–210. https://doi.org/10.1016/0003-2697(78)90586-9 PMID: 98070

39. Schägger H, von Jagow G. Blue native electrophoresis for isolation of membrane protein complexes in enzymatically active form. Anal Biochem. 1991; 199: 223–231. https://doi.org/10.1016/0003-2697(91)90094-A PMID: 1812789

40. Schägger H, von Jagow G. Tricine-sodium dodecyl sulfate-polyacrylamide gel electrophoresis for the separation of proteins in the range from 1 to 100 kDa. Anal Biochem. 1987; 166: 368–379. https://doi.org/10.1016/0003-2697(87)90587-2 PMID: 2449095

41. Yoshida M, Sone N, Hirata H, Kagawa Y. A highly stable adenosine triphosphatase from a thermophillie bacterium. Purification, properties, and reconstitution. J Biol Chem. 1975; 250: 7910–6. Available: http://www.ncbi.nlm.nih.gov/pubmed/240842 PMID: 240842

42. Salinas LS, Maldonado E, Navarro RE. Stress-induced germ cell apoptosis by a p53 independent pathway in *Caenorhabditis elegans*. C1 Salinas LS, Maldonado E, Navarro RE Stress germ cell apoptosis by a p53 Indep Pathw *Caenorhabditis elegans* Cell Death Differ,2006; 13(12)2129–39 https://doi.org/10.1038/sj.cdd.4401976 PMID: 16729024

43. Arun P, Moffett JR, Ives JA, Todorov TI, Centeno JA, Namboodiri MAA, et al. Rapid sodium cyanide depletion in cell culture media: Outgassing of hydrogen cyanide at physiological pH. Anal Biochem. 2005; 339: 282–289. https://doi.org/10.1016/j.ab.2005.01.015 PMID: 15797569

44. Saldanha JN, Parashar A, Pandey S, Powell-Coffman JA. Multiparameter behavioral analyses provide insights to mechanisms of cyanide resistance in *Caenorhabditis elegans*. Toxicol Sci. 2013; 135: 156–168. https://doi.org/10.1093/toxsci/kft138 PMID: 23805000

45. Labbadia J, Morimoto RI. Repression of the Heat Shock Response Is a Programmed Event at the Onset of Reproduction. Mol Cell. Elsevier Inc.; 2015; 59: 1–12. https://doi.org/10.1016/j.molcel.2015.06.027 PMID: 26212459

46. Wilkinson DS, Taylor RC, Dillin A. Analysis of Aging in *Caenorhabditis elegans*. Methods Cell Biol. 2012; 107: 353–381. https://doi.org/10.1016/B978-0-12-394620-1.00012-6 PMID: 22226530

47. Merritt C, Rasoloson D, Ko D, Seydoux G. Report 3 0 UTRs Are the Primary Regulators of Gene Expression in the *C. elegans* Germline. 2008; 1476–1482.

48. Pulak R, Anderson P. mRNA surveillance by the *Caenorhabditis elegans smg* genes. Genes Dev. 1993; 7: 1885–1897. https://doi.org/10.1101/gad.7.10.1885 PMID: 8104846

49. Andreux PA, Mouchiroud L, Wang X, Jovaisaite V, Mottis A, Bichet S, et al. A method to identify and validate mitochondrial modulators using mammalian cells and the worm *C. elegans*. Sci Rep. 2014; 4: 5285. https://doi.org/10.1038/srep05285 PMID: 24923838

50. Braeckman BP, Houthoofd K, De Vreese A, Vanfleteren JR. Assaying metabolic activity in ageing *Caenorhabditis elegans*. Mech Ageing Dev. 2002; 123: 105–119. https://doi.org/10.1016/S0047-6374(01)00331-1 PMID: 11718805

51. Liu X, Long F, Peng H, Aerni SJ, Jiang M, Sánchez-Blanco A, et al. Analysis of Cell Fate from Single-Cell Gene Expression Profiles in *C. elegans*. Cell. 2009; 139: 623–633. https://doi.org/10.1016/j.cell.2009.08.044 PMID: 19879847

52. Schumacher B, Schertel C, Wittenburg N, Tuck S, Mitani S, Gartner a, et al. *C. elegans* ced-13 can promote apoptosis and is induced in response to DNA damage. Cell Death Differ. 2005; 12: 153–61. https://doi.org/10.1038/sj.cdd.4401539 PMID: 15605074

53. Twig G, Elorza A, Molina AJA, Mohamed H, Wikstrom JD, Walzer G, et al. Fission and selective fusion govern mitochondrial segregation and elimination by autophagy. EMBO J. 2008; 27: 433–446. https://doi.org/10.1038/sj.emboj.7601963 PMID: 18200046

54. Schleyer M, Schmidt B, Neupert W. Requirement of a Membrane Potential for the Posttranslational Transfer of Proteins into Mitochondsria. Eur J Biochem. 1982; 125: 109–116. https://doi.org/10.1111/j.1432-1033.1982.tb06657.x PMID: 6213410

55. Ly JD, Grubb DR, Lawen a. The mitochondrial membrane potential (deltapsi(m)) in apoptosis; an update. Apoptosis. 2003; 8: 115–128. PMID: 12766472

56. Tait SWG, Green DR. Mitochondria and cell death: outer membrane permeabilization and beyond. Nat Publ Gr. Nature Publishing Group; 2010; 11: 621–632. https://doi.org/10.1038/nrm2952 PMID: 20683470

57. Petronilli V, Cola C, Massari S, Colonna R, Bernardi P. Physiological effectors modify voltage sensing by the cyclosporin A- sensitive permeability transition pore of mitochondria. J Biol Chem. 1993; 268: 21939–21945. PMID: 8408050

58. Schertel C, Conradt B. C. elegans orthologs of components of the RB tumor suppressor complex have distinct pro-apoptotic functions. Development. 2007; 134: 3691–3701. https://doi.org/10.1242/dev.004606 PMID: 17881492

59. Gumienny TL, Lambie E, Hartwieg E, Horvitz HR, Hengartner MO. Genetic control of programmed cell death in the *Caenorhabditis elegans* hermaphrodite germline. Development. 1999; 126: 1011–1022. PMID: 9927601

60. Schumacher B, Hofmann K, Boulton S, Gartner A. The *C. elegans* homolog of the p53 tumor suppressor is required for DNA damage-induced apoptosis. Curr Biol. 2001; 11: 1722–1727. PMID: 11696333

61. Láscarez-Lagunas LI, Silva-García CG, Dinkova TD, Navarro RE. LIN-35/Rb causes starvation-induced germ cell apoptosis via CED-9/Bcl2 downregulation in C. elegans. Mol Cell Biol. 2014; 34: 2499–2516. https://doi.org/10.1128/MCB.01532-13 PMID: 24752899

62. Jagasia R, Grote P, Westermann B, Conradt B. DRP-1-mediated mitochondrial fragmentation during EGL-1-induced cell death in *C. elegans*. Nature 2005; 433(7027):754–60. https://doi.org/10.1038/nature03316 PMID: 15716954

63. Wang X, Yang C, Chai J, Shi Y. Mechanisms of AIF-Mediated Apoptotic DNA Degradation in Caenorhabditis elegans. Science. 2002; 298: 1587–1592. https://doi.org/10.1126/science.1076194 PMID: 12446902

64. Parrish J, Li L, Klotz K, Ledwich D, Wang X, Xue D. Mitochondrial endonuclease G is important for apoptosis in *C. elegans*. Nature. 2001; 412: 0–4.

65. Seervi M, Xue D. Mitochondrial Cell Death Pathways in *Caenorhabiditis elegans* [Internet]. 1st ed. Apoptosis and Development. Elsevier Inc.; 2015. https://doi.org/10.1016/bs.ctdb.2015.07.019 PMID: 26431563

66. Gottlieb E, Armour S, Harris M, Thompson C. Mitochondrial membrane potential regulates matrix configuration and cytochrome c release during apoptosis. Cell Death Differ. 2003; 10: 709–717. https://doi.org/10.1038/sj.cdd.4401231 PMID: 12761579

Cysteine Sulfenylation Directs IRE-1 to Activate the SKN-1/Nrf2 Antioxidant Response.

John M. Hourihan, Lorenza E. Moronetti Mazzeo, L. Paulette Fernández-Cárdenas and T. Keith Blackwell

En este trabajo se encontró que las especies reactivas de oxígeno producidas en el retículo endoplásmico y en la mitocondria provocan la sulfenilación de una cisteína localizada en el asa de activación de la cinasa IRE-1. Esta modificación inhibe la respuesta UPR "Unfolded Protein Response) del retículo endoplásmico y propicia la activación de la respuesta antioxidante que inicia p38/SKN-1 (Nrf-2) que incrementa la resistencia al estrés y la vida del animal. También se encontró que existen otras cinasas como AKT, p70S6K, PKC y ROCK1 que se regulan de manera similar indicando que las modificaciones en las cisteínas inducida por ROS puede dirigir a proteínas a adoptar funciones inesperadas y coordinar procesos celulares.

DPFF-1 transcription factor deficiency causes the aberrant activation of MPK-1 and meiotic defects in the *Caenorhabditis elegans* germline

Emmanuel Villanueva-Chimal, Laura S. Salinas, Laura P. Fernández-Cardenas, Gabriela Huelgas-Morales, Alejandro Cabrera-Wrooman, Rosa E. Navarro

En este trabajo se estudió a DPFF-1, el cual es similar en mamíferos a DPF2/requiem/ubi-d4. Se encontró que la mutante nula de *dpff-1* produce menos progenie que los nematodos silvestres posiblemente debido a defectos en la meiosis. Los animales mutantes en *dpff-1* muestran más células germinales en paquíteno y una sobre-expresión de P-MPK-1. Adicionalmente, los animales presentaron niveles altos de apoptosis inducidos por p53. Además los animals mutantes en *dpff-1* mostraron ser más sensibles al choque de calor. Este es el primer estudio en donde un factor transcripcional está involucrado en la meiosis y en la protección de estrés.

Article

Molecular Cell

Cysteine Sulfenylation Directs IRE-1 to Activate the SKN-1/Nrf2 Antioxidant Response

Graphical Abstract

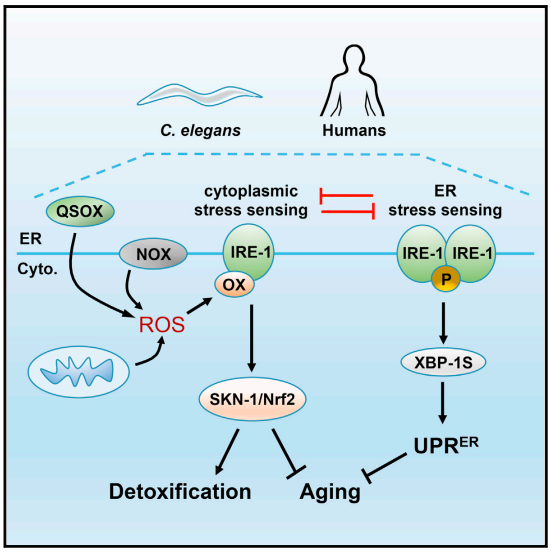

Authors

John M. Hourihan,
Lorenza E. Moronetti Mazzeo,
L. Paulette Fernández-Cárdenas,
T. Keith Blackwell

Correspondence

keith.blackwell@joslin.harvard.edu

In Brief

We report that the transmembrane endoplasmic reticulum (ER) stress sensor IRE-1 has a redox-regulated cytoplasmic signaling function. Localized ROS sulfenylate an IRE-1 cysteine, inhibiting its ER functions and initiating the antioxidant response. IRE-1 therefore monitors cytoplasmic homeostasis through localized ROS signaling, suggesting that cysteine modifications have broad and diverse regulatory functions.

Highlights

- The ER stress sensor IRE-1 has a distinct function in cytoplasmic homeostasis
- Local redox signals block IRE-1 ER signaling by sulfenylating a kinase cysteine
- This functional switch initiates the p38/SKN-1(Nrf2) antioxidant response at IRE-1
- The IRE-1 paradigm implies broad and versatile functions for signaling at cysteines

Hourihan et al., 2016, Molecular Cell *63*, 553–566
August 18, 2016
http://dx.doi.org/10.1016/j.molcel.2016.07.019

CellPress

Molecular Cell
Article

Cysteine Sulfenylation Directs IRE-1 to Activate the SKN-1/Nrf2 Antioxidant Response

John M. Hourihan,[1,2] Lorenza E. Moronetti Mazzeo,[1,2] L. Paulette Fernández-Cárdenas,[1,2] and T. Keith Blackwell[1,2,*]
[1]Research Division, Joslin Diabetes Center, Boston, MA 02215, USA
[2]Department of Genetics and Harvard Stem Cell Institute, Harvard Medical School, Boston, MA 02115, USA
*Correspondence: keith.blackwell@joslin.harvard.edu
http://dx.doi.org/10.1016/j.molcel.2016.07.019

SUMMARY

Emerging evidence suggests that many proteins may be regulated through cysteine modification, but the extent and functions of this signaling remain largely unclear. The endoplasmic reticulum (ER) transmembrane protein IRE-1 maintains ER homeostasis by initiating the unfolded protein response (UPR^{ER}). Here we show in *C. elegans* and human cells that IRE-1 has a distinct redox-regulated function in cytoplasmic homeostasis. Reactive oxygen species (ROS) that are generated at the ER or by mitochondria sulfenylate a cysteine within the IRE-1 kinase activation loop. This inhibits the IRE-1-mediated UPR^{ER} and initiates the p38/SKN-1(Nrf2) antioxidant response, thereby increasing stress resistance and lifespan. Many AGC-family kinases (AKT, p70S6K, PKC, ROCK1) seem to be regulated similarly. The data reveal that IRE-1 has an ancient function as a cytoplasmic sentinel that activates p38 and SKN-1(Nrf2) and indicate that cysteine modifications induced by ROS signals can direct proteins to adopt unexpected functions and may coordinate many cellular processes.

INTRODUCTION

Organisms encounter stresses that include reactive small molecules from metabolic or exogenous sources, and accumulation of misfolded or damaged proteins. To defend against these perturbations, complex stress responses have evolved that attempt to restore homeostasis and repair damage (Fulda et al., 2010). It is an intriguing question as to how stresses might be perceived in a rapid manner that minimizes damage, and how stress responses might be coordinated with each other and with other cellular processes.

In the endoplasmic reticulum (ER), where secretory and membrane-bound proteins are synthesized, accumulation of misfolded ER proteins (ER stress) triggers a complex unfolded protein response (UPR^{ER}) (Ron and Walter, 2007; Wang and Kaufman, 2014). This response includes activation of genes that promote ER homeostasis. The most ancestral transducer of the transcriptional UPR^{ER} is the ER transmembrane kinase/RNase Ire1 (Figure S1A) (Maly and Papa, 2014; Ron and Walter, 2007). In the presence of unfolded proteins, IRE-1 oligomerizes and is autophosphorylated by its cytoplasmic kinase (Ron and Walter, 2007; Wang and Kaufman, 2014). These events activate the Ire1 RNase, which splices the mRNA that encodes the UPR^{ER} transcription factor XBP1 (Figure S1A). IRE-1 is important in development, immunity, and metabolism and is dysfunctional or a potential therapeutic target in many human diseases (Fu et al., 2012; Hetz et al., 2013; Wang and Kaufman, 2014). The various biological functions of IRE-1 are thought to derive from its role as an unfolded protein sensor.

ER protein folding depends upon appropriate crosslinking of cysteines (Cys), which requires that the ER maintain an oxidizing environment that would be deleterious to the cell at large (Kakihana et al., 2012; Sevier and Kaiser, 2008). An antioxidant response that defends against reactive oxygen species (ROS) and other small molecules is orchestrated by the transcription factor Nrf2 and its *C. elegans* ortholog SKN-1 (Blackwell et al., 2015; O'Connell and Hayes, 2015; Suzuki and Yamamoto, 2015). This response promotes redox homeostasis, detoxifies small molecules, enhances proteostasis, regulates metabolism, and has been implicated in lifespan extension in various organisms. Nrf2 activity is increased when electrophiles interact with the Nrf2-binding ubiquitin ligase adaptor Keap1, allowing Nrf2 to escape degradation (Suzuki and Yamamoto, 2015). The paradigm of Nrf2 regulation by Keap1 has been studied in great detail, but it is still unclear how Nrf2 is regulated by some ROS-based stimuli (Jomova et al., 2011; Lau et al., 2013). Moreover, *C. elegans* lacks a *Keap1* ortholog, implying that additional mechanisms regulate SKN-1/Nrf2 responses to stress. In *C. elegans*, ROS and other stresses increase SKN-1 levels in nuclei within the intestine, the digestive system counterpart (Blackwell et al., 2015). This generally requires phosphorylation of SKN-1 by the p38 mitogen-activated protein kinase (MAPK) (Figure S1B) (Inoue et al., 2005). ROS activate p38 pathway signaling in *C. elegans* and mammals (Inoue et al., 2005; Nadeau et al., 2007), but the primary trigger of this response is unknown.

While high levels of ROS damage proteins, a growing body of evidence suggests that ROS also have physiological signaling functions that are mediated through oxidation of specific Cys residues (D'Autréaux and Toledano, 2007; Gould et al., 2015; Holmström and Finkel, 2014; Paulsen et al., 2012; Tonks, 2005). Many examples have been described in which stress or exogenously provided ROS induce modifications that affect protein function (D'Autréaux and Toledano, 2007; Holmström and Finkel, 2014), and in some cases endogenously generated

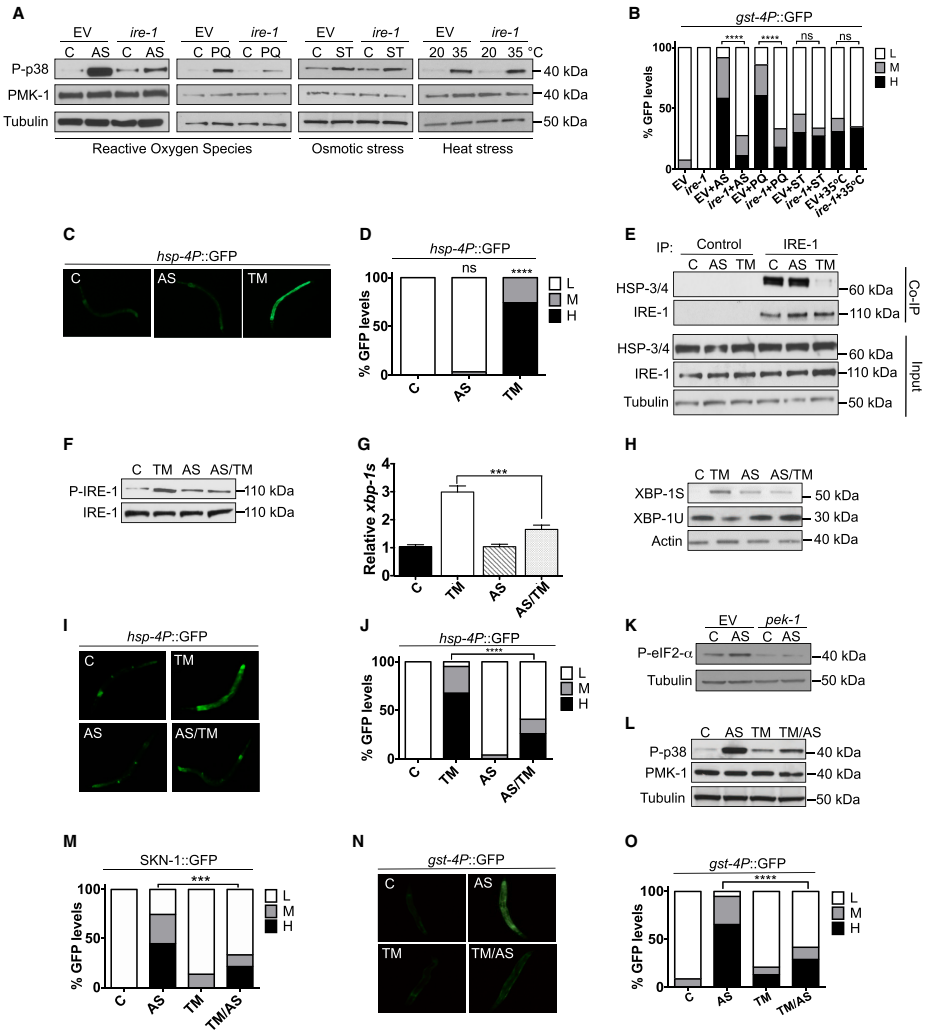

Figure 1. Distinct IRE-1-Dependent Responses to ROS and ER Stress

(A and B) IRE-1 is required for the *C. elegans* p38/SKN-1 response to ROS. *ire-1* RNAi diminished the p38 (A) and *gst-4P*::GFP (B) responses to sublethal exposure to AS (30 min) or PQ (30 min), but not Sorbitol (ST, 30 min) or heat (30 min). Phosphorylation of p38 (P-p38) indicates p38 activation (Inoue et al., 2005).

(C–E) Acute AS treatment does not activate the UPR^{ER}. AS (30 min) did not upregulate *hsp-4P*::GFP (C), with intestinal GFP scoring in (D), or promote IRE-1 and HSP-3/4 dissociation as determined by co-immunoprecipitation (co-IP) (E).

(F–J) AS pre-treatment blocks IRE-1 and UPR^{ER} activation in response to ER stress. Prior AS exposure (30 min) inhibited IRE-1 phosphorylation (F), *xbp-1* mRNA splicing, as indicated by qPCR assay of levels of the indicated mRNA forms (G), XBP-1S protein accumulation (H), and *hsp-4P*::GFP induction by ER stress (I), with scoring shown in (J) (TM; 5 hr). AS-treated samples were allowed to recover for 30 min prior to TM exposure. In (G), error bars are ±SEM.

(legend continued on next page)

ROS have been demonstrated to regulate proteins physiologically. For example, certain growth factors induce NADPH oxidase (NOX) enzymes to generate ROS that inhibit phosphatases (Bae et al., 1997; Finkel, 2011; Sundaresan et al., 1995; Tonks, 2005) and potentiate epidermal growth factor receptor kinase activity (Paulsen et al., 2012). In brown adipocytes, cold induces production of mitochondrial ROS that oxidize uncoupling protein 1, leading to thermogenesis (Chouchani et al., 2016). Remarkably, in cultured human cells over 700 proteins are prone to Cys oxidation, in patterns that can be altered by oxidizing or growth conditions (Gould et al., 2015; Yang et al., 2014). The number of cellular processes that might be regulated physiologically through such modifications remains an open question, and it is largely unknown how versatile these modifications are with respect to their effects on protein function.

Here we show that Ire1 not only acts in the secretory pathway, but also has an evolutionarily conserved function as a sentinel that maintains cytoplasmic redox homeostasis. Localized ROS production at the ER leads to rapid oxidation of a single Cys within the Ire1 kinase active site. This modification inhibits the UPR^{ER} and directs Ire1 to adopt a distinct function in which it activates p38/SKN-1(Nrf2) and thereby promotes both stress resistance and longevity in *C. elegans*. This molecular switch reveals remarkable versatility in redox-based signaling and suggests a paradigm by which physiological Cys modifications may coordinate numerous cellular processes.

RESULTS

Mutually Exclusive UPR^{ER} and Antioxidant Response Functions of IRE-1

Previously, we observed that in *C. elegans*, RNA interference (RNAi) knockdown of *ire-1* largely blocked activation of the p38/SKN-1 antioxidant response (Glover-Cutter et al., 2013). We investigated why this would be the case, first by asking whether *ire-1* is required for p38 to be activated specifically by ROS. RNAi against *ire-1* diminished acute p38 activation by the ROS generators sodium arsenite (AS) and paraquat (PQ), but not osmotic or heat stress (Figure 1A). The SKN-1 antioxidant response can be monitored in vivo with the *gst-4*P::GFP reporter, in which the SKN-1 target *gst-4* promoter drives GFP expression (Glover-Cutter et al., 2013). Only AS and PQ required *ire-1* to activate *gst-4*P::GFP (Figure 1B), and *ire-1(ok799)* nulls were defective in AS-induced p38 activation and sensitive to oxidative stress (Figures S1C and S1D; Table S1). Treatment with the antioxidant glutathione (GSH) inhibited AS-induced ROS production, p38 activity, and *gst-4P*::GFP expression (Figures S1E–S1H). *ire-1* therefore appears to be required specifically for ROS to activate p38/SKN-1 and is important for redox homeostasis.

Our current understanding of IRE-1 predicts that this requirement would be mediated through its canonical UPR^{ER} function. Prolonged ER stress may lead to cytoplasmic oxidative stress (Chaudhari et al., 2014; Kakihana et al., 2012), but we had assayed p38 activity after AS treatment for only 30 min under conditions that required 12 hr to result in death (Figure S1D). *C. elegans* UPR^{ER} activation can be monitored with a transcriptional reporter for *hsp-4*, an ortholog of the ER chaperone BiP (Figure S1A) (Calfon et al., 2002; Henis-Korenblit et al., 2010; Taylor and Dillin, 2013). In contrast to ER stress from tunicamycin (TM), acute AS treatment did not activate *hsp-4p*::GFP (Figures 1C and 1D) or increase levels of the fluorescent protein P$_{nhx\text{-}2}$*cpl-1*^{W32AY35A}::YFP, which misfolds and accumulates under ER stress conditions (Miedel et al., 2012) (Figure S1I). AS also did not induce disruption of the IRE-1/HSP-4(BiP) complex, a key step in UPR^{ER} activation (Figures 1E and S1A) (Ron and Walter, 2007). On the other hand, ER stress did not increase p38 activity (Figure S1J). We conclude that AS-induced ROS trigger rapid IRE-1-dependent p38/SKN-1 antioxidant signaling without activating the UPR^{ER}.

We next asked whether the IRE-1-dependent responses to ROS and ER stress might interfere with each other. Remarkably, short-term AS treatment reduced the IRE-1-mediated response to ER stress, as indicated by IRE-1 phosphorylation, *xbp-1* mRNA splicing, production of the spliced form of the XBP-1 protein (XBP-1S), and *hsp-4P*::GFP expression (Figures 1F–1J). This suggests that acute ROS exposure inhibits the UPR^{ER} function of IRE-1. The UPR^{ER} also involves IRE-1-independent mechanisms, including suppression of protein synthesis that is triggered by activation of the ER membrane kinase PERK (Ron and Walter, 2007; Wang and Kaufman, 2014). Treatment with AS increased activity of the *C. elegans* PERK ortholog PEK-1 (Figure 1K), suggesting that ROS exposure interferes specifically with IRE-1 and not all UPR^{ER} mechanisms. Having observed that pre-exposure to ROS antagonized IRE-1/XBP-1S signaling, we investigated whether ER stress might interfere with IRE-1-dependent p38/SKN-1 activation by ROS. Pretreatment with the ER stressor TM at a sub-lethal dose (Glover-Cutter et al., 2013) suppressed AS-induced p38 signaling, accumulation of a SKN-1::GFP fusion in intestinal nuclei, and *gst-4P*::GFP reporter activation (Figures 1L–1O). p38 and SKN-1 target gene activation were similarly diminished when we activated the UPR^{ER} genetically by knocking down the retro-translocon regulator *tfg-1* (Levi-Ferber et al., 2014) (Figures S1K–S1M). IRE-1 therefore mediates responses to acute ER stress and ROS through mechanisms that are distinct and mutually exclusive.

IRE-1 Kinase Domain Sulfenylation Drives the Antioxidant Response

Having determined that ROS exposure acutely inhibits the canonical UPR^{ER} activity of IRE-1, we investigated whether IRE-1 might become modified by ROS. The initial step in Cys oxidation is conversion of the thiol group (SH) to sulfenic acid (SOH)

(K) AS does not inhibit the PERK kinase PEK-1, as indicated by phosphorylation of its substrate eIF2-α. In the right panels PEK-1 expression was blocked by RNAi. (L–O) Pre-exposure to ER stress inhibits the antioxidant response. Exposure to TM (5 hr) prior to AS treatment (30 min) decreased p38 activation (L), SKN-1 nuclear localization (M), and intestinal *gst-4P*::GFP expression (N), with scoring shown in (O).

In all figures, mock incubations and zero time points are indicated by "C." For (B), (D), (J), (M), and (O), GFP quantification is with high (H), medium (M), or low (L) scoring. $p < 0.0001$****; $p < 0.001$***; $p < 0.01$**. All immunoblots in the paper are representative of at least two, and in most cases three, experiments. See also Figure S1.

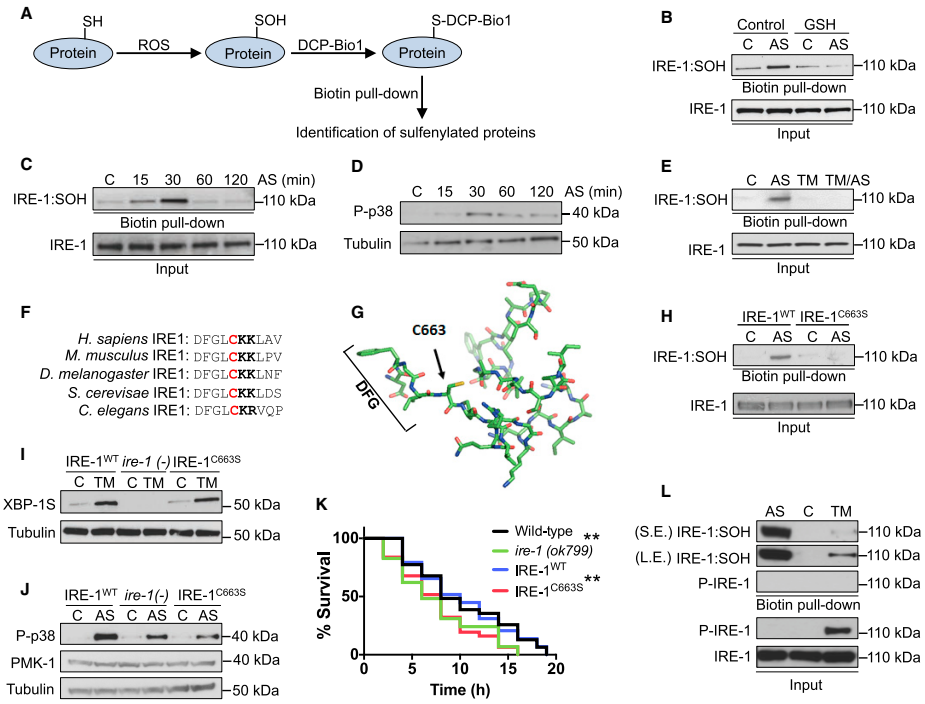

Figure 2. IRE-1 Sulfenylation within the Kinase Activation Loop

(A) Capture of sulfenylated (SOH) proteins with DCP-BIO1.

(B) ROS induce sulfenylation of IRE-1. Lysates from animals treated with AS (30 min) in the absence or presence of GSH were incubated with DCP-BIO1, with sulfenylated IRE-1 (IRE-1:SOH) identified by immunoblot.

(C and D) sulfenylation of IRE-1 parallels p38 activation. Animals treated with AS for 0–120 min were assessed for IRE-1:SOH (C) and active p38 (D) by immunoblot.

(E) ER stress interferes with IRE-1 sulfenylation. Animals pretreated with TM (5 hr) show reduced IRE-1:SOH in response to AS (30 min).

(F and G) Conservation of C663 within the IRE-1 kinase domain. In (F), adjacent basic amino acids are labeled in bold. A model of the IRE-1 kinase domain based upon the human Ire1α crystal structure (PDB ID: 3P23) shows C663 protruding into the ATP-binding pocket (G).

(H) C663 is the site of IRE-1 sulfenylation. IRE-1:SOH was not detected in IRE-1^{C663S} animals after AS treatment (30 min).

(I) C663 mutation does not interfere with ER stress-induced XBP-1S production. XBP-1S protein levels were determined in *ire-1 (ok799)* animals and animals expressing either IRE-1^{WT} or IRE-1^{C663S} following TM (5 hr) treatment.

(J) C663 is required for ROS-induced p38 activation. IRE-1^{C663S} animals exhibit diminished AS-induced p38 activity comparable to *ire-1(ok799)* null animals. In (H)–(J), results are representative of two independent transgenic lines.

(K) IRE-1^{C663S} animals exhibit enhanced oxidative stress sensitivity compared to *ire-1(ok799)* that was rescued with WT IRE-1. Day 1 adult worms were exposed to 5 mM AS (**$p < 0.01$).

(L) IRE-1 sulfenylation is not compatible with IRE-1 phosphorylation. The sulfenylated IRE-1 fraction, which was isolated by Biotin (Dimedone) pull down, does not contain any detectable phosphorylated IRE-1. S.E., short exposure; L.E., long exposure.

See also Figure S2 and Table S1.

(Figures 2A and S2A). This modification can be detected specifically with a chemical probe (Dimedone or its derivatives) (Yang et al., 2014) (Figure 2A). Using a biotin-linked Dimedone derivative (DCP-BIO1), we discovered that *C. elegans* IRE-1 is readily and transiently sulfenylated (IRE-1:SOH) in vivo by AS-generated ROS, with the extent of sulfenylation peaking at around 30 min (Figures 2B and 2C). The AS dependence of this SOH signal eliminated the possibility that it arose through post-lysis oxidation. AS treatment did not alter the gel mobility distribution of IRE-1 (Figure S2B), suggesting that sulfenylated IRE-1 did not progress

to disulfide bond formation. The time course of AS-induced p38 activity roughly paralleled that of IRE-1 sulfenylation (Figure 2D), consistent with the idea that IRE-1 sulfenylation might be involved in MAPK activation. Our finding that ER stress antagonizes the IRE-1/p38/SKN-1 response to ROS (Figures 1L–1O) suggested that IRE-1 sulfenylation might also be inhibited. Accordingly, ER stress induced by either TM or *tfg-1* RNAi blocked subsequent IRE-1 sulfenylation (Figures 2E and S2C).

We sought to identify the sulfenylated cysteine in IRE-1. Cys residues are differentially prone to oxidation if they are located near basic amino acids that may stabilize their thiol group as an anion (Poole, 2015). C663 of IRE-1 is widely conserved, and located adjacent to basic amino acids within the activation loop of the IRE-1 kinase domain (Figures 2F and 2G). It is also close to the Mg^{2+}-binding DFG motif, which is critical for kinase function (Bayliss et al., 2012). We generated *ire-1(ok799)* nulls that transgenically expressed wild-type IRE-1 (IRE-1^{WT}), or IRE-1 in which C663 was mutated to serine (IRE-1^{C663S}). AS induced rapid in vivo sulfenylation of IRE-1^{WT}, but not IRE-1^{C663S}, suggesting that IRE-1 is sulfenylated uniquely at C663 (Figure 2H). Rescue with IRE-1^{WT} and IRE-1^{C663S} comparably allowed *xbp-1* mRNA splicing in response to ER stress, indicating that this mutation does not disrupt IRE-1 folding or its canonical UPR^{ER} functions (Figure 2I). In striking contrast, the IRE-1^{C663S} mutation prevented AS from activating p38 above the *ire-1(-)* mutant background (Figure 2J). Accordingly, the IRE-1^{C663S} transgenics and *ire-1(ok799)* nulls were comparably sensitive to oxidative stress (Figure 2K; Table S1). We speculated that sulfenylation of IRE-1 at C663 might inhibit its kinase activity, given the critical location of this residue. ER stress strongly increased IRE-1 phosphorylation, as predicted (Ron and Walter, 2007), but elicited only a low level of IRE-1 sulfenylation (Figure 2L). In striking contrast, the sulfenylated IRE-1 population appeared to be completely unphosphorylated (Figure 2L), consistent with evidence that AS inhibited ER stress-induced IRE-1 phosphorylation (Figure 1F). Together, the data suggest that when IRE-1 is exposed to ROS in the cytoplasm, sulfenylation at C663 inhibits its canonical kinase and UPR^{ER} activities but is required for p38/SKN-1 pathway activation.

Localized ROS Production Initiates the p38 Cascade at IRE-1

We next investigated how IRE-1 sulfenylation promotes p38 signaling. In *C. elegans*, the p38/SKN-1 antioxidant response depends largely upon the p38 MAPKKK NSY-1 (Figure S1B) (Inoue et al., 2005). We found that NSY-1 forms a complex with IRE-1 and that this was increased by AS treatment (Figure 3A). In mammalian cells, tumor necrosis factor-alpha and other peptide factors activate p38 by recruiting MAPKKK to their membrane receptor through bridging by TRAF2 (Cuadrado and Nebreda, 2010). Knockdown of *C. elegans* TRAF2 (*trf-1*) decreased IRE-1/NSY-1 complex formation, AS-induced p38 phosphorylation, SKN-1 nuclear accumulation, and *gst-4P*::GFP activation and increased oxidative stress sensitivity (Figures 3B–3F and S3A; Table S1). By contrast, *trf-1* RNAi did not interfere with AS-induced sulfenylation of IRE-1 (Figure 3G), indicating that TRF-1 is not required for AS-induced ROS production. Knockdown of *trf-1* also did not reduce UPR^{ER} activation by ER stress, indicating that TRF-1 is not required for this aspect of IRE-1 function (Figures S3B and S3C). The data indicate that TRF-1 allows the MAPKKK NSY-1 to be recruited to IRE-1 and that this interaction is essential for activation of the p38 response to ROS.

We examined how NSY-1 becomes activated when bound to IRE-1. Phosphorylation within the kinase activation loop is critical for MAPKKK activation (Raman et al., 2007). Importantly, AS treatment induced activating phosphorylation of NSY-1 independently of *ire-1* (Figure 3H), indicating that IRE-1 must be required for a different NSY-1 activation step. NSY-1 lacks a Cys at DFG+2 (not shown) but was sulfenylated robustly in response to AS treatment (Figures 3G and 3I). This NSY-1 sulfenylation required both *ire-1* and *trf-1*, in contrast to NSY-1 phosphorylation (Figures 3G–3I). Thus, while IRE-1 sulfenylation at C663 inhibits its kinase, sulfenylation of NSY-1 at a different position correlates with its interaction with IRE-1 and p38 cascade activation (Figure S3D). Together, the data suggest that AS-induced activation of the p38 cascade depends upon TRF-1-dependent recruitment of phosphorylated NSY-1 to an oxidizing environment at IRE-1 and the cytoplasmic surface of the ER membrane (Figure S3D).

Cellular antioxidant mechanisms limit the extent of ROS diffusion, making it necessary for ROS signals to be produced locally with respect to the target (Winterbourn, 2008). How might AS induce production of a localized pool of ROS in the vicinity of IRE-1? AS can damage proteins and lipids directly, but it is not known how AS exposure induces ROS production (Hughes et al., 2011). NOX enzymes represent a potential source of inducible ROS production. These enzymes generate superoxide anions by reducing NADPH, are produced in the ER, and are present in membrane structures (Lambeth and Neish, 2014; Laurindo et al., 2014). They have well-described roles in pathogen defense and have been implicated in signaling by some growth factors, but less is known about their other functions. The two *C. elegans* NOX enzymes (BLI-3 and DUOX-2) are dual oxidases (DUOXs), which may directly convert superoxide to hydrogen peroxide (van der Hoeven et al., 2011). Knockdown of *bli-3*, but not *duox-2*, dramatically attenuated the *gst-4p::GFP* response to AS (Figures 3J, 3K, and S3E). AS treatment increased BLI-3 activity, leading to ROS production that was blocked by a NOX inhibitor (Figure 3L). Accordingly, *bli-3* RNAi diminished AS-induced IRE-1 sulfenylation and p38 activation (Figures 3M and 3N). IRE-1 and BLI-3 interacted physically, and their association was increased by AS treatment (Figure 3O). We conclude that AS causes stress that leads to activation of BLI-3 that is at or near the ER, leading to ROS production. These ROS signal locally through IRE-1 to activate the p38/SKN-1 antioxidant response.

p38 Activation and Longevity Induced by ROS at the ER

Our model predicts that any stimulus that generates ROS in the vicinity of the ER could activate the IRE-1/p38/SKN-1 pathway. Mitochondria are a major source of cellular ROS, and perturbations in mitochondrial respiration can increase ROS production to levels that are devastating. The ER interacts physically with mitochondria (Kornmann, 2013), raising the question of whether mitochondrially produced ROS might signal through IRE-1. PQ induces mitochondrial ROS production by inhibiting complex 1

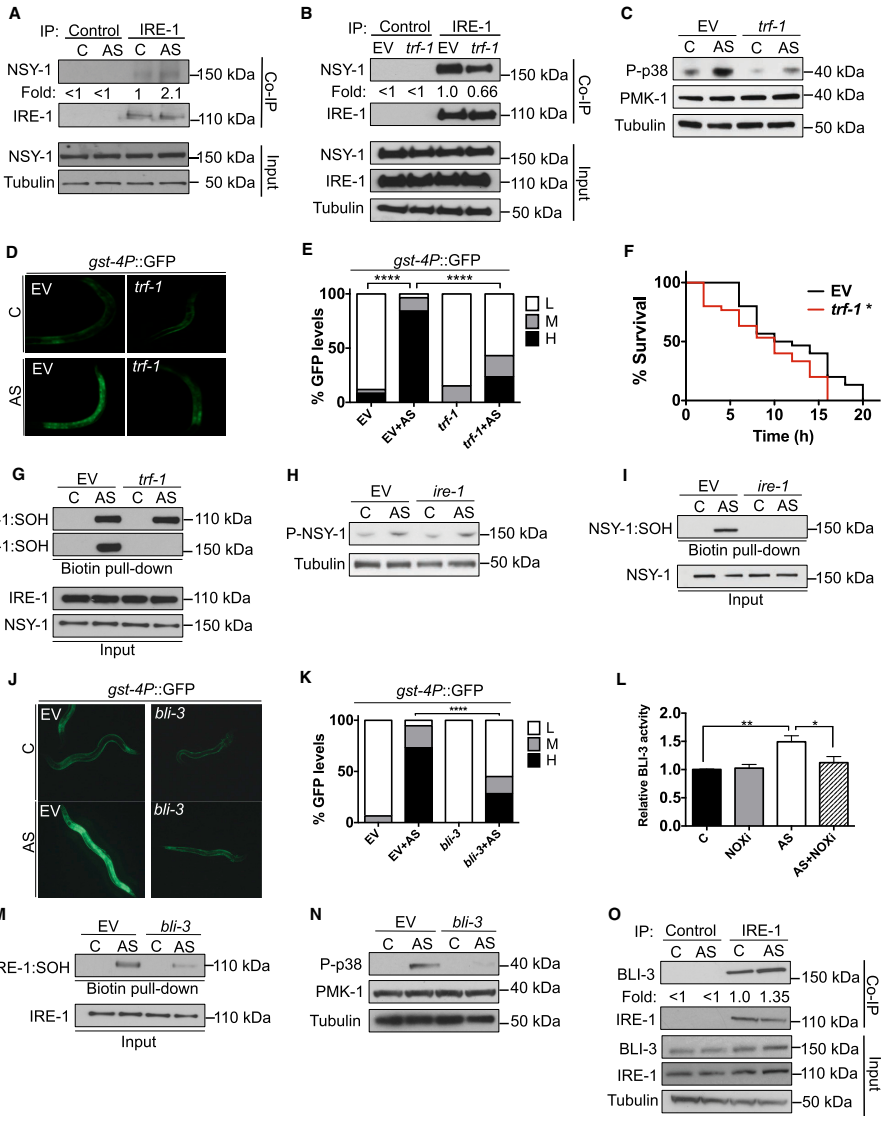

Figure 3. A Local ROS Signal Initiates the IRE-1/p38/SKN-1 Response

(A) AS promotes IRE-1 and NSY-1 complex formation. IRE-1 was immunoprecipitated from *C. elegans* that had been treated with vehicle or AS (30 min), then assayed by immunoblot for NSY-1. Non-specific IgG acted as control.

(legend continued on next page)

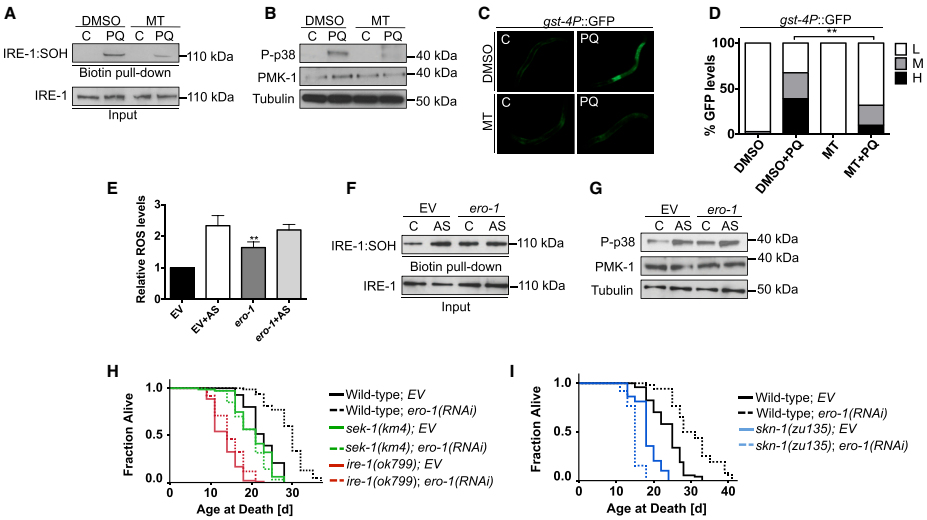

Figure 4. ER-Associated ROS Activate the IRE-1/p38/SKN-1 Pathway to Increase Lifespan

(A) IRE-1 is sulfenylated in response to mitochondrial ROS production. IRE-1 sulfenylation (SOH) that is induced by PQ (30 min) was inhibited by pre-treatment of *C. elegans* with the mitochondrial ROS scavenger mito-tempo (MT) (1 hr).

(B–D) Mitochondrial ROS activate the p38/SKN-1 response. Mito-tempo (MT) (1 hr) reduced the p38 response to PQ (30 min) (B) and diminished PQ-induced *gst-4P*::GFP expression (C), with GFP scoring shown in (D). GFP was quantified as high (H), medium (M), or low (L).

(E–I) *ero-1* RNAi induces ROS production (E), IRE-1:SOH (F), and p38 signaling (G) to extend lifespan (H and I). The MAPKK SEK-1 phosphorylates p38 in response to ROS and is required for p38 activity (Inoue et al., 2005). Lifespan extension from *ero-1* RNAi depended upon *ire-1*- and *sek-1* (H), and in a presumed null *skn-1* mutant *ero-1* RNAi shortened lifespan (I).

Additional lifespan experiments and statistics are described in Table S2. ****p < 0.0001; *p < 0.05. See also Figure S4 and Table S2.

of the electron transport chain (Yang and Hekimi, 2010). Accordingly, PQ, but not AS, activated the mitochondrial UPR (Pellegrino et al., 2014), a biomarker of mitochondrial ROS production (Figure S4A). PQ rapidly induced IRE-1 sulfenylation (Figure 4A), as expected from the *ire-1* dependence of the p38/SKN-1 response to PQ (Figures 1A and 1B). PQ-induced appearance of IRE-1/p38/SKN-1 response markers was diminished by the antioxidant Mito-Tempo (MT), which scavenges mitochondrial ROS specifically (Figures 4A–4D). Importantly, and in contrast to AS, PQ activated this response independently of the NOX enzyme *bli-3* (Figure S4B) (van der Hoeven et al., 2011). We conclude that the p38 antioxidant response is initiated at IRE-1 in response to localized ROS that can be generated by either NOX activation or mitochondria.

(B) *trf-1* promotes AS-induced IRE-1 and NSY-1 interaction. Lysates of animals fed control (*EV*) or *trf-1* RNAi and treated with AS (30 min) were assayed by immunoblot for IRE-1/NSY-1 interaction.

(C–E) *trf-1* is required for the p38/SKN-1 response to AS. Knockdown of *trf-1* diminished the p38 (C) and *gst-4P*::GFP (D) responses to AS (30 min), with GFP scoring shown in (E).

(F) Reduced TRF-1 levels sensitize to oxidative stress. Day 1 adults were scored for survival in 5 mM AS.

(G) Sulfenylation of NSY-1, but not IRE-1, requires *trf-1*. Knockdown of *trf-1* blocked AS-induced (30 min) sulfenylation of NSY-1.

(H) AS induces NSY-1 phosphorylation comparably in control (*EV*) and *ire-1(RNAi)* animals.

(I) AS induces NSY-1 sulfenylation in an *ire-1*-dependent manner. Animals fed either control or *ire-1* RNAi were assessed for NSY-1:SOH after AS (30 min) treatment.

(J and K) *bli-3* (DUOX) is required for the p38/SKN-1 response to AS. *bli-3* RNAi reduced intestinal *gst-4P*::GFP activation by AS (30 min) (J), with intestinal GFP scoring in (K).

(L) AS exposure (30 min) increases BLI-3 activity. NOX-dependent superoxide production was measured by chemiluminescence.

(M) AS-induced sulfenylation of IRE-1 was diminished by *bli-3* RNAi.

(N) *bli-3* is required for the p38 response to AS. *bli-3* RNAi decreased AS-induced p38 activity.

(O) Interaction of IRE-1 and BLI-3 is enhanced by AS, assessed by co-IP.

For (E) and (K), GFP scored as high (H), medium (M), or low (L). ****p < 0.0001; **p < 0.01; *p < 0.05. See also Figure S3.

We also investigated whether the IRE-1/p38/SKN-1 pathway could be activated by ROS that are produced by the ER itself, through the process of secretory protein folding. ER oxidoreducin 1 (ERO1) drives disulfide bond formation within the ER lumen by participating in a redox relay that generates hydrogen peroxide (Kakihana et al., 2012; Sevier and Kaiser, 2008; Tu and Weissman, 2004). Surprisingly, in mice deletion of both *ERO1* genes only subtly impaired ER disulfide formation, implying that an alternative mechanism can drive Cys thiol oxidation (Zito et al., 2012). These mutant mice exhibited increased sulfenylation of membrane-associated proteins, depletion of the antioxidant ascorbic acid, and a greater proportion of oxidized glutathione (Zito et al., 2012), suggesting that ROS levels were increased. As these mouse studies predict, knockdown of *ero-1* in adult *C. elegans* increased ROS levels, IRE-1 sulfenylation, *ire-1*-dependent p38 phosphorylation, and SKN-1 target gene activity (Figures 4E–4G, S4C, and S4D). This p38 activation was abolished by GSH, suggesting that it is ROS driven (Figure S4E). Knockdown of *ero-1* therefore resulted in ROS production that activated the IRE-1/p38/SKN-1 antioxidant response. Consistent with our evidence that this response and the UPR^{ER} are mutually exclusive, *ero-1* RNAi also interfered with TM-induced production of the spliced form of XBP-1 (Figure S4F).

Quiescin-Sulfhydryl Oxidase (QSOX) proteins are produced in the ER and catalyze disulfide formation, thereby generating peroxide, but their contributions to ER protein folding in vivo are unknown (Kodali and Thorpe, 2010; Sevier, 2012). Strikingly, *ero-1* RNAi failed to generate ROS and activate p38 when *C. elegans* QSOX genes were knocked down (Figures S4G and S4H). This suggests that when ERO-1 activity is low, QSOX generates high levels of ROS and might play a compensatory role in the ER. Consistent with this idea, a strong genetic interaction between *ero1* and *qsox1* was previously detected in *Drosophila* (Tien et al., 2008). We conclude that when ER redox homeostasis is perturbed sufficiently to increase cytoplasmic ROS levels, the IRE-1/p38/SKN-1 antioxidant response becomes activated.

ROS can damage cellular macromolecules and have long been presumed to promote aging. However, it is now known that *C. elegans* lifespan can be increased when mitochondrial ROS production is modestly elevated, apparently because protective mechanisms are mobilized (Lee et al., 2010; Ristow, 2014; Yang and Hekimi, 2010). *ero-1* is required for *C. elegans* development (not shown) but was detected in a screen that identified genes for which RNAi knockdown during adulthood increases lifespan (Curran and Ruvkun, 2007). We confirmed that lifespan is increased substantially when *ero-1* is knocked down in adults (18%–48% extension of mean lifespan). Across multiple trials, this increased longevity largely or completely depended upon both *ire-1* and p38 signaling (Figure 4H and Table S2). Moreover, in *skn-1* mutants *ero-1* RNAi consistently decreased lifespan (Figure 4I and Table S2). Taken together, our data suggest that ER-derived ROS that are generated upon *ero-1* knockdown increase lifespan by activating the *ire-1*/p38/SKN-1 pathway. Knockdown of *ero-1* was notably deleterious when the SKN-1-mediated antioxidant response was completely absent, illustrating the importance of this protective response for defending against ER-derived ROS. The lifespan extension enjoyed by *ero-1(RNAi)* animals (Figures 4H and 4I) also suggests that the *ire-1*/p38/SKN-1 response promotes both homeostasis and health.

Conservation of the IRE-1 Antioxidant Response Function

The DFG+2 Cys in Ire1 is evolutionarily conserved (Figure 2F), suggesting that Ire1 might initiate the p38 antioxidant response in mammals. Accordingly, AS treatment rapidly induced Ire1α sulfenylation and p38 activation in human (HepG2) cells (Figures 5A and 5B). AS also activated the stress-response kinase JNK, but only p38 activation was blocked by *Ire1α* knockdown (Figure 5B). Similar to *C. elegans* results with *bli-3* RNAi, the mammalian p38 response to AS was attenuated by a NOX inhibitor, indicating that it was initiated by enzymatically produced ROS (Figure 5C). The human Ire1α responses to acute ROS and ER stress were also mutually exclusive: short-term AS preconditioning blocked ER stress-induced XBP-1S induction, and pre-treatment with TM inhibited AS-induced p38 activation (Figures 5D and 5E). Human Ire1α therefore initiates an acute p38 response to ROS analogously to its *C. elegans* counterpart. In *C. elegans*, stress responses can be influenced profoundly by signals between tissues (Prahlad and Morimoto, 2011; Taylor and Dillin, 2013), but our detection of this response in cultured cells demonstrates that it occurs cell-autonomously.

In mammalian cells, AS treatment appears to activate Nrf2 independently of the canonical Nrf2 inhibitor Keap1 (Wang et al., 2008). Earlier work suggested a possible role for p38 signaling in the Nrf2 antioxidant response (Zipper and Mulcahy, 2000), but this has not been elucidated. Nrf2 upregulates its own expression and becomes activated through stabilization, making Nrf2 protein levels a reliable indicator of the antioxidant response (O'Connell and Hayes, 2015; Suzuki and Yamamoto, 2015). Remarkably, the Nrf2 response to AS was dramatically attenuated by treatment with Ire1α siRNA, a NOX inhibitor, or a p38 inhibitor (Figures 5B, 5C, and 5F), as would be predicted from our *C. elegans* data. By contrast, the classical Keap1 inhibitor sulforaphane increased Nrf2 levels independently of Ire1 (Figure 5G), suggesting that the Ire1α-regulated antioxidant response is parallel to and distinct from the Keap1-Nrf2 axis. Treatment with an Ero1 inhibitor activated p38 signaling and Nrf2 in human cells (Figure 5H), indicating conservation of this response to ER-derived ROS. Together, our *C. elegans* and mammalian data demonstrate the existence of a conserved ancestral Ire1α/p38 pathway that activates Nrf2 when ROS accumulate at the ER (Figure S5).

Sulfenylation of Related Kinases by NOX-Generated ROS

Oxidative stress affects numerous cellular functions, including protein synthesis and proliferation (Martindale and Holbrook, 2002), but the mechanisms involved are largely not understood. Interestingly, a conserved Cys is present at the same DFG+2 position as IRE-1 in approximately 8% of human kinases, including most members of the AGC family (Figure 6A) (Liu et al., 2013). In many cases, this Cys is predicted to be redox-reactive (not shown), suggesting that these kinases might be modified similarly to IRE-1 when NOX enzymes produce ROS in response to stress. To test this idea, we examined AGC kinases in which

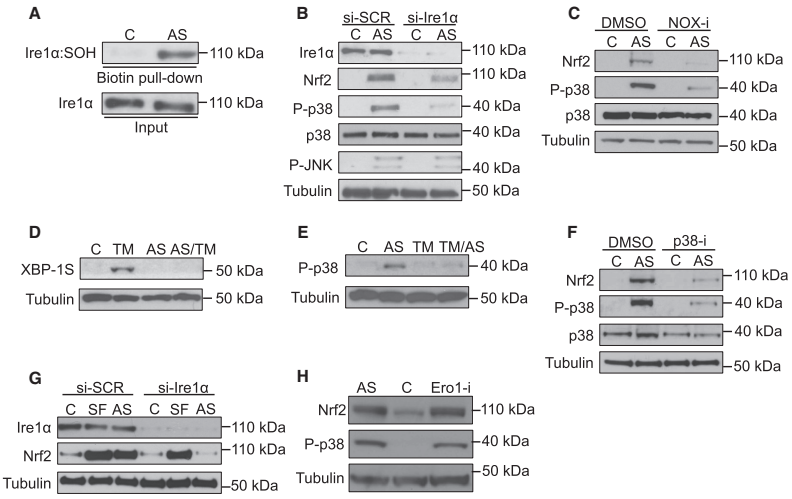

Figure 5. Evolutionary Conservation of the IRE-1 Antioxidant Response Function

(A) Human Ire1α senses ROS. Ire1α sulfenylation was assessed in HepG2 cells following AS (30 min) treatment.

(B) Ire1α is required for the p38 and Nrf2 response to AS-induced ROS. Levels of Nrf2 accumulation, p38 phosphorylation, and activation were assayed in HepG2 cells treated with either control siRNA (si-SCR) or *Ire1α* siRNA (si-Ire1α) following AS (30 min) treatment.

(C) NOX-derived ROS activate the p38/Nrf2 pathway. Levels of Nrf2 and p38 activation were determined in HepG2 cells treated with AS (30 min) in the absence or presence of the pan-NOX inhibitor VAS2870 (NOX-i) (1 hr).

(D and E) Ire1α senses ROS and ER stress in a mutually exclusive manner. HepG2 cells were treated with AS (30 min) prior to TM (5 hr) treatment, with Xbp1S protein assayed by immunoblot (D). Levels of active p38 were determined in HepG2 cells following treatment with AS (30 min) alone, TM (5 hr) alone, or pre-treatment with TM prior to acute AS exposure (E).

(F) Nrf2 activation by AS requires p38. HepG2 cells were treated with vehicle control or the p38 inhibitor SB203580 (p38-i) (2 hr) prior to AS (30 min).

(G) Ire1α regulates Nrf2 independently of Keap1. HepG2 cells treated with either control siRNA (si-SCR) or *Ire1α* siRNA (si-Ire1α) were exposed to either the Keap1 inhibitor sulforaphane (SF) (30 min) or AS (30 min).

(H) Activation of the p38/Nrf2 response by ER-derived ROS. Treatment of HepG2 cells with Ero1 inhibitor II (2 hr) activated p38 and Nrf2 comparably to AS.

See also Figure S5.

the DFG+2 Cys is predicted to be reactive (Rock1, Akt, Pkc-δ, and p70S6K) or non-reactive (Pak1) (Figure 6A). Using available antibodies, we found that AS rapidly induced sulfenylation of Rock1 (LET-502) and p70S6K (RSKS-1) orthologs in *C. elegans* (Figure 6B). In human cells, AS similarly induced sulfenylation of each AGC kinase tested except for Pak1 (Figure 6C). Remarkably, NOX inhibition blocked sulfenylation of these kinases (Figure 6C), suggesting that many kinases with a DFG+2 Cys may be susceptible to conserved modification and regulation by NOX-produced ROS signals.

DISCUSSION

A Conserved IRE-1 Function that Is Distinct from the UPR^{ER}

Over 23 years of study have yielded deep insights into the canonical IRE-1 function of responding to unfolded proteins within the ER (Maly and Papa, 2014; Ron and Walter, 2007). Here we describe a mechanistically distinct IRE-1 function in which its cytoplasmic kinase transduces ROS signals from the ER, NOX enzymes, and mitochondria (Figure 7A). IRE-1 assumes this unexpected function through a conserved molecular switch in which a Cys within its kinase activation loop becomes sulfenylated when exposed to a ROS signal. This addition of a single oxygen atom appears to inhibit the IRE-1 kinase and RNase and promotes recruitment and activation of p38 signaling at IRE-1. Our data provide a striking example of a well-described protein having an unexpected function and suggest that Cys-based signaling can regulate proteins in diverse ways.

IRE-1 initiates this antioxidant response upon exposure to ROS that are generated nearby and need not be dispersed throughout the cytoplasm. Stress-induced phosphorylation of the MAPKKK NSY-1 was not sufficient to activate p38 signaling, which depended upon NSY-1 also being physically associated with IRE-1 within an oxidative environment and becoming sulfenylated (Figure 3). At the ER, IRE-1 is in an opportune location to sense ROS and stimuli that trigger ROS signals. The ER lumen maintains oxidizing conditions (Kakihana et al., 2012; Sevier

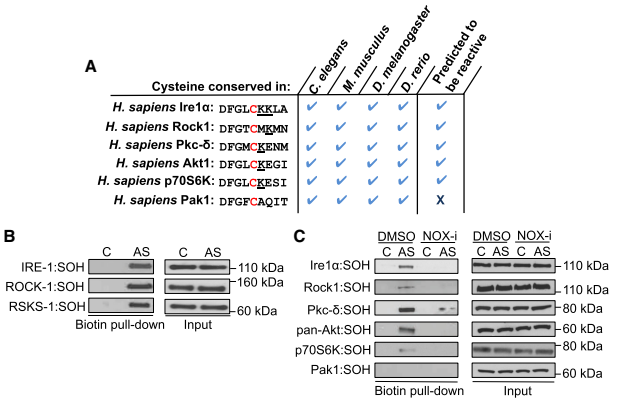

Figure 6. Sulfenylation of AGC Kinases by NOX-Derived ROS

(A) Alignment of the DFG+2 Cys of selected human AGC kinases. Basic amino acids are underlined.

(B) The *C. elegans* Rock1 ortholog (LET-502) and p70S6K (RSKS-1) are sulfenylated in vivo. Lysates from animals treated with AS (30 min) were assessed for levels of Rock1:SOH and RSKS-1:SOH.

(C) NOX-derived ROS sulfenylate multiple AGC kinases. HepG2 cells were treated with AS (30 min) in the absence or presence of the NOX inhibitor (NOX-i) VAS2870 (1 hr).

and Kaiser, 2008) apparently by balancing ERO-1 and QSOX activities (Figure S4G). IRE-1 is ideally poised to detect ER-derived ROS that appear in the cytoplasm and is well placed to detect mitochondrial ROS (Figures 4A–4D) because of extensive ER-mitochondrial communication (Kornmann, 2013). In addition, NOX enzymes that interact with IRE-1 transduce AS stress into a ROS signal (Figure 7A). This suggests that certain stresses, possibly lipid or protein damage in the vicinity of the ER (Laurindo et al., 2014), send an adaptive signal through IRE-1 to activate p38. By sensing these perturbations at the ER, IRE-1 acts as a sentinel that may limit their deleterious effects on the cell at large.

The requirement for IRE-1 sulfenylation would prevent ROS from activating p38 signaling without a "go ahead" signal from the ER environment. In *C. elegans*, SKN-1 and XBP-1 regulate each other's expression, suggesting underlying cooperation between their respective stress responses (Glover-Cutter et al., 2013). However, the UPR^{ER} and ROS signaling functions of IRE-1 are mutually exclusive (Figures 1F–1J, 1L–1O, 5D, and 5E). Under ER stress conditions it could be advantageous to suppress antioxidant response activation because this response could impair oxidative protein folding by increasing GSH levels. In the other direction, when the antioxidant response is needed it may be advantageous to "tap the brakes" on the IRE-1-initiated UPR^{ER} and oxidative protein folding until redox homeostasis is restored. Accordingly, when the ER becomes overly oxidizing, BiP undergoes oxidation that inhibits its chaperone function and allows it to stabilize misfolded proteins by acting as a holdase (Wang et al., 2014). The mutual exclusivity between the these two IRE-1 functions could explain evidence that the ER and cytoplasm are mutually antagonistic with respect to redox status, so that proteostasis perturbations that make the cytoplasm more oxidizing (and thus should inhibit the IRE-1 UPR^{ER}) render the ER more reducing (Kirstein et al., 2015).

It will be important to elucidate how post-translational modification of the IRE-1 kinase discriminates between these two distinct IRE-1 functions (Figure 7A) and influences the UPR^{ER} and antioxidant responses over time. For example, a considerable body of evidence indicates that the IRE-1 kinase is important for *xbp-1* mRNA splicing (Prischi et al., 2014; Ron and Walter, 2007), a model consistent with our results, but in yeast the Ire1 kinase limits the duration of the UPR^{ER} (Chawla et al., 2011; Rubio et al., 2011). One interesting question is whether the sulfenylated IRE-1 Cys progresses to further oxidation steps (Figure S2A) or can be "reset" to a thiol so that this IRE-1 molecule can reassume its UPR^{ER} function. Another question is how UPR^{ER} activation might inhibit IRE-1 from responding to ROS (Figure 7A). Perhaps oligomerized IRE-1 is resistant to sulfenylation within the kinase loop. Formation of a signalosome that initiates p38 signaling might require a subtle interaction with sulfenylated IRE-1, or it might be sufficient simply to inhibit the IRE-1 kinase and oxidatively modify the p38 MAPKKK. In mammalian cells, exogenous ROS administration induces the p38 MAPKKK ASK1 to form an internal disulfide that promotes signalosome assembly (Nadeau et al., 2007). Our finding that Ire1α is required for ROS-induced mammalian p38 activation suggests that ASK1 oxidation is not the initiating signaling event but might play a similar role to NSY-1 sulfenylation in *C. elegans*. In earlier cell culture experiments, sustained ER stress from TM led to JNK activation that was prevented by mutational Ire1 kinase inactivation (Urano et al., 2000). It is possible that p38 and JNK signaling are activated at IRE-1 through distinct mechanisms, with only the former involving sulfenylated kinase-inactive IRE-1 (Figure 7A). In HepG2 cells, we observed AS-induced JNK activation that did not require Ire1α (Figure 5B) but failed to detect TM-induced JNK activation (not shown), suggesting that the latter pathway might be context dependent.

A surprising aspect of our findings was that IRE-1 functions as a direct ROS sensor for the Nrf2/SKN-1 antioxidant pathway. In mammals, analyses of Nrf2 responses to stress have been focused almost entirely around the solidly established Keap1 inhibitory paradigm (Figure S5) (Suzuki and Yamamoto, 2015). p38 phosphorylates Nrf2 and has been implicated in its regulation in mammalian cells (Sun et al., 2009; Zipper and Mulcahy, 2000), but the functional significance of these findings has remained unclear. We determined that AS activates Nrf2 by stimulating the conserved NOX/Ire1α/p38 pathway, which apparently functions independently of Keap1 (Figures 5 and S5). Similarly, inhibition of mammalian Ero1 activated p38 and Nrf2

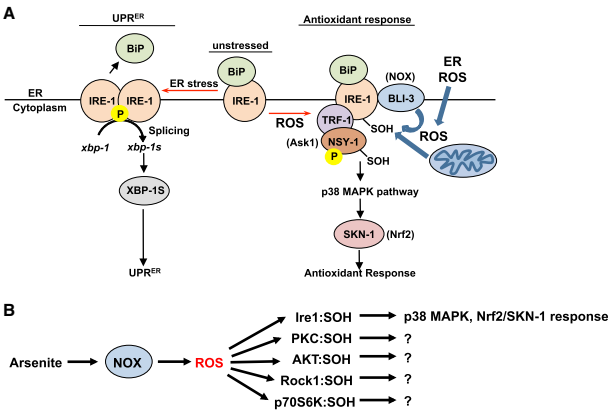

Figure 7. A Sulfenylation-Mediated Switch between IRE-1 Functions

(A) Model of the UPR^{ER} and antioxidant response functions of IRE-1 (see text).

(B) NOX-generated ROS sulfenylate multiple AGC kinases, resulting in IRE-1 adopting a distinct function.

(Figure 5H), indicating that this pathway is a conserved response to the presence of ROS at the ER. The presence of this IRE-1/p38 pathway in *C. elegans*, which lacks a Keap1 ortholog, suggests that it may represent the ancestral mode through which ROS and other stresses activate the antioxidant response. Perhaps Keap1 arose in higher organisms to broaden or speed responsiveness to diverse electrophilic compounds. Nrf2 is either pathogenic or protective in certain cancers, diabetes, and other diseases (Murakami and Motohashi, 2015; O'Connell and Hayes, 2015; Uruno et al., 2013). It will be important to elucidate the extent to which the normal and disease-related functions of Nrf2 involve its regulation by Ire1α and ER-associated ROS.

IRE-1 Redox Regulation in Aging and Disease

Ire1 is required for normal development and is dysfunctional or a potential therapeutic target in diseases that include cancer, diabetes, and neurodegeneration (Fu et al., 2012; Hetz et al., 2013; Wang and Kaufman, 2014). Our results indicate that functional requirements for Ire1 are likely to involve its regulation of p38/SKN-1(Nrf2) as well as its UPR^{ER} functions. In mice, obesity can lead to nitric oxide modifying Ire1α within its RNase, thereby perturbing *Xbp1* splicing and glucose homeostasis (Yang et al., 2015). Overall protein oxidation patterns change with age, possibly reflecting damage or maladaptive modifications (Brandes et al., 2013; Stadtman, 2006). Age- or disease-related oxidation of residues that have physiological regulatory functions, like IRE-1 C663, could have devastating effects.

Ire1 also appears to play a positive role in promoting longevity, as indicated by its being required for some genetic or dietary interventions to increase lifespan in *C. elegans* (Chen et al., 2009; Henis-Korenblit et al., 2010). This requirement is likely to involve not only the canonical UPR^{ER} function of IRE-1, but also activation of p38/SKN-1, a pathway linked to longevity across species (Blackwell et al., 2015). The observation that mitochondrially produced ROS can extend lifespan has generated considerable interest because it shows that ROS-based signals can promote longevity (Lee et al., 2010; Ristow, 2014; Yang and Hekimi, 2010). Some studies indicate that SKN-1 is essential for this beneficial effect of mitochondrial ROS (Blackwell et al., 2015). Here we determined that ER-derived ROS extend lifespan by activating the IRE-1/p38/SKN-1 pathway but are harmful when the SKN-1 antioxidant response is completely ablated (Figures 4H and 4I). The data emphasize the importance of SKN-1-regulated mechanisms as potent drivers of longevity, identify the ER as another source of ROS that can extend lifespan, and suggest that physiological ROS-mediated signaling may profoundly affect longevity and health.

Importance of Localized Redox Signaling for Homeostasis

A conserved Cys is present at the DFG+2 position in numerous kinases (Figure 6A) (Liu et al., 2013). In each case in which this Cys was predicted to be redox-reactive, these kinases became sulfenylated in response to AS treatment and NOX activation (Figure 6C). The precedent of IRE-1 suggests that sulfenylation might not simply inhibit their kinase activity, but also could induce unexpected functions (Figure 7B). It is not understood how oxidative stress affects so many cellular processes, including protein synthesis and proliferation (Martindale and Holbrook, 2002). The sulfenylated kinases we identified are involved in cell polarity (Rock1), cell growth and survival (Akt, Pkc), and protein synthesis (p70S6K), providing a possible explanation. ROS-scavenging antioxidants have largely failed as disease therapies, possibly because they may suppress protective mechanisms (Ristow, 2014). The idea that ROS have many physiological regulatory functions provides another note of caution concerning such treatments. Great interest has arisen in designing covalent inhibitors that target Cys residues, which are present in over 200 human kinase domains (Liu et al., 2013), and recently an Ire1 inhibitor has been designed that binds its DFG+2 Cys (Waller et al., 2016). Our results suggest that many of these potential Cys targets are likely to be physiological regulatory sites and that pharmacological targeting of such residues might allow specific activities to be modulated in multifunctional proteins like IRE-1.

We suspect that many more targets and processes are regulated physiologically by post-translational Cys modifications than is appreciated currently. At least 700 proteins are sulfenylated in mammalian cells, in patterns that are altered by ROS

or growth factor treatment (Yang et al., 2014). The paradigm of IRE-1 and NSY-1 regulation we have described suggests that many of these modified Cys residues are likely to be play regulatory roles and that this Cys-based regulation is remarkably versatile: sulfenylation inhibited the IRE-1 kinase and UPR^{ER} and induced IRE-1 to adopt a distinct function, whereas p38 signaling was activated through sulfenylation of NSY-1 that is associated with IRE-1. We propose that Cys modification by ROS from NOX enzymes or other sources allows various perturbations and signals to be transduced into a language that can be interpreted by kinases and transcription factors, or other regulators. Elucidating these regulatory interactions and the stimuli that trigger them, and determining how they influence their protein targets, is likely to yield profound insights into physiology, development, aging, and disease.

EXPERIMENTAL PROCEDURES

ROS Detection

Synchronized *C. elegans* were incubated with the ROS sensitive fluorescent probe CM-H_2DCFDA (Life Technologies), with ROS levels indicated relative to total protein concentration.

GFP Scoring

Expression or nuclear accumulation of transgenically expressed GFP proteins was scored as "low," "medium," or "high," as described previously (Glover-Cutter et al., 2013).

Sulfenylation Assay

Sulfenylated proteins were isolated from *C. elegans* and HepG2 cells using the DCP-Bio1 probe (KeraFast), prior to immunoblotting with antibodies.

Details and other methods are in the Supplemental Experimental Procedures.

SUPPLEMENTAL INFORMATION

Supplemental Information includes Supplemental Experimental Procedures, five figures, and two tables and can be found with this article online at http://dx.doi.org/10.1016/j.molcel.2016.07.019.

AUTHOR CONTRIBUTIONS

J.M.H. and T.K.B. designed the experiments, J.M.H., L.E.M.M., and L.P.F.-C. conducted the experiments and organized and interpreted the data, and J.M.H., L.P.F.-C., and T.K.B. wrote the paper.

ACKNOWLEDGMENTS

We thank Blackwell lab members and Eric Greer for helpful discussions, Sonja Bertram for experimental contributions, and Elizabeth Veal, Kunihiro Matsumoto, and Sivan Henis-Korenblit for reagents. Some strains were provided by the *Caenorhabditis* Genetics Center (CGC), which is funded by the NIH Office of Research Infrastructure Programs (P40 OD010440). The work was supported by funding from the NIH to T.K.B. (R01GM094398) and a Diabetes Center Research Award from the NIDDK (P30DK036836). L.P.F.-C is a doctoral student from Programa de Doctorado en Ciencias Bioquímicas, UNAM and received a fellowship from CONACyT and the PAEP program.

Received: April 11, 2016
Revised: July 1, 2016
Accepted: July 20, 2016
Published: August 18, 2016

REFERENCES

Bae, Y.S., Kang, S.W., Seo, M.S., Baines, I.C., Tekle, E., Chock, P.B., and Rhee, S.G. (1997). Epidermal growth factor (EGF)-induced generation of hydrogen peroxide. Role in EGF receptor-mediated tyrosine phosphorylation. J. Biol. Chem. *272*, 217–221.

Bayliss, R., Fry, A., Haq, T., and Yeoh, S. (2012). On the molecular mechanisms of mitotic kinase activation. Open Biol. *2*, 120136.

Blackwell, T.K., Steinbaugh, M.J., Hourihan, J.M., Ewald, C.Y., and Isik, M. (2015). SKN-1/Nrf, stress responses, and aging in Caenorhabditis elegans. Free Radic. Biol. Med. *88* (Pt B), 290–301.

Brandes, N., Tienson, H., Lindemann, A., Vitvitsky, V., Reichmann, D., Banerjee, R., and Jakob, U. (2013). Time line of redox events in aging postmitotic cells. eLife *2*, e00306.

Calfon, M., Zeng, H., Urano, F., Till, J.H., Hubbard, S.R., Harding, H.P., Clark, S.G., and Ron, D. (2002). IRE1 couples endoplasmic reticulum load to secretory capacity by processing the XBP-1 mRNA. Nature *415*, 92–96.

Chaudhari, N., Talwar, P., Parimisetty, A., Lefebvre d'Hellencourt, C., and Ravanan, P. (2014). A molecular web: endoplasmic reticulum stress, inflammation, and oxidative stress. Front. Cell. Neurosci. *8*, 213.

Chawla, A., Chakrabarti, S., Ghosh, G., and Niwa, M. (2011). Attenuation of yeast UPR is essential for survival and is mediated by IRE1 kinase. J. Cell Biol. *193*, 41–50.

Chen, D., Thomas, E.L., and Kapahi, P. (2009). HIF-1 modulates dietary restriction-mediated lifespan extension via IRE-1 in Caenorhabditis elegans. PLoS Genet. *5*, e1000486.

Chouchani, E.T., Kazak, L., Jedrychowski, M.P., Lu, G.Z., Erickson, B.K., Szpyt, J., Pierce, K.A., Laznik-Bogoslavski, D., Vetrivelan, R., Clish, C.B., et al. (2016). Mitochondrial ROS regulate thermogenic energy expenditure and sulfenylation of UCP1. Nature *532*, 112–116.

Cuadrado, A., and Nebreda, A.R. (2010). Mechanisms and functions of p38 MAPK signalling. Biochem. J. *429*, 403–417.

Curran, S.P., and Ruvkun, G. (2007). Lifespan regulation by evolutionarily conserved genes essential for viability. PLoS Genet. *3*, e56.

D'Autréaux, B., and Toledano, M.B. (2007). ROS as signalling molecules: mechanisms that generate specificity in ROS homeostasis. Nat. Rev. Mol. Cell Biol. *8*, 813–824.

Finkel, T. (2011). Signal transduction by reactive oxygen species. J. Cell Biol. *194*, 7–15.

Fu, S., Watkins, S.M., and Hotamisligil, G.S. (2012). The role of endoplasmic reticulum in hepatic lipid homeostasis and stress signaling. Cell Metab. *15*, 623–634.

Fulda, S., Gorman, A.M., Hori, O., and Samali, A. (2010). Cellular stress responses: cell survival and cell death. Int. J. Cell Biol. *2010*, 214074.

Glover-Cutter, K.M., Lin, S., and Blackwell, T.K. (2013). Integration of the unfolded protein and oxidative stress responses through SKN-1/Nrf. PLoS Genet. *9*, e1003701.

Gould, N.S., Evans, P., Martínez-Acedo, P., Marino, S.M., Gladyshev, V.N., Carroll, K.S., and Ischiropoulos, H. (2015). Site-Specific Proteomic Mapping Identifies Selectively Modified Regulatory Cysteine Residues in Functionally Distinct Protein Networks. Chem. Biol. *22*, 965–975.

Henis-Korenblit, S., Zhang, P., Hansen, M., McCormick, M., Lee, S.J., Cary, M., and Kenyon, C. (2010). Insulin/IGF-1 signaling mutants reprogram ER stress response regulators to promote longevity. Proc. Natl. Acad. Sci. USA *107*, 9730–9735.

Hetz, C., Chevet, E., and Harding, H.P. (2013). Targeting the unfolded protein response in disease. Nat. Rev. Drug Discov. *12*, 703–719.

Holmström, K.M., and Finkel, T. (2014). Cellular mechanisms and physiological consequences of redox-dependent signalling. Nat. Rev. Mol. Cell Biol. *15*, 411–421.

Hughes, M.F., Beck, B.D., Chen, Y., Lewis, A.S., and Thomas, D.J. (2011). Arsenic exposure and toxicology: a historical perspective. Toxicol. Sci. *123*, 305–332.

Inoue, H., Hisamoto, N., An, J.H., Oliveira, R.P., Nishida, E., Blackwell, T.K., and Matsumoto, K. (2005). The C. elegans p38 MAPK pathway regulates nuclear localization of the transcription factor SKN-1 in oxidative stress response. Genes Dev. *19*, 2278–2283.

Jomova, K., Jenisova, Z., Feszterova, M., Baros, S., Liska, J., Hudecova, D., Rhodes, C.J., and Valko, M. (2011). Arsenic: toxicity, oxidative stress and human disease. J. Appl. Toxicol. *31*, 95–107.

Kakihana, T., Nagata, K., and Sitia, R. (2012). Peroxides and peroxidases in the endoplasmic reticulum: integrating redox homeostasis and oxidative folding. Antioxid. Redox Signal. *16*, 763–771.

Kirstein, J., Morito, D., Kakihana, T., Sugihara, M., Minnen, A., Hipp, M.S., Nussbaum-Krammer, C., Kasturi, P., Hartl, F.U., Nagata, K., and Morimoto, R.I. (2015). Proteotoxic stress and ageing triggers the loss of redox homeostasis across cellular compartments. EMBO J. *34*, 2334–2349.

Kodali, V.K., and Thorpe, C. (2010). Oxidative protein folding and the Quiescin-sulfhydryl oxidase family of flavoproteins. Antioxid. Redox Signal. *13*, 1217–1230.

Kornmann, B. (2013). The molecular hug between the ER and the mitochondria. Curr. Opin. Cell Biol. *25*, 443–448.

Lambeth, J.D., and Neish, A.S. (2014). Nox enzymes and new thinking on reactive oxygen: a double-edged sword revisited. Annu. Rev. Pathol. *9*, 119–145.

Lau, A., Zheng, Y., Tao, S., Wang, H., Whitman, S.A., White, E., and Zhang, D.D. (2013). Arsenic inhibits autophagic flux, activating the Nrf2-Keap1 pathway in a p62-dependent manner. Mol. Cell. Biol. *33*, 2436–2446.

Laurindo, F.R., Araujo, T.L., and Abrahão, T.B. (2014). Nox NADPH oxidases and the endoplasmic reticulum. Antioxid. Redox Signal. *20*, 2755–2775.

Lee, S.J., Hwang, A.B., and Kenyon, C. (2010). Inhibition of respiration extends C. elegans life span via reactive oxygen species that increase HIF-1 activity. Curr. Biol. *20*, 2131–2136.

Levi-Ferber, M., Salzberg, Y., Safra, M., Haviv-Chesner, A., Bülow, H.E., and Henis-Korenblit, S. (2014). It's all in your mind: determining germ cell fate by neuronal IRE-1 in C. elegans. PLoS Genet. *10*, e1004747.

Liu, Q., Sabnis, Y., Zhao, Z., Zhang, T., Buhrlage, S.J., Jones, L.H., and Gray, N.S. (2013). Developing irreversible inhibitors of the protein kinase cysteinome. Chem. Biol. *20*, 146–159.

Maly, D.J., and Papa, F.R. (2014). Druggable sensors of the unfolded protein response. Nat. Chem. Biol. *10*, 892–901.

Martindale, J.L., and Holbrook, N.J. (2002). Cellular response to oxidative stress: signaling for suicide and survival. J. Cell. Physiol. *192*, 1–15.

Miedel, M.T., Graf, N.J., Stephen, K.E., Long, O.S., Pak, S.C., Perlmutter, D.H., Silverman, G.A., and Luke, C.J. (2012). A pro-cathepsin L mutant is a luminal substrate for endoplasmic-reticulum-associated degradation in C. elegans. PLoS ONE *7*, e40145.

Murakami, S., and Motohashi, H. (2015). Roles of Nrf2 in cell proliferation and differentiation. Free Radic. Biol. Med. *88* (Pt B), 168–178.

Nadeau, P.J., Charette, S.J., Toledano, M.B., and Landry, J. (2007). Disulfide Bond-mediated multimerization of Ask1 and its reduction by thioredoxin-1 regulate H(2)O(2)-induced c-Jun NH(2)-terminal kinase activation and apoptosis. Mol. Biol. Cell *18*, 3903–3913.

O'Connell, M.A., and Hayes, J.D. (2015). The Keap1/Nrf2 pathway in health and disease: from the bench to the clinic. Biochem. Soc. Trans. *43*, 687–689.

Paulsen, C.E., Truong, T.H., Garcia, F.J., Homann, A., Gupta, V., Leonard, S.E., and Carroll, K.S. (2012). Peroxide-dependent sulfenylation of the EGFR catalytic site enhances kinase activity. Nat. Chem. Biol. *8*, 57–64.

Pellegrino, M.W., Nargund, A.M., Kirienko, N.V., Gillis, R., Fiorese, C.J., and Haynes, C.M. (2014). Mitochondrial UPR-regulated innate immunity provides resistance to pathogen infection. Nature *516*, 414–417.

Poole, L.B. (2015). The basics of thiols and cysteines in redox biology and chemistry. Free Radic. Biol. Med. *80*, 148–157.

Prahlad, V., and Morimoto, R.I. (2011). Neuronal circuitry regulates the response of Caenorhabditis elegans to misfolded proteins. Proc. Natl. Acad. Sci. USA *108*, 14204–14209.

Prischi, F., Nowak, P.R., Carrara, M., and Ali, M.M. (2014). Phosphoregulation of Ire1 RNase splicing activity. Nat. Commun. *5*, 3554.

Raman, M., Chen, W., and Cobb, M.H. (2007). Differential regulation and properties of MAPKs. Oncogene *26*, 3100–3112.

Ristow, M. (2014). Unraveling the truth about antioxidants: mitohormesis explains ROS-induced health benefits. Nat. Med. *20*, 709–711.

Ron, D., and Walter, P. (2007). Signal integration in the endoplasmic reticulum unfolded protein response. Nat. Rev. Mol. Cell Biol. *8*, 519–529.

Rubio, C., Pincus, D., Korennykh, A., Schuck, S., El-Samad, H., and Walter, P. (2011). Homeostatic adaptation to endoplasmic reticulum stress depends on Ire1 kinase activity. J. Cell Biol. *193*, 171–184.

Sevier, C.S. (2012). Erv2 and quiescin sulfhydryl oxidases: Erv-domain enzymes associated with the secretory pathway. Antioxid. Redox Signal. *16*, 800–808.

Sevier, C.S., and Kaiser, C.A. (2008). Ero1 and redox homeostasis in the endoplasmic reticulum. Biochim. Biophys. Acta *1783*, 549–556.

Stadtman, E.R. (2006). Protein oxidation and aging. Free Radic. Res. *40*, 1250–1258.

Sun, Z., Huang, Z., and Zhang, D.D. (2009). Phosphorylation of Nrf2 at multiple sites by MAP kinases has a limited contribution in modulating the Nrf2-dependent antioxidant response. PLoS ONE *4*, e6588.

Sundaresan, M., Yu, Z.X., Ferrans, V.J., Irani, K., and Finkel, T. (1995). Requirement for generation of H2O2 for platelet-derived growth factor signal transduction. Science *270*, 296–299.

Suzuki, T., and Yamamoto, M. (2015). Molecular basis of the Keap1-Nrf2 system. Free Radic. Biol. Med. *88* (Pt B), 93–100.

Taylor, R.C., and Dillin, A. (2013). XBP-1 is a cell-nonautonomous regulator of stress resistance and longevity. Cell *153*, 1435–1447.

Tien, A.C., Rajan, A., Schulze, K.L., Ryoo, H.D., Acar, M., Steller, H., and Bellen, H.J. (2008). Ero1L, a thiol oxidase, is required for Notch signaling through cysteine bridge formation of the Lin12-Notch repeats in Drosophila melanogaster. J. Cell Biol. *182*, 1113–1125.

Tonks, N.K. (2005). Redox redux: revisiting PTPs and the control of cell signaling. Cell *121*, 667–670.

Tu, B.P., and Weissman, J.S. (2004). Oxidative protein folding in eukaryotes: mechanisms and consequences. J. Cell Biol. *164*, 341–346.

Urano, F., Wang, X., Bertolotti, A., Zhang, Y., Chung, P., Harding, H.P., and Ron, D. (2000). Coupling of stress in the ER to activation of JNK protein kinases by transmembrane protein kinase IRE1. Science *287*, 664–666.

Uruno, A., Furusawa, Y., Yagishita, Y., Fukutomi, T., Muramatsu, H., Negishi, T., Sugawara, A., Kensler, T.W., and Yamamoto, M. (2013). The Keap1-Nrf2 system prevents onset of diabetes mellitus. Mol. Cell. Biol. *33*, 2996–3010.

van der Hoeven, R., McCallum, K.C., Cruz, M.R., and Garsin, D.A. (2011). Ce-Duox1/BLI-3 generated reactive oxygen species trigger protective SKN-1 activity via p38 MAPK signaling during infection in C. elegans. PLoS Pathog. *7*, e1002453.

Waller, D.D., Jansen, G., Golizeh, M., Martel-Lorion, C., Dejgaard, K., Shiao, T.C., Mancuso, J., Tsantrizos, Y.S., Roy, R., Sebag, M., et al. (2016). A Covalent Cysteine-Targeting Kinase Inhibitor of Ire1 Permits Allosteric Control of Endoribonuclease Activity. ChemBioChem *17*, 843–851.

Wang, M., and Kaufman, R.J. (2014). The impact of the endoplasmic reticulum protein-folding environment on cancer development. Nat. Rev. Cancer *14*, 581–597.

Wang, X.J., Sun, Z., Chen, W., Li, Y., Villeneuve, N.F., and Zhang, D.D. (2008). Activation of Nrf2 by arsenite and monomethylarsonous acid is independent of Keap1-C151: enhanced Keap1-Cul3 interaction. Toxicol. Appl. Pharmacol. *230*, 383–389.

Wang, J., Pareja, K.A., Kaiser, C.A., and Sevier, C.S. (2014). Redox signaling via the molecular chaperone BiP protects cells against endoplasmic reticulum-derived oxidative stress. eLife *3*, e03496.

Winterbourn, C.C. (2008). Reconciling the chemistry and biology of reactive oxygen species. Nat. Chem. Biol. *4*, 278–286.

Yang, W., and Hekimi, S. (2010). A mitochondrial superoxide signal triggers increased longevity in Caenorhabditis elegans. PLoS Biol. *8*, e1000556.

Yang, J., Gupta, V., Carroll, K.S., and Liebler, D.C. (2014). Site-specific mapping and quantification of protein S-sulphenylation in cells. Nat. Commun. *5*, 4776.

Yang, L., Calay, E.S., Fan, J., Arduini, A., Kunz, R.C., Gygi, S.P., Yalcin, A., Fu, S., and Hotamisligil, G.S. (2015). METABOLISM. S-Nitrosylation links obesity-associated inflammation to endoplasmic reticulum dysfunction. Science *349*, 500–506.

Zipper, L.M., and Mulcahy, R.T. (2000). Inhibition of ERK and p38 MAP kinases inhibits binding of Nrf2 and induction of GCS genes. Biochem. Biophys. Res. Commun. *278*, 484–492.

Zito, E., Hansen, H.G., Yeo, G.S., Fujii, J., and Ron, D. (2012). Endoplasmic reticulum thiol oxidase deficiency leads to ascorbic acid depletion and noncanonical scurvy in mice. Mol. Cell *48*, 39–51.

Received: 30 September 2016 | Revised: 15 September 2017 | Accepted: 20 September 2017
DOI: 10.1002/dvg.23072

RESEARCH ARTICLE

WILEY genesis
The Journal of Genetics and Development

DPFF-1 transcription factor deficiency causes the aberrant activation of MPK-1 and meiotic defects in the *Caenorhabditis elegans* germline

Emmanuel Villanueva-Chimal[1] | Laura S. Salinas[1] | Laura P. Fernández-Cardenas[1] | Gabriela Huelgas-Morales[1] | Alejandro Cabrera-Wrooman[2] | Rosa E. Navarro[1]

[1]Departamento de Biología Celular y Desarrollo, Instituto de Fisiología Celular, Universidad Nacional Autónoma de México, México, D.F., México

[2]Laboratorio de Tejido Conjuntivo, Centro Nacional de Investigación y Atención de Quemados, Instituto Nacional de Rehabilitación "Luis Guillermo Ibarra Ibarra," México, D.F, México

Correspondence
Rosa E. Navarro, Departamento de Biología Celular y Desarrollo, Instituto de Fisiología Celular, Universidad Nacional Autónoma de México. Apartado Postal 70-600. México D.F., 04510 México.
Email: rnavarro@ifc.unam.mx

Funding information
NIH Office of Research Infrastructure Programs, Grant Number: P40 OD010440; National BioResource Project for the Experimental Animal "Nematode C. elegans," Tokyo, Japan; Consejo Nacional de Ciencia y Tecnología (CONACyT-México); Grant Number: 103856-Q, 220987; Programa de Apoyo a Proyectos de Investigación e Innovación Tecnológica (PAPIIT-UNAM), Grant Number: IN207412, IN207415

Summary

The d4 family of transcription factors consists of three members in mammals. DPF1/neuro-d4 is expressed mainly in neurons and the peripheral nervous system, and is important for brain development. DPF2/requiem/ubi-d4 is expressed ubiquitously and presumably functions as an apoptotic factor, especially during the deprivation of trophic factors. DPF3/cer-d4 is expressed in neurons and in the heart, and is important for heart development and function in zebrafish. In *Drosophila*, there is only one member, dd4, whose function is still unknown, but it is expressed in many tissues and is particularly abundant in the brain of developing embryos and in adults. Here, we present DPFF-1, the only member of this family of proteins in the nematode *C. elegans*. DPFF-1 is similar to its mammalian homolog DPF2/requiem/ubi-d4 because it is ubiquitously expressed during embryogenesis and in adult tissues, and because it is important for the induction of germ cell apoptosis during stress. Here, we show that *dpff-1* null mutant animals produce less progeny than wild-type nematodes, presumably due to meiotic defects. Gonads of *dpff-1* deficient animals showed more germ cells in pachytene and overexpressed the P-MPK-1 signal. Additionally, these animals presented higher levels of p53-induced germ cell apoptosis than wild-type animals. Furthermore, we observed that *dpff-1* deficient animals are more sensitive to heat shock. This is the first report showing that the d4 family of transcription factors could be involved in meiosis and stress protection.

KEYWORDS
apoptosis, DPF1/neuro-d4, DPF2/requiem/ubi-d4, DPF3/cer-d4, dpff-1, *C. elegans*, meiosis, MPK-1, stress

1 | INTRODUCTION

Members of the evolutionarily conserved d4 family of transcription factors DPF1/*neuro-d4*, DPF2/*requiem/ubi-d4* and DPF3/*cer-d4* play important roles in programmed cell death and development (Buchman et al., 1992; Gabig, Mantel, Rosli, & Crean, 1994; Lange et al., 2008; Lim, Seah, Mantalaris, Yap, & Wong, 2010; Tando et al., 2010; Wu et al., 2007). DPF1/*neuro-d4* and DPF3/*cer-d4* were originally described as transcription factors that are expressed only in the central and peripheral nervous systems of mice (Buchman et al., 1992; Kulikova, Mertsalov, & Simonova, 2013; Lessard et al., 2007; Mertsalov et al., 2000). In contrast, DPF2/*requiem/ubi-d4* is expressed in all tissues and organs of mice and is required for the apoptotic response upon IL-3 withdrawal in myeloid cells (Gabig et al., 1994, 1998). DPF2/REQ overexpression in Chinese hamster ovary (CHO) cells has a negative effect on cell growth and sensitizes cells to increased caspase-9 activities under control and staurosporine-induced apoptotic conditions (Lim et al., 2010).

Few groups have studied the requirements of this family of proteins in whole animals. Whereas mice with mutated DPF1/*neuro-d4* or DPF3/*cer-d4* do not show any reproductive or tissue defects (Mertsalov et al., 2008), morpholino knockdown of *dpf3* in zebrafish leads to

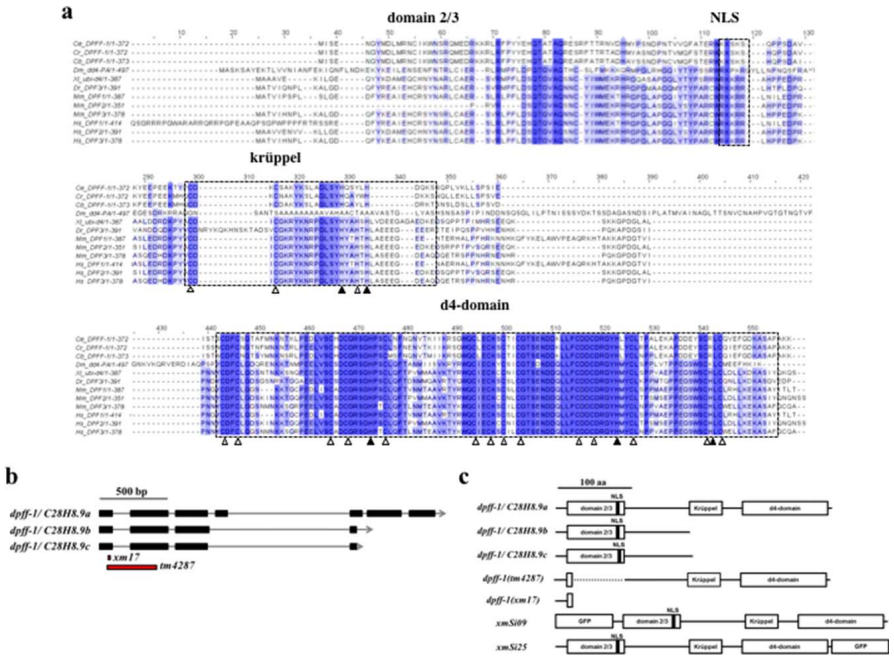

FIGURE 1 DPFF-1 is a member of the D4 zinc and double PHD finger transcription factor family. (a) Amino acid sequence alignment of D4 zinc and double PHD fingers transcription factor family. The alignment was performed with Ce-DPFF-1 (*C. elegans*), Cr-DPFF-1 (*C. remanei*), Cb-DPFF-1 (*C. briggsae*), Dm-dd4-PA (*Drosophila melanogaster*), Xl-ubi-d4 (*Xenopus laevis*), Dr-DPF3 (*Danio rerio*), Mm-DPF1, Mm-DPF2, Mm-DPF3 (*Mus musculus*), Hs-DPF-1, Hs-DPF2 and Hs-DPF3 (*Homo sapiens*) sequences, using the Muscle method. Conserved residues are marked with the same color. The conserved motifs are enclosed in dotted boxes. Domain 2/3: N-terminal region encoded by exons 2 and 3; NLS: nuclear localization signal; Krüppel-type zinc finger and d4-domains: within the domains, conserved cysteine and histidine residues are marked with open and closed arrowheads, respectively. (b) Schematic representation of *dpff-1* gene, isoforms and alleles (in red). (c) Schematic representation of DPFF-1 wild-type, mutant and transgenic proteins. GFP: green fluorescent protein; NLS: nuclear localization signal

incomplete cardiac looping and severely reduced ventricular contractility with disassembled muscular fibers (Lange et al., 2008).

The nematode *Caenorhabditis elegans* has only one member of this family of proteins, *dpff-1*. In this article, we show that DPFF-1 is important for fertility and the correct progression of germ cells through meiosis. *dpff-1* mutant animals had ectopic and higher expression of the active phosphorylated form of MPK-1 (P-MPK-1) than wild-type animals, and this expression was never down-regulated in the proximal gonad. We show that *dpff-1* mutant animals showed increased germ cell apoptosis, which we attributed to the activation of a meiotic checkpoint because was dependent on the p53 homolog of *C. elegans* CEP-1. Here, we also show that DPFF-1 is important for the heat shock response because animals lacking this protein were unable to induce germ cell apoptosis under these conditions, were more sensitive to heat shock and were unable to turn on heat shock stress reporters.

2 | RESULTS

2.1 | *C. elegans* has only one member of the D4 family of transcription factors

Searching for members of the d4 family of transcription factors in the *C. elegans* genome, we found the open reading frame C28H8.9, which is also called *dpff-1* (http://www.wormbase.org, release WS252, Dec 04, 2015). Protein alignment showed that *C. elegans* DPFF-1 is almost identical to its putative orthologs in *Caenorhabditis remanei* (86% identity) and *Caenorhabditis briggsae* (82% identity) (Figure 1a). *C. elegans* DPFF-1 is also closely related to *Drosophila melanogaster* dd4-PA (60% identity) and, to a lesser extent, is similar to its orthologs from vertebrates [~38% identity with the d4 family of transcription factors from *Xenopus laevis*, *Danio rerio*, *Mus musculus* and *Homo sapiens*; (Figure 1a)]. Similar to other members of the d4 family of transcription factors, *C. elegans* DPFF-1 contains a putative nuclear localization signal (NLS),

a Krüppel-type zinc finger domain and two C-terminal tandem plant homeodomains (PHD/d4-domain; Figure 1a,c). There are three predicted *dpff-1* spliced isoforms in the *C. elegans* genome, but only the longest isoform encodes a protein that possesses the Krüppel and d4 domains, which are characteristic of this family of proteins (Figure 1b,c).

2.2 | DPFF-1 is expressed in nuclei during development

To determine the expression pattern of *dpff-1* during *C. elegans* development, we made amino- and carboxy-terminus green fluorescent protein (GFP) reporter transgenes driven by *dpff-1's* own regulatory regions. To generate these transgenes, we cloned in tandem: *dpff-1's* putative promoter region (965 bp), defined as the intergenic sequence upstream of *dpff-1* (Dupuy et al., 2004), and the genomic coding region from ATG to the end of the longest 3'UTR reported (2632 bp) (http://www.wormbase.org, release WS252, Dec 04, 2015). Then, we fused the *gfp* coding gene without a stop codon after *dpff-1* ATG or before the *dpff-1* stop codon using a Gibson reaction (Gibson et al., 2009). Transgenic animals were generated by Mos1-mediated single copy insertion (MosSCI) (Frokjaer-Jensen, Davis, Ailion, & Jorgensen, 2012; Frokjaer-Jensen et al., 2008). The transgenic line *xmSi09* expresses the GFP reporter fused to DPFF-1 in the amine-terminus (Figure 1c), and the line *xmSi25* expresses the GFP reporter fused to DPFF-1 in the carboxy-terminus (Figure 1c). For simplicity, in this work, we will refer to the transgenic line *xmSi09* as GFP::DPFF-1 and the transgenic line *xmSi25* as DPFF-1::GFP.

A mixture of live GFP::DPFF-1 embryos, larvae and adult hermaphrodite animals were placed on a slide and observed under an epifluorescence microscope to determine the fusion protein expression pattern. GFP::DPFF-1 positive cells could be observed throughout all embryonic and post-embryonic stages, at high levels in nuclei, and at lower levels diffused throughout the cytoplasm (Figure 2). Both transgenic lines had the same expression pattern (Supporting Information Figure S1).

To confirm GFP::DPFF-1 nuclear localization, we stained extruded gonads of 1-day-old *xmSi09* hermaphrodite and male animals with 4′,6′-diamidino-2-phenylindole dihydrochloride (DAPI). As expected, the fluorescent signal of GFP::DPFF-1 overlapped with the DAPI fluorescent signal in hermaphrodite (Supporting Information Figure S2a–c) and male (Supporting Information Figure S2d–f) germ and somatic gonad cells. GFP::DPFF-1 was also observed at lower levels diffused throughout the cytoplasm of hermaphrodite (Supporting Information Figure S2a–c) and male (Supporting Information Figure S2d–f) germ cells. These observations demonstrate that GFP::DPFF-1 is expressed ubiquitously throughout all embryonic and postembryonic stages and is, mainly localized in the nuclei and at lower levels is diffused throughout the cytoplasm.

To validate the fluorescent signal of the GFP::DPFF-1 transgene, we silenced the *dpff-1* gene in *xmSi09* animals using RNAi by feeding. As a negative control for the RNAi studies, we used an empty pPD129.36 plasmid (EP) as previously recommended by Conte and Mello (2003). *xmSi09* animals were grown under control (EP) or *dpff-1 (RNAi)* conditions at 24°C. One-day-old *xmSi09(EP)* and *xmSi09;dpff-1 (RNAi)* animals were observed under an epifluorescence microscope. The GFP::DPFF-1 fluorescent signal was clearly reduced in *dpff-1(RNAi)* animals (Supporting Information Figure S3i–p) compared to that of control RNAi animals (Supporting Information Figure S3a–h). However, all *xmSi09;dpff-1(RNAi)* animals retained some fluorescent background in some unidentified cells in the head, tail and along the body (Supporting Information Figure S3m,p, arrowheads). We hypothesized that some of these unidentified cells could be neurons because they are resistant to RNAi by feeding in *C. elegans* (Asikainen, Vartiainen, Lakso, Nass, & Wong, 2005; Kamath, Martinez-Campos, Zipperlen, Fraser, & Ahringer, 2001). Our observations demonstrate that the fluorescent signal observed in the GFP::DPFF-1 animals corresponds to the expression of the fusion protein and that the dsRNA used to silence *dpff-1* works efficiently.

2.3 | *dpff-1* mutant animals have fertility defects

To better understand the role of *dpff-1* in *C. elegans*, we studied *dpff-1* mutants carrying *xm17* or *tm4287* alleles (Figure 1c). The *xm17* allele was generated in our laboratory by the CRISPR-Cas-9 genome editing system (Friedland et al., 2013) and it consists of a five-base pair deletion and a four-base pair insertion between nucleotides 46 to 56 after the *dpff-1* ATG codon (Supporting Information Figure S4a). *xm17* results in a *dpff-1* nonsense mutation that leads to the production of a truncated hypothetical protein that contains only the first 23 amino acids (Figure 1c). The *tm4287* allele was obtained from the National BioResource Project in Tokyo, Japan, and is a 318 bp deletion that eliminates 16 bp (out of 83 bp) from exon 1, all of intron 1 and 176 bp (out of 254 bp) of exon 2 but conserves the open reading frame (Supporting Information Figure S4b). Translation of the *tm4287* allele results in the production of a hypothetical shortened version of the DPFF-1 protein that lacks amino acids 22 to 85 (Figure 1c) but conserves the rest of the protein. *dpff-1(xm17)* and *dpff-1(tm4287)* animals grew, moved and looked like the wild-type animals and we did not detect any evident somatic defects.

To study the effects of *dpff-1* mutations on *C. elegans* fertility and embryonic lethality, we performed a self-progeny count experiment. We assessed fertility at different temperatures because some germline phenotypes are more evident in higher temperatures (Kawasaki et al., 1998). In some experiments, we performed a temperature shift to ensure that the embryonic and larval development occurred at lower temperatures such that when these animals were about to reach adulthood (L4 larvae), they were switched to higher temperatures thus allowing us to observe the effects of *dpff-1* loss in the adult animals mainly in the germline. Offspring of wild-type and *dpff-1* mutant animals were studied at 20 and 24°C and upon shifting the temperature from 20 to 24°C (see the Materials and Methods). *dpff-1(tm4287)* and *dpff-1(xm17)* animals had less offspring than wild-type animals, independent of the temperature (Table 1). Although *dpff-1(tm4287)* and *dpff-1(xm17)* animals had slightly higher embryonic lethality than wild-type animals, none of these differences were statistically significant

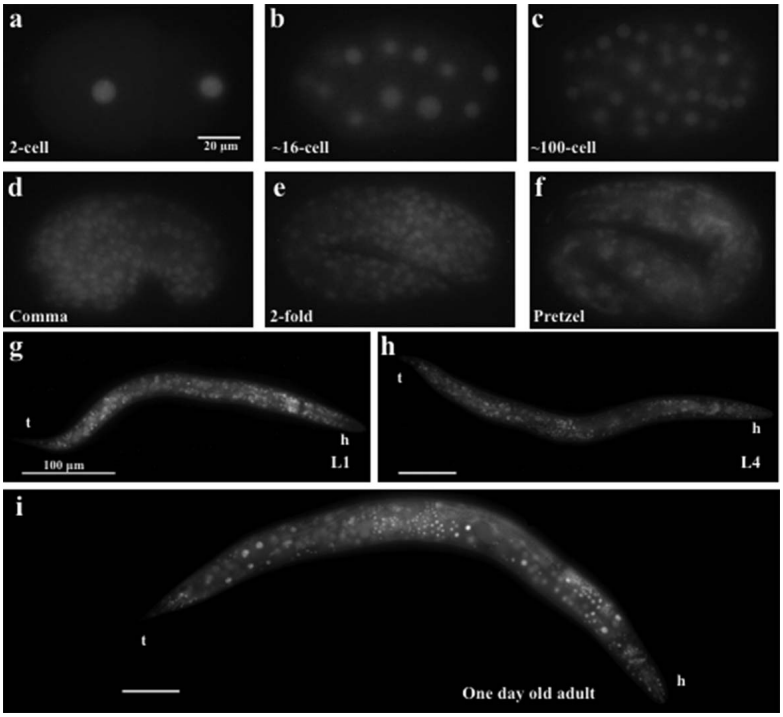

FIGURE 2 GFP::DPFF-1 is expressed ubiquitously throughout all of *C. elegans* development. Live *xmSi09* transgenic animals were mounted and observed under an epifluorescence microscope to analyze their expression pattern at the indicated developmental stages. (a–f) Embryos, (g) L1, (h) L4 larval stages and (i) 1-day-old hermaphrodites are shown. (g–i) Images were captured as a montage, with overlapping cell boundaries and processed using MosaicJ. h: head; t: tail

(Table 1). Our data show that *dpff-1* is important for *C. elegans* optimal fertility, and does not seem to play an evident role in embryogenesis although we cannot discard this possibility.

2.4 | *dpff-1* mutant animals overexpress the P-MPK-1 signal and have meiotic defects

To study the effects of *dpff-1* mutations on germ cell proliferation and meiosis at the nuclear morphological level, we stained extruded gonads of 1-day-old wild-type and *dpff-1* mutant animals grown at 24°C or under temperature shift experiments with DAPI. A small proportion of 1-day-old *dpff-1(tm4287)* and *(xm17)* animals grown with the temperature shift had longer distal gonad arms than wild-type animals [5% ($N = 39$) and 3% ($N = 35$), respectively]. This phenotype was more evident in 1-day-old animals grown at 24°C, in which 19% of *dpff-1 (tm4287)* ($N = 37$) and 11% of *dpff-1(xm17)* ($N = 44$) had longer distal gonad arms. We quantified the number of germ cells in mitosis and meiosis with DAPI staining and found that some *dpff-1* mutant animals with longer distal gonad arms had more germ cells in pachytene (~60% more when compared to the wild-type) but a normal proliferation zone. Indeed, the penetrance of germline phenotypes was higher in *dpff-1* mutants grown at 24°C. For example, we observed germ cells that looked like oocytes in the distal gonad arm of *dpff-1(tm4287)* and *(xm17)* [8% ($N = 37$) and 5% ($N = 44$), respectively] whereas wild-type animals had only pachytene-stage germ cells. Because animals grown at 24°C had a more penetrant phenotype and both alleles behaved similarly, we continued evaluating the meiotic defects in *dpff-1(xm17)* animals grown at 24°C. As we will show later, some phenotypes were clearer in older animals; therefore, experiments were performed in 1- or 2-day-old adults.

We further examined the proliferation zone in *dpff-1* mutant animals by using an antibody against the phosphorylated form of Histone H3, a commonly used marker for mitosis (Kadyk and Kimble, 1998). Two-day-old *dpff-1(xm17)* animals had an average of 4.6 nuclei positive for phospho-Histone H3 ($N = 34$) while the wild-type animals had 4.2

TABLE 1 *dpff-1* mutant animals produce fewer offspring than wild-type animals

Genotype	% Offspring (*N*)			% Embryonic lethality (*N*)		
	20°C	24°C	20 to 24°C	20°C	24°C	20 to 24°C
N2	100 ± 2.99 (22)	100 ± 3.93 (22)	100 ± 1.75 (15)	0.19 ± 0.05 (22)	0.68 ± 0.12 (22)	0.72 ± 0.13 (15)
dpff-1 (tm4287)	77.5 ± 4.20 (21) $p < 0.001$	81.53 ± 6.21 (19) $p = 0.017$	78.24 ± 2.29 (15) $p < 0.001$	1.89 ± 1.14 (21) $p = 0.168$	1.21 ± 0.25 (19) $p = 0.214$	1.51 ± 0.34 (15) $p = 0.149$
dpff-l(xm17)	81.12 ± 2.58 (22) $p < 0.001$	71.51 ± 4.71 (22) $p < 0.001$	83.02 ± 1.53 (14) $p < 0.001$	0.46 ± 0.10 (22) $p = 0.084$	1.17 ± 0.3 (22) $p = 0.539$	1.2 ± 0.34 (14) $p = 0.406$

Hermaphrodite animals of the indicated genotype were individually selected as L4 larvae and then transferred to new plates every 24 h over the course of 3 or 4 days, depending on the temperature. Plates were scored for dead embryos and surviving offspring every 24 h. Embryos that did not hatch within 24 h after laying were considered dead. The percentages of each category are shown with the SEM. The number of animals tested is given in parentheses. All *t* tests are two-tailed unpaired *t* tests (Mann-Whitney).

(*N* = 34). Because we did not observe any significant differences in the proliferation zone of *dpff-1* mutant and wild-type animals, we concluded that the longer distal arms observed in some *dpff-1* mutant animals were not the result of proliferation defects.

When we examined the germ cells nuclear morphology of 2-day-old *dpff-1(xm17)* animals with DAPI staining, we observed more evident defects than those of 1-day-old animals. For example, *dpff-1(xm17)* animals had more condensed nuclei that were not positive for phospho-Histone H3 staining in the distal gonad (4.4, *N* = 79) than wild-type animals (2.1, *N* = 81) (Figure 3a,b). We also observed transition nuclei (crescent shape) in the loop area in 66% of *dpff-1(xm17)* animals (*N* = 64), whereas these type of nuclei are exclusively located adjacent to the mitotic cells in wild-type animals (Figure 3c, inset). Indeed, the penetrance of phenotypes such as long distal arm gonads and the presence of cells that looked like oocyte-like in the distal part was higher in 2-day-old animals. Therefore, we further studied *dpff-1(xm17)* mutant animal phenotypes at this age and at 24°C.

To confirm that some germ cells looked like "oocyte" at the distal gonad, we immuno-stained extruded gonads of 2-day-old wild-type and *dpff-1* mutant animals for the oocyte marker RME-2, which is the yolk receptor (Grant and Hirsh, 1999), and DAPI. As previously described (Grant and Hirsh, 1999), all wild-type animal gonads were RME-2 positive only in the proximal part of the gonad where oocytes had exited the pachytene stage of meiotic pro-phase I and had progressed to diplotene and diakinesis (Figure 3d). In total, 67.6% of gonads of *dpff-1* mutant animals had RME-2-positive cells in the proximal area (Figure 3e), whereas the rest (32.4%) had them in both the distal and proximal gonad (Figure 3f) (*N* = 37).

In the *C. elegans* gonad, meiotic cell cycle progression occurs in spatially restricted regions. Immediately, after leaving the distal mitotic region, germ cells enter meiosis and thereafter remain in the pachytene stage of the first meiotic prophase for an extended period. Germ cells exit pachytene at the loop area, in a process that depends on the phosphorylation of the MAP kinase MPK-1 (ERK homolog) (Church, Guan, & Lambie, 1995). MPK-1 is rapidly dephosphorylated when the oocytes enter diplotene and diakinesis (Hajnal and Berset, 2002). As oocytes move proximally, a signal from the sperm (MSP, major sperm protein), reactivates the phosphorylation of MPK-1 on the most proximal oocyte to allow their maturation (Miller et al., 2001). Because one of the phenotypes observed in *dpff-1* mutant animals was a longer pachytene zone, we stained the gonads of 2-day-old *dpff-1(xm17)* animals grown at 24°C with an antibody that binds specifically to the phosphorylated form of MPK-1 (P-MPK-1). In 65% of *dpff-1(xm17)* animals, P-MPK-1 was observed in the pachytene zone (Figure 4c,d) similar to the wild-type (Figure 4a,b). However this signal persisted all the way to the proximal oocytes and its intensity appeared to be higher than in the wild-type animals (Figure 4c,d). To confirm that the intensity of the P-MPK-1 signal was higher in *dpff-1(xm17)* animals, we performed Western blotting. By this means, we confirmed that the expression of the P-MPK-1 signal was higher in *dpff-1(xm17)* than in wild-type animals (Figure 4e). These results demonstrate that *dpff-1* deficient animals showed up-regulation as well as ectopic expression of the P-MPK-1 signal, and this correlates with the observed meiotic defects.

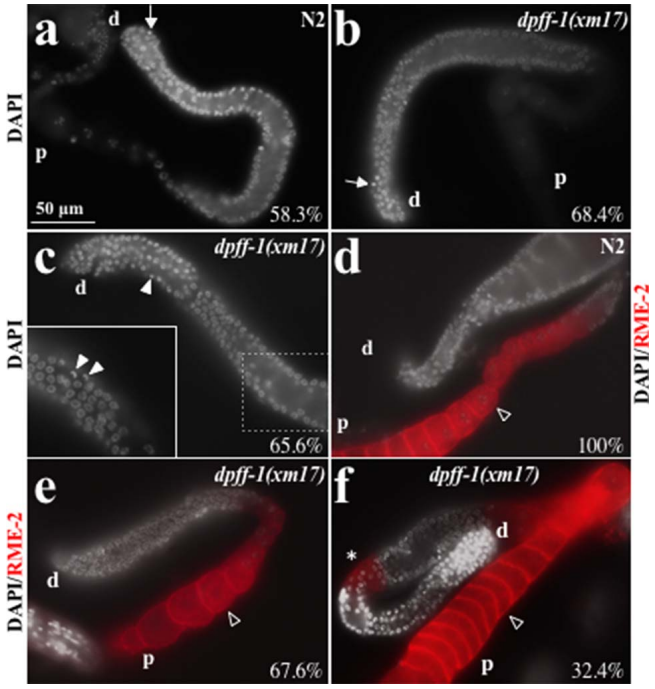

FIGURE 3 Loss of *dpff-1* results in meiotic defects. DAPI and Immunofluorescent images of extruded gonads from 2-day-old adult hermaphrodites of the indicated genotypes. (a) DAPI-stained gonads of the wild-type animal. (b and c) DAPI-stained gonads of *dpff-1(xm17)* animals. (d–f) DAPI-stained and anti-RME-2-immunostained gonads of wild-type (d) and *dpff-1(xm17)* animals (e and f). The percentage of animals presenting each phenotype is indicated inside each panel. In **c,** a detail of the gonad is shown in a different focal plane where crescent nuclei are observed (arrowhead). Full arrows point towards condensed nuclei, empty arrowheads point towards RME-2-positive germ cells and asterisks indicate ectopic RME-2-positive germ cells. d:distal and p:proximal

2.5 | *dpff-1* mutant animals activate germ cell apoptosis via p53

As we mentioned earlier, when we stained gonads of *dpff-1* mutant animals with DAPI, we observed condensed nuclei in the distal gonad (Figure 3b) that were not positive for phospho-histone-H3 antibody. Because condensed nuclei are a common feature of cells undergoing apoptosis, we hypothesized that *dpff-1* mutations could trigger this type of cell death. To test our hypothesis, we crossed *dpff-1(xm17)* animals with the strain MD701 that carries an apoptotic marker (*bcIs39* [*Plim-7::ced-1::gfp; lin-15(+)*]), which we will refer to hereafter as *ced-1::gfp* (Schumacher et al., 2005). *ced-1::gfp* (control) and *ced-1::gfp; dpff-1 (xm17)* animals were grown at 24°C for up to 3 days after the L4 stage, mounted and observed under an epifluorescence microscope to quantify germ cell corpses. One-day-old *dpff-1(xm17)* and control animals had a similar number of germ cell corpses (Table 2). However, 2-day-old and 3-day-old *dpff-1(xm17)* animals had more germ cell corpses than the wild-type animals (Table 2). In the control strain, germ cell corpses localized to the loop area (Figure 5a). Unexpectedly, some *dpff-1(xm17)* 2-day-old animals had ectopic germ cell corpses in the distal gonad (Figure 5b). To corroborate our data, we used a different method to quantify apoptosis. We performed RNAi in *ced-1*, which is required for germ cell corpse degradation (Zhou, Hartwieg, & Horvitz, 2001). In a *ced-1* mutant background, corpses are easily detected by Nomarski microscopy. By means of this methodology, we confirmed that *dpff-1 (xm17)* mutant animals had an increased number of germ cell corpses and that this phenotype was more severe as the animals aged (Table 2).

Double-strand breaks occur normally during meiotic prophase as the initiating events in meiotic recombination (Bailly and Gartner, 2013). Among other events, the success in repairing double strand breaks is monitored during meiotic checkpoints (Alpi, Pasierbek, Gartner, & Loidl, 2003; Gartner, Milstein, Ahmed, Hodgkin, & Hengartner, 2000; Martin, Winkelmann, Petalcorin, McIlwraith, & Boulton, 2005). During the meiotic checkpoints, a failure to repair the double strand breaks activates

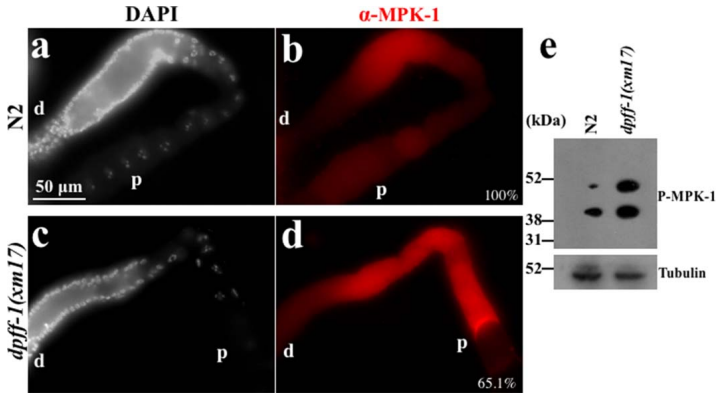

FIGURE 4 *dpff-1* mutant animals have an expanded zone of expression of the P-MPK-1 signal. (a–d) Dissected gonads of 2-day-old wild-type and *dpff-1(xm17)* animals were extruded, fixed and stained with DAPI (gray) and an anti-phosphorylated-MPK-1 antibody (red). The percentage of animals having the observed phenotype are indicated in each panel. d:distal and p:proximal. (e) Western blot of whole extracts of wild-type and *dpff-1(xm-17)* where an antibody against an anti-phosphorylated-MPK-1 antibody (top panel) or tubulin (lower panel) was used

DNA damage-induced apoptosis via the p53 worm homolog *cep-1* (Alpi et al., 2003). We hypothesized that germ cell apoptosis in *dpff-1* mutant animals could be triggered by the activation of a meiotic checkpoint. To test our hypothesis, we silenced *dpff-1* by RNAi in a *cep-1(gk138);ced-1:gfp* background. Silencing *dpff-1* in the *ced-1:gfp* background resulted in higher germ cell apoptosis, similar to *dpff-1* loss of function (Table 2). *cep-1(gk138);ced-1:gfp* animals had similar numbers of germ cell corpses as the *ced-1:gfp* (EP) animals (Table 2). Silencing *dpff-1* in *cep-1 (gk138);ced-1:gfp* animals resulted in similar germ cell corpse numbers as in control animals (*cep-1(gk138);ced-1:gfp*, EP) (Table 2). Our results demonstrate that the increase in germ cell apoptosis of *dpff-1*-deficient animals is dependent on *cep-1*/p53, suggesting that the high levels of germ cell apoptosis in *dpff-1* mutant animals might be a consequence of the activation of the DNA damage apoptosis program that is triggered when meiosis defects are found in the system.

2.6 | *dpff-1* is important in the induction of germ cell apoptosis under heat shock

In tissue culture, it has been observed that *dpf2/requiem/ubi-d4* is required for the apoptotic response upon IL-3 withdrawal in myeloid cells (Gabig et al., 1994). In *C. elegans* several stress conditions lead to an increase of germ cell apoptosis (Derry, Putzke, & Rothman, 2001; Salinas, Maldonado, & Navarro, 2006; Stergiou, Doukoumetzidis, Sendoel, & Hengartner, 2007); therefore, we tested the role of *dpff-1* in the induction of apoptosis under different stress conditions. For starvation, 1-day-old *ced-1::gfp* and *ced-1::gfp; dpff-1* mutant animals were grown at 24°C and divided into two groups: one that was fed with bacteria and another one that lacked bacteria for 6 h. After treatment, animals were mounted and observed under an epifluorescence microscope to quantify germ cell corpses. Starved *ced-1::gfp* control

TABLE 2 Germ cell apoptosis in different genetic backgrounds.

	24 h	48 h	72 h
dpff-1 mutant animals have higher germ cell apoptosis			
ced-l::gfp	6.3 ± 0.3 (47)	9.6 ± 0.3 (69) 1.5	14.5 ± 0.5 (32) 2.3
ced-l::gfp ;dpff-1 (xml 7)	6.3 ± 0.2 (54) $p = 0.915$	19.6 ± 0.6 (60) 3.1 $p < 0.001$	21.2 ± 0.6 (41) 3.4 $p < 0.001$
ced-1(RNAi)	5.6 ± 0.2 (48)	10.2 ± 0.2 (115) 1.8	13.1 ± 0.3 (46) 2.3
dpff-1 (xml 7);ced-l(RNAi)	5.5 ± 0.3 (45) $p = 0.877$	20.8 ± 0.4 (140) 3.8 $p < 0.001$	20.1 ± 0.5 (38) 3.7 $p <$ O.00l
dpff-1 increased germ cell apoptosis is CEP-1-dependent			
ced-l::gfp-, EP	5.2 ± 0.3 (57)	9.7 ± 0.3 (93) 1.9	15.5 ± 0.3 (62) 3.0
ced-1 ::gfp; dpff-1 (RNAi)	5.4 ± 0.2 (78) $p = 0.557$	14.7 ± 0.3 (106) 2.7 $p < 0.001$	19.6 ± 0.5 (83) 3.6 $p <$ O.OOl
ced-l::gfp ;cep-l(gkl38); EP	5.8 ± 0.3 (37)	11.5 ± 0.3 (97) 2	14.3 ± 0.3 (85) 2.4
ced-l::GFP;cep-l (gkl38); dpff-1 (RNAi)	5.9 ± 0.3 (34) $p = 0.928$	10.1 ± 0.2 (105) 1.7 $p \leq 0.001$	12.4 ± 0.3 (108) 2.1 $p <$ O.OOl

Animals of the indicated genotype were grown at 24°C, mounted and observed under an epifluorescence microscope or Nomarski microscopy to quantify germ cell corpses. The mean number of apoptotic cells per gonad arm with the SEM was scored with CED-1::GFP at 24, 48, and 72 h post L4 stage. The number of animals tested is given in parentheses. All *t* tests are two-tailed unpaired *t* tests (Mann-Whitney; *** < 0.001).

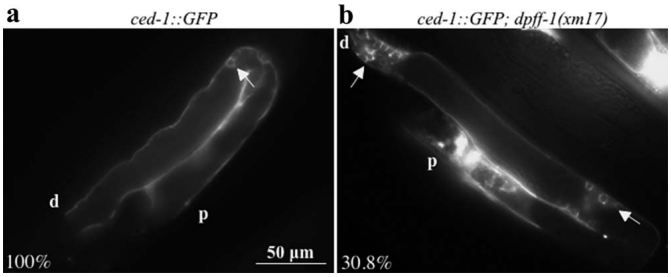

FIGURE 5 *dpff-1* mutant animals have ectopic cell corpses. (a and b) Two-day-old adult animals of the indicated genotype were grown at 24°C, mounted and observed under an epifluorescence microscope to quantify germ cell corpses. Full arrows point towards germ cell corpses. The percentage of animals showing the observed phenotype is indicated in each panel. d:distal and p:proximal

animals had increased germ cell apoptosis by up to 1.8-fold at 24°C (Figure 6). Starved *ced-1::gfp; dpff-1* mutant animals had only partially increased germ cell apoptosis (1.4-fold) (Figure 6). Our data suggest that DPFF-1 might play a partial role in inducing germ cell apoptosis under starvation.

For heat shock experiments, 1-day-old *dpff-1* mutant animals grown at 24°C were exposed to 31°C for 3 h as we have previously reported (Salinas et al., 2006). Heat-shocked *ced-1::gfp* control animals had increased germ cell apoptosis by up to 1.4-fold (Figure 6). Heat-shocked *ced-1::gfp; dpff-1* mutant animals did not increase germ cell apoptosis (Figure 6). Our data suggest that DPFF-1 might play a role in inducing germ cell apoptosis under heat shock conditions.

To determine if *dpff-1* is important for germ cells and/or embryo protection from heat shock, we performed an assay published earlier by our group (Huelgas-Morales, Silva-Garcia, Salinas, Greenstein, D., & Navarro, 2016) in which embryogenesis success is used as a measure of germ cell quality. In this assay, 1-day-old adult animals were exposed to heat shock, and their progeny were sorted into three groups thereafter: Group I was composed of embryos already formed before the heat shock (inside the uterus) and embryos formed during or shortly after heat shock, which likely came from diakinesis-stage oocytes (Figure 7a). Group II was composed of embryos laid between 12 and 24 h after stress (late pachytene-stage germ cells at the moment of stress). Finally, group III was composed of those embryos laid between 24 and 48 h after stress (early pachytene-stage germ cells at the moment of stress) (Figure 7a) (Huelgas-Morales et al., 2016).

For performing this assay, 1-day-old wild-type and *dpff-1* mutant hermaphrodites were grown at 24°C and divided into two groups: one that was kept as a control (24°C) and another that was heat shocked for 3 h at 31°C. After that, the progeny of these animals was divided into three groups, and embryonic lethality was quantified. Non-heat-shocked wild-type and *dpff-1* mutant animals showed low to no embryonic lethality (Figure 7b). Heat-shocked wild-type and *dpff-1* mutant animals from group I showed an increase in embryonic lethality (Figure 7b). However, heat-shocked *dpff-1* mutant and wild-type animals from group II and III showed low percentages of embryonic lethality that were not significantly different between the groups (Figure 7b). Our data suggest that germ cells from *dpff-1* mutant animals are not sensitive to heat shock and that DPFF-1 is not important for the protection of germ cells and embryos from heat shock, despite its importance in the induction of germ cell apoptosis under this condition.

2.7 | *dpff-1* is important for adult stress survival

We have previously observed that proteins required for stress-induced germ cell apoptosis are also important to protect the whole animal from stressful conditions (Huelgas-Morales et al., 2016; Rousakis et al., 2014; Silva-Garcia and Estela Navarro, 2013). Because we found that DPFF-1 is important in the induction of germ cell apoptosis under heat shock conditions, we decided to test whether this protein could protect the whole organism from stress. We tested heat shock stress resistance in wild-type and *dpff-1* mutant animals following standard protocols (Arsenovic, Maldonado, Colleluori, & Bloss, 2012; Paz-Gomez, Villanueva-Chimal, & Navarro, 2014; Rodriguez, Snoek, De Bono, &

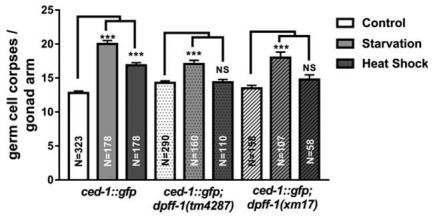

FIGURE 6 DPFF-1 is important for stress-induced germ cell apoptosis. One-day-old adult animals of the indicated genotype were grown at 24°C and exposed to 6 h of starvation or at 31°C for 3 h to induce heat shock. Afterwards, treat animals were mounted and observed under an epifluorescence microscope to quantify germ cell corpses. The mean number of apoptotic germ cells per gonad arm of at least two independent experiments was scored with CED-1::GFP and is shown in the graph. Error bars indicate SEM and asterisks show that each treatment is different from untreated control. All *t* tests are two-tailed unpaired *t* tests (Mann–Whitney; *** $p < 0.001$)

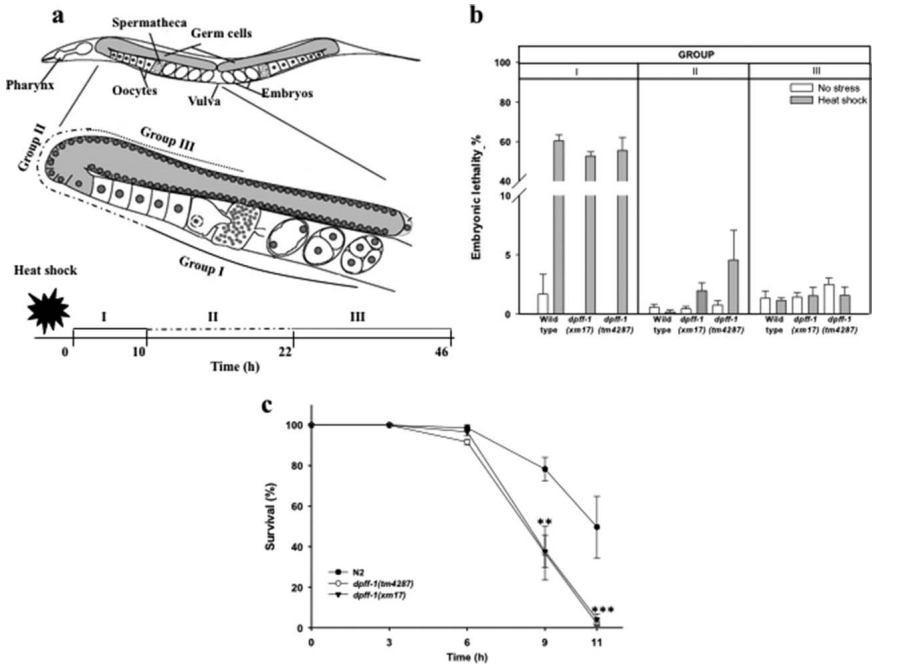

FIGURE 7 *dpff-1* participates in adult stress survival. (a) Scheme representing how the groups of embryos were assigned for the heat shock assay. (b) Animals of the indicated genotype were grown at 24°C and were divided into two groups: one kept at the same temperature an another that was heat-shocked at 31°C for 3 h. The embryos produced were sorted into three groups: embryos that had been fertilized (I) before or during the heat-shock, (II) shortly after heat-shock and (III) long after heat-shock. Embryonic lethality is represented by the percentage of embryos that did not hatch after 24 h of being laid. The data from one of two replicates, with each condition having a ≥989, are depicted. Error bars indicate SEM. One-way-ANOVA (**$p < 0.01$). (c) Synchronized 1-day-old adult hermaphrodites of the indicated genotype were grown at 24°C and exposed to a heat shock stress at 36°C for the indicated time. The data from three different experiments were obtained, and the percentage of surviving animals was graphed. Error bars indicate SEM. Two-way ANOVA analysis with Bonferroni's test was used to compare each condition to the control. ** $p < 0.01$; *** $p < 0.001$

Kammenga, 2013). One-day-old wild-type and *dpff-1* mutant animals grown at 24°C were exposed to heat shock at 36°C and analyzed every hour to monitor their survival over the course of 11 h. During the first 6 h of incubation, there was no difference in survival between *dpff-1* mutant and wild-type animals (Figure 7c). After 9 h of heat shock, 78% of wild-type animals were still alive (Figure 7c). However, at the same time, only 36% of *dpff-1* mutant animals survived (Figure 7c). After 11 h of heat shock, 49% of wild-type animals survived (Figure 7c); in contrast, only 3% of *dpff-1* mutant animals did (Figure 7c). These data demonstrate that *dpff-1* mutant animals have a compromised heat shock response.

To continue studying the role of DPFF-1 in the heat shock response, we tested whether *dpff-1* mutant animals were able to turn on two heat shock reporters: *hsp-16.2::gfp(gpls1)* (Rea, Wu, Cypser, Vaupel, & Johnson, 2005) and *$_P$sod-3::gfp* (Libina, Berman, & Kenyon, 2003). We exposed *hsp-16.2::gfp(gpls1) and dppf-1(xm17)*; *hsp-16.2::gfp* animals to 35°C for 2 h and recovered them for 4 h at 20°C as recommended by (Rea et al., 2005). After incubation, the animals were mounted and observed under a fluorescence microscope. As expected, *hsp-16.2::gfp* animals expressed the reporter after heat shock (Figure 8a,b,e) nevertheless *dpff-1(xm17); hsp-16.2::gfp* animals showed significantly lower expression (Figure 8a–e).

We performed RNAi by feeding in a *$_P$sod-3::gfp* background using bacteria that expressed *dpff-1* dsRNA or an empty plasmid as a control. We exposed *$_P$sod-3::gfp(EP)* and *$_P$sod-3::gfp; dpff-1(RNAi)* animals to 35°C for 2 h as recommended by Dues et al. (2016), but we were not able to detect an induction of *$_P$sod-3::gfp* expression. Therefore, we optimized the temperature to detect *$_P$sod-3::gfp* expression and found that 8 h at 31°C were optimal for the observation of gfp expression. *$_P$sod-3::GFP(EP)* animals had higher GFP expression during heat shock

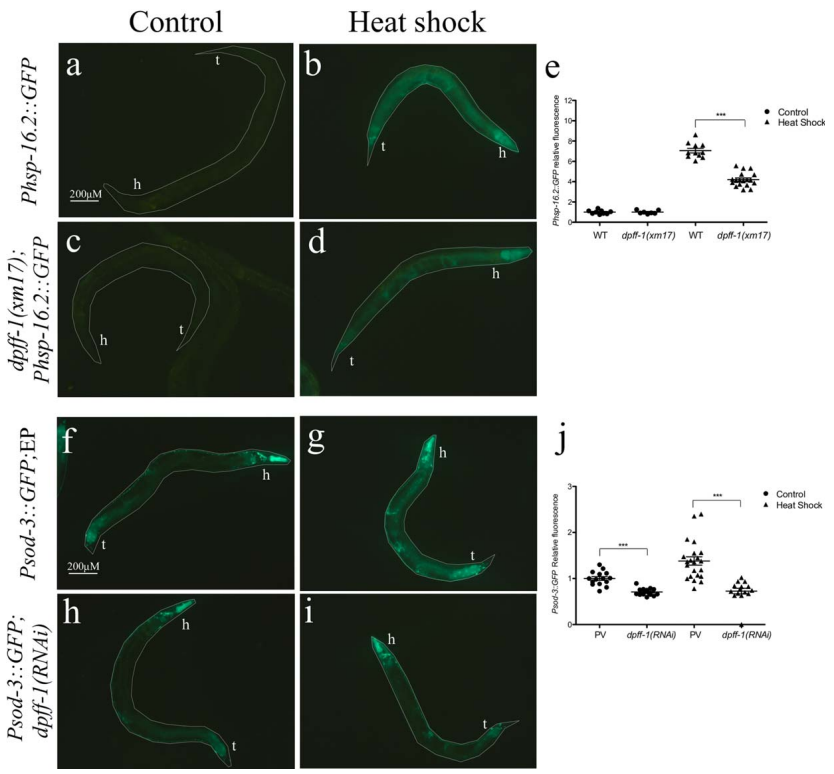

FIGURE 8 *dpff-1 (xm17)* animals are unable to respond to heat shock. (a–e) One-day-old adult hermaphrodites of (a and b) *hsp16.2::gfp* and (c and d) *dpff-1*; *hsp16.2::gfp* strains grown at 20°C were subjected to heat shock at 35°C for 2 h or were kept at 20°C (control, no stress). After heat shock animals were recovered for 4 h at 20°C, they were mounted and observed under an epifluorescence microscope to obtain photomicrographs of representative animals for each strain and condition. (f–j) Animals expressing a heat shock reporter (*Psod-3::gfp*) were fed with an empty plasmid (EP, f and g) or *dpff-1* dsRNA to induce RNAi (h and i). EP or *dpff-1(RNAi)* 1-day-old adult animals of the indicated background were exposed to 8 h at 31°C to induce heat shock (g and i) or kept at 20°C (no stress condition; f and h). Right after heat shock animals were mounted and observed under a fluorescence microscope and representative pictures are shown. (e and j) Quantitative analysis to compare the expression levels of GFP in indicated backgrounds. The data of one of two independent replicates with similar results are shown. One-way ANOVA *** $p < 0.001$. *hsp-16::gfp*: (control) $n = 17$, (heat shock) $n = 17$; *hsp-16::gfp*; *dpff-1(xm17)*: (control) $n = 29$, (heat shock) $n = 33$. *sod-3:gfp*; EP: (control) $n = 27$, (heat shock) $n = 29$; *sod-3:gfp;dpff-1(RNAi)*: (control) $n = 43$, (heat shock) $n = 31$. h:head and t:tail

than in normal conditions (Figure 8f,g,j). In contrast, *Psod-3::gfp; dpff-1 (RNAi)* animals had less expression of the *sod-3::gfp* reporter in control conditions and after heat shock in comparison to control animals (Figure 8h–j). Our results show that DPFF-1 plays an important role in the activation of heat shock response in *C. elegans*.

3 | DISCUSSION

In this work, we explored the expression and function of the putative transcriptional factor *dpff-1* in *C. elegans* fertility and during the stress response. We found that the fusion protein GFP::DPFF-1 is ubiquitously expressed throughout all embryonic and post-embryonic stages, mainly in the nuclei, and at lower levels diffused in the cytoplasm of somatic and germ cells. Here, we show for the first time that a member of the d4 family of transcription factors participates in meiosis. Some *dpff-1* mutant animals had an extended pachytene zone and ectopic oocyte-like cells in the distal gonad. We also found that the P-MPK-1 signal is higher and persists from pachytene to diakinesis. *dpff-1* mutant animals had higher, and in some cases, ectopic germ cell apoptosis that was activated through the p53 (CEP-1) pathway. In addition to DPFF-1

function in fertility and meiosis, we also showed that DPFF-1 is important to protect the animal from heat shock and to turn on heat shock reporters. This is the first report showing that a member of this family of proteins plays a role in meiosis and heat shock protection. Because DPFF-1 is a putative transcription factor is possible that its function is to regulate the expression of some genes important for meiosis, apoptosis and/or stress.

3.1 | *dpff-1* mutant animals have fertility and meiosis defects

dpff-1 mutant animals, grew, appeared and moved like the wild-type animals, and we did not observe any evident somatic phenotype. Because in other organisms DPF1 and DPF3 play a role in the nervous system (Lange et al., 2008; Mertsalov et al., 2008), we do not discard the possibility that DPFF-1 could have a role in the soma.

Here, we showed that *dpff-1* mutant animals have less offspring independent of the temperature tested (Table 1). However, meiotic defects were more evident in older animals that grew at 24°C. This finding is not surprising since some germline phenotypes are more penetrant at higher temperatures (Kawasaki et al., 1998). Nevertheless, is possible that somatic defects accumulated when animals grew from early larval stages at 24°C potentially compromising the germline's performance. Another possibility is that older animals had higher penetrance of the studied phenotypes because their gonads accumulated defects as oogenesis progressed.

We attributed low fertility problems in *dpff-1* mutant animals to meiotic defects since several defects were observed during this process by several techniques. Among the defects observed are: an extended transition zone that in some instances could be observed in the loop area, an expanded pachytene zone, in some cases, ectopic oocyte-like germ cells in the distal gonad and condensed nuclei in the distal gonad (Figure 3).

Here, we show that the expression of the phosphorylated MPK-1 is ectopic and higher in *dpff-1* mutant animals (Figure 4). MPK-1 signal is necessary for germ cells to progress through the meiotic prophase I from pachytene to diplotene and diakinesis (Church et al., 1995). We speculate that upregulation of the P-MPK-1 could be contributing to meiotic defects observed in *dpff-1* deficient animals although it is possible that it is a consequence of other meiotic defects. Currently, we do not know why MPK-1 expression is ectopic or higher in *dpff-1* animals. Further studies are required to test if DPFF-1 regulates the expression of MPK-1 directly or indirectly. Because DPFF-1 is a putative transcription factor, it is possible that it could be directly regulating *mpk-1* expression or other genes important for meiosis, but it is also possible that DPFF-1 plays an indirect role.

dpff-1 mutant animals had increased germ cell apoptosis (Table 2 and Figure 5). We observed that high levels of germ cell apoptosis in *dpff-1* mutant animals were dependent on CEP-1 (Table 2), and for this reason, we suggest that germ cell apoptosis is triggered in these animals due to the activation of a meiotic checkpoint. Double-strand breaks occur not only following DNA damage but also normally during meiotic prophase as the initiating events of meiotic recombination. During meiotic prophase, the integrity of both meiotic recombination and meiotic chromosome synapsis is monitored by checkpoints, and such checkpoint activation leads to a cell cycle arrest phenotype in yeast and apoptosis in animals. In mutations that lead to the accumulation of recombination intermediates such as *rad-51* (Gartner et al., 2000) or *brcA* (Martin et al., 2005), germ cell apoptosis is activated via the DNA damage pathway, which is induced by CEP-1/p53 (Alpi et al., 2003; Bailly and Gartner, 2013; Gartner et al., 2000). It is important to note that not all meiotic defects lead to activation of the DNA damage checkpoint. For example, in synapsis-defective animals (such as *him-3* mutants) and those with translocated chromosomes (such as *rec-8* mutants), germ cell apoptosis is not triggered (Alpi et al., 2003).

In some *dpff-1* mutant animals, germ cell corpses were found ectopically in the distal gonad. In the wild-type, germ cell apoptosis occurs only in the loop area, where germ cells are in late pachytene and become competent for apoptosis due to the phosphorylation of MPK-1 (Gumienny, Lambie, Hartwieg, Horvitz, H. R., & Hengartner, 1999). We believe that the ectopic germ cell apoptosis observed in the distal gonad of *dpff-1* animals is due to the activation of a meiosis checkpoint because it is completely blocked by the absence of *cep-1*/p53. We do not believe that DPFF-1 or any of its putative targets regulates germ cell apoptosis during meiosis directly.

Germ cell apoptosis can be triggered by different and independent pathways (Bailly and Gartner, 2013). As we mentioned above, DNA damage is regulated by checkpoint genes and can be induced by meiosis defects (Bailly and Gartner, 2013; Gartner et al., 2000). We previously found that heat shock can trigger germ cell apoptosis in a CEP-1/p53 independent pathway via the MAPKKs MEK-1 and SEK-1 (Salinas et al., 2006). Starvation can trigger germ cell apoptosis via LIN-35/Rb and in a CEP-1/p53 and MEK-1/SEK-1 independent pathways (Lascarez-Lagunas, Silva-Garcia, Dinkova, & Navarro, 2014; Salinas et al., 2006). Here, we found that DPFF-1 is important in the induction of apoptosis during starvation (although partially) and heat shock in *C. elegans*. It is possible that DPFF-1 could play a direct role in the induction of apoptosis by stress because DPF2/*requiem/ubi-d4* was originally found in a screening to identify factors that provide apoptosis resistance in murine myeloid cells (Gabig et al., 1994). Until now, it is not know what role the DPF family members could be playing in this type of cell death and whether their function is direct or indirect. However is possible that this family of proteins has a conserved role in the induction of apoptosis during stress conditions and further studies are needed to investigate this possibility.

3.2 | *dpff-1* protects animals from stress

Until this report, there was no evidence that members of the d4 family of transcription factors could play a role in stress protection. Here, we show that DPFF-1 is important for adult hermaphrodites to survive heat shock conditions (Figure 7c) and to activate the heat shock stress response (Figure 8). Despite DPFF-1 having an important role in oocyte development, it does not seem to play an important role into protecting the germ cells from heat shock because *dpff-1* mutant

animals exposed to heat shock produce embryos that are able to successfully complete embryogenesis (Figure 7b). The role of DPFF-1 in protecting animals from heat shock still remains to be elucidated but it is intriguing that DPFF-1 is not needed for stress protection until animals have been exposed for several hours to extreme heat shock. It will be interesting to test if DPFF-1 plays a role in chromatin remodeling and stress in *C. elegans* because some members of the d4 family of transcription factors of vertebrates interact with BAF-class SWI/SNF complexes (Middeljans et al., 2012; Tando et al., 2010) and in *C. elegans*, it has been shown that DAF-16/FOXO, a transcriptional activator essential for the stress response, acts with a BAF-like subclass of SWI/SNF components to provide stress resistance (Riedel et al., 2013).

The DPFF-1:GFP transgene is expressed mainly in the nuclei of all the *C. elegans* cells. This pattern of expression is congruent with DPFF-1's putative DNA binding domains and nuclear localization signal. Until now, not much is known about the putative targets of this family of transcription factors. It is possible that DPFF-1 might directly regulate the expression of genes implicated in meiosis, apoptosis, stress-induced apoptosis and/or genes that are important for the activation of the heat shock response, and further studies are needed to better understand the role of this protein in these processes. It also would be interesting to test the roles of members of the d4 family of transcription factors in meiosis and stress resistance in higher organisms.

4 | MATERIALS AND METHODS

4.1 | *C. elegans* strains and growth conditions

C. elegans strains were maintained according to standard procedures (Brenner, 1974) on NGM-lite and grown at 20, 24°C for all of their life cycle or at 20°C from embryos to L4 larvae and then shifted to 24°C. The following *C. elegans* strains were used: the wild-type variety Bristol strain N2 (var Bristol), *dpff-1(tm4287)*, MD701 *bcIs39* [*Plim-7::ced-1::gfp*; *lin-15(+)*] (Schumacher et al., 2005), EG6699 [*ttTi5605* II; *unc-119 (ed3)* III; *oxEx1578*] (Frokjaer-Jensen et al., 2008, 2012), TJ375 *hsp-16.2:gfp(gpIs1)* (Rea et al., 2005), RN019 *xmSi09* [P*dpff-1::gfp::dpff-1::dpff-1 3'UTR*; *Cbr-unc-119(+)*] II (this study), RN031 *xmSi09* [P*dpff-1::dpff-1::gfp::dpff-1 3'UTR*; *Cbr-unc-119(+)*] II (this study), RN045 [*dpff-1 (xm17)*] (this study), RN046 [*ced-1::gfp; dpff-1(tm4287)*] (this study), RN048 [*ced-1::gfp; dpff-1(xm17)*] (this study), TJ1 *cep-1(gk138)*. and CF1553 *muIs84 [(pAD76) psod-3::gfp + rol-6(su1006)]*.

4.2 | RNA interference

RNAi silencing was performed by feeding at 24°C using standard methods (Conte and Mello, 2003; Timmons, Court, & Fire, 2001). Briefly, empty pPD129.36 plasmid (EP) and RNAi vectors were grown into the *E. coli* strain HT115(DE3). To induce RNAi in *dpff-1*, the clone was obtained from the RNAi library (OpenBiosystems) (Rual et al., 2004) and confirmed by sequencing. To induce RNAi in *ced-1* a plasmid previously cloned in our lab was used (Salinas et al., 2006). The transformed bacteria were cultured overnight in LB broth containing 50 mg/ml of ampicillin and 12.5 mg/ml of tetracycline. For RNAi experiments to quantify apoptosis, double stranded RNA for *ced-1* and *dppf-1* was induced in liquid as previously described by (Salinas et al., 2006). To test *dpff-1* RNAi efficiency double stranded RNA synthesis was induced overnight on NGM plates supplemented with ampicillin (50 mg mL^{-1}), tetracycline (12.5 mg mL^{-1}) and IPTG (1 mM). L4 larvae were placed onto NGM-lite plates containing induced bacteria and incubated at 24°C for one generation, and then, L4 animals were cloned for experiments.

4.3 | Transgene and sgRNA targeting construction

The cloning of *dpff-1* for single-copy insertion was performed using the Multisite Gateway Three Fragment Vector Construction Kit (Invitrogen, Carlsbad, CA). For the promoter, we amplified a 965-bp fragment of the intergenic region upstream of *dpff-1*. For the coding region containing the 3'UTR, we amplified the region from the ATG to the end of the longest 3'UTR reported (http://www.wormbase.org, release WS252, Dec 04, 2015).

The following primers were used: attB4_*dpff-1*_FOW GGGGACAACTTTGTATAGAAAAGTTGATGATGACCCTAAAAATTATCATAC; attB1r_*dpff-1*_REV, GGGGACTGCTTTTTTGTACAAACTTGCTTAGATTATTCAGATTTCAAATGGATC; attB1_*dpff-1*_FOW, GGGGACAAGTTTGTACAAAAAAGCAGGCTTAATGATAAATCTTTAGAGCATTTAGG; attB2r_*dpff-1*_REV, GGGGACCACTTTGTACAAGAAAGCTGGGTTAAGATCCACAATTATGTGAAGAAG; attB2_*dpff-1*_FOW, GGGGACAGCTTTCTTGTACAAAGTGGTCAAATGTATTAGCTTCCTTCCTCTC and attB3_*dpff-1*_REV, GGGGACAACTTTGTATAATAAAGTTGTGATTCTTTGAAACTTCCAATATTG. PCR products were gel-purified by standard procedures and cloned through recombination in to the donor vectors pDONRP4-P1R, pDONR221 and pDONRP2R-P3 to generate entry clones. In all cases, genomic N2 DNA was used as a template. The inserts were confirmed by sequencing.

pDONRP4-P1R-*dpff-1* and pDONRP2R-P3-*dpff-1* were linearized by PCR with primers P4-P1R-*dpff-1*_FOW, GCTTCCGCCGGTACCTCCACTGCCACCGCTAGTACTCATTGTCTGTAAGATTAGCTGTCTTGGATTATTTTTAAAC; P4-P1R-*dpff-1*_REV, GGTGGCACAGGAGGAACGGGCGGTAGTGGAGGCACTGGTATCTCGGAAAACGGATATATGGACCTGATGC; 2R-P3-*dpff-1*_FOW, GCTTCCGCCGGTACCTCCACTGCCACCGCTAGTACTCTTCTTGGCCGGTGCAC and 2R-P3-*dpff-1*_REV, GGTGGCACAGGAGGAACGGGCGGTAGTGGAGGCACTGGTTAATGGTTCTCAAATATTATATTTATTCCAATATTT, respectively. The GFP sequence was amplified from the entry clone pCM1.53 (Addgene plasmid 17250) (Merritt, Rasoloson, Ko, & Seydoux, 2008) with primers GFP_FOW, AGTACTAGCGGTGGCAGTGGAGGTACCGGCGGAAGCAGTAAAGGAGAAGAACTTTTCAC and GFP_REV, ACCAGTGCCTCCACTACCGCCCGTTCCTCCTGTGCCACCTTTGTATAGTTCATCCATGCC. PCR products were digested with DpnI and gel-purified following standard procedures. Then, we fused the GFP coding gene after the *dpff-1* ATG or before the *dpff-1* stop codon using a Gibson reaction (Gibson et al., 2009) by mixing pDONRP4-P1R-*dpff-1* or pDONRP2R-P3-*dpff-1* PCR products with GFP PCR products. Finally, the desired PCR products on each entry clone

vector were cloned in tandem through recombination into the destination vector pCFJ150 (Addgene plasmid 19329) (Frokjaer-Jensen et al., 2008).

To generate the *dpff-1* sgRNA expression vector, we used the pU6::*unc-119* sgRNA vector (Addgene plasmid 46169) (Friedland et al., 2013) as a template. pU6::*unc-119* sgRNA was linearized by PCR with the primers sgRNA_*dpff-1*_FOW, ACTGCATTAAATGGAATTCCGTTTTAGAGCTAGAAATAGCAAGTTAAAATAAG and sgRNA_*dpff-1*_FOW, CGGAATTCCATTTAATGCAGTAAACATTTAGATTTGCAATTCAATTATATAGG. The PCR product was digested with DpnI, gel-purified and transformed into competent cells. pU6::*dpff-1* sgRNA was confirmed through sequencing.

4.4 | Generation of transgenic and mutant strains

Transgenic animals were generated through Mos1-mediated single copy insertion (Frokjaer-Jensen et al., 2008, 2012). Briefly, 1-day-old EG6699 [*ttTi5605* II; *unc-119(ed3)* III; *oxEx1578*] animals were microinjected into the gonad with a mixture containing the following plasmids: pCFJ601 (P*eft-3*::Mos1 transposase, 50 ng μL^{-1}), the negative selection marker pMA122 (P*hsp-16.1*::*peel-1*, 10 ng μL^{-1}), the coinjection markers pCFJ104 (P*myo-3*::mCherry, 5 ng μL^{-1}), pGH8 (P*rab-3*::mCherry, 10 ng μL^{-1}), pCFJ90 (P*myo-2*::mCherry, 2.5 ng μL^{-1}) and the template plasmid pCFJ150 with the transgene P*dpff-1*::*gfp*::*dpff-1*::*dpff-1 3′UTR* (20 ng μL^{-1}) or pCFJ150 with the transgene P*dpff-1*::*dpff-1*::*gfp*::*dpff-1 3′UTR* (20 ng μL^{-1}). The injected worms were grown at 24°C for several days. *unc-119* (+) animals were heat shocked at 34°C for 2 h. The living animals were isolated, and their progeny were analyzed using a fluorescence microscope. GFP-expressing animals with no mCherry expression were selected.

The mutant RN042 *dpff-1(xm17)* line was generated by CRISPR-Cas-9 genome editing (Friedland et al., 2013). Briefly, 1-day-old wild-type N2 animals were microinjected using a mixture containing the following plasmids: P*eft-3*::*cas9*-SV40 (Addgene plasmid 46168, 50 ng μL^{-1}) (Friedland et al., 2013), pU6::*dpff-1* sgRNA (45 ng/μl) and pCFJ104 (P*myo-3*::mCherry, 5 ng μL^{-1}). F1 animals with mCherry expression were selected using a fluorescence stereomicroscope. We genotyped 66 F1 worms by PCR using the primers *dpff-1*_EcoRI_FOW, GCGTAGCTACATATTAATCAATTATCGC and *dpff-1*_EcoRI_REV, AGCCGTTTGATGTTCATAGTATG. PCR products were digested with EcoRI and visualized in a 2% agarose gel. Using this approach, we identified two independent restriction fragment length polymorphisms in PCR amplicons generated from mutant genomic DNA. *xm17* and *xm20* alleles were sequenced and analyzed. The *xm17* allele resulted in a nonsense mutation (Supporting Information Figure S2). The *xm20* allele resulted in a silent mutation and was not used in this study (data not shown).

4.5 | Fertility assay

To study the effect of *dpff-1* mutations on *C. elegans* fertility, wild-type N2, *dpff-1(tm4287)* and *dpff-1(xm17)* hermaphrodite animals were grown at 20°C, 24°C and with the temperature shift (as previously described). These hermaphrodite animals were individually selected as L4 larvae and then transferred to new plates every 24 h over the course of 3–4 days, depending on the temperature. Embryos that did not hatch within 24 h after being laid were considered dead.

4.6 | Immunostaining

RME-2 and P-MPK-1 immunolocalization in dissected gonads were performed as previously described (Salinas, Maldonado, Macias-Silva, Blackwell, & Navarro, 2007) with the following modifications. Briefly, dissected gonads were frozen in liquid nitrogen, freeze-cracked, fixed in methanol at −20°C for 1 min and treated with a mix of 1X PBS, 3.7% paraformaldehyde, 80 mM HEPES, 1.6 mM $MgSO_4$, and 0.8 mM EGTA for 20 min at room temperature for RME-2 and 12 min for P-MPK-1. Fixed gonads were incubated with RME-2 antibody (1:100) as previously described (Grant and Hirsh, 1999), a commercial antibody against phospho-histone-H3 (Upstate Biotechnology, Catalogue number: 06-570) (1:10) or a commercial phospho-MPK-1 antibody (1:400) (Sigma-Aldrich, Catalogue number: M8159), washed in PBT and finally incubated with a mix of Alexa Fluor 594-conjugated goat anti-rabbit secondary antibody (1:100; Molecular Probes) for MPK-1, Alexa Fluor 488-conjugated goat anti-mouse Ig(G) secondary antibody (1:100 Molecular Probes) for phospho-histone-H3 or Cy3 anti-mouse secondary antibody (1:100; Jackson Immunology) and DAPI (4′ 6′-diamidino-2-phenylindole dihydrochloride, 1 ng μL^{-1}).

To observe nuclear morphology, DAPI staining was performed as previously described (Lee et al., 2007). Briefly, dissected gonads were fixed in 3% formaldehyde and 100% methanol in a 100 mM K_2HPO_4 (pH 7.2) buffer for 20 min at −20°C. Fixed gonads were incubated with DAPI (4′, 6′-diamidino-2-phenylindole dihydrochloride, 1 ng μL^{-1}) in PBT (PBS and 0.5% Tween 20) for 10 min at room temperature and washed in PBT. Stained gonads were mounted with Vectashield Mounting Medium (Vector Labs, Burlingame, CA) to prevent photobleaching.

4.7 | Western blot analysis

For the Western blot analysis, 100 two-day-old adult animals from the indicated backgrounds were grown at 24°C, collected and washed in phosphate-buffered saline (PBS 1X). To lyse animals, the samples were boiled for 5 min in 171.5 mM DTT and loading buffer and centrifuged at 13,000 rpm for 1 min. The resulting supernatant was loaded onto 10% polyacrylamide gels. The gels were transferred onto an Immobilon-P polyvinylidene di-fluoride (PVDF) membrane (Millipore) according to standard procedures. Blots were incubated using a commercial antibody for Phospho-ERK (Cell Signaling Technology, Catalogue number: 9101) 1:1000. Primary antibody was diluted in 0.5% nonfat commercial milk, 0.1% TBT and incubated overnight at 4°C. To detect to the Phospho-ERK protein, we used the secondary antibody peroxidase-conjugated Goat Anti-Rabbit (H + L) (Thermo Scientific, Catalogue number: 32460) diluted to a final concentration of 1:1000 (same dilution buffer) and incubated for I h at room temperature. An α-tubulin monoclonal antibody (Sigma–Aldrich, Catalogue number:

T9026) was used as a loading control at a dilution of 1:500. Bound antibody was detected using a Super Signal West Femto Trial Kit (Thermo Scientific, Catalogue number: 34096).

4.8 | Apoptosis assays

To investigate the role of *dpff-1* in germ cell apoptosis, we crossed *dpff-1(tm4287)* and *dpff-1(xm17)* animals with the strain MD701 (Schumacher et al., 2005). Control *ced-1::gfp, ced-1::gfp; dpff-1(tm4287)*, and *ced-1::gfp; dpff-1(xm17)* animals were grown at 24°C, mounted in 2% agarose pads, anesthetized with 10 mM tetramisole and observed under an epifluorescence microscope to quantify germ cell corpses at the indicated developmental stages or stress conditions. For *ced-1 (RNAi)*, animals of the indicated genotypes were grown at 24°C, mounted on 2% agarose pads, anesthetized with 10 mM tetramisole and observed by Nomarski microscopy to observe cell corpses. All statistical analyses were performed using SIGMA-PLOT. Error bars indicate SEM. All t-tests are two-tailed unpaired *t* tests (Mann–Whitney).

4.9 | Stress conditions

For stress-induced germ cell apoptosis, we followed (Salinas et al., 2006) and (Silva-Garcia and Estela Navarro, 2013). Briefly, control *ced-1::gfp, ced-1::gfp; dpff-1(tm4287)*, and *ced-1::gfp; dpff-1(xm17)* animals were grown at 24°C. For starvation conditions, 1-day-old animals of the indicated genotype were transferred to NGM plates without bacteria and incubated for 6 h at 24°C. For inducing germ cell apoptosis by heat shock, 1-day-old animals of the indicated background were transferred to NGM plates with bacteria, incubated for 3 h at 31°C in a water bath, and then allowed to recover for 4.5 h at 24°C. After every treatment, animals of the indicated genotypes were anesthetized with 10 mM tetramisole, mounted on 2% agarose pads and observed under an epifluorescence microscope to quantify germ cell corpses. All statistical analyses were performed using SIGMA-PLOT. Error bars indicate SEM. All *t* tests are two-tailed unpaired *t* tests (Mann-Whitney).

Synchronized *hsp-16.2::GFP* and *dpff-1(xm17); hsp-16.2::GFP* were grown at 20°C, and when animals reached the L4 stage, 30–40 animals were passed to 35 mm plates of NGM-lite seeded with OP50-1 bacteria. The next day, 1-day-old adults were heat shocked at 35°C for 2 h and then recovered for 4 h (Dues et al., 2016). Animals were mounted and observed under a fluorescence microscope. EP and *dpff-1(RNAi)* animals in the L4 stage expressing the transgene *Psod-3::GFP* were selected and transferred to 35 mm plates of NGM-lite seeded with OP50-1 bacteria. The next day, the animals were heat shocked at 31°C for 8 h. Control animals in both experiments were grown at 20°C (without stress). Fluorescence quantification was performed using ImageJ software as previously described (Huelgas-Morales et al., 2016).

4.10 | Quantification of embryonic lethality after heat shock

Quantitation of embryonic lethality after heat shock was performed as previously described (Huelgas-Morales et al., 2016). Briefly, 1-day-old hermaphrodites were grown at 24°C and heat shocked at 31°C for 3 h in a controlled temperature water bath. Control groups were kept at 24°C. Immediately after the heat shock, animals were mounted in 2% agarose pads and observed under a microscope. The number of embryos in the uterus and the number of fully grown oocytes inside each gonad arm of every hermaphrodite were counted. Then, animals were recovered and allowed to lay as many embryos as previously averaged for 10 h, constituting group I. Afterwards, the hermaphrodites were transferred to new plates and were allowed to lay embryos for 12 h, constituting group II. Once again, the hermaphrodites were transferred and allowed to lay embryos for another 24 h, constituting group III. Embryonic lethality was determined as the percentage of embryos that did not hatch after 24 h of being laid. In parallel, the embryonic lethality of control hermaphrodites that were not heat shocked was scored.

4.11 | Survival assays

Heat shock was performed as previously described (Paz-Gomez et al., 2014). Synchronized L1 worms were grown at 24°C for 40 h and subsequently transferred to several 35-mm NGM plates for heat shock (30 worms per plate). Plates with 1-day-old hermaphrodites were incubated at 36°C for 12 h, and every hour a plate was taken from the incubator to observe animals under a stereoscopic microscope. Animals without pharyngeal pumping that did not respond to touch were scored as dead and burst animals were discarded. Data from three different experiments were obtained, and the percentage of survival was graphed.

4.12 | Image acquisition and processing

The images were obtained on a Nikon Eclipse E600 microscope equipped with an AxioCam MRc camera (Zeiss). Pictures were captured using AxioVision software (Zeiss). Images were processed using ImageJ (1.50b, Wayne Rasband National Institutes of Health). Some images were captured as a montage with overlapping cell boundaries and processed using MosaicJ (Thévenaz and Unser, 2007).

Quantification of GFP fluorescence used ImageJ (1.5ob, Wayne Rasband, National Institutes of Health). The whole area of each animal was selected, and its relative levels of fluorescence (intensity) were measured and graphed. The corrected total fluorescence was calculated as follows: corrected total fluorescence (CTF) = integrated density – (area of the selected animal x mean fluorescence of the background readings). In which the background reading was determined independently by selecting a region next to the animal that had no fluoresce.

ACKNOWLEDGMENTS

The authors thank Drs. Erik M. Jorgensen, C. Frøkjær-Jensen, and G. Hollopeter for kindly providing technical advice and reagents. They also thank Dr. Barth Grant for kindly providing the RME-2 antibody. Some strains were provided by the CGC, which is funded by the NIH Office of Research Infrastructure Programs (P40 OD010440) and by the National BioResource Project for the Experimental Animal "Nematode *C. elegans*," Tokyo, Japan. They also thank the WormBase release WS252 (Dec 04, 2015) for gathering information

and making it available. A.E.V.C. is a doctoral student from the Programa de Doctorado en Ciencias Biomédicas, UNAM, and received fellowship 335767 from CONACyT. A.E.V.C. received additional financial support from the Programa de Apoyo a los Estudios de Posgrado (PAEP) program and PAPIIT-UNAM (IN207412 and IN207415). This work was supported by grants from Consejo Nacional de Ciencia y Tecnología (CONACyT-México) (103856-Q and 220987) and from Programa de Apoyo a Proyectos de Investigación e Innovación Tecnológica (PAPIIT-UNAM) (IN207412 and IN207415).

ORCID

Rosa E. Navarro http://orcid.org/0000-0003-4992-4450

REFERENCES

Alpi, A., Pasierbek, P., Gartner, A., & Loidl, J. (2003). Genetic and cytological characterization of the recombination protein RAD-51 in *Caenorhabditis elegans*. *Chromosoma*, *112*, 6–16.

Arsenovic, P. T., Maldonado, A. T., Colleluori, V. D., & Bloss, T. A. (2012). Depletion of the *C. elegans* NAC engages the unfolded protein response, resulting in increased chaperone expression and apoptosis. *PLoS One*, *7*, e44038.

Asikainen, S., Vartiainen, S., Lakso, M., Nass, R., & Wong, G. (2005). Selective sensitivity of *Caenorhabditis elegans* neurons to RNA interference. *Neuroreport*, *16*, 1995–1999.

Bailly, A., & Gartner, A. (2013). Germ cell apoptosis and DNA damage responses. *Advances in Experimental Medicine and Biology*, *757*, 249–276.

Brenner, S. (1974). The genetics of *Caenorhabditis elegans*. *Genetics*, *77*, 71–94.

Buchman, V. L., Ninkina, N. N., Bogdanov, Y. D., Bortvin, A. L., Akopian, H. N., Kiselev, S. L., … Georgiev, G. P. (1992). Differential splicing creates a diversity of transcripts from a neurospecific developmentally regulated gene encoding a protein with new zinc-finger motifs. *Nucleic Acids Research*, *20*, 5579–5585.

Church, D. L., Guan, K. L., & Lambie, E. J. (1995). Three genes of the MAP kinase cascade, mek-2, mpk-1/sur-1 and let-60 ras, are required for meiotic cell cycle progression in *Caenorhabditis elegans*. *Development*, *121*, 2525–2535.

Conte, D., Jr., & Mello, C. C. (2003). RNA interference in *Caenorhabditis elegans*. *Current Protocols in Molecular Biology* 26.3.1–26.3.20.

Derry, W. B., Putzke, A. P., & Rothman, J. H. (2001). *Caenorhabditis elegans* p53: role in apoptosis, meiosis, and stress resistance. *Science*, *294*, 591–595.

Dues, D. J., Andrews, E. K., Schaar, C. E., Bergsma, A. L., Senchuk, M. M., & Van Raamsdonk, J. M. (2016). Aging causes decreased resistance to multiple stresses and a failure to activate specific stress response pathways. *Aging (Albany NY)*, *8*, 777–795.

Dupuy, D., Li, Q. R., Deplancke, B., Boxem, M., Hao, T., Lamesch, P., … Vidal, M. (2004). A first version of the *Caenorhabditis elegans* promoterome. *Genome Research*, *14*, 2169–2175.

Friedland, A. E., Tzur, Y. B., Esvelt, K. M., Colaiacovo, M. P., Church, G. M., & Calarco, J. A. (2013). Heritable genome editing in *C. elegans* via a CRISPR-Cas9 system. *Nature Methods*, *10*, 741–743.

Frokjaer-Jensen, C., Davis, M. W., Ailion, M., & Jorgensen, E. M. (2012). Improved Mos1-mediated transgenesis in *C. elegans*. *Nature Methods*, *9*, 117–118.

Frokjaer-Jensen, C., Davis, M. W., Hopkins, C. E., Newman, B. J., Thummel, J. M., Olesen, S. P., … Jorgensen, E. M. (2008). Single-copy insertion of transgenes in *Caenorhabditis elegans*. *Nature Genetics*, *40*, 1375–1383.

Gabig, T. G., Crean, C. D., Klenk, A., Long, H., Copeland, N. G., Gilbert, D. J., … Weber, G. (1998). Expression and chromosomal localization of the Requiem gene. *Mammalian Genome*, *9*, 660–665.

Gabig, T. G., Mantel, P. L., Rosli, R., & Crean, C. D. (1994). Requiem: a novel zinc finger gene essential for apoptosis in myeloid cells. *Journal of Biological Chemistry*, *269*, 29515–29519.

Gartner, A., Milstein, S., Ahmed, S., Hodgkin, J., & Hengartner, M. O. (2000). A conserved checkpoint pathway mediates DNA damage-induced apoptosis and cell cycle arrest in *C. elegans*. *Molecular Cell*, *5*, 435–443.

Gibson, D. G., Young, L., Chuang, R. Y., Venter, J. C., Hutchison, C. A., III, & Smith, H. O. (2009). Enzymatic assembly of DNA molecules up to several hundred kilobases. *Nature Methods*, *6*, 343–345.

Grant, B., & Hirsh, D. (1999). Receptor-mediated endocytosis in the *Caenorhabditis elegans* oocyte. *Molecular Biology of the Cell*, *10*, 4311–4326.

Gumienny, T. L., Lambie, E., Hartwieg, E., Horvitz, H. R., & Hengartner, M. O. (1999). Genetic control of programmed cell death in the *Caenorhabditis elegans* hermaphrodite germline. *Development*, *126*, 1011–1022.

Hajnal, A., & Berset, T. (2002). The *C. elegans* MAPK phosphatase LIP-1 is required for the G(2)/M meiotic arrest of developing oocytes. *EMBO Journal*, *21*, 4317–4326.

Huelgas-Morales, G., Silva-Garcia, C. G., Salinas, L. S., Greenstein, D., & Navarro, R. E. 2016. The stress granule RNA-binding protein TIAR-1 protects female germ cells from heat shock in *Caenorhabditis elegans*. G3 (Bethesda).

Kadyk, L. C., & Kimble, J. (1998). Genetic regulation of entry into meiosis in *Caenorhabditis elegans*. *Development*, *125*, 1803–1813.

Kamath, R. S., Martinez-Campos, M., Zipperlen, P., Fraser, A. G., & Ahringer, J. (2001). Effectiveness of specific RNA-mediated interference through ingested double-stranded RNA in Caenorhabditis elegans. *Genome Biology*, *2*, RESEARCH0002.

Kawasaki, I., Shim, Y. H., Kirchner, J., Kaminker, J., Wood, W. B., & Strome, S. (1998). PGL-1, a predicted RNA-binding component of germ granules, is essential for fertility in *C. elegans*. *Cell*, *94*, 635–645.

Kulikova, D. A., Mertsalov, I. B., & Simonova, O. B. (2013). D4 family genes in vertebrates: Genomic organization and expression. *Ontogenez*, *44*, 3–9.

Lange, M., Kaynak, B., Forster, U. B., Tonjes, M., Fischer, J. J., Grimm, C., … Sperling, S. (2008). Regulation of muscle development by DPF3, a novel histone acetylation and methylation reader of the BAF chromatin remodeling complex. *Genes & Development*, *22*, 2370–2384.

Lascarez-Lagunas, L. I., Silva-Garcia, C. G., Dinkova, T. D., & Navarro, R. E. (2014). LIN-35/Rb causes starvation-induced germ cell apoptosis via CED-9/Bcl2 downregulation in *Caenorhabditis elegans*. *Molecular & Cellular Biology*, *34*, 2499–2516.

Lee, M. H., Ohmachi, M., Arur, S., Nayak, S., Francis, R., Church, D., … Schedl, T. (2007). Multiple functions and dynamic activation of MPK-1 extracellular signal-regulated kinase signaling in *Caenorhabditis elegans* germline development. *Genetics*, *177*, 2039–2062.

Lessard, J., Wu, J. I., Ranish, J. A., Wan, M., Winslow, M. M., Staahl, B. T., … Crabtree, G. R. (2007). An essential switch in subunit composition of a chromatin remodeling complex during neural development. *Neuron*, *55*, 201–215.

Libina, N., Berman, J. R., & Kenyon, C. (2003). Tissue-specific activities of *C. elegans* DAF-16 in the regulation of lifespan. *Cell*, *115*, 489–502.

Lim, Y., Seah, V. X., Mantalaris, A., Yap, M. G., & Wong, D. C. (2010). Elucidating the role of requiem in the growth and death of Chinese hamster ovary cells. *Apoptosis*, *15*, 450–462.

Martin, J. S., Winkelmann, N., Petalcorin, M. I., McIlwraith, M. J., & Boulton, S. J. (2005). RAD-51-dependent and -independent roles of a *Caenorhabditis elegans* BRCA2-related protein during DNA double-strand break repair. *Molecular & Cellular Biology*, *25*, 3127–3139.

Merritt, C., Rasoloson, D., Ko, D., & Seydoux, G. (2008). 3' UTRs are the primary regulators of gene expression in the *C. elegans* germline. *Current Biology*, *18*, 1476–1482.

Mertsalov, I. B., Kulikova, D. A., Alimova-Kost, M. V., Ninkina, N. N., Korochkin, L. I., & Buchman, V. L. (2000). Structure and expression of two members of the d4 gene family in mouse. *Mammalian Genome*, *11*, 72–74.

Mertsalov, I. B., Ninkina, N. N., Wanless, J. S., Buchman, V. L., Korochkin, L. I., & Kulikova, D. A. (2008). Generation of mutant mice with targeted disruption of two members of the d4 gene family: neuro-d4 and cer-d4. *Doklady Biochemistry & Biophysics*, *419*, 65–68.

Middeljans, E., Wan, X., Jansen, P. W., Sharma, V., Stunnenberg, H. G., & Logie, C. (2012). SS18 together with animal-specific factors defines human BAF-type SWI/SNF complexes. *PLoS One*, *7*, e33834.

Miller, M. A., Nguyen, V. Q., Lee, M. H., Kosinski, M., Schedl, T., Caprioli, R. M., & Greenstein, D. (2001). A sperm cytoskeletal protein that signals oocyte meiotic maturation and ovulation. *Science*, *291*, 2144–2147.

Paz-Gomez, D., Villanueva-Chimal, E., & Navarro, R. E. (2014). The DEAD Box RNA helicase VBH-1 is a new player in the stress response in *C. elegans*. *PLoS One*, *9*, e97924.

Rea, S. L., Wu, D., Cypser, J. R., Vaupel, J. W., & Johnson, T. E. (2005). A stress-sensitive reporter predicts longevity in isogenic populations of *Caenorhabditis elegans*. *Nature Genetics*, *37*, 894–898.

Riedel, C. G., Dowen, R. H., Lourenco, G. F., Kirienko, N. V., Heimbucher, T., West, J. A., … Ruvkun, G. (2013). DAF-16 employs the chromatin remodeller SWI/SNF to promote stress resistance and longevity. *Nature Cell Biology*, *15*, 491–501.

Rodriguez, M., Snoek, L. B., De Bono, M., & Kammenga, J. E. (2013). Worms under stress: *C. elegans* stress response and its relevance to complex human disease and aging. *Trends in Genetics*, *29*, 367–374.

Rousakis, A., Vlanti, A., Borbolis, F., Roumelioti, F., Kapetanou, M., & Syntichaki, P. (2014). Diverse functions of mRNA metabolism factors in stress defense and aging of *Caenorhabditis elegans*. *PLoS One*, *9*, e103365.

Rual, J. F., Ceron, J., Koreth, J., Hao, T., Nicot, A. S., Hirozane-Kishikawa, T., … Vidal, M. (2004). Toward improving *Caenorhabditis elegans* phenome mapping with an